
UNIVERSITY OF BIRMINGHAM

# The relationship between senescence and autophagy in human inflamed joint cell populations

Vincent Gauthier

Supervisors:

Prof Christopher D. Buckley

Prof Karim Raza

Dr Ghada Alsaleh

Thesis submitted for

the Degree of Doctor of Philosophy

June 2024

**ABREVIATIONS**

| | |
|---|---|
| **ACPA** | Anti-citrullinated protein antibodies |
| **BMI** | Body mass index |
| **BV** | Blood vessel |
| **CCP** | Cyclic citrullinated peptide |
| **CD(+number)** | Cluster differentiation |
| **CDKs** | cyclin-dependent kinases |
| **CDKN1A** | Cyclin-dependent kinase inhibitor 1A |
| **CDKN2A** | Cyclin-dependent kinase inhibitor 2A |
| **CRP** | C-Reactive Protein |
| **CX3CR1** | CX3C motif chemokine receptor 1 |
| **ER** | Endoplasmic reticulum |
| **ESR** | Erythrocyte sedimentation rate |
| **DAS28** | Disease activity score 28 |
| **DDR** | DNA damage response |
| **DMARDs** | Disease-modifying antirheumatic drugs |
| DMM | Destabilisation of the medial meniscus |
| **ECs** | Endothelial cells |
| **ECAR** | Extracellular acidification rate |
| **ECM** | Extracellular matrix |
| **FISH** | fluorescence in situ hybridization |
| **FLS** | fibroblast like synoviocytes |
| **HLA** | Human Leukocyte Antigen |
| **HUVEC** | Human Umbilical cord Endothelial Cell |
| **IF** | Immunofluorescence |
| **ICC** | Immunocytochemistry |
| **IHC** | Immunohistochemistry |
| **IQR** | Interquartile range |
| **JRP** | Joint replacement |
| **LL** | Lining layer |
| **MCs** | Mural cells |

| | |
|---|---|
| **MERTK** | Myeloid-epithelial-reproductive tyrosine kinase |
| **MFI** | Mean fluorescence intensity |
| **MMP** | Matrix metalloproteinase |
| **mTOR** | Mechanistic target of rapamycin |
| **MTX** | Methotrexate |
| **OA** | Osteoarthritis |
| **OCR** | Oxygen consumption rate |
| **PDPN** | Podoplanin |
| **PFFE** | Paraffin embedded |
| **PRG4** | Lubricin |
| **RA** | Rheumatoid Arthritis |
| **RANKL** | Receptor activator of nuclear factor kappa-B ligand |
| **ROS** | Reactive oxygen species |
| **SA-β Gal** | Senescence associated β Galactosidase |
| **SAHFs** | Senescence-associated heterochromatin foci |
| **SASP** | Senescence associated secretory phenotype |
| **SDFs** | Senescence DNA damages foci |
| **scRNA-seq** | Single cells RNA sequencing |
| **SL** | Sub-lining |
| **SMCs** | Smooth muscle cells |
| **TFEB** | Transcription factor EB |
| **TRMs** | Tissue resident macrophages |
| **NET** | Neutrophils Extracellular Traps |
| **NSAID** | non-steroidal anti-inflammatory drugs |
| **yH2AX** | gamma Histone 2A.X |

**Statement of originality**

I certify that this thesis is the results of my own work. I declare that all data, text, and figures have not been submitted for another award, degree or diploma at any other institution.

The use of published public data has been acknowledged.

This work was completed between the RRG in Queen Elisabeth Hospital in Birmingham, the Kennedy institute of Rheumatology in Oxford, and the BOTNAR research centre in Oxford.

**Abstract:** Rheumatoid arthritis (RA) and osteoarthritis (OA) are both diseases of the articular joint affecting the synovium. The synovium is critical to maintain joint homeostasis by protecting the articular cartilage and secreting synovial fluid. In OA and RA, the synovial lining layer (LL) and sub-lining (SL) are challenged by many stressors such as inflammation. Although RA and OA have different origins, age is a relevant factor for both. However, the role of aging in the degenerative processes occurring in the synovium remain poorly understood. By using multiplex immunofluorescence and spectral flow cytometry, we investigated aging through the perspective of cellular senescence, DNA damage and autophagy regulation via TFEB in the fibroblasts, tissue resident macrophages (TRMs), lymphocytes and endothelial cells (ECs) in OA and RA. We found that the lining layer is highly affected by DNA damage, up regulated p53 and accumulation of p16+ cells in both diseases. Notably, the LL fibroblasts have a higher DNA damage response o activation and senescence compared to the SL populations. Other cell types such as ECs also up regulated the DNA damage response through p21 and p53 expression. This pro damage context promotes the master regulator of autophagy TFEB. We found that TFEB activity and expression is decreased in OA compared to RA specifically in the LL fibroblasts. Together, these data provide the first map of the cellular stressors involved in inflamed synovium, paving the way to promising new regulation involving autophagy, metabolism, inflammation and cellular senescence in arthritis.

**CONTENTS**

# 1 Introduction

## 1.1 Arthritis:

### 1.1.1 Rheumatoid arthritis

Rheumatoid arthritis (RA) is a systemic autoimmune disease caused by genetic and environmental factors leading to chronic inflammation of the synovium (synovitis). The local inflammation of the joint destabilized the homeostasis of the synovium driving cartilage and bone damage and increasing articular pain. Genetic factors are estimated to contribute around 50 to 60% to the susceptibility of RA. The most significant genetic variants are found within the human leukocyte antigen (HLA) genes, notably, the HLA-DRB1 alleles (1). One important feature in the diagnosis of RA is the presence of multiples autoantibodies such as rheumatoid factor (RF) or anti-citrullinated protein antibodies (ACPA). The presence of ACPA in RA patients is associated with diseases severity and can be detected in the pre-clinical phase before the establishment of the disease (2). ACPA play an important role in the development of the pathology by activating synovial macrophages or promoting osteoclasts activity among others (3).

Due to multi-factorial origin and gradual inflammation, many modifications occur in the cell populations of the synovium creating an heterogenous clinical background among patients (4).

### 1.1.2 Osteoarthritis

Osteoarthritis (OA) is the most common form of arthritis, affecting millions of people globally. OA is a chronic condition characterized by joint pain and swelling, which reduces articular mobility (5). Factors such as aging, obesity, and heart diseases increase the risk of OA and can decrease lifespan (5, 6). Although OA primarily affects elderly individuals, it can also occur in younger people following traumatic joint injuries (7). In the knee, the progression and development of OA depends on various factors impacting different joint components, including cartilage and synovial tissue.

Specifically, cartilage fractures, known as fibrillation, and alterations in the extracellular matrix (ECM)—marked by a loss of proteoglycan and collagen—undermine cartilage's protective function. Furthermore, the formation of osteophytes (fibro-cartilage structures that represent abnormal bone growth at the joint margin) and reduced lubrication in the synovial cavity contribute to increased pain and mechanical stress in the joint (6). Synovial tissue is deeply affected during OA, notably structural changes characterized by an expansion of the lining layer (LL) accompanied by synovitis in the sub-lining (SL).

### 1.1.3 Perspective and treatment

The first line of treatment in RA consists of nonsteroidal anti-inflammatory drugs (NSAIDs) and corticosteroids to rapidly reduce pain and inflammation (8). In order to promote the remission of the disease, disease-modifying antirheumatic drugs (DMARDs) are then also added. The most commonly used DMARD is methotrexate (MTX), a metabolic inhibitors which promotes T cells apoptosis, inhibits nuclear factor-κB (NF-κB) activation, and acts on other anti-inflammatory processes via the accumulation of adenosine (9). However, only 40% of the patients are responsive to MTX leaving many patients in need to other DMARDs or biologic treatments (10).

Biologics inhibiting TNF-α such as etanercept, adalimumab or infliximab are effective options in the treatment of RA, although have adverse side effects (8). Rituximab targeting CD20 and promoting B cells depletion, is often used in combinations with MTX in case of anti TNF-α failure (11).

Nevertheless, a significant proportion of patients are still refractory to conventional treatments increasing the need for new therapies targeting other actors of inflammation such as fibroblasts.

The treatment of other arthritic diseases such as OA remains today a challenge. Many pre-clinical and clinical trials aim to address different aspect of OA by targeting degradation molecules, inflammatory mediators, or neurone growth to alleviate pain (12). However, no current therapies are successfully

preventing or reversing cartilage and bone damage underscoring the desperate need to novel line of treatment in OA.

Thanks to the discoveries implicating stromal cells in the progression of RA and OA, new therapies based on the modulation of synovial fibroblasts are emerging (13).

## 1.2 Cellular populations of the synovium in disease

### 1.2.1 Fibroblasts

The synovial membrane consists of two distinct compartments: the lining layer and the sub-lining layer. PRG4+CD55+CLIC5+ fibroblasts, which are highly specific and responsible for synovial fluid secretion, are located in the synovial lining layer. In contrast, sub-lining fibroblasts are not well characterized under normal conditions (14, 15). However, in patients with active synovial inflammation, there is a marked increase in fibroblast heterogeneity, contributing to both inflammation and bone/cartilage erosion. Under normal conditions, fibroblasts adjust to the needs of their local environment, modulating specific tissue niches. Emerging single-cell RNA sequencing (scRNA-seq) data on human fibroblasts in healthy individuals are uncovering new roles for fibroblasts beyond their traditional function in ECM formation.

Indeed, a heterogenous inflammatory phenotype has been identified in the CD90+ synovial fibroblast subset in inflamed human synovium (16, 17). The recent scRNA-seq data set investigating the inflammatory populations in RA have identified 7 sub-clusters named SL CD90+ fibroblasts: CD34+, POSTN+, DKK3+, $CD74^{high}$ $HLA^{high}$, CXCL12+ SFRP1+, NOTCH3+, and RESPO3+. Most of those populations positively regulates inflammation by promoting the secretion of pro-inflammatory cytokines and chemokines leading to the recruitment and retention/survival of infiltrated lymphocytes (16). Interestingly, a cross-disease study indicates the existence of common inflammatory phenotypes enriched upon inflammation in the fibroblasts characterized by SPARC+COL3A1+ and CXCL10+CCL19+. Their equivalents in RA pathology will probably be the perivascular NOTCH3 corresponding to

SPARC+COL3A1+ and both $CD74^{high}$ $HLA^{high}$, CXCL12+ corresponding to CXCL10+CCL19+ (14, 18). In RA, SL fibroblasts proliferate from the perivascular region toward the lining layer, with endothelial cells providing guidance through NOTCH3 signalling. Activation of NOTCH3 in fibroblasts not only influences their expansion but also shapes their pathogenic sub-lining phenotype. Inhibition of NOTCH3, either through genetic depletion or antibody blockade, reduces synovial inflammation and damage, underscoring the significance of endothelial-fibroblast interaction in RA progression (19).

Emerging evidence suggests that the DKK3+ fibroblasts have a regulatory role in different forms of arthritis (20, 21). Therefore, this population may represent a new therapeutic avenue for refractory patients to conventional therapies (22).

It has been demonstrated that pathological processes supported by the LL fibroblasts differ from the SL fibroblasts. Notably, under arthritis LL fibroblast expressed many degradation associated molecules such as RANKL which increase bone and cartilage erosion. Indeed, adoptive transfer of LL fibroblast at the joint site increase osteoclast activity and cartilage destruction. Conversely, adoptive transfer of fibroblast THY-1+ populations is sufficient to increase inflammation suggesting their pro-inflammatory role (16).

However, recent research revealed a new transcriptional control dictating the fate of synovial fibroblasts towards an ECM degrading phenotype. The transcription factor ETS1 might be a key driver in this process, positively regulating genes such as Tnfsf11 (coding for RANKL), MMP13, and MMP3 in arthritic synovial fibroblasts (23).

### 1.2.2 Tissue resident macrophages

In the manner of synovial fibroblasts, tissues resident macrophages (TRMs) in the synovium have a myriad of phenotypes and differential activation states according to their role and localization. TRMs act as a protective barrier of the synovial cavity by maintaining the structure of the LL (24). Indeed, in mice, CX3CR1+ TRMs expressed tight junctions to form an epithelium-like barrier to support the

integrity of the LL. Those specialized TRMs are renewed by a proliferating pool of interstitial SL CX3CR1- TRMs (24). According to scRNA seq in human synovium, TRM populations express MERTK, CD206. Among them, the LL associated TRMs are TREM2+, CX3CR1+ and FOLR2+ while the interstitial macrophages are FOLR2$^{HIGH}$, LYVE1+. In contrast, the tissue infiltrated monocytes are MERTK-, CD206-, CD48+, HLA$^{HIGH}$ (25). Under arthritis the number of infiltrating macrophages rises while the LL TRMs are disturbed. This increase of infiltrating MERTK- HLA$^{HIGH}$ is associated with increased inflammation. Interestingly, disease remission is associated with an enrichment of MERTK+ TRMs leading to pro repair mechanisms via a crosstalk with synovial fibroblasts underlining the protective role of the TRMs in the joint (26).

### 1.2.3 Lymphocytes

Chronic inflammation is marked by the failure of resolution. This prevents the immune cells recruited at the site of inflammation to exits the tissue or being eliminated by apoptosis (27, 28). Rearrangement of the stromal niche supported by SL fibroblasts favoured the accumulation of immune cells in the synovium leading to the formations of lymphocytes aggregates and in certain occasion to the formation of Tertiary lymphoid Structures (TLS) (29, 30, 31). The accumulation of T and B cells infiltration in the synovium is a synonym of poor outcomes by maintaining a pro-inflammatory environment through the secretion of cytokines and pro damaging molecules(32).

### 1.2.4 Endothelial and Mural cells

Blood vessels are formed by a layer of endothelial cells (ECs) that assure the exchange between the circulatory system and the peripheric tissue. ECs are critical for vessels growth through VEGF signalling in a process is called angiogenesis to create a dynamic network to supply oxygen and nutrient in the tissue (33). The vasculature found in peripheral tissue like the synovium is called microcirculation which characterizes the end of the vascular network. This network is composed by the capillaries, arterioles, and venules with a diameter inferior or equal to 100µm (34, 35). In addition, mural cells are important to regulate the blood flow throughout the vasculature system. Mural cells comprise smooth muscle

cells (SMCs) and pericytes both expressing MCAM (19, 36). For instance, SMCs will usually form a uniform layer around the arterioles, while pericytes are unevenly distributed around capillaries and post-capillary venules (37). Under synovitis, more vessels are formed within the SL of the synovium as a result of the pro-inflammatory environment facilitating the infiltration of immune cells(38). Moreover, at the site of inflammation, ECs promote the infiltration of immune cells through the secretion of many chemokines and cytokines (39, 40, 41). ECs also permits the trafficking of circulating lymphocytes through a process called diapedesis essential in the establishment of the immune response in peripheral tissue(42). In addition, endothelial cells and pericytes induced the expansion of the CD90+ pro-inflammatory SL fibroblasts via NOTCH3 in synovitis (19).

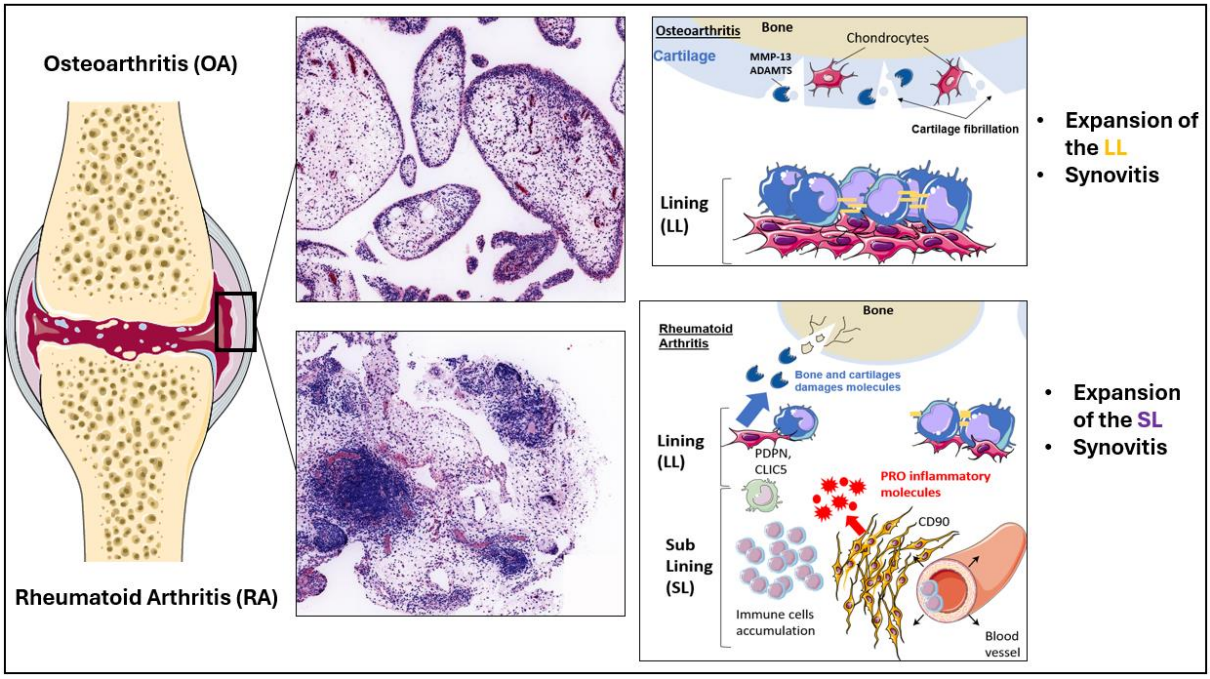


**Figure 1.1:** Synovial architecture during Osteoarthritis (OA) and Rheumatoid arthritis (RA).

Virtual haematoxylin and eosin staining of OA synovium (top) and RA synovium (bottom) displaying the main structural differences between the two diseases. OA synovium often features hyperplasia of the lining layer (LL) while in RA the LL is disrupted. On the other hand, RA sub-lining (SL) is often associated with infiltration of immune cell, including T cells, B cells and pro-inflammatory monocytes. In addition, SL fibroblasts expand from the perivascular niche and promote the pro inflammatory environment called “synovitis”. Furthermore, the LL fibroblasts adopt a pro damage phenotype leading to bone and cartilage degradation. While RA is mainly driven by pro inflammatory mechanisms, synovitis is often seen in OA synovium affecting the SL organisation.

## 1.3 Aging

### 1.3.1 What is aging?

Aging is now considered by many as a disease on its own (43). As human lifespan has significantly increase towards the last decades, aging is becoming one of the major economic and societal burden. While the idea of an ultimate cause of aging is unknown, our understanding of aging supports the theory that aging is a multi-factorial molecular and cellular disorder (44). Aging could be described as the accumulation of degenerative processes leading to organismal dysfunction. Therefore, explaining the aging required the integration of multiple processes classified as “Hallmarks of aging” (45). This comprises genetic instability, loss of proteostasis, epigenetic regulation, mitochondrial dysfunction, autophagy decline and cellular senescence increase to name just a few (45). Those mechanisms happen to a certain extent and may overlap with each other depending on the context. For example, autophagy decline leads to mitochondrial dysfunction which will eventually lead to the increase of Reactive Oxygen Species (ROS) decreasing DNA stability. Integrating environmental causes with the molecular hallmarks in a specific context (disease, cell type, metabolism) represents the next challenges of the field and need to be addressed to delay or prevent age related diseases.

### 1.3.2 Cellular senescence and evolutionary aging

Cellular senescence is an evolutionarily conserved mechanism, beneficial early in life. However, the protective effect of senescence early in life is impaired and becomes harmful in elderly individuals. In 1957 Georges C. Williams introduced the concept of *antagonist pleiotropy (46)*. This theory proposes that beneficial genes selected for fertility and individual fitness early in life have a deleterious effect later in life, driving aging. In 2019 J.F. Mitteldorf proposed that aging has a long-term benefit when placed in the context of community benefit rather than individual fitness (47). He explains that having a long life, combined with high fertility, could unbalance the adaptation of a group, especially in the context of predation. Long lifespan individuals with high fertility could disturb the prey/predator ratio

and so, be detrimental for both groups. It is possible that a group could adapt its longevity and fertility to fit the demands of its environment. Unfortunately, at the individual level, senescence mechanisms eventually exhibit side effects that could be detrimental to the individual's survival. This theory applies to cellular senescence duality, where the beneficial aspect early in life is compromised in aged individuals. However, the cost-benefit is favourable to the population.

### 1.3.3 Characteristics of senescence

The viability of complex organisms such as mammals requires adapted responses from their cells. This viability is maintained by one property of the tissue termed "renewable tissue". Renewable tissue is characterized by its ability to induce proliferation or recruit mitotic cells to ensure regeneration or tissue repair (48). In this context, cells undertake important molecular changes that allow DNA replication. Proliferation is essential to renewing tissues, but it can also be the source of cancer development. One effective mechanism to avoid cancer development is cellular senescence. Senescence (from the Latin word senex meaning old age) was originally described by Hayflick in 1965 as a limitation in the lifespan of "old" fibroblasts in vitro (49). He observed that despite growth factors and nutrients in the medium, cells gradually lost their ability to divide but remained viable. This mechanism is termed replicative senescence. Later, many authors speculated that this mechanism was related to age and provided protection against cancer. Today, senescence is understood to represent a complex cellular state involved in many processes and pathologies (both related to ageing and not).

Senescence is characterized by the inability of a cell to grow. It is conceptually different to quiescence, which is defined by a resting state where cells leave the cell cycle and undergo other functions. In contrast, post-mitotic cells (e.g. cardiac and skeletal muscle cells and differentiated neurons) lose their ability to proliferate due to differentiation. Other cell types such as fibroblasts, vascular, and epithelial cells are classified as mitotic and can become senescent under certain conditions. Senescent cells cannot begin a new cycle of proliferation when they encounter oncogenic events and become resistant to apoptosis. However, replicative senescence can occur and defines a limited number of divisions

before an absolute arrest of the cell cycle. The primary cause of replicative senescence is telomere shortening, described as the main characteristic of cellular ageing.

### 1.3.4 Telomere shortening

Telomeres are repeated sequences found at the ends of chromosomes. In humans, the repeated sequence (TTAGGG/CCCTAA) forms in complex with several proteins a loop structure referred to as "Shelterin" (50). During DNA replication, DNA polymerases need RNA primers to replicate in a 5' to 3' direction. On the lagging strand, DNA synthesis is discontinuous due to its opposite direction to the leading strain. This process creates the Okazaki fragments which are subsequently ligated by a DNA ligase. RNA primers are removed to create a completed DNA strain. However, replication at chromosome ends is challenging. Indeed, when the last primer has been removed, DNA polymerase is unable to entirely complete the lagging strand due to its incapacity to fix the reading frame. This leads to the shortening of the size of a primer at the telomere end. Over a long series of replications, the shortening of telomeres will be more important, leading to DNA damage. To counter this process, a specific DNA polymerase RNA dependent termed telomerase reverse transcriptase (TERT) elongates the repeated sequences of the telomere, ensuring DNA polymerase attachment and completed DNA synthesis (51). In humans, TERT expression is highly regulated and occurs only during a short period of time during development, in the germline and in progenitor cells (51, 52). The regulation and silencing of the telomerase complex is essential to prevent cancer formation as TERT is up regulated in 85-95% of cancers (51). Cellular ageing is characterized by the shortening of telomeres which leads cells to senescence after a certain number of divisions. The progressive shortening at the ends of telomeres destabilizes the loop structure and exposes single strain DNA which is recognized by the DNA damage response (DDR) (48). This is termed "The end replication problem".

### 1.3.5 DNA damage response

It is well known that DNA damage, especially double-strand breaks (DSBs), trigger many cells to undergo senescence. Indeed, as described previously, telomere shortening mimics DSBs and recruits

the DDR. In most cases, DSBs are induced by factors such as ionizing radiation, reactive oxygen species (ROS), or VDJ recombination. Two pathways, homologous recombination (HR) and non-homologous end-joining (NHEJ), play roles in repairing DSBs (53). The HR pathway is active during the S- and G2-phases of the cell cycle. Indeed, the homologous sister chromatid is required as a structural base for repairing. In contrast, when DSBs occur in the G1 phase, the NHEJ pathway is required. The NHEJ pathway starts with the recognition and binding of the Ku70/Ku80 heterodimer at DNA ends. This is followed by the recruitment of the DNA dependent protein kinase (DNA-PK), which can then recruit nucleases or DNA polymerases. Finally, the formation of a protein complex including XRCC4, Lig4, and XLF permits DNA ligation (The Cell, 2nd edition: A Molecular Approach). Senescent cell often exhibits a persistent DDR signalling. After telomere shortening, the DNA damage sensor is activated and comprises many protein interactors and DNA modifications. The most important chromatin modification is phosphorylation of the histone H2AX (γH2AX). The accumulation of γH2AX on the damaged site increases DNA accessibility to facilitate repairing machinery and to reduce chromatin density (54). The three main kinases which directly phosphorylate H2AX at DSBs sites are ataxia telangiectasia mutated (ATM), RAD3-related (ATR), and DNA-PK. Thus, a protein complex composed of NSB1, RAD50, and MRE11 (NRM) can directly bind to DNA and facilitate the phosphorylation of H2AX by ATM. This collaboration allows the recruitment of mediator of DNA damage checkpoint-1 MDC1 or 53BP1 which orchestrates the DDR and maintains the local phosphorylation of H2AX. It also leads to the recruitment and activation of downstream kinases such as the checkpoint-1 kinase-1 (CHK1) and checkpoint-2 kinase-2 (CHK2) which will activate the effector molecules to stop the cell cycle (48). Those effectors are essential to blocking cell cycle progression transiently or permanently in case of senescence. For instance, CKH1 and 2 can activate phosphatase such as CDC25, a regulator of the cell cycle in G1. More importantly, CHK2 and ATM can phosphorylate the tumor suppressor p53, a major effector involved in senescence (55, 56). Indeed, p53 activates the cyclin-dependent kinases (CDK) inhibitor p21 that belongs to the INK4/CiP1 family protein. DDR activation can also activate the P16INK4a pathway after p53 activation. This is especially observed in humans where telomere

shortening can trigger both p53 and $p16^{INK4a}$ /pRb pathways. Once $p16^{INK4a}$ is activated, it enables the phosphorylation of pRb. Therefore, the Rb/E2F complex is maintained, and specific genes activated by E2F remain silenced; those foci are termed senescence-associated heterochromatin foci (SAHFs) (48). In multicellular organisms, cell division is an essential mechanism to allow tissue growth and maintenance. In somatic cells, the division process is referred to as the cell-cycle which is characterized by a series of highly regulated steps (57). Before undergoing a division, cycling cells are termed quiescent (G0). Cell growth starts with interphase. Before the beginning of DNA replication (S phase), cells enter a gap phase (G1) (58). However, the mechanism that allows DNA replication is conserved and relies on the activation of cyclin-dependent kinases (CDKs). CDKs coordinate in time the main events of the cell cycle in association with a specific cyclin subunit. In G1, CDK4/6 interacts with cyclin D to drive cell proliferation; this complex phosphorylates retinoblastoma protein Rb which release E2F. E2F activates the transcription of the proteins involved in cell cycle progression such as CDK1, cyclin E (cyE), or cyclin A (cyA). Moreover, the CDK2/cyE complex continues to phosphorylate Rb to overcome the first checkpoint of the cell cycle (58). Therefore, many inhibitors, including those belonging to the p21 and p16 family, can block the progression of the cell cycle in G1. $p16^{INK4a}$ directly inhibits CDK4 and CDK activities, enabling the phosphorylation of Rb. However, p21 interferes with the CDK2/cyE interaction to block the entry in S phase (59). As described earlier, telomere shortening via DSBs can induce activation and overexpression of p53 which will activate p21 to inhibit the cell cycle and induce senescence. However, many other signals can cause cellular senescence.

### 1.3.6 Oncogenes activated senescence

Oncogenes are the mutant version of genes that can transform normal cells into cancerous cells. Senescence occurs when certain types of genes are overexpressed, or in an oncogene form. This is the case for the gene RAS and its mutant form which induces the formation of SAHFs by the activation of p16. Consequently, many other genes involved in the RAS pathway such as MEK or BRAF in oncogenic versions cause senescence (48, 60). Oncogene induced senescence is an essential process to prevent

cancer development. When tumour suppressors such as p53 or p16 are mutated in the presence of oncogenes, senescence cannot be activated without other signals and cells undergo tumorigenesis (48).

### 1.3.7 Oxidative stress

Oxidative stress is one of the main causes of senescence. Indeed, reactive oxygen species (ROS) are responsible for many damages in DNA. Ageing can be associated with different parameters such as metabolic changes, oncogene accumulation and high production of ROS (45). It is known that a high level of ROS, despite their role in DNA damage, mediates p53 activation which can also promote oxidant production (61). Moreover, ROS damage mitochondrial DNA (mtDNA) in synergy with p53 pathway activity and telomere shortening. This creates a mitochondrial dysfunction characteristic of senescent cells. Also, p21 is necessary and sufficient to induce mitochondrial dysfunction and increased ROS production through the p38MAPK GRB2-TGFBR2-TGFB signalling and maintain DDR (62).

### 1.3.8 Senescence and epigenetics

Chromatin perturbation can cause senescence (63). Chromatin state determines which genes are expressed or are silent. Euchromatin corresponds to decompaction of DNA to provide an active state for transcription. In contrast, heterochromatin is a compact state of chromatin where genes are silenced. Those mechanisms depend on different histone modifications (acetylation or methylation) (63). For instance, the inhibition of histones deacetylase which promote euchromatin may induces senescence. It is conflicting with the formation of SAHFs which are heterochromatin regions. However, histone deacetylase inhibitions activate the p21 and p16 expression in human fibroblasts while the p53 pathway is involved in mouse (64).

### 1.3.9 Hallmarks of senescence

Senescence activation is very heterogeneous and depends on the cell type, tissue context, nature of stress among others (65). However, some common markers exist which can be used to define senescent

cells (66, 67). Senescent cells can be distinguished in vitro by their lack of proliferation. For instance, immunostaining of proteins such as Ki67, or the incorporation of 5-bromodeoxyuridine (BrdU) during DNA replication distinguishes proliferative cells from senescent cells. However, it will not tell us if the non-proliferative cells are truly senescent or just quiescent or differentiated post-mitotic cells (48). One of the first markers used to detect senescent cells was the senescence-associated β-galactosidase (SA-βgal). Indeed, senescent cells exhibit higher lysosomal activity, and the lysosomal β-galactosidase can be detected by histological staining on fresh frozen tissue. As mentioned earlier, p16 can be a good marker of senescent cells via its important role in cell cycle arrest(59). Furthermore, p38MAPK pathway promote the phosphorylation of Bmi1 a directed regulator of the INK4A promoter. Once phosphorylated, Bmi1 loses its repressive activity leading to the transcription of p16 (68). In addition, p38MAPK is activated by different stress stimuli, including telomere shortening or oxidative stress, making the p38MAPK pathway a common activator of senescence (69). However, the expression of p16 is not involved in all senescence processes. For instance, during oxidative stress, autophagy and senescence can simultaneously activate p38 MAPK signalling leading to the up regulation of p21 but not p16 (70). Moreover, senescence associated DNA-damage foci (SDFs) can be identified by the presence of specific markers such as phosphorylated histone H2AX (yH2AX) or the H3 lys9 methylation (H3K9 me3) (71, 72). Furthermore, DNA damage activates the p53/p21 pathway, increasing the level of expression of both of those hallmarks (73). While the p52/p21 is observed in most senescence cells, the activation of this pathway might result in a transient cell cycle arrest promoting repair and genetic stability without engaging the irreversible cell cycle arrest seen in senescent cells. However, a prolonged p53 activation will lead to senescence (67, 74).

Besides protein biomarkers, the presence of ROS is a good indication of the cellular stress state which often leads to apoptosis or senescence (45, 66). Therefore, mitochondrial dysfunction can be investigated to confirm the altered metabolic state.

Finally, nucleus size, ER stress, lack of proliferation, decreased expression of LAMINB1 and SASP are also good hallmarks of senescent cells (67, 75, 76, 77). Nevertheless, it remains difficult to fully characterized senescent cells as their heterogeneity is reflected by the numerous contexts of activation.

## 1.4 Senescence and tissue regulation

### 1.4.1 Benefits of cellular senescence

Like many aspects of biology, the biological outcomes of cellular senescence are highly dependent on the cellular and tissue context. One of the principal roles of senescence is to contain DNA damage by stopping the cell cycle with the removal of senescent cells and restoration of homeostasis This is a primordial role to prevent early cancer formation but is also important in tissue remodelling and repair following tissue damage. This is particularly the case in wound healing where cellular senescence plays a major role via the secretion of platelet-derived growth factor AA (PDGF-AA). Indeed, microenvironmental changes after wounding show an increase of the matricellular protein CCN1 which induces senescence in fibroblasts (78). The senescence-associated secretory phenotype (SASP) factor PDGF-AA, secreted by these senescent fibroblasts, promotes myofibroblast differentiation and accelerated wound healing (79).

Recently, a novel role for senescence has been identified in the development of various structures such as the mesonephros, the endolymphatic sac of the inner ear, the neural roof plate, and the apical ectodermal ridge, among several other tissues (80). Depletion of the senescence activator p21 results in abnormal development of those structures. However, the absence of programmed developmental senescence is partially reversed by cellular apoptosis, suggesting a link between these two mechanisms, possibly via the clearance of both apoptotic and senescent cells.

Moreover, cellular senescence is important to regulate the structure of the placenta(81). Unlike the developmentally programmed senescence which requires the activation of p21 by the transforming growth factor (TGF)-β/SMAD and PI3K/FOXO pathways (80), the formation of the placenta is controlled

by a similar activation observed during DNA damage response induced senescence and result through the activation of the p53 and p16 axis. The activation of p53 in this context depends on the viral fusogen ERVWE1 which mediates cell fusion of syncytiotrophoblasts to provide a maternal/foetal interface at the placenta (80, 82). Interestingly, senescence is also activated during cell fusion induced by oncogenic or viral origins. This is thought to facilitate their elimination by NK cells adapted to recognize abnormal cell fusion (82). Senescence in RA has been understudied due to the inefficiency of senolytics treatment. Interestingly, a recent study demonstrated that the therapeutics activation of monocarboxylate transporter 1 (MCT1), promotes cellular senescence in fibroblasts and ameliorate diseases prognosis (83). In this specific context, the induction of senescence exchanges the pathological pro-inflammatory phenotype of the fibroblasts to a pro repair phenotype dampen inflammation (83). This underlining the fact that the context of cellular senescence activation plays a critical role on the outcomes. Due to its predominant role in the regulation of early tumorigenesis, and tissue remodelling, cellular senescence appears as a vital mechanism early in life explaining its high conservation through evolution.

### 1.4.2 Darkside of senescence

As described previously, cellular senescence is classified as a hallmark of aging (45). Cellular senescence impacts aging at different levels. Notably, the expression of pro-inflammatory SASP such as IL-6 or IL-8 induces a low-grade inflammation termed “inflammaging” that actively participates to tissue specific aging (65). Conversely, cellular senescence in fibroblasts and alveolar cells is known to be involved in pulmonary fibrosis by promoting excessive matrix secretion through a pro repair SASP (84, 85, 86). In addition, cellular senescence is a cause of stem cells exhaustion, induced by the paracrine effect of senescence through the SASP, leading to a loss of the regenerative tissue capacity. This has major impact on many age-related diseases such as sarcopenia, heart diseases, or neurodegenerative diseases (87, 88, 89). Osteoarthritis is not exempt of the negative impact of cellular senescence. In fact, the transplant of senescent cells into the joint in mice is sufficient to induce an OA-like state (90).

Furthermore, removal of p16+ senescent cells attenuate post traumatic induced OA (91). In addition, correlation between senescence-associated β-galactosidase (SA-βgal) in chondrocytes and diseases severity in knee OA has been reported (92). Yet, the implication of senescence in the synovial tissue on OA progression remains mostly unknown. Because of its pleiotropism cellular senescence is a paradoxical mechanism involves in both repair and damage depending on the context (65).

## 1.5 Autophagy

### 1.5.1 Regulation of autophagy via TFEB

On the opposite side of cellular stress response, autophagy contrasts with senescence as a global catabolic mechanism permitting the recycling of dysfunctional organelles and misfolded proteins. Three types of autophagy can be distinguished, macro autophagy (referred as autophagy here), micro autophagy and chaperone mediated autophagy. Autophagy starts with the formation of a lipid bilayer, termed the phagophore, originating from the endoplasmic reticulum and/or the trans-Golgi. It then engulfs proteins aggregates, ribosomes and organelles in a structure called the autophagosome which fuses with a lysosome. The acidic environment and the high lysosomal proteases activity of the lysosome degrade the autophagolysosomal contents to amino acid, which are transported to be used in anabolism processes and metabolism. Autophagy machinery in mammals begins with the interaction of Beclin-1 and the class III PI-3 kinase Vps34 required for the elongation of the phagophore. At the phagophore membrane, the conjugation of Atg5 and Atg12 is critical to the recruitment of LC3 (converted in LC3II) involved in the membrane fusion and the selective or random capture of cargo for degradation (93). Autophagy is mainly activated during nutrient, growth factor or energy deprivation while the mammalian target of rapamycin complex 1 (mTORC1), a master regulator of metabolism which promotes cells growth, is inhibited. In this context, mTORC1 can also inhibit autophagy in the presence of a high amino acid level. Indeed, mTORC1 regulates autophagy by inhibiting Beclin-1/Vps34 interaction, but also through the phosphorylation of the transcription factor EB (TFEB) resulting in its sequestration at the lysosome membrane (94, 95). Beside mTOR1, Sirtuin 1 (SIRT1) enhances the

activity of TFEB by promoting its deacetylation within the nucleus (96). TFEB is often referred to as the master regulator of autophagy. Indeed, TEFB coordinates lysosomal biogenesis and autophagy by the activation of the gene network called Coordinated Lysosomal Expression and Regulation (CLEAR) (97, 98, 99). Therefore, characterizing the regulation of TFEB within the tissue is critical to understand autophagy **(Fig 1)**.

### 1.5.2 Autophagy as hallmark of aging

Many studies report a decrease in autophagy in many tissues (including the joint) with ageing. The decline of autophagy is considered as a hallmark of aging due to its implication in many aged related molecular processes including mitochondrial dysfunction, proteostasis loss, damage accumulations, or metabolic aging amongst others (100, 101). Many studies report the beneficial role of active autophagy in disease but also the adverse effect when it declines (102). The role of autophagy declines with age in arthritic diseases is actively investigated. It has been reported that enhancing autophagy by inhibiting mTOR with rapamycin limit chondrocytes death (103). Furthermore, the expression of beclin-1 and LC3 is reduced in mild OA and OA cartilage compared to normal cartilage (104). In addition, TFEB expression is decreased in the articular cartilage of OA patients, and a similar effect is observed in destabilized medial meniscus (DMM) mouse OA models. Moreover, the overexpression of TFEB in DMM mice reduce cartilage degradation (105). Nonetheless, the mechanism by which TFEB is regulated in the synovium in health and disease is still unknow.

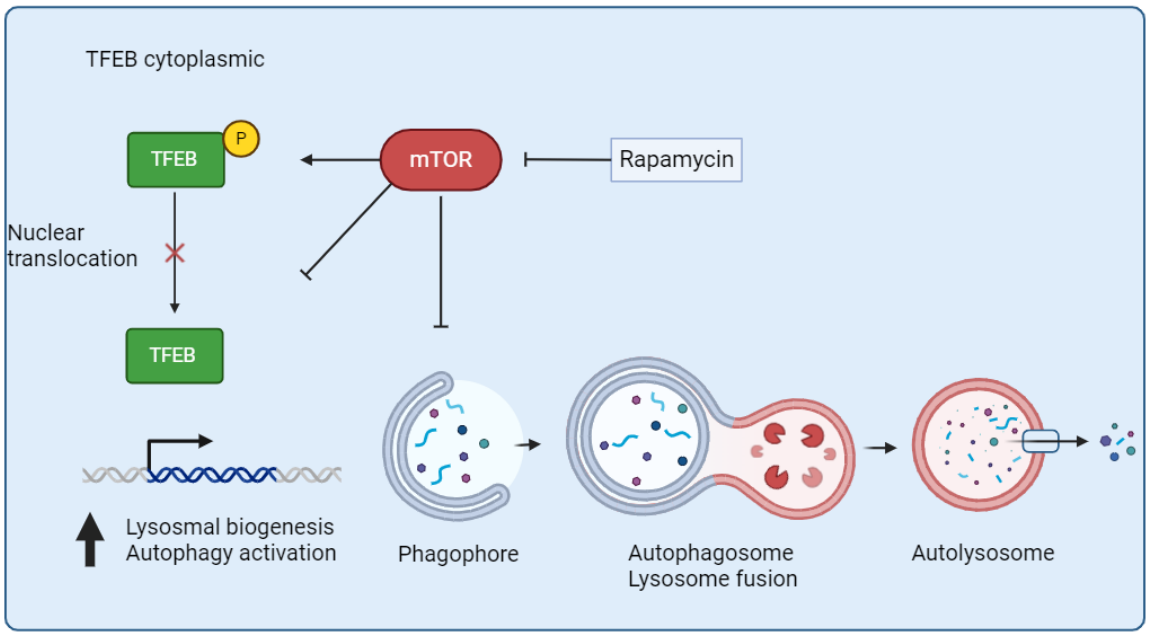


**Figure 1: Schematic overview of TFEB regulation in autophagy**

*TFEB is the master regulator of lysosomal and autophagosome biogenesis genes and participates to the global regulation of autophagy. mTOR inhibits TFEB activity by promoting its phosphorylation. Phosphorylated TFEB is sequestered at the lysosome membrane in the cytoplasm blocking its translocation into nucleus.*

## 1.6 Autophagy, cellular senescence and arthritis

### 1.6.1 Cellular senescence and arthritis

The incidence of many forms of arthritis increases with age. This is particularly relevant in OA, yet the relevance of cellular senescence on disease progression remains unclear. For decades, multiple studies have detected the accumulation of senescent chondrocytes in articular cartilage (91, 106, 107). While the incidence of the senescent chondrocytes on disease progression remains debated, some evidence suggests that the presence and localization of those cells correlate with OA severity (92). Similarly, the removal of p16+ cells using p16-3MR transgenic mouse models promotes regeneration of the articular cartilage (91). As chondrocytes rarely proliferate in cartilage, the origin of senescence in this population might not be related to replicative senescence but other senescence inducers (107). Among the possible origins of senescence in OA chondrocytes, many processes could be involved including

mechanical stress, inflammation, oxidative stress, metabolism or autophagy dysfunction (108). A recent study proposes that extracellular vesicles secreted by senescent chondrocytes activate senescence in non-senescent cells in a paracrine manner limiting articular cartilage production (109). In addition, senescent cells have also been detected within the synovium, but the cell types involved remains unclear (91). Similarly, the role of cellular senescence in the synovium and its influence on joint health are not known.

In RA, despite the fact that it is more common in the elderly population, little is known about the impact of age on the disease establishment. Due to the auto-immune origin of the disease, most studies are focusing on ways to prevent inflammation with a very limited focus on aging processes. However, some studies have tried to characterize senescence accumulation in synovial tissue in RA and associated SASP expression (110). The authors of that study found that senescent synovial fibroblast *in vitro* have an enhanced inflammatory phenotype potentially detrimental to disease outcomes. Oppositely, therapeutics approaches aiming to trigger senescence in specific context may reduce inflammation (83). Nonetheless, none of those studies investigated the specific populations impacted by cellular senescence.

### 1.6.2 Autophagy and arthritis

Since autophagy decrease have been addressed as one key hallmark of aging, many studies tried to understand the context of autophagy in normal aging and in age related diseases (111). In 2011, a study highlighted the protective role of autophagy in DMM models of OA (112). The authors found that the inhibition of mTOR with rapamycin ameliorated cartilage health, increased the number of chondrocytes, and reduced the production of ADAMTS-5, the main proteinase involved in aggrecan degradation (112). More recently, a study suggested that TFEB activation may have a protective role in OA via the activation of autophagy (105). Indeed, overexpression of TFEB in DMM mouse OA models limited cartilage degradation, prevented apoptosis and cellular senescence of the chondrocyte (105). However, the protective role of autophagy in the synovium was not addressed until recently. A recent

publication addressed one relationship between autophagy in OA synovial fibroblasts. The authors proposed a novel post translational regulation of autophagy mediated by the methyltransferase-like 3 (METTL3) which destabilized ATG-7 mRNA, decreasing autophagy, promoting senescence and SASP associated damage in the synovial fibroblasts (113). This study also proposed that the inhibition of autophagy promoted cellular senescence via the activation of the transcription factor GATA4 paving the way for novel anti-aging targets (113). Interestingly, another study demonstrated that METTL3 supressed TFEB epigenetically in OA chondrocytes (114). This process is mediated by the regulation of miR-273, an inhibitor of METTL3 (114). Altogether, those studies propose new post translational regulation of autophagy in the context of arthritis in both synovium and articular cartilage.

# 2 Aims of the thesis and hypothesis

The synovium, a thin mesenchymal membrane encapsulating and lubricating the joint space, is a major site of pathology in RA and combined with cartilage destruction, in the pathology of OA. Yet despite the remarkable progress in elucidating the environmental and genetic factors associated with RA and OA, embarrassingly little is known about the cell subsets in the synovium and cartilage that are responsible for pathogenicity and whether these subsets are subject to differential ageing and senescence.

**In this thesis I will test the hypothesis that differential senescence in synovial lining layer fibroblasts compared to sub-lining subsets underpins the clinical differences in age of onset and articular manifestations between RA and OA**

I will test this hypothesis by addressing two aims

Aim1: Molecular characterization of a panel of senescence markers in synovial tissues in patients across the spectrum of ages (31ys-78ys) with OA and RA using multiplex immunofluorescence (CellDive), RNAscope analysis and spectral flow cytometry aurora analysis

Aim 2: Establish the expression of the master regulator of autophagy TFEB in synovial subsets in OA and RA and correlate to the senescence panel to understand the relationship between autophagy and cellular senescence in the context of inflamed arthritis.

# 3 Methods

## 3.1 Human tissue act:

All relevant human tissues were manipulated under valid HTA certification. All the ethics were applied as well as the complete anonymization. Our study was undertaking under valid MTAs between Oxford and the university of Birmingham (Human Tissue MTA Sept 17 Provider Ref: 2115853 Recipient Ref: R80892/CN002; Human Tissue MTA Sept 17 Provider Ref: 1296639). Ethical approval for the Oxford Musculoskeletal Biobank (09/H0606/11 and 19/SC/0134). OA patient JRP collection were asked a written consent for tissue collection.

| | OA JRP (n=13) | RA JRP (n=8) | RA biopsy (n=4) | Normal (n=1) |
|---|---|---|---|---|
| **Age; median (IQR)** | 70 (62 - 76.75) | 67 (41,75 - 73.5) | 65.6 (55.13 - 73.05) | 43 |
| Female; number (%) | 10 (76.9) | 5 (62.5) | 3 (75) | 0 (0) |
| NSAID; number (%) | / | / | 1 (25) | / |
| CRP (mg/ml); median (IQR) | / | 7 (2.75 -135) | 23 (11.25 - 55.75) | / |
| ESR (mm/h); median (IQR) | / | 30.5 (5 - 66) | 45 (40.5 - 53.25) | / |
| Rf positive; number (%) | / | 4 (100) | 2 (50) | / |
| CCP positive; number (%) | / | 6 (75) | 2 (50) | / |
| DAS28 ; median (IQR) | / | / | 6.66 (5.88 - 7.87) | / |
| BMI ; number; median (IQR) | 5; 32.6 (27.73 - 36.73) | / | / | / |

**Table 1: Patient information**

*IQR: Interquartile range; JRP: joint replacement; NSAID: non-steroidal anti-inflammatory drugs, ESR: erythrocyte sedimentation rate, CRP: C-Reactive Protein, CCP: cyclic citrullinated peptide, DAS28: disease activity score 28, BMI: body mass index.*

## 3.2 Histology:

### 3.2.1 Tissue preparation

Synovial tissues from joint replacement surgery were separated between histology and flow-cytometry after collection. Samples used in Flow cytometry were cut into pieces of approximatively 4mm$^3$ and place in cryovials in media with 45% FBS, 45% RPMI, 10% DMSO and frozen overnight at minus 80 before being stored in liquid nitrogen.

Samples used in the histology analysis were washed in PBS and fixed for 24h in neutral buffered Formalin 10% (4% formaldehyde) at 4°C. After fixation, the samples were washed in PBS overnight under low agitation and transfer in 70% ethanol. Samples were place in cassettes and place in the tissue processor (Leica ASP300) to be dehydrated and paraffinized. Then, synovial tissues were embedded in paraffin blocks and cuts using a microtome. All the slides in this study were cut with a thickness of 5µm and placed on Fisherbrand™ Superfrost™ Plus microscopes slides and immediately baked at 60°C overnight.

### 3.2.2 Cell DIVE

After baking overnight at 60°C, OA and RA PFFE slides were deparaffinized using the Epredia Gemini™ Stainer which automatically transfer slides into Xylene and ethanol solution. Slides were permeabilized in PBS triton 0,3% for 10 min at RT. Slides were transfer in antigen unmasking solution citric acid based (Vector lab; H-3300-250) when temperature reach 70°C in the pressure cooker then baked for 20 min. During this time the temperature keep rising until 110°C for 4min before progressively decreasing. After 20 min slides were transfer in the pH9 TRIS based antigen retrieval solution (already heated in the cooker) and incubate 20 min, and 10 min outside to let them cool. After one wash in PBS, slides were blocked PBS with 0,02% triton, 10% Human serum, 1% BSA for 1H at RT. Slides were stained in DAPI solution and mounted using mounting media (4% propyl gallate, 50% glycerol; Sigma-Aldrich). Slides were imaged with an initial scan plan using 10X magnification to select the regions of interest (ROI) and

then image at 20X in all channels (FITC, Cy3, Cy5) to determine the background autofluorescence which will be removed for the following staining. Slides were decoverslipped in PBS. Before being incubate with Primary TFEB (4240S) at 1/100 dilution, overnight at 4°C in PBS 0,02% triton, 1% BSA. Secondary αRabbit AF647 at 1/250 was incubated 45min at RT and slides were coverslipped in mounting media. Slides were imaged at 20X. Once the images were acquired, the slides were decoverslipped and bleach using 0.5M NaHCO3 (pH 11.2) and 3% H2O2 solution twice for 15 with a 1-min wash in between, before being wash 3 times for 5 min and incubated 2min in DAPI. After a re-coverslip step slides were imaged using the same parameter for background imaging to subtract autofluorescence for the next round. Those steps are repeated for each staining round in the following order: staining round, bleaching round, staining round etc. After the second round, only directly conjugated antibodies were used to avoid cross species nonspecific interactions. The list of antibodies and round used are listed in table 3.

### 3.2.3 RNAscope

RNAscope® Fluorescent Multiplex Reagent Kit (Cat. No. 320850) was used to perform the RNAscope analysis. This technique uses RNA probes, and a molecular amplification method coupled with enzymatic fluorescent revelation.

OA and RA synovial tissue slides were baked 1h at 60°C prior being processed. Slides were deparaffinized in xylene for 5min with occasional shaking. This step is repeated with fresh xylene. Then slides were placed in 100% ethanol for 2 min repeated with fresh ethanol. Then, slides were dried 5min at 60°C. Once dried, the tissue was covered with hydrogen peroxide and incubate 10 min at RT. Slides were washed in distilled water 2 times before being placed 10 seconds in hot distilled water (80°C) and immediately transferred in 1X retrieval regent warmed at 99°C in a steam cooker and incubated 15 min. The temperature was monitored to be maintained at 99°C. Then, slides were quickly rinsed in distilled water and place in 100% ethanol for 3 min before being placed in the oven at 60°C for drying. Once dried, slides were labelled, placed in a horizontal rack and the hydrophobic barrier was applied around the tissue. Next, tissues sections were incubated in Protease plus reagent for 30 min at 40°C and

washed 2 times in distilled water. Probes C2 (*CDKN2A, CDKN1A, TFEB*) and probes C3 (*PRG4*) were diluted 50 times in probe C1 (*THY1*) already diluted in probes diluent solution, and all the amplification reagents were place at RT. Probes were incubated on the samples for 2h at 40°C. After incubation, slides were washed in 1X wash buffer for 2 min and transferred in fresh washed buffer for an additional 2 min. All the next washes were performed this way.

Slides were incubated in Hybridized AMP1 solution for 30 min at 40°C and washed. This step was repeated with AMP2 solution for 30 min at 40°C, washed, and incubated in AMP3 solution for 15 min at 40°C and washed. At this stage the TSA Vivid Fluorophore 520 (FITC), TSA Vivid Fluorophore 570 (Cy3), and TSA Vivid Fluorophore 650 (Cy5) were diluted at 1 in 5000 in TSA buffer. Next, slides were incubated in solution containing the HRP specific for the probe C1 for 15 min at 40°C, then slides were washed, and the TSA Vivid Fluorophore 520 (FITC) was added for 30 min at 40°C to develop the C1 probes in FITC. After the incubation, the slides were washed and blocked with the HRP blocker for 15 min at 40°C. Those steps were consecutively repeated to develop the probes C2 using TSA Vivid Fluorophore 650 (Cy5) and the probes C3 using Vivid Fluorophore 570 (Cy3). After the last washed, slides were incubated in the DAPI solution provide in the kit for 30 sec and coverslip using ProLong Gold Antifade Mountant. Slides were dried overnight 30 min and stored overnight at 4°C. Images were taken no longer than 1 day after the staining on confocal microscope Zeiss LSM 780.

### 3.2.4 Immunofluorescence staining

PFFE RA and OA sections were deparaffinized in Histoclear solution before being progressively rehydrated. Antigen retrieval was performed in phosphate buffer at ph9. Permeabilization was performed in PBS/Triton 0,4% for10 min at RT. Blocking was made in 10% human serum, 1% BSA in PBS incubated for 1H at RT. Rabbit anti-human P16 antibody (AB_2809424), yH2AX (ab81299), rabbit anti-human p53 (ab3238) were used at 1/100 dilution and incubated overnight at 4°C. Rat anti-human PDPN (clone NZ-1.3) and sheep anti-human CD90 antibodies were used at 1/100 and 1/200 dilution respectively before been incubated in PBS 10% Horse serum, 1% BSA, 0.2% Triton overnight at 4°C.

Washes were made in PBS. Secondary donkey anti-rabbit AF488, goat anti-rat AF647, and donkey anti-sheep AF546 were used at 1/200 dilution for 45 min at RT. Nuclear staining was performed with Hoechst for 10 min at RT. Slides were mounted in ProLong Gold mounting media and kept at 4°C.

### 3.2.5 Immunohistochemistry and immunocytochemistry

Immunohistochemistry (IHC): P53 human antibodies (ab3238) were optimized for the human synovium tissue. p53 antibody was used at 1/100 concentration. Optimal staining was obtained overnight at 4°C incubation with a pH 6 antigen retrieval buffer. Secondary goat anti-rabbit IgG coupled with streptavidin was used. The revelation was made with HRP coupled with biotin and brown enzymatic dye.

Immunocytochemistry (ICC): Autoclaves round glass coverslips were coated with rat tails collagen I (50 µg/mL) and places in 6 wells plate. RA fibroblasts were seeded at 5 x $10^4$ per well and incubate for 24h at 37°C with 5% $CO_2$. RA fibroblasts were fixed 10 min in 4% PFA before Permeabilization with 0,1% TRITON X100 for 10 min at RT. Primary antibodies p53 (ab3238), p16 (AB_2809424), p21 (sigma: 05-655), and yH2AX (ab81299) were incubated at 1/100 for 1H at RT. Secondary donkey anti-rabbit and anti-mouse AF488 or AF647 were used at 1/500 for 1H at RT. Coverslips with cells were flipped on a microscope slides mounted in ProLong Gold mounting media and kept at 4°C.

## 3.3 Flow cytometry:

### 3.3.1 Synovial Digestion

Cryovials containing chopped synovium were thawed at RT and rinsed with RPMI without FBS through a 70µm nylon cell strainer. Rinsed synovia were placed in bijoux with 2 ml of digestion media containing Liberase™ TL (Roche: 05401020001) at 0,1 mg/ml and DNase I (Roche:10104159001) at 100µg/ml in RPMI no FBS prewarmed at 37°C. Digestion tubes were placed at 37°C on high agitation for 30min. After, 30min the digestion was evaluated, and placed back at 37°C under agitation for another 30 min until most of the pieces were dissolved. Once digested, the tissue was filtered using 70µm nylon cell strainer and washed with 40ml of RMPI with 10% FBS. Cells were centrifuged at 450g for 5min at 4°C

and resuspend in 40 ml of cold PBS. This step was repeated 2 more time in 20 ml of PBS to removed most of debris and proteins. Cells were place on ice before being processed with the staining AURORA protocol.

### 3.3.2 Aurora

Aurora is a spectral flow cytometer allowing the simultaneous staining of 40 markers that uses unmixing to separate fluorescence to separate the spectrum of each individual fluorochrome. This required beads or single antibody control on cells with an equal or brighter signal than the tested sample. As the sample size were limited and rare I used peripheral blood mononuclear cells (PBMCs) as single antibody control for immune markers.

To avoid batch effect 10 OA and 10 RA synovium were digested and stained simultaneously. Synovial cells from the digestion were washed in 20 ml of PBS and kept on ice. In parallel, 2 million of PBMCs were thawed and wash in PBS. Hunam dermal fibroblasts (HDF) treated with zeocin and HDF non treated were harvested using trypsin and washed in PBS. Synovial cells, PBMCs and HDF were placed in a 1ml deep well plate according to each conditions. PBMCs were used as single antibody controls for the immune markers CD45, CD11c, CD19, CD4, CD8, CD68, CX3CR1, HLA-DR, and HLA-ABC. HDF were used as internal control of the senescence antibodies and were divided into the following condition: HDF zeocin stained, HDF zeocin unstained, HDF control stained, HDF control unstained. Finally, 30% of each synovial samples were mixed to create the control surface panels for CD90, PDPN, CD31, MERTK, CD34 and intracellular panels p21, p16, p53, yH2AX and TFEB. Unstained and L LIVE/DEAD™ (LD) Blue (L23105) control was made with synovial cells too. The rest of synovial cells were placed in the plate. LD was diluted at 1/100 in PBS and incubate for 15 min at 4°C in the dark on the appropriate conditions. Cells were washed with PBS and plate centrifugated at 400g for 5 min at 4°C. Surface antibodies CD45, CD11c, CD19, CD4, CD8, CD68, CX3CR1, HLA-DR, HLA-ABC, CD90, PDPN, CD31, MERTK, and CD34 were mixed in FACS buffer (PBS 1% BSA, 2mM EDTA). The concentrations and labelling are listed in table 4. The surface staining mix was incubated for 20 min at RT in the dark. At the same time, single antibody

controls were incubated with their corresponding surface antibody 20min at RT in the dark. Compensation beads (UltraComp eBeads™: 01-2222-42) were also prepared at this step and incubated for 20 min at RT. The isotype of p16 and p21 antibodies is rabbit IgG and do not attach on UltraComp eBeads™. Therefore, compensation beads from Biolegends (424602) were used for those antibodies. After surface staining incubation, cells and beads were washed in FACS buffer and fixed in 100 µl of fix buffer for 30 min at RT using the eBioscience™ Foxp3 / Transcription Factor Fixation/Permeabilization (00-5521-00) kit. Cells and beads were washed with 1ml of perm buffer. Intracellular staining mix was prepared in permeabilization buffer and applied to the samples. At the same time single antibody controls were incubated with appropriate intracellular antibody. Intracellular antibodies were incubated overnight at 4°C. The next day, cells and beads were washed with permeabilization buffer and wash again in FACS buffer before being resuspended in 400 µL of FACS buffer. Each digested sample was filtered using 70 µm nylon cell strainers and resuspend in 400 µl of FACS buffer before acquisition the Aurora flow cytometer.

## 3.4 Cell culture

### 3.4.1 Cellular models

Primary fibroblasts from OA and RA were isolated after synovial tissue digestion and resuspend in an equal mix of RPMI 1640 Medium without glutamine (21870076) and Medium 199, GlutaMAX™ (41150087), 10% FBS, 1% Penicillin-Streptomycin (15140122). Cells in suspension were washed the next day and incubate at 37°C in 5% $CO_2$. Adherent cells were passed for the first time when they reach 80% of confluence. Human dermal fibroblasts (HDF) were cultured in the same media described above.

Human Umbilical Cord Endothelial Cells (HUVECs) were cultured in EGM™-2 Endothelial Cell Growth Medium-2 BulletKit™ (Lonza: Catalog #: CC-3162). All cells were fed every 2 days and passed when they reached at least 90% of confluence.

### *3.4.2* DNA damage induced senescence *in vitro*

DNA damage agents Bleomycin and Zeocin were used to induced senescence in fibroblasts in vitro. Fibroblasts (primary synovial fibroblasts and HDF) were incubated with 5µg/ml of either Bleomycin or Zeocin for 24h. After 24h cells were washed with fresh media. Any Data acquisition was performed at least 7 days after the drug incubation.

### 3.4.3 Organoids

Synovial organoids were generated according to the STAR methods protocol published alongside study performed by Wei et. al. (19). In brief, primary fibroblasts from RA and OA patients were mixed equally with early passaged HUVECs. After centrifugation, all the media was removed, and the cell pellet was resuspended carefully in cold Matrigel. Per each organoids 35µl of Matrigel was placed on a warmed 6 well plate and incubate 1h at 37°C until complete polymerization. Each organoids contained on average 100 000 fibroblasts and 100 000 HUVECs. Once polymerized, Organoids were carefully resuspended in HUVECs media not supplemented with hydrocortisone. After 21 days, the organoids are ready to be analysed.

### 3.4.4 SA-βGal assay

RA fibroblasts from early and late passages were seeded at $1x10^5$ in 6 well plate and incubate for 24h. Cells were fixed and stained according to the Senescence β-Galactosidase Staining Kit (#9860) from cell signalling. Pictures were taken using bright a filter microscope.

### 3.4.5 Migration assay

For the scratch test assay $3x10^4$ RA fibroblasts treated with Bleomycin and non-treated were seeded in 24 well plate and incubate for 24h in presence or absence of 10 mM of sodium lactate in triplicate. Cells were starved 2 hours the experiment in fibroblasts media with 1% FBS. The scratch was made in the centre of each well using a sterile pipette tips. The surface area of the scratch was measured after the scratch (T0), after 24h (T2), after 48h (T3) and after 72h (T4) using ImageJ software. The difference of the ratio was calculated from the value starting at TO until T4.

### 3.4.6 Seahorse analysis

RA fibroblasts from early passage and late passage were harvested using Trypsin and seeded at $3x10^4$ fibroblasts per well in a 96 Seahorse XF cell culture plates for 24h. After, 24h fibroblasts were stimulated with 10ug/ml with recombinant TNF-α (210-TA) for 24h. The cells plate was incubated 1h at 37°C without $CO_2$ for equilibration prior the measurement of Oxygen consumption rate (OCR) and Extracellular acidification rate (ECAR). OCR media was prepared with XF RPMI, 1mM Sodium Pyruvate, 2mM L-glutamine and 10mM glucose. ECAR media was prepared with XF RPMI, 2mM L-glutamine. Oligomycin was used at 2µM, FCCP at 5µM, Rotenone at 3µM, Antimycin A at 3µM in OCR media. 2-DG was prepared at 50Mm in ECAR media. To start glycolysis detection 10mM of glucose was added in the ECAR media. All compounds were purchased from Sigma Aldrich. Three technical replicates were used in each condition.

## 3.5 Analysis

### 3.5.1 CellDIVE analysis

All multiplex immunofluorescence staining were analysed using the free image software analysis QuPath (Copyright (C) 2007 Free Software Foundation, Inc.). Regions of interested (ROIs) or the total synovium were delimited using the drawing tools. Cells were segmented based on the final DAPI staining using the Cell detection tool and the area of each cells were set on a 5µm radius. The detection threshold for positive cells were determined based on the Mean + 1 SD of the total fluorescence the total area of the cells for the marker of interest. For instance, only the cells that have a mean fluorescence for PDPN (nucleus + cytoplasm) equal to the mean+ 1SD will be considered positive. This allows a standardized method of detection between tissue with different intensity for the same marker. 3 exceptions were made with p16, p21 and yH2AX where the threshold was determined based on the mean + 1 SD of the fluorescence in the nucleus instead of the total cell (nucleus + cytoplasm). Classified cells were combined in different composite classifier to determine the percentage of each sub

populations. For instance, the percentage of p16 in PDPN+ was calculated by the number of p16+ PDPN+ divided by the number of PDPN+ (excluding all the other combination possible such as MERTK+ PDPN+, MERTK+ PDPN+ P16+, etc). Nuclear and cytoplasmic mean fluorescence intensity of TFEB to determine its activation state was measure in each cells classified TFEB+ using the object detection measurement tools.

### 3.5.2 RNAscope analysis

RNAscope stained slides were analysed using QuPath image software. Cells were detected based on the DAPI in each ROIs and segmented with a radius of 5 µM. Dots in each cells were detected using the Sub-cellular detection tools based on the fluorescence of the interest marker. The fluorescence detection threshold was adjusted manually until most of the dots were detected. The minimum size of a detection for a dot was set at 0,1µm and the maximum to 0,6 µm for each slides. Every dot superior to 0,6 µm was classified as a clusters. Depending on the number of dot cells were classified in different bins as follows: Bin 0 (0 dots/Cells), Bin 1 (1-3 Dots/Cells), Bin 2 (4-9 Dots/Cells), Bin 3 (10-15 Dots/Cells), and Bin 4 (>15 Dots/Cells). Then, the H-score was calculated as follows: (0 x % cells Bin0) + (1 x %cells Bin1) + (2 x %cells Bin 2) + (3 x %cells Bin 3) + (4 x %cells Bin 4). The average number of dots per cells was calculated from the total number of dots divided by the number of cells with dots.

### 3.5.3 Statistical analysis

All the results were calculated using GraphPad Prism 5.0 software (GraphPad Software, San Diego, CA). Standard deviation (SD) is presented after the symbol ±. Paired or Unpaired T test were used to assess statistical significance between two groups, p values ≤ 0.05 were considered as statistically significant (*$p < 0.05$; **$p < 0.01$; ***$p < 0.001$; ****$p < 0,0001$).

# 4 Results Chapter One: Senescence in the synovium

## 4.1 Hallmarks of senescence in human cells populations in arthritic diseases

### 4.1.1 Aims

Defining the aging phenotype of the key synovial populations in human. Investigated the localisation of the senescence hallmarks in those populations to underline one aspect of the aging in the joint.

### 4.1.2 Identification of the fibroblast population in OA and RA synovium using multiplex histology

In a first time we wanted to localise those cells population, including the fibroblasts subsets of the LL and SL, the tissue resident macrophages (TRMs), endothelial cells (ECs) and infiltrated lymphocytes. One technique was to use multiplex histology to address a phenotype allowing the separation of Immune cells including T cells, B cells, myeloid and the stromal population including LL fibroblasts, SL fibroblasts and endothelial cells.

The main cell populations in OA and RA synovium were identified by using Cell DIVE imaging system which allows consecutive immunofluorescence staining on the same tissue slide. To have a representative samples size, synovial tissue from of 10 patients from RA and 9 from OA were analysed in a total of 7 staining rounds with the following panel: CD90, PDPN, CD31, CD34, CD68, CD206, CD3, CD20/CD19, CD45, MERTK, VIMENTIN, p16, p21, p53, yH2AX and TFEB to cover most of the main cell types.

The lining layer fibroblasts in pathological context were characterized many times by different studies over the last years (16, 17, 115). However, due to the plasticity of the fibroblasts those markers can vary in expression according to the context of their micro-environmental niche. This concept will be further explored in the discussion. Nevertheless, it is widely accepted that LL fibroblasts expressed PDPN, CD55, CliC5 and PRG4. According to my staining I found that PDPN was almost exclusively localized in the LL region of the synovium. We decided to use PDPN as the primary marker of the LL

fibroblasts in both OA and RA. However, the lining layer includes many tissues resident macrophages (TRMs) that also express PDPN. To be able to differentiate the fibroblasts from the TRM we stained the macrophages with MERTK and CD68 both markers use in the classification of macrophages in human synovium (25). Therefore, to select the LL fibroblasts we classified the PDPN positive, MERTK negative and CD68 negative. As expected, PDPN and CD68 staining overlap in the LL layers with MERTK positive macrophages, MERTK+ abundance vary according to the patient **(Fig 4.1.2 A)**. Overall, the PDPN+ CD68- MERTK- cells represent 43,44% (±10,68) of the LL region while the CD68+ MERTK+ TRMs make 28,6% (±9,38) of the total cells LL cells in RA with a ratio of 0,6 TRM per 1 fibroblast **(Fig 4.1.2 B)**. Interestingly, in OA the ratio of macrophage to fibroblasts is close to 1 as 26,34% (±7,9) of the LL is composed by PDPN+CD68-MERTK- and 29,9% (±5,11) by the TRMs **(Fig 4.1.2 B)**. Then, we asked what the remaining cells were by looking at all the other markers. Besides CD34 that represent on average 6,76% (±3,32) of the total cells in the LL, the other markers such as CD3, CD90, CD31 were not expressed in the LL. Therefore, 36,99% of the cells in the OA LL were not annotated in my panel (Data not shown).

Most of the sub-lining fibroblasts in RA were classified by the expression of CD90 (16, 17, 19). However, the phenotypical and mechanistic heterogeneity within the CD90 positive fibroblasts is still heavily studied. To simplify the study of the SL fibroblasts, CD90 was use as the main SL marker. As CD90+ fibroblasts expend from the perivascular niche, the highest expression is found around the blood vessel in both OA and RA **(Fig 4.1.2 C)**. To avoid the overlaps between endothelial cells and CD90 + fibroblasts during the analysis the SL fibroblasts were characterized by the negative expression of CD31. In a similar way, the infiltration of immune cells was often observed within perivascular region leading to close contact between the CD90+ cells and immune cells. To prevent any false positive and keep the fibroblasts population as clean as possible the double positive CD45 CD90+ were exclude from the classification of the SL fibroblasts. Therefore, we observed that in average 11,85% (±3,14) of the SL is composed by CD90+ fibroblasts in RA and 9,16% (±2,33) in OA **(Fig 4.1.2 D)**.

Finaly, to verify that the markers CD90 and PDPN are exclusive to the SL and LL respectively, we compared the proportion of CD90+ cells in the LL region and the PDPN+ in the SL. As expected, the CD90+ are almost entirely localized in the sub-lining, while the PDPN+ fibroblasts proportion is significantly higher in the lining **(Fig 4.1.2 E)**.

In addition, the stromal marker CD34 was used to better understand the fibroblast populations phenotype. Originally, CD34 was described as a SL marker; it is also expressed on all synovial fibroblasts once they are put in culture (116). Interestingly, CD34 is also expressed in the PDPN+ LL fibroblasts. Moreover, the proportion of CD34+ LL fibroblasts is higher than the CD90+ CD34+ SL population of the sub-lining in most of the patients in RA and significantly higher in OA **(Fig 4.1.2 F)**. However, the expression is very heterogenous among the patients with out of layer profile. For instance, one OA patient does not show any CD34 expression in the PDPN+ population while 68% of CD34+ are endothelial. In contrast, another OA patient had a strong CD34 staining in the LL while the endothelial cells were mostly negative **(Fig 4.1.2 G)**. The possibility that those differences are coming from an experimental artefact cannot be excluded. However, the heterogeneity of CD34 expression between patients might indicates different dynamics of cell adhesion/migration within the synovium. Indeed, CD34 is a highly glycosylated transmembrane protein expressed in hematopoietic stem cells but also on vascular and stromal cells playing a role in angiogenesis and in the recruitment of immune cells (117, 118). Depending on the context, CD34 facilitates the adhesion of trafficking lymphocytes to the vascular cells at the inflamed site. Therefore, the high expression of CD34 in the endothelial compartment might be an indication of infiltration. Indeed, in most patients, CD34 is colocalizing with CD31+ cells with 39,43% of CD34 positive cells in the CD31 population in RA and 36,77% in OA **(Fig 4.1.2 F)**.

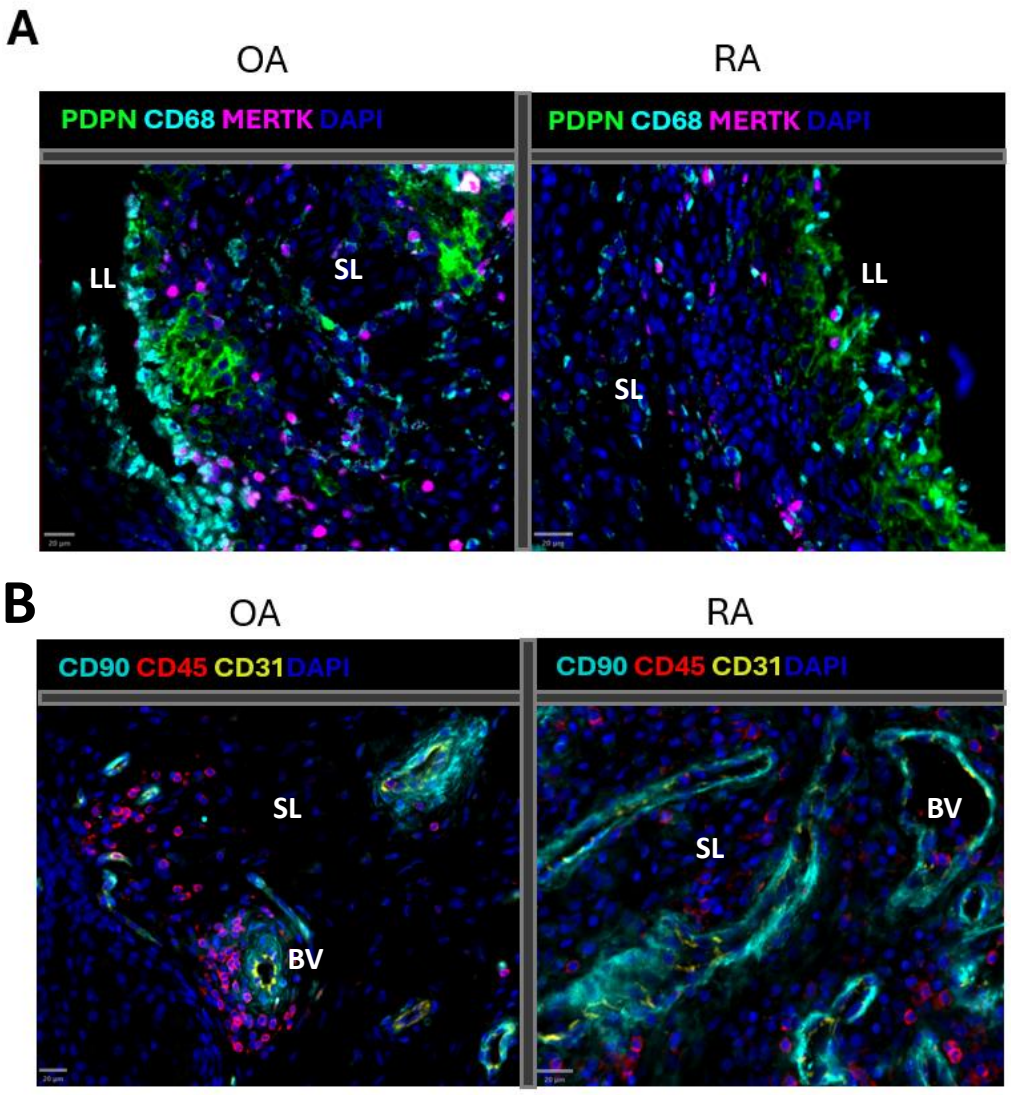


**Figure 4.1.2: Identification of the synovial fibroblasts in multiplex histology**

**A:** Multiplex IF image of the LL in OA synovium (left) and RA synovium (right) showing macrophages and fibroblasts. PDPN (green) MERTK (magenta), CD68 (cyan), DAPI (blue). **B:** Multiplex IF image of the SL in OA synovium (left) and RA synovium (right) showing CD90+ perivascular fibroblasts (cyan), CD31+ ECs (yellow) and CD45+ immune cells (red), DAPI (blue). LL=Lining layer; SL=Sub-lining; BV=Blood vessels.

C

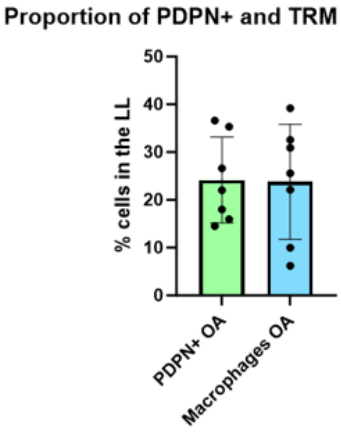
Proportion of PDPN+ and TRM in the LL in OA
% cells in the LL
PDPN+ OA
Macrophages OA

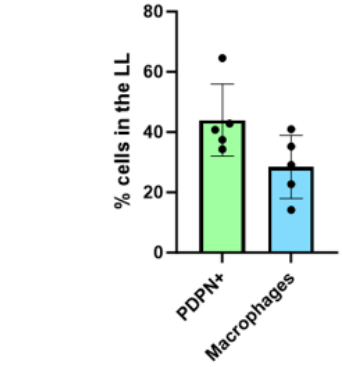
Proportion of PDPN+ and TRM in the LL in RA
% cells in the LL
PDPN+
Macrophages

D

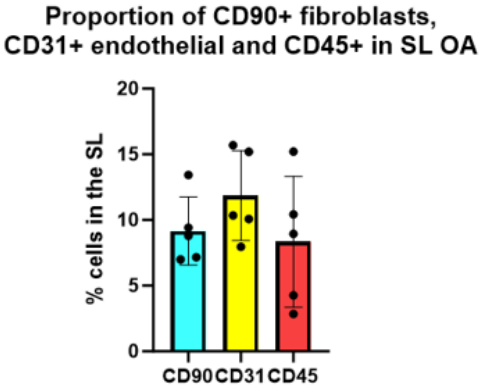
Proportion of CD90+ fibroblasts, CD31+ endothelial and CD45+ in SL OA
% cells in the SL
CD90 CD31 CD45

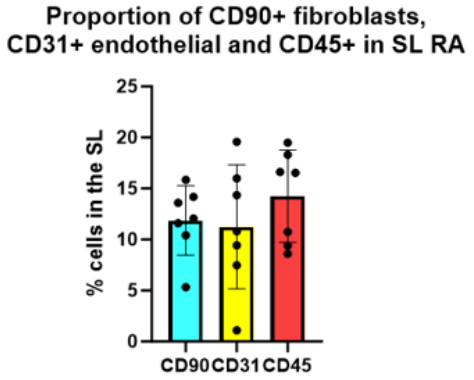
Proportion of CD90+ fibroblasts, CD31+ endothelial and CD45+ in SL RA
% cells in the SL
CD90 CD31 CD45

F

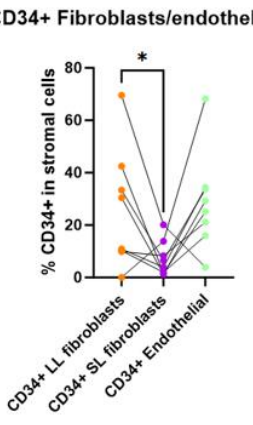
CD34+ Fibroblasts/endothelial in OA
% CD34+ in stromal cells
CD34+ LL fibroblasts
CD34+ SL fibroblasts
CD34+ Endothelial

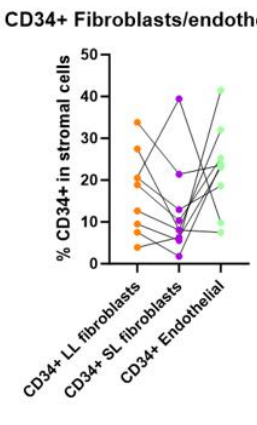
CD34+ Fibroblasts/endothelial in RA
% CD34+ in stromal cells
CD34+ LL fibroblasts
CD34+ SL fibroblasts
CD34+ Endothelial

E

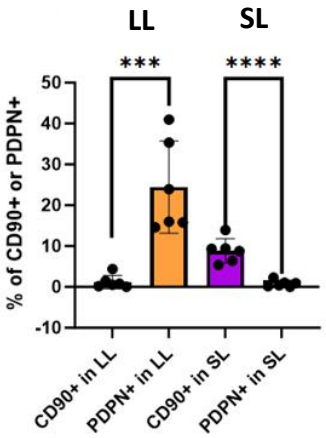
LL
SL
% of CD90+ or PDPN+
CD90+ in LL
PDPN+ in LL
CD90+ in SL
PDPN+ in SL

G

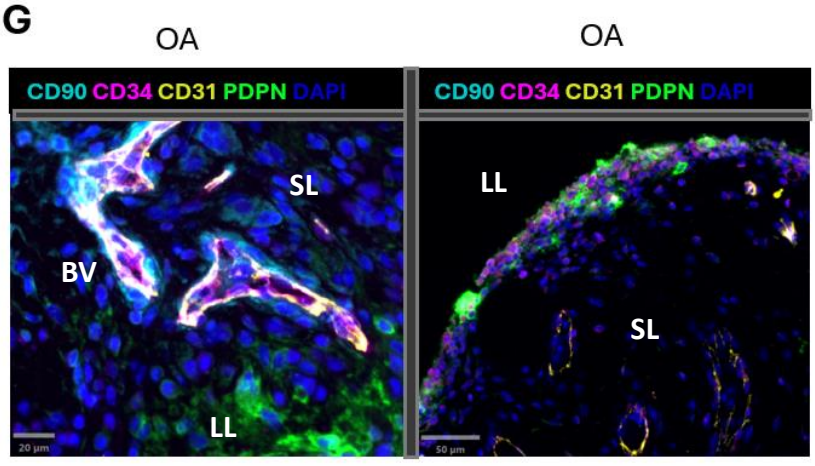
OA
OA
CD90 CD34 CD31 PDPN DAPI
CD90 CD34 CD31 PDPN DAPI
SL
BV
LL
LL
SL

**Figure 4.1.2: Identification of the synovial fibroblasts in multiplex histology**

**C:** Quantification of LL fibroblasts PDPN+ MERTK- CD68- (green bar) and macrophages MERTK+, CD68+ and CD68+MERTK+ (blue bar) in the LL of OA (Top graph) and RA (bottom graph). The proportion is reported on the total number of cells in the LL. OA (n=7); RA (n=5). **D:** Quantification of SL fibroblasts CD90+ CD31- CD45- (cyan bar), CD31+ ECs (yellow bar), and CD45+ (red bar) in the SL of OA (Top graph) and RA (bottom graph). The proportion is reported on the total number of cells in the SL. OA (n=5); RA (n=7). **E:** Percentage of CD90+ and PDPN+ in the LL and SL respectively in OA synovium (n=5). F: Proportion of CD34+ in LL fibroblasts, SL fibroblasts and ECs in OA (left) and RA (right). **G:** Multiplex IF image showing 2 OA patients with different CD34 localization. Patient on the left has high CD34 in ECs but not in LL, patient on the right has low in ECs and high in the LL. CD90 (cyan), CD31 (yellow), CD34 (magenta), PDPN (green). LL=Lining layer; SL=Sub-lining; BV=Blood vessels. (*p < 0.05; ***p < 0.001; ****p < 0,0001).

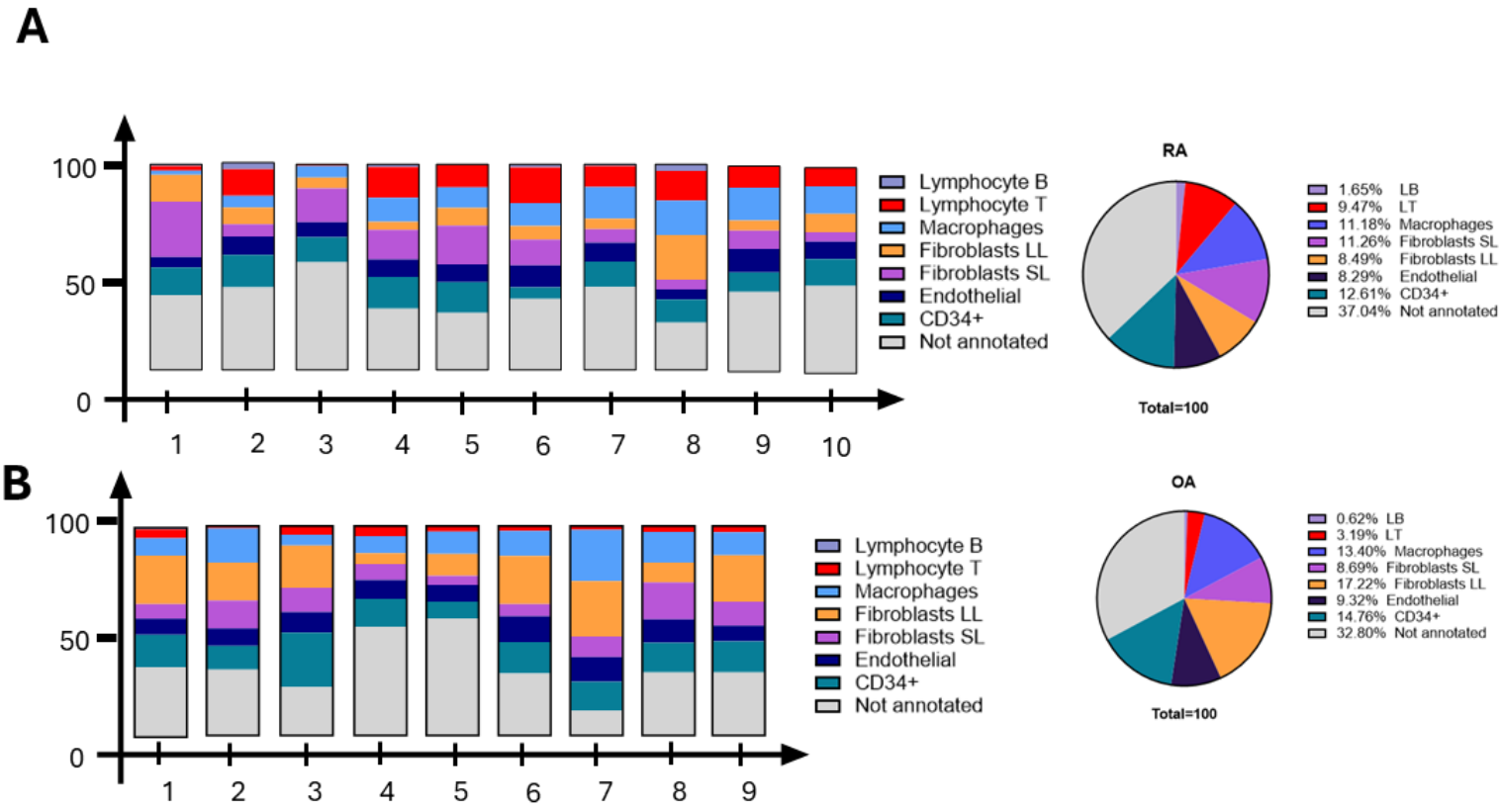


**Figure 4.1.3: Representation of the percentage of synovial populations identified by multiplex IF in OA and RA**

**A:** Graphical representation of the different synovial population in each RA patient (n=10) classified using the following panel CD90, PDPN, CD31, CD34, CD68, CD206, CD3, CD20/CD19, CD45, MERTK, VIMENTIN. The average percentage of each population between patients is displayed in the graphic pie chart (left). LB = B lymphocyte, LT = T lymphocytes SL= Sub-lining, LL = Lining layer. **B:** Same graphical representation in OA patients and the average population on the left (n=9).

### 4.1.3 Proportion of the synovial populations in OA and RA by multiplex IF

The percentage of LL fibroblasts (17,3 ± 7,001) in OA varies more between patient than the percentage of SL fibroblasts (8,73 ± 2,26). On the other hand, the SL fibroblasts (11,36 ± 6,97) in RA exhibits a higher variation than the LL fibroblasts (8,65 ± 4,85) **(Fig 4.1.3 A, B)**. As expected, the proportion of LL fibroblasts is greater in OA patients compared to RA patients. Furthermore, the proportion of SL fibroblasts is higher in RA compared to OA. Thus, the observation corresponds with the consensus that RA fibroblasts expand more in the SL while OA fibroblasts expand in the LL. This might explain the variability observed between the patients as in each diseases the population with the highest variation is the population associated with the pathology.

The proportion of endothelial cells (CD31+) is constant between OA and RA patients and represents 9,36% (± 2,06) and 8,36% (± 1,88) of the total synovium cells, respectively. Interestingly, the percentage on EC is similar between the 2 diseases although RA patients present more infiltrated T cells (CD3+) with 9,55% (± 5,47) of the total cell on average compared to 3,19% (± 1,31) in OA. The percentage of infiltration is heterogenous between the RA patients **(Fig 4.1.3 A, B)**.

The macrophages heterogeneity and the role of the sub population in both OA and RA remains unclear. According to single cells, histology, and flow cytometry staining, Synovial TRMs are MERTK+, CD68+, CD206+ in opposition to infiltrated macrophages MERTK-, CD206-, CD48+, and $HLA^{high}$. Based on the expression of CD206, MERTK and CD68, I found that TRMs represent on average 13,4% (±6,08) of the synovium in OA and 11,18% (±4,04) in RA **(Fig 4.1.3 A, B)**.

Infiltration of the synovium by immune cells including B lymphocytes and T lymphocytes is a characteristic feature of the inflammatory status of the synovium. The absence or presence and numbers of infiltrated cells is an essential criterion in determining the histological classification of RA patients. It is interesting to notice that OA synovium is also susceptible to mild inflammation despite the different origin of the disease. As expected, the proportion of T cells (CD3+) in RA synovium in on average 3 times higher than the proportion observed in the OA cohort and represent 9,47% of the total

synovium **(Fig 4.1.3 A, B)**. Moreover, this proportion is variable according to the patient as infiltration is variable in RA. For instance, in a high infiltrated synovium with more than one aggregates the proportion of T cells represents up to 17% of the total number of cells **(Fig 4.1.3 A, B)**.

Similarly, B cells were mostly present in RA synovium compared to OA. Indeed, in OA synovium B cells (CD20+) were detected in 2 patients out of 9 tested. While in RA, B cells were detected in 8 patients out of 11. The percentage of CD20+ cells in the synovium is low in both diseases by representing 1,6% and 0,6% of the total number of cells in both RA and OA respectively **(Fig 4.1.3 A, B)**. It is also important to notice than the vast majority of CD20+ or CD19+ cells are localized within the aggregates while some individual CD3+ T cells can be found throughout tissue.

Finally, a significant proportion of the cells remains unclassified. Among this population a small proportion expressed the stromal marker Vimentin while other cells are CD45+. However, once all the cells were classified between 20% and 30% were negative for all the markers. Thus, this suggests that the panel needs more markers to fully identified all the sub-population as well as the infiltrated monocyte/myeloid cells.

### 4.1.4 Analysis of the synovial populations using spectral flow cytometry

According to histology, the hallmarks of senescence are found in the LL and the LL fibroblasts are more senescent than the perivascular and SL fibroblasts. However, many senescent cells are also present in the synovium beside the fibroblasts and their classification will be discussed later. Furthermore, to validate to findings in the fibroblasts population we decide to investigate senescence in another experimental context. A good way to dissect the cell composition of a tissue is to use flow cytometry. Therefore, we designed a flow cytometry panel to cover the main population in RA and OA synovium and run it on JRP tissues from 10 OA and 10 RA after tissue digestion. Unfortunately, due to a very small quantity of tissue obtained for each patient only 4 RA and 6 OA patients were analysable. The panel contain the stromal markers described earlier: PDPN for LL fibroblasts, CD90 for SL, CD31 for endothelial and CD34 for fibroblasts and endothelial **(Fig 4.1.4 A)**. A pan immune cell marker, CD45 was

used to separate the stromal populations from the immune cells). Within the immune compartment, we used CD4 and CD8 to characterize the T lymphocytes and CD20 for the B cells. Moreover, among the myeloid population CD11c was used to separate dendritic cells from tissue resident macrophages expressing CD68 and MERTK. Furthermore, CX3CR1 and HLA-DR were used to classify the LL and SL macrophages respectively. Finally, a pan class I HLA was used to help the separation of cells from debris induced by the digestion protocol.

Once those population were classified, we investigated the expression of the intracellular markers of senescence p16, p21, p53, yH2AX and the autophagy maker TFEB that will be discussed in the next chapter. All the data were acquired on the Cytek Aurora spectral flow cytometer and analysed using Spectro flow, FlowJo and OMIQ **(Fig 4.1.4 A, B)**.

Initially, we analysed the proportions of cell populations to determine the heterogeneity between patients and compared data generated using this technique to those generated via CellDIVE analysis. By using Flowjo, we determined the main classes of cells using the gating strategy shown in figure 1.4 A. After eliminating most of the debris and exclude dead cells, the stromal and immune populations were separated by the expression of CD45. Within the stromal population, we isolated the fibroblasts from the endothelial cells using CD31 expression. Interestingly, 30,2% of the PDPN+ population expressed CD31 and will be further investigated in this chapter. Then, the LL fibroblasts were classified as $PDPN^{HIGH}$, the SL fibroblasts as $PDPN^{LOW}$.

Furthermore, the expression of CD90 in this experiment was low. Only a fraction of the stromal cell expressed CD90 while in the histology and the literature the proportion of CD90 and PDPN especially in RA should be in majority. To better classified the fibroblasts population, I decided to use the online bio-informatics tools called OMIQ to analyse those Data **(Fig 4.1.4 B)**.

We used a commonly used pipeline to study the data, starting by adjusting the spillover, scaling the samples and exclude debris and dead cells using the gating strategy **(Fig 4.1.4 A)**. Then, the data were cleaned by using the algorithm FlowAI and sub-sampling to homogenize the number of cells per

patient. In this step we separated the CD45+ and stromal cells and continued with the dimensional analysis on the 2 groups. We generated the UMAP for the stromal population and annotated using FlowSOM elbow based on the expression of CD34, PDPN, CD90, and CD31 to automatically detect the number of clusters. After adjusting the cluster and annotated them with heatmaps **(Fig 4.1.4 B)** I detected in both OA and RA, the presence of the following populations: PDPN high, PDPN+, PDPN+CD34+, CD34+, CD31+CD34+, CD31+, CD90+ and a large not annotated population close to the CD90 and PDPN **(Fig 4.1.4 B)**. Similarly to the first analysis using flowJo the SL fibroblasts population remains difficult to classify in this experiment. However, in previous FACS staining and literature the proportion of CD90+ fibroblasts should be higher and present within the PDPN+ cells to form the intermediate phenotype. Moreover, the CD90+ cells in this experiment resemble mural cells (pericytes and smooth muscle cells) due to the lack of expression of other marker and the size of the population. Therefore, we decide to classify the CD90+ as mural cells (pericytes) and the PDPN+ based on the level of PDPN expression. Indeed, we observed 2 population within the PDPN, a $PDPN^{HIGH}$ and a $PDPN^{LOW}$

Then we investigated the proportion of all the cell populations within the live cells in each patient and on average in both OA and RA cohort **(Fig 4.1.4 C).** First, in OA patients the proportion of LL fibroblasts $PDPN^{HIGH}$ is higher than the SL $PDPN^{LOW}$ fibroblasts in all patients tested. Moreover, in RA the percentage of LL fibroblasts (mean=13,06 ± 16,15) is higher on average compared to the percentage of SL fibroblasts (mean=2,71 ± 1,03). This result is in contradiction with the observation obtain with histology. Surprisingly, OA and RA profile by flow cytometry is very similar at the exception of the percentage of infiltrated T and B cells **(Fig 4.1.4 C)**.

The phenotype of the CD31+ is more complex than anticipated and is characterized by differential expression of CD34, PDPN. In addition, I notice a strong co-expression of CD31 and immune markers in both CD45+ and CD45- groups suggesting non-specific staining due to Fc receptor expressed on myeloid cells. This is analysed in detail in the endothelial section. Preliminary results only based on the CD31 expression shows RA the proportion of CD31+ cells observed in flow cytometry is similar to the one

measure in histology and represent 8,20% (±2,8) of the total live cells. However, in OA, 2 patients have a higher proportion of CD31+ cells compared to the others 2. Indeed, in OA patient 3 and 5, CD31+ represent 20,3% and 24,1% of the total live cells respectively when the other 4 patients on average 11,4% of the cells are CD31+. This higher proportion in OA patient number 3 and 5 increase the average proportion in the cohort to 14,93% compared to the 9,32% observed in histology.

Within the stromal cells, the pericytes and smooth muscle cells are important in the good function of the circulatory system and are called mural cells. In synovium, mural cells are characterized by the expression of CD146 (MCAM) and are important in the expansion of the CD90+ SL pro-inflammatory fibroblasts via NOTCH3 signalling. Unfortunately, we were not able to obtain a consistent staining in histology and CD146 antibody was not fitting in my flow cytometry panel. However, I observed a population with a higher expression of CD90. At first, we thought this population was the SL fibroblasts, but the size of the population did not correspond to the "physiological" expected proportion of the SL fibroblasts. Moreover, when looking at multiplex histology, the brightest CD90 staining is often coming from the first layer of the perivascular niche where pericytes reside. As there was a close promiscuity between the CD31+ and the bright CD90+ they were excluded from the CellDIVE analysis and not counted as fibroblasts. However, in the context of flow cytometry cells are isolated from each other allowing the separation between the two cell types. Nevertheless, the percentage of CD90+ observe using flow cytometry was 1,49% (±0,71) of live cells in RA and 1,63% (±1,07) in OA (**Fig 4.1.4 C**) which correspond to the expected proportion of pericytes in a tissue with capillaries.

When we look at the immune compartment, the proportion of T cells and B cells observe in OA synovium using flow cytometry is similar the one observe with CellDIVE and composed 3,80% (± 2,24) and 0,76% (± 0,57) of the living cells respectively. Furthermore, the increase proportion of lymphocytes in RA synovium compared to OA is also reported by flow cytometry where T cells represent on average 19,48% (± 15,39) of the total live cells while the B cells represent 6,30% (±3,19). Moreover, we can

notice that RA patient number 2 do not present a high proportion of lymphocytes characteristics of a low infiltration.

In the flow cytometry panel, the marker CD11c was added to distinguish the dendritic cells (DC) from the macrophages in opposition to the multiplex analysis where the staining was not optimized for this marker. Interestingly, a recent study shows that CD11c is also expressed on neutrophils (119). Similarly to the histology, we used MERTK and CD68 to characterize the TRMs with the addition of a LL macrophages marker CX3CR1 and HLA-DR as an inflammatory associated maker more represented in the SL macrophages. Moreover, in the classification of the cell populations the DC were selected based on the expression of CD11c and the TRMs as CD11c- CD68+ and CD11c- CD68-. Based on this phenotype we notice that in OA the percentage of TRMs is heterogenous amongst patients (mean=5,15%, SD=9,2). For instance, the percentage of macrophages in OA patient number 3, 4, and 5 represent only 3,93%; 1,25%, and 3,22% of the live cells respectively while the synovium of the 3 other patients is composed of 12,69% to 26,56% by macrophages. Interestingly in RA synovium, the dispersion between patient is lower (SD=2,8) and on average 11,35% of the live cells are macrophages **(Fig 4.1.4 C)**. However, the number of patient analysable in RA is lower than in OA making prediction on larger population even more speculative than in OA.

In a similar way, the proportion of CD11c+ annotated as DC is very heterogenous between patient in both diseases. Indeed, in OA patients 1, 2, and 3 the proportion of CD11c+ is on average 29,32% while the in patients 4, 5, and 6 this percentage drop to 9,12%. Moreover, in RA, we also observe 2 patients with a high proportion of CD11c+ as patient number 1 and 2 have 33,13% and 58,9% of the total synovium cells are CD11c+ respectively **(Fig 4.1.4 C)**. On the other hand, the proportion of CD11c+ in live cells of patients 3 and 4 only represent 9,17% and 4,25% respectively **(Fig 4.1.4 C)**. Globally, in OA CD11c+ cells make on averages 13,45% ±10,43 of the total synovial cells while in RA this proportion is increase to 26,37% +21,73. This might indicate more myeloid infiltration in RA compared to OA

including dendritic and neutrophils but the variation between patient is too high to conclude to any difference between the diseases.

Finaly, the percentage of non-annotated cells was reduced in the flow cytometry analysis compared to the multiplex classification. Indeed, in the OA patients the percentage of non-annotated cells represent on average 17,25% (±2,61) compared to 32,80% found with CellDIVE. Similarly, in RA patients after the classification only 4,88% (±2,47) of the live cells could not be annotated compared to 37,04% in CellDIVE experiments. This difference might be explained by the presence of CD11c in the flow cytometry panel which include DC and neutrophils representing 13,45% and 26,37% of the synovial cells in my analysis in OA and RA respectively. Altogether, the classification of the cell population using flow cytometry gives slightly different results compared to the classification made in histology. However, the main populations are represented in both techniques.

A

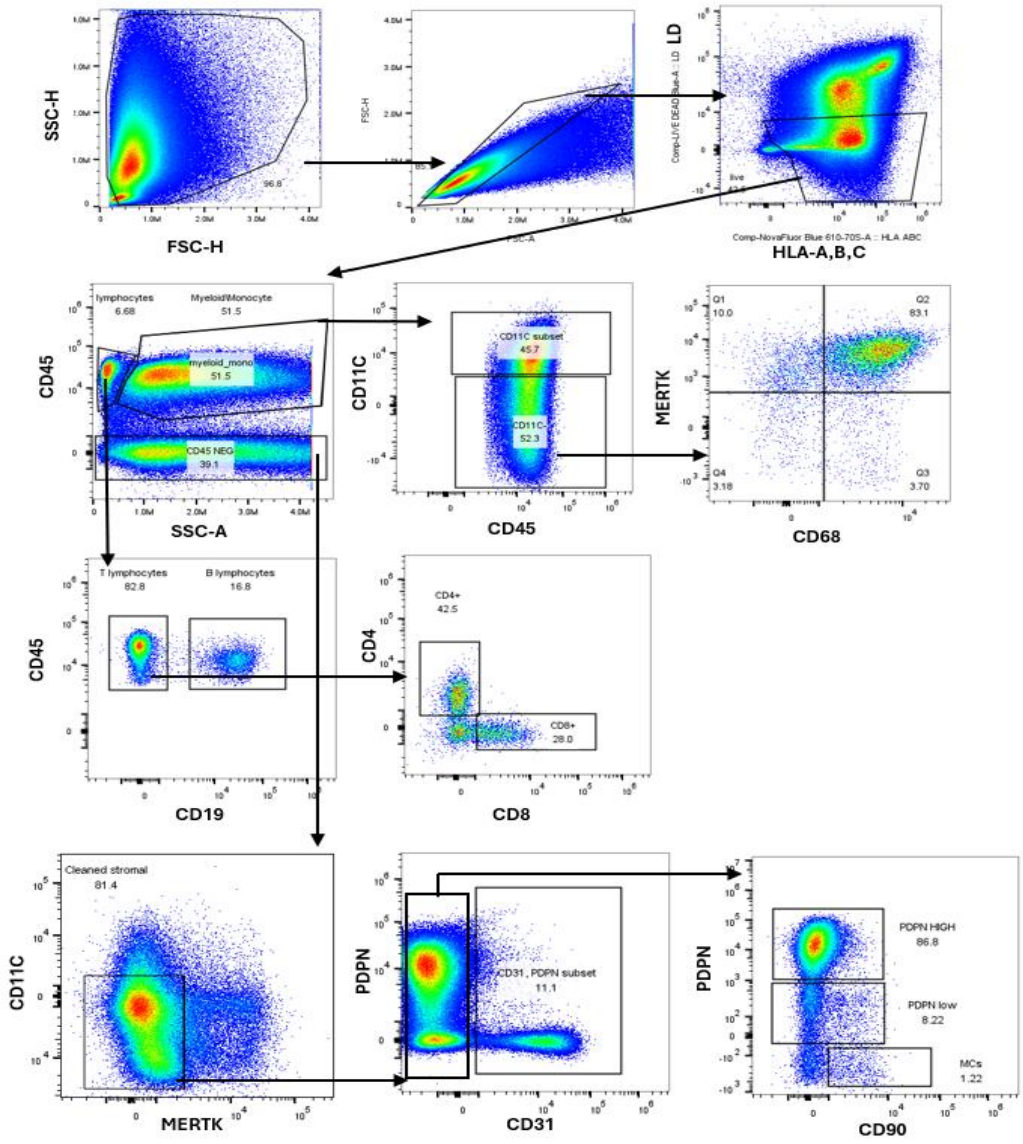


**Figure 4.1.4: Identification of the synovial populations using spectral flow cytometry**

**A:** Gatting strategy used to classify the main synovial populations in both OA and RA synovium after tissues digestion. Most of the debris were removed using size, live/dead and HLA-ABC. Stromal cells and immune were separated based on the CD45 expression. Whitin CD45, macrophages were classified CD11c-, B cells with CD19+, T cells as CD4+ and CD8+. In the CD45-, MERTK and CD11c positives cells were removed. Fibroblasts and ECs were separated by the expression of CD31. Fibroblasts were classified based on CD90 and PDPN expression.

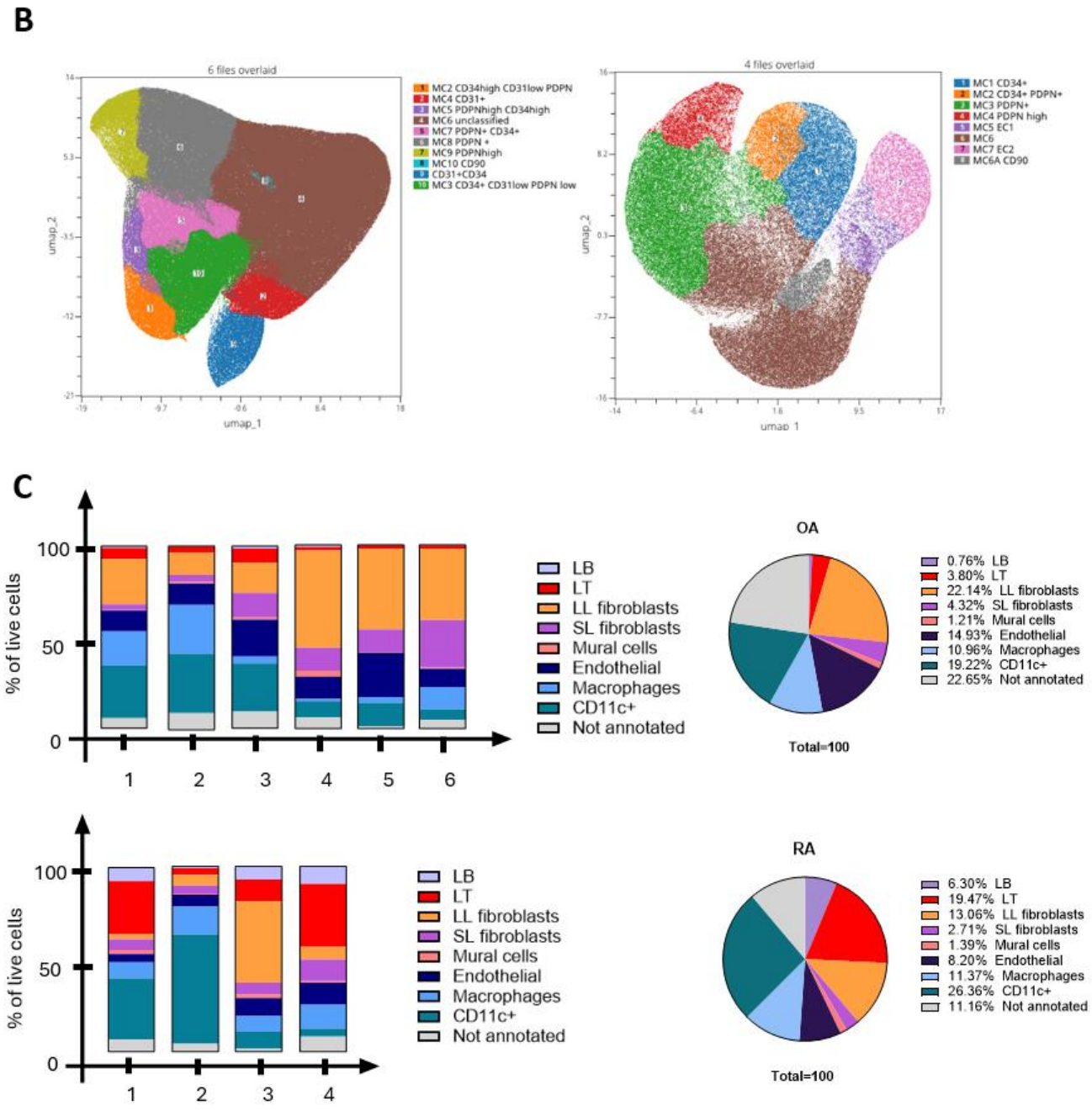


**Figure 4.1.4 (continued): Identification of the synovial populations using spectral flow cytometry**

**B:** UMAPs of the stromal population clusters generated using the online flow cytometry software OMIQ© (Dotmatics) based on the expression of PDPN, CD31, CD34 and CD90 in the CD45- in concatenated OA patients (n=6) and RA patients (n=4). **C:** Graphical representation of the different synovial population in each RA patient (n=4) and each OA patient (n=6) classified using the following panel CD90, PDPN, CD31, CD34, CD68, CD11C, CD4, CD8, CD19, CD45, MERTK. The average percentage of each population between patients is displayed in the graphic pie chart (left). LB = B lymphocyte, LT = T lymphocytes SL= Sub-lining, LL = Lining layer.

## 4.2 Hallmarks of Senescence in Human Cells Populations in Arthritic Diseases

### 4.2.1 Fibroblasts and Senescence

#### *4.2.1.1 Preliminary Characterization of Cellular Senescence in Synovium*

Before using the multiplex IF described earlier, I try to validate the senescence antibodies in primary RA fibroblasts and in synovial sections using confocal microscopy. To validate the antibodies, I stained RA fibroblasts in culture at passage 8 for yH2AX, p53, p16, p21. Apart from p16, p53, p21 and yH2AX were detected in the nucleus of RA cultured. SA β-gal staining was used to address the percentage of senescence expected in each condition **(Fig 4.2.1.1 A)**. Those preliminary data allowed me to test those antibodies in OA and RA synovium using IF staining and confocal imaging.

The localization of yH2AX appeared associated with the LL in both OA and RA **(Fig 4.2.1.1 B)**. This was further confirmed by quantifying the fluorescence intensity of yH2AX in the sub-regions. Indeed, we noticed a significant accumulation of DNA damage in the LL compared to the SL **(Fig 4.2.1.1 C)**.

To investigate cellular senescence, the expression of the tumour suppressor p53 and p16 were investigated using immunofluorescence staining of human synovium from OA and RA joint replacement (JRP) tissue. Many optimizations were performed to find antibodies and staining conditions to obtain a specific signal and a limited background. This leads to the first steps in localisation of senescent cells in the synovium. Preliminary staining of p16 indicate the presence of positive cells in the LL and in the BV endothelium OA while the perivascular region as well as the SL connective tissue remains negative **(Fig 4.2.1.1 D)**. Interestingly, p53 was also found in the LL in OA but also in some infiltrated immune cells immune in this patient **(Fig 4.2.1.1 D)**. Similar observations were found in RA synovium with the presence of p16 in the LL. Furthermore, p53 is strongly associated with the BV endothelium in RA **(Fig 4.2.1.1 E)**. As a result, the hypothesis that differential senescence between the LL and SL exists was promising yet the staining needed to be improved, and the cell populations involved was unknown.

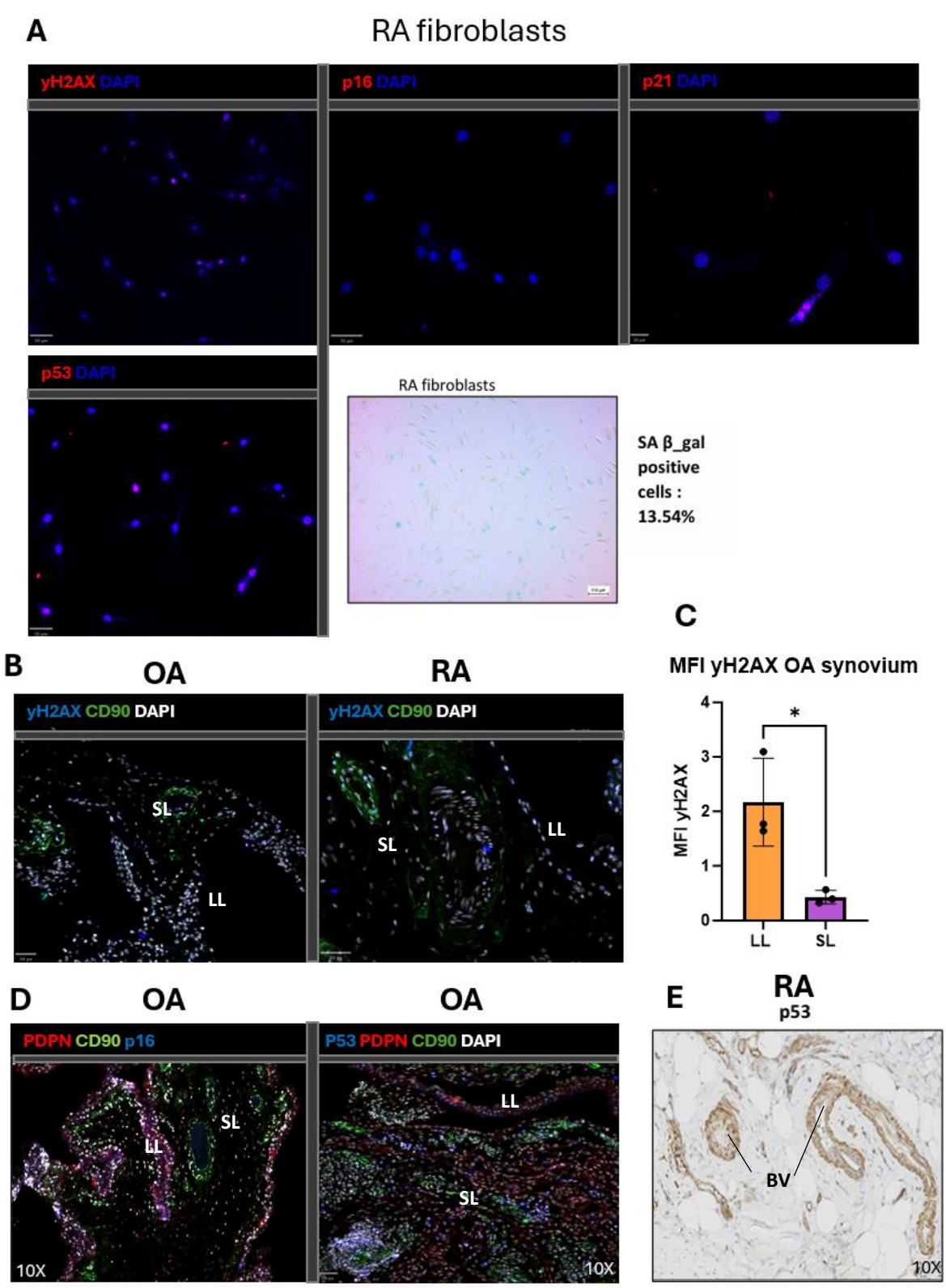


**Figure 4.2.1.1: Preliminary investigation of the hallmarks of senescence in histology.**

**A:** ICC staining of RA fibroblasts (P8) for yH2AX, p16, p21, p53 (red) and DAPI (blue). Same fibroblasts were stained for β-gal. Percentage of β-gal+ cell is indicated on the right. **B:** IF staining of yH2AX (blue) and CD90 (green) in OA and RA synovium. Nuclei are grey. **C:** quantification of the yH2AX MFI measured in the LL and the SL in OA synovium (n=3), paired student t-test. **D:** IF staining of p16 and p53 (blue) in OA synovium with CD90 (green) and PDPN (red) 10x magnification. **E**: IHC staining of p53 (brown) in RA synovium. (*$p < 0.05$).

#### *4.2.1.2 Investigating the cellular senescence profile of the fibroblast populations in human synovium by multiplex Histology*

After the classification of the LL fibroblasts (PDPN+MERTK-CD68-) and the SL fibroblasts (CD90+CD31-CD45-) we investigated the expression hallmarks of senescence in those cells in the OA and RA cohort.

To characterize the senescence profile, I used the expression of the CDK inhibitor p16, classically used to detect senescent cells undergoing cell cycle arrest. Moreover, we investigated the presence of DNA damage by targeting the phospho-epitope of the Histone H2AX (yH2AX). Finally, we determined the expression of the tumour suppressor p53 and its downstream target CDK inhibitor p21.

Firstly, we observed that the signal of p21, p16 and yH2AX is almost exclusively nuclear while p53 is cytoplasmic **(Fig 4.2.1.2 A)**. Indeed, we expect to find the phosphorylated form of H2AX at the site of DNA damage. Similarly, due to their cycle arrest capacity, we were expecting to find p16 and p21 within the nucleus. However, little is known about the role of the sub-cellular localization of p16 on its activation. Moreover, most of the published histological staining of p16 are not clear about the link between the localisation of p16 or p21 and their respective activity. For those reasons, the detection threshold to classify p21+, p16+ and yH2AX+ was based on the mean fluorescence intensity within the nucleus only while p53+ cells were detected the whole cell mean fluorescence intensity. Similarly to the classification of the cell phenotype describe in part 1.2, all the cells exhibiting an MFI superior to the mean + 1 time the SD were consider positive. Examples of p16, p21, yH2AX and p53 staining in the fibroblasts in OA and RA are presented in figure 2.1.2 A and B respectively **(Fig 4.2.1.2 A, B)**.

Then, the proportion of p16, p21, p53 and yH2AX was investigated in the previously defined fibroblast populations of the LL and SL in all the OA and RA patients.

Following the findings made on confocal microscopy, most of the positive cells for the 4 studied hallmarks are localized in the LL. This is confirmed by a significantly higher proportion senescent PDPN+ LL fibroblasts compared to the CD90+ SL fibroblasts for the 4 markers **(Fig 4.2.1.2 C)**. Interestingly, this differential cellular senescence is observed in both OA and RA cohorts suggesting that the mechanism

behind the increased of cellular senescence in the LL is not dependant on the disease but rather on the architecture of the synovium.

In details, p16 in RA is higher in the LL fibroblasts in the 10 patients tested (p=0,0001) compared to the SL fibroblasts. Furthermore, on the 9 patients tested in OA, p16 was detectable in 7 patients and among them 6 had more p16 in the PDPN+ fibroblasts (p=0,0124) in comparison to the SL population. Furthermore, on average 23,95% ± 5,76 of the PDPN+ fibroblasts were p16 positive against 7,93% ± 4,69 in the CD90+ in RA **(Fig 4.2.1.2 C)**. The average proportion of p16 positive in the SL is similar in OA (mean=7,88% ± 5,32) while the proportion of p16 in the LL is slightly lower (mean=19,28% ± 8,05) **(Fig 4.2.1.2 C)**.

Moreover, in RA the presence of DNA damage is higher in the LL fibroblasts compared to the SL fibroblasts (n=11, p=0,0003). Similarly, in OA the DNA damage detected by the yH2AX in significantly higher in the PDPN+ fibroblasts compared to the CD90+ SL population (n=8, p=0,0015) **(Fig 4.1.2.2 A)**. On average, 18,93% ± 7,95 of the LL fibroblasts are yH2AX+ cells in RA and 5,22% ± 2,54 of the SL fibroblasts present DNA damage associated staining. We notice a slight increase in OA compared to RA with 26,07% ± 8,94 yH2AX positives cells in the LL fibroblast population and 8,56% ± 5,41 amongst the SL fibroblasts on average **(Fig 4.1.2.2 A)**.

Next, we investigated the differences between OA and RA senescence in the LL fibroblasts. Whereas no differences in p16 and p53 proportions is observed between OA and RA, we noticed a significant increase of the proportion of p21 in RA LL compared to OA **(Fig 4.2.1.2 D)**. Interestingly, the proportion of yH2AX+ in OA LL fibroblasts is increased compared to RA **(Fig 4.2.1.2 D)**. This suggest might suggest higher DNA damage in OA LL fibroblasts, while RA fibroblasts have more p21 as a consequence of the activation of the DNA damage response.

**Figure 4.2.1.2: Cellular senescence profile of the fibroblast populations in human synovium by Multiplex Histology**

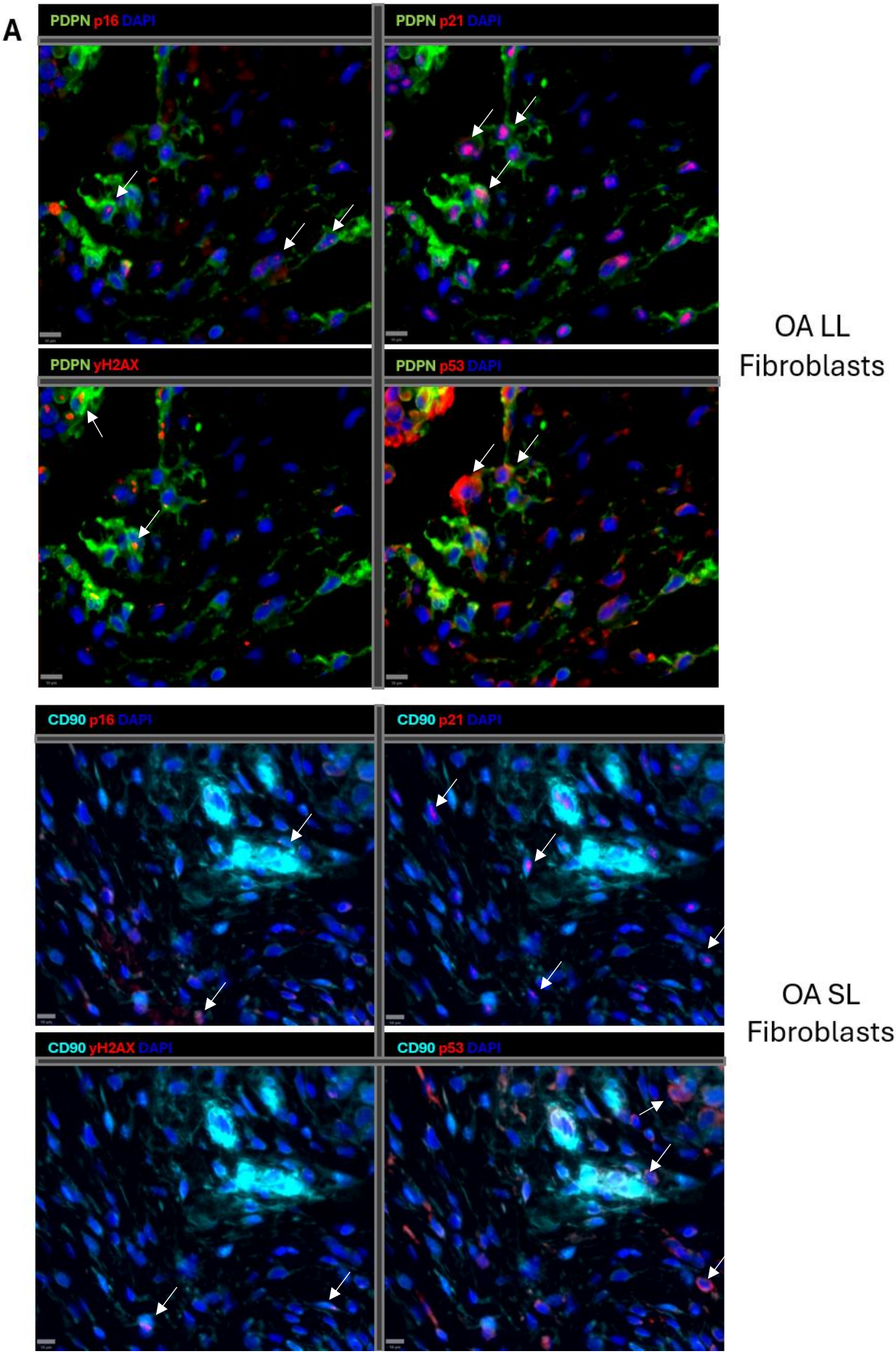
A
PDPN p16 DAPI
PDPN p21 DAPI
PDPN γH2AX
PDPN p53 DAPI
OA LL Fibroblasts
CD90 p16 DAPI
CD90 p21 DAPI
CD90 γH2AX DAPI
CD90 p53 DAPI
OA SL Fibroblasts

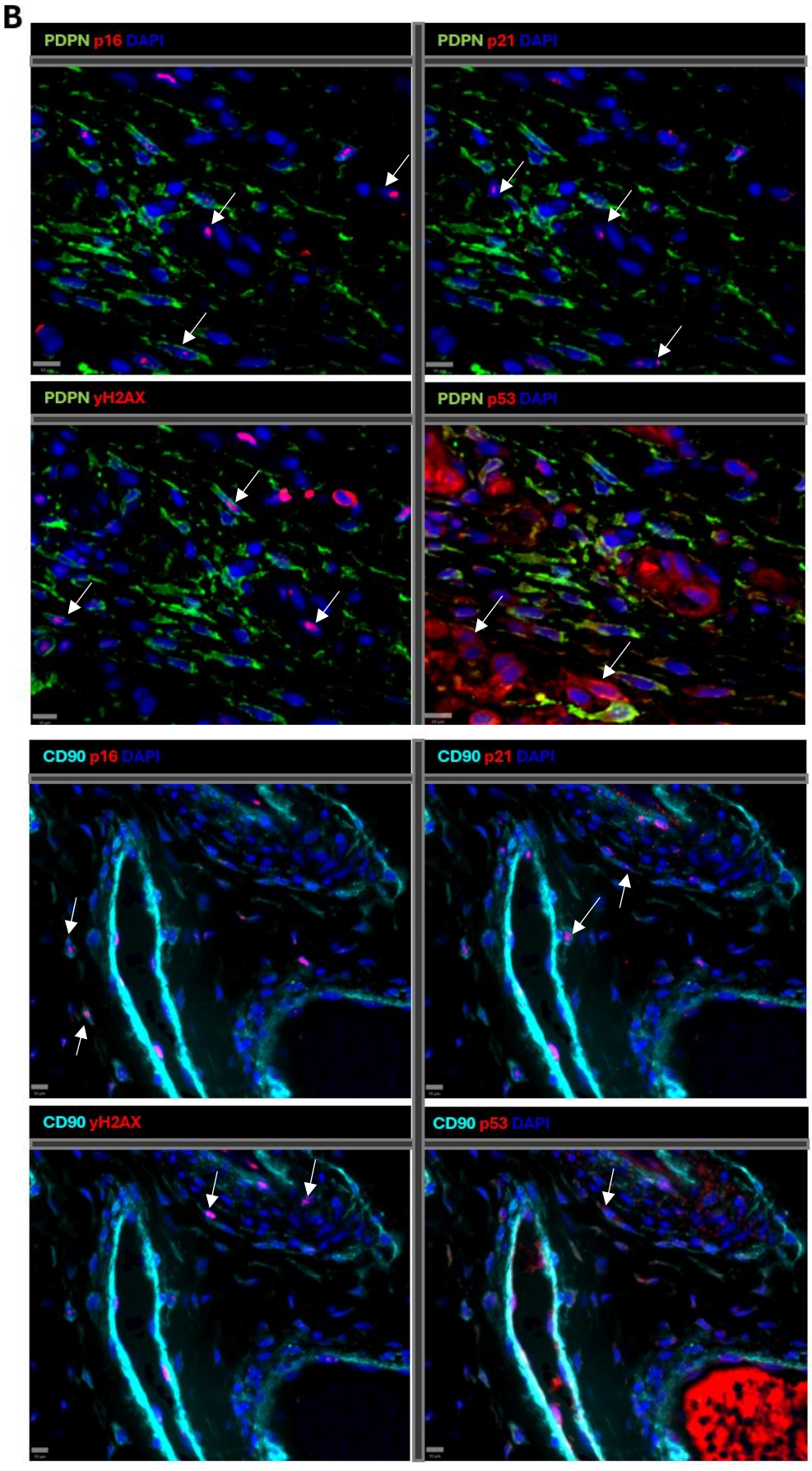
B
PDPN p16 DAPI
PDPN p21 DAPI
PDPN yH2AX
PDPN p53 DAPI
RA LL Fibroblasts
CD90 p16 DAPI
CD90 p21 DAPI
CD90 yH2AX
CD90 p53 DAPI
RA SL Fibroblasts

v

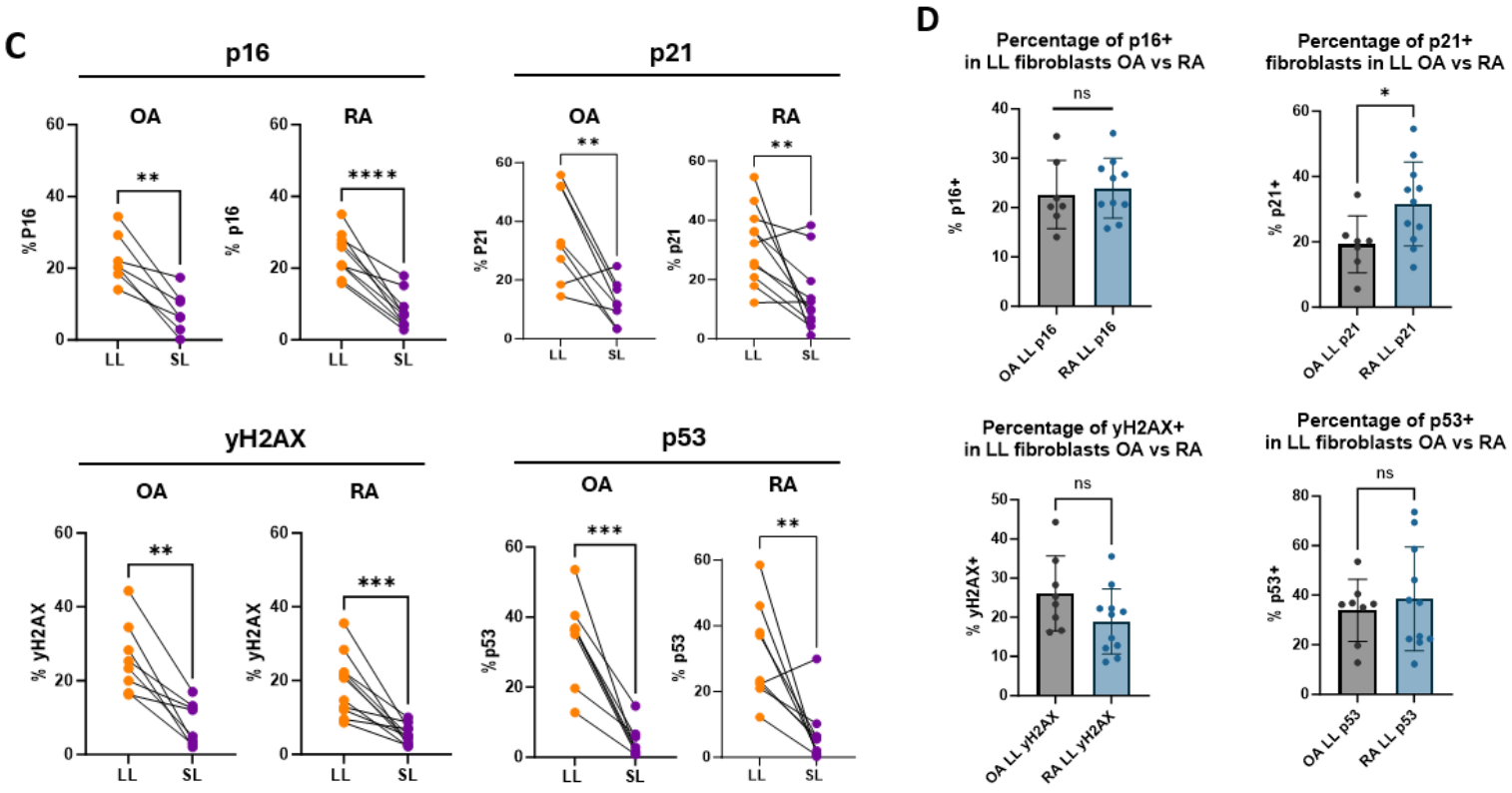


**Figure 4.2.1.2: Cellular senescence profile of the Fibroblast populations in human synovium by Multiplex Histology**

**A:** Multiplex IF image showing p16, p21, yH2AX, and p53 in the LL PDPN+ fibroblasts (top panels) and in the SL CD90+ fibroblasts (bottom panels) in OA synovium. PDPN (green); CD90 (cyan); p16, p21, yH2AX, and p53 (red). White arrows=positive cells **B:** Multiplex IF image showing p16, p21, yH2AX, and p53 in the LL PDPN+ fibroblasts (top panels) and in the SL CD90+ fibroblasts (bottom panels) in RA synovium. PDPN (green); CD90 (cyan); p16, p21, yH2AX, and p53 (red). White arrows=positive cells **C:** Quantification of the percentage of p16, p21, yH2AX, and p53 in the PDPN+ MERTK- CD68- LL fibroblasts (orange) and in the CD90+ CD31- CD45- SL fibroblasts (Purple) in OA and RA synovium. Student paired t-test, OA (n=7) RA (n=10). Exception for p16: OA (n=6). **D:** Comparisons of p16, p21, yH2AX, and p53 proportion in LL between OA (grey) and RA (blue). Student Unpaired t-test, OA (n=7) RA (n=10). Exception for p16: OA (n=6). (*p < 0.05; **p < 0.01; ***p < 0.001; ****p < 0,0001).

#### *4.2.1.3 DNA damage induced senescence in synovial fibroblasts*

As the DNA damage response starts with the phosphorylation of H2AX and then the activation p53-p21 pathway, we investigated the proportion of p53+ p21+ in absence of yH2AX, then the proportion of cells with the complete pathway yH2AX+ p53+ p21+ and finally the cells that are yH2AX+ p53+ but without the activation of p21. Interestingly, when pull together we found 2 groups of patients in RA and in OA. Thus, in the first RA group (RA G1) a third of the p53+ LL fibroblasts are p21+ yH2AX negative (mean=28,96 ± 7,37) **(Fig 4.2.1.3 A**). Furthermore, 15% of the LL fibroblasts have the complete pathway (P53+ p21+ yH2AX+) while only 8,15% ± 1,76 are yHA2X+ P21 negative. In opposition, the second group (RA G2) have a lower proportion of P53+p21+ (mean=9,21 ± 2,73) but a higher proportion of p53+ yH2AX+ p21- (mean=28,71 ± 8,74). Interestingly the proportion of the triple positive is also lower (8,66% ± 4,8) compared to the first group. This suggest that the induction of senescence in G2 seems more linked to DNA damage than in G1. Moreover, a similar trend is observed in OA. Indeed, in OA G1, the proportion of P53+P21+ is 2 times higher than the p53+ yH2AX+ P21- **(Fig 4.2.1.3 A**). The opposite is observed in OA G2 where 8,83% are p53+ p21+ and 25,48% are p53+ yH2AX+ P21 negative. Moreover, the proportion of triple positive LL fibroblasts is similar between the 2 groups with 14,87% ± 6,64 in G1 and 18,66% ± 1,6 **(Fig 4.2.1.3 A**). One explanation could be that in group 2, the high proportion of DNA damage is leading to an irreversible cell cycle arrest independent of p21 by the activation of p16 while in the group 1 the activation of p21 by p53 do not require p16 activation and is reversible. To test this hypothesis, we investigated the proportion of p16+ within the 3 senescent populations, p53+p21+, yH2AX+p53+p21+, and yH2AX+p53+ **(Fig 4.2.1.3 B**). Surprisingly, no difference was observed in RA between the DNA damage induced senescence yH2AX+p53+ and the p53+p21+ in the 2 groups regarding activation of p16. However, the proportion of p16 fibroblasts within the DNA damage induced yH2AX+p53+p21+ was significantly higher compared to the 2 others senescent fibroblasts phenotype in both groups **(Fig 4.2.1.3 B**). This might suggest a strong activation of the

senescence hallmarks characteristics of an irreversible senescence status. More interestingly, this is exacerbated in the group 2 in RA where the proportion of p53+p21+ are the lowest suggesting a failure in DDR mechanism in those patients and therefore more senescence.

In literature, p21 and p16 have been shown to be rarely co-expressed and have distinct associated secretory phenotype (120, 121). However, among all the p21 positives cells 47,95% are p16 in RA synovium and 45,56% in OA **(Fig 4.2.1.3 C**). Despite a high variability between patients in RA (SD=21,39) the proportion of double positive p16/p21 cells was not negligeable and need to be further investigated**.**

Together, those data suggest that the LL fibroblasts compared to the SL fibroblasts are more exposed to DNA damages characterized by a significant increases of p53, p21 ad, yH2AX. As a consequence of this LL fibroblasts are more senescent than the SL fibroblasts demonstrated by a significant increase of p16+ proportions. Interestingly, a different response to DNA damages activation is found among patients. Nevertheless, LL fibroblasts positives for yH2AX alongside p53 and p21 are also p16+ in RA suggesting a senescence activation in response to unresolved DNA damage despite the activation of the DDR. This is not observed in OA, but it may be explained by a small number of patients in this analysis.

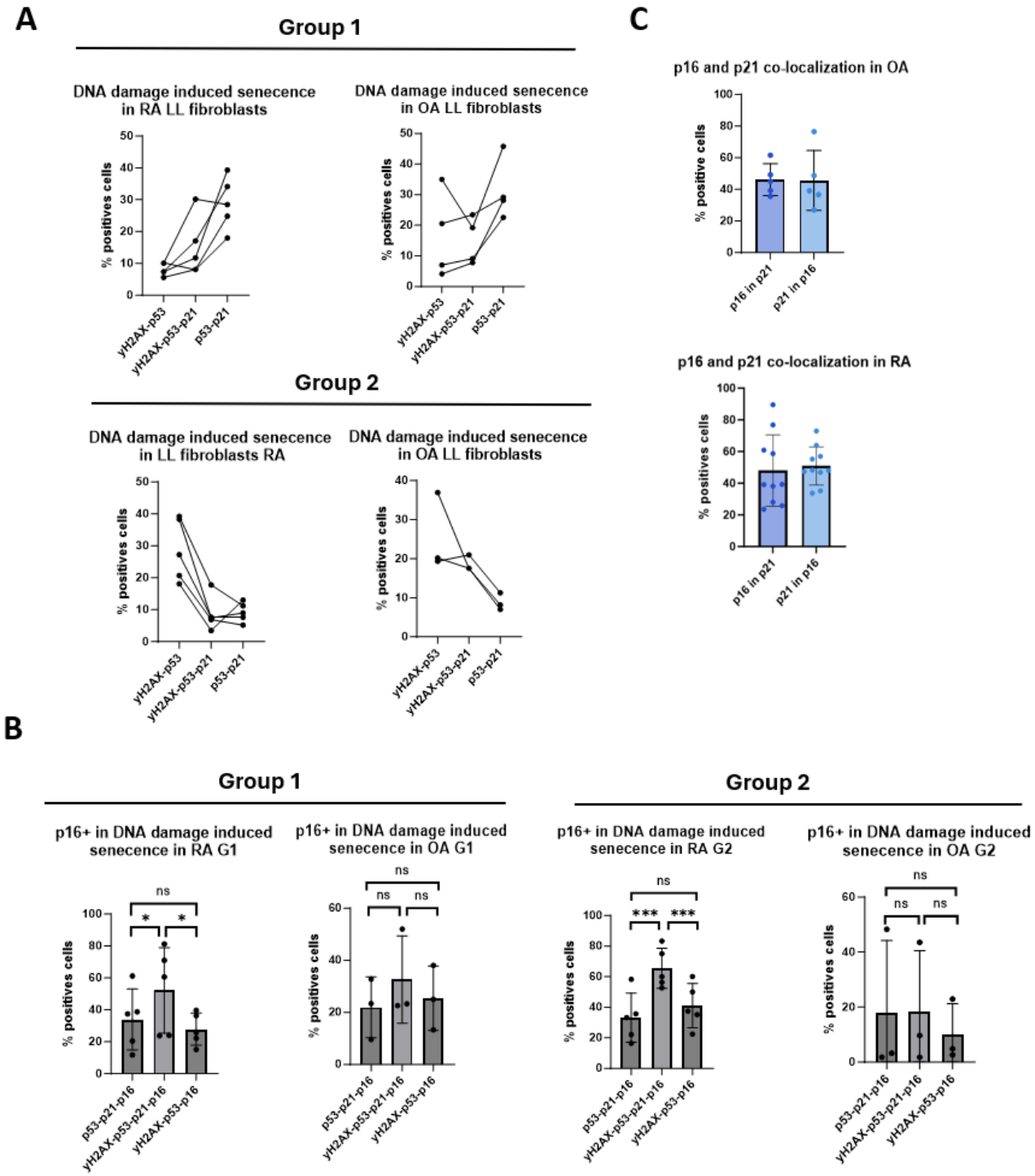


**Figure 4.2.1.3: DNA damage induces senescence in synovial fibroblasts**

**A:** Percentage of yH2AX+p53+, yH2AX+p53+p21+, and p53+p21+ in LL fibroblasts in the identified groups of patients in OA (right) and RA (left). **B:** Percentage of p16+yH2AX+p53+, P16+yH2AX+p53+p21+, and p16+p53+p21+ in LL fibroblasts in OA and RA. Student paired t-test; RA G1 (n=5), RA G2 (n=5), OA G1 (n=4), OA G2 (n=3). **C:** Respective proportion of p16+ in p21+ and p21+ in p16+ of all synovial cells in OA (top panel) and in RA (bottom panel). (*$p < 0.05$; ***$p < 0.001$).

#### *4.2.1.4 Cellular senescence in the fibroblast populations analysed by flow cytometry.*

As described earlier, LL fibroblasts were classified mainly by the expression of PDPN leading to the identification of 2 populations in the CD45 negative live cells: one PDPN$^{high}$ and the second PDPN$^{low}$ (**Fig 4.2.1.4 A)**. The expression of CD90 was lower than usual it this experiment which limits the identification of the SL populations. However, according to transcriptomic DATA and FACS analysis, PDPN is expressed by all the synovial fibroblasts (16, 17). Although in histology, the PDPN expression is confined to the lining layer and no colocalization is observed between PDPN+ and CD90+ fibroblasts **(Fig 4.1.2 E)**. Some Hypothesis can explain this difference. First, comes directly from the technique, where FACS is able to pick lower signal due to a higher sensitivity, histology will show the highest expression. Secondly, alternative slicing of PDPN might be involved in the detection of the signal as different antibody clones were used between the two techniques. Nevertheless, the PDPN$^{HIGH}$ population is most probably the population detected in the LL in histology, while the PDPN$^{low}$ might correspond to the SL. Furthermore, most of double positive PDPN+/CD90+ are detected in the PDPN$^{low}$ population. However, this is not true in some patients, which might not exclude some overlapping between the SL and LL in the selected populations for the analysis. In addition, the PDPN- CD90+ are classified as mural cells (MCs).

Thus, based on the above classification, we investigated the proportion of p16+, p21+, yH2AX+ and p53+ in the PDPN$^{HIGH}$ LL fibroblasts compared to the PDPN$^{low}$ SL fibroblasts in both OA and RA synovium. The main difference observed is that the proportion of p16+ in the PDPN$^{HIGH}$ is significantly higher compared to the PDPN$^{LOW}$ fibroblasts **(Fig 4.2.1.4 B, C)**. Indeed, on average 43,47% (±12,30; n=6) of OA PDPN$^{HIGH}$ fibroblasts are p16+ while we observed 14,39% (±6,78; n=6) of p16+ in OA PDPN$^{LOW}$ fibroblasts **(Fig 4.2.1.4 C)**. Furthermore, in RA, there is also an increase in p16+ proportion in PDPN$^{HIGH}$ compared to PDPN$^{LOW}$. However, this difference is not significant may be because of the small sample size (n=4) **(Fig 4.2.1.4 C)**. Moreover, the proportion of p21+ in PDPN$^{HIGH}$ is significantly higher compared to the PDPNlow fibroblast in OA, while in RA no difference is observed **(Fig 4.2.1.4 C)**. On the global

senescence profile, we noticed that p21+ are the most abundant cells in all the populations in both OA and RA **(Fig 4.2.1.4 B)**. Furthermore, there is a significant decrease of the proportion yH2AX+ in the PDPNlow compared to the LL PDPN$^{high}$ fibroblasts **(Fig 4.2.1.4 B, C)**. This decrease is also observed in RA but is not significant. Interestingly, the proportion of p53+ do not vary between the 2 populations in both OA and RA **(Fig 4.2.1.4 C)**. While in histology, the proportion of p53+ is almost exclusively present in the LL, here we observed 33,17% (±15,93; n=6) and 46,97% (±9,29; n=4) of p53+ in PDPN$^{low}$ in OA and RA respectively **(Fig 4.2.1.4 C)**.

Then, we investigated the DNA damage associated senescence profile through yH2AX+/p53+/p21+ pathway. In opposition the findings in histology, we do not observe the two patient groups with inverted yH2AX+/p53+ and p21+/p53+ proportion **(Fig 4.2.1.4 D)**. Instead, there is higher proportion of p21+/p53+ in all OA PDPN$^{high}$ compared to the proportion of yH2AX+/p53+/p21+ **(Fig 4.2.1.4 D)**. Similarly, in the PDPN$^{low}$ we observed the same profile for most patients at the exception of 1 that have a high proportion of yH2AX+/p53+/p21+. In RA, 1 patient out of 3 have more yH2AX+/p53+/p21+ in both PDPN high and PDPN low compared to p21+/p53+, may be due to a high proportion of yH2AX+ **(Fig 4.2.1.4 D)**.

Together, those results may suggest that the activation of p53 and subsequently p21 might not be associated directly by H2AX phosphorylation in most patients. However, we can hypothesize that the strong activation of p53 and p21 in this patient may promote a transitory cell cycle arrest in order to establish the DNA damage response leading to a decrease of yH2AX. Although some patients have a high proportion of yH2AX+/p53+/p21+ suggesting that the DNA damage activated the cells a cycle arrest after activation of p53 via the phosphorylation of the histone H2AX. In opposition to the patients with high p53 and p21, they failed to repair leading to and the accumulation of yH2AX+. To verify this, we investigated the MFI of p16 in the above populations. Surprisingly, p16 is higher in the p21+/ P53+ compared to the yH2AX+/p53+/p21+ in the PDPN$^{high}$ and PDPNI$^{ow}$ in both disease and do not vary across patients **(Fig 4.2.1.4 E)**. This result is not in accord with the findings in histology, where the

proportion of p16+ was higher in yH2AX+/p53+/p21+ suggesting that fibroblasts that accumulate yH2AX despite the activation of p53 and p21 increase p16 expression **(Fig 4.2.1.4 E).**

Finally, in the MCs, we observed a high proportion (above 60%) of p16+ and p53+ in both OA and RA **(Fig 4.2.1.4 F)**. Moreover, the proportion of p21+ in also high in RA CD90+PDPN- MCs with an average of 50,95 (±13,26; n=4) while in OA only 35,18% (±14,03; n=6) are p21+ but this difference is not significant **(Fig 4.2.1.4 F)**. The proportion of yH2AX+ is lower compared to the other senescence markers in this population in OA and RA, although one RA patient have a high proportion of yH2AX+ compared to the other two analysed **(Fig 4.2.1.4 F).**

In summary, multiplex histology indicates that LL fibroblasts have a significant increase of p16, p21, yH2AX and p53 compared to the CD90+ SL fibroblasts in both OA and RA. Further investigation of the DNA damage associated senescence shows 2 groups of patients with different proportion of yH2AX+/p53+ and p21+/p53+ suggesting different response to DNA damages. In the group where the most of LL fibroblasts are yH2AX+/p53+, we can hypothesize that a lot of fibroblasts are subjects to DNA damage leading to the activation of p53. Conversely, a high proportion of p53+/p21+ could suggest the establishment of the cycle arrest allowing the DNA damage response activation leading to a reduction of H2AX phosphorylation. Moreover, a failure to resolve the damage could lead to an increase of p16 expression to establish an irreversible cellular senescence.

Furthermore, the FACS analysis on the $PDPN^{high}$ LL fibroblasts and the $PDPN^{low}$ SL fibroblasts show a higher p16 and p21 activation as well as an increase of the yH2AX+ proportion in the LL fibroblasts in OA. Similar trend is shown in RA, but no significative difference is observed may be due to the limited number of patients analysed. Moreover, the DNA damage pathway, indicates a higher proportion of p21+/p53+ compared to the yH2AX+/p53+/p21+ still suggesting that the DNA damage response is established to activate the DNA repair mechanism. However, the fluorescence intensity of p16 is higher in the p21+/p53+ compared to yH2AX+/p53+/p21+, questioning further the activation of senescence is those cells.

**Figure 4.2.1.4: Cellular senescence in the fibroblast populations analyzed by flow cytometry**

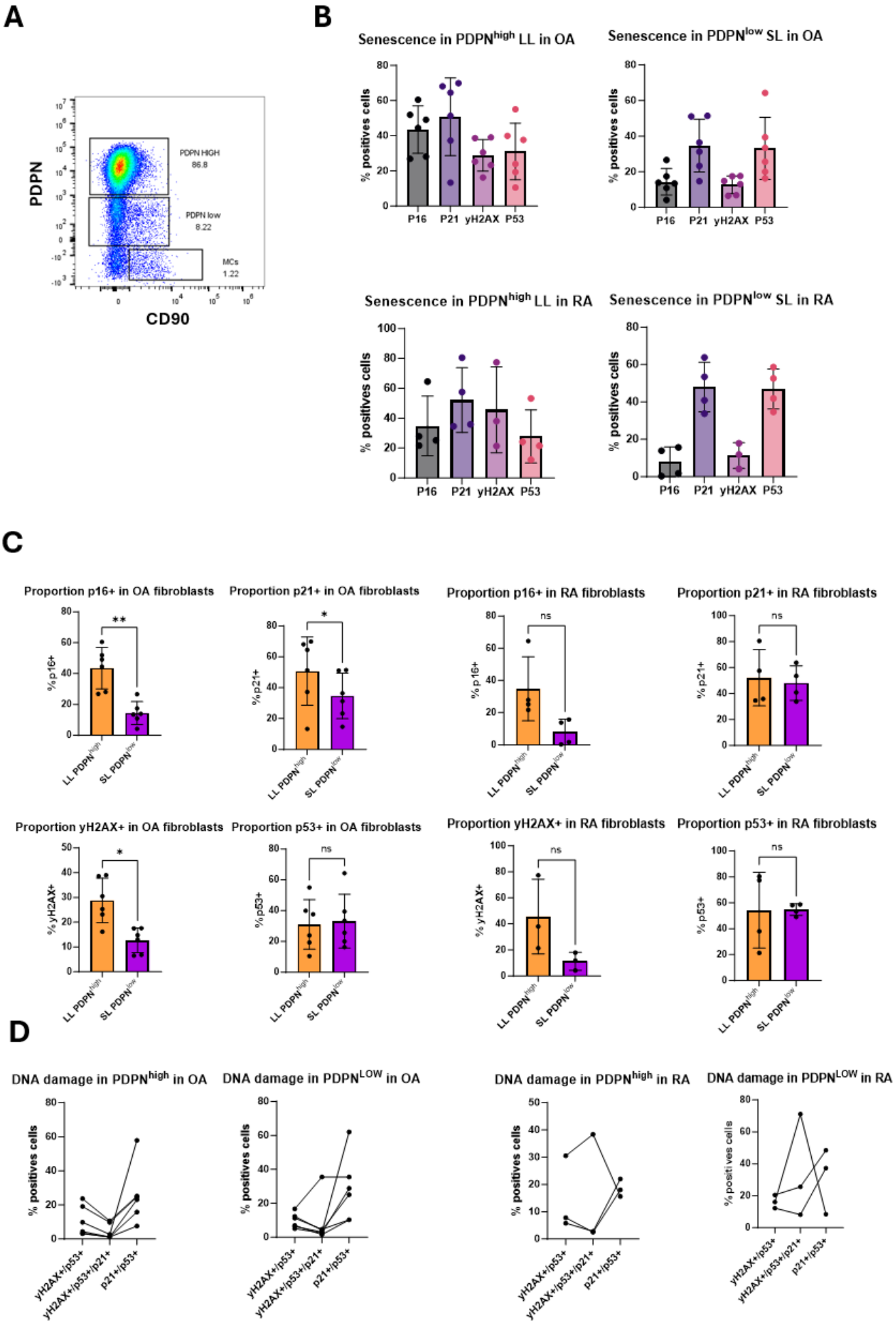

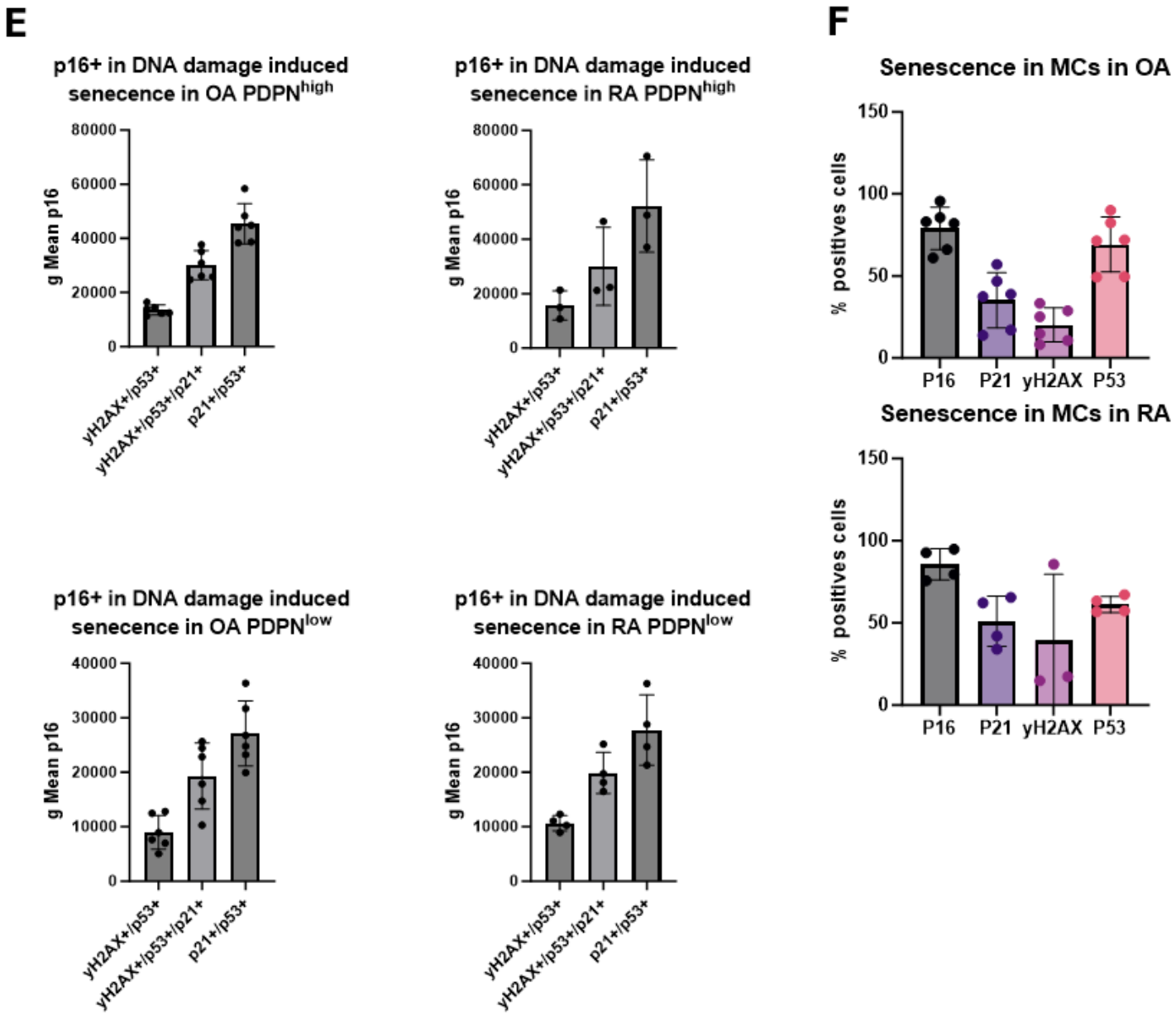


**Figure 4.2.1.4: Cellular senescence in the fibroblast populations analyzed by flow cytometry**

**A:** Gating strategy of the synovial fibroblasts. LL fibroblasts were characterized based on CD45- CD31- PDPN$^{HIGH}$ and the SL fibroblasts based on CD45- CD31- PDPN$^{LOW}$. Murals cells (MCs) were classified as PDPN- CD90+. **B:** Percentage of p16, p21, yH2AX, p53 in PDPN$^{HIGH}$ and PDPN$^{LOW}$ fibroblasts populations in OA (top panel) and in RA (bottom panel). **C:** Statistical comparison of the percentage of p16, p21, yH2AX, p53 in PDPN$^{HIGH}$ and PDPN$^{LOW}$ fibroblasts populations in OA and RA. Paired student t-test. **D:** Percentage of yH2AX+p53+, yH2AX+p53+p21+, and p53+p21+ in PDPN$^{HIGH}$ and PDPN$^{LOW}$ fibroblasts populations in OA (left) and RA (right). **E:** MFI of p16 in yH2AX+p53+, yH2AX+p53+p21+, and p53+p21+ in PDPN$^{HIGH}$ and PDPN$^{LOW}$ fibroblast populations in OA and RA. **F:** Percentage of p16, p21, yH2AX, p53 in mural cells (MCs) in OA (top) and I RA (bottom). (*$p < 0.05$).

### 4.2.2 Macrophages and senescence

#### *4.2.2.1 Characterization the Tissue Resident Macrophages populations in human synovium*

Tissue resident macrophages (TRMs) play a dominant role in synovial homeostasis. Beside their immune surveillance and clearing roles, synovial TRMs participate to the organization of the lining layer by creating a barrier between the synovial sub-lining and the synovial cavity. Indeed, they express tight junction molecules to form a pseudo epithelium structure preventing the infiltration of cells into the synovial fluid and maintaining its homeostasis. In synovial joints affected by arthritis, the LL is challenged in different ways. While RA will often be associated with a loss of the macrophages barrier, OA will be associated with hyperplasia resulting in aberrant function of the LL. Moreover, maintaining the integrity of the LL have been shown to be important for remission in RA underlining the protective role of the LL macrophages (26). Transcriptomic analyses have been pivotal in the discovery of the different TRMs subsets involved in synovial organization and their role during arthritis (24, 25, 26). Transcriptomic data have revealed that TRMs in human synovium are CD64+, CD11b+, and CD68+ and can be subcategorised into the tissue resident (MERTK+ CD206+) and the tissue infiltrating (MERTK- CD206-) macrophages. In addition, within the TRMs, TREM2 and CXCR1 expression is associated with the LL subset while LYVE1 is associated with the SL population.

In our multiplex analysis we used the expression of CD68, MERTK and CD206 to characterize the TRMs and to investigate their localization and senescence in both OA and RA. As tissues sections came from different origin, the staining was inconsistent for CD68 and CD206 resulting in the absence of CD68 and/or CD206 signal for some patients in the cohort. Therefore, the number of patients in each separated analysis will be indicated.

Following the data in part 1.2, we investigated further the proportion of TRMs within the sub regions of the synovium and their phenotype. As the LL expansion and destabilization are both respective features of OA and RA synovium, we compared the percentage of TRMs in the LL and in the SL in both diseases. Thus, in OA synovium, 33,56% (± 7,53; n=6) of the LL and 12,86% (± 4,68; n=6) of the SL is

composed by TRMs **(Fig 4.2.2.1 A)**. Similarly in RA, the majority of the TRMs are in the lining and represent 29,87% (± 8,73; n=6) of the LL cells while the SL is composed by 16,83% (± 8,88; n=6) of TRMs **(Fig 4.2.2.1 A)**. Interestingly, we observe a decrease of 3,69% of the LL TRMs in RA compared to OA synovium. On the other hand, we see an increase of 3,97% in the proportion of TRMs of RA SL compared to OA SL. On all the tissue, this represents a decrease of 2,42% of the proportion of TRMs in RA compared to OA **(Fig 4.2.2.1 B)**. However, these differences are not significant probably as a result of the heterogeneity between the patients and limited by the size of the cohort. Next, we wanted to determine if we observed differences between the different TRMs populations in both diseases. Therefore, we investigated the total proportion of CD68+, CD206+ and MERTK+ between OA and RA synovium. The proportion of MERTK+, CD68+ and CD206+ do not show any significant differences between OA and RA synovium **(Fig 4.2.2.1 B)**. Indeed, on average MERTK+ TRMs represent 7,36% (± 2,9; n=7) of total cells in OA synovium and 6,22% (± 2,9; n=9) of RA synovium. Although the proportion of MERTK+ is slightly lower on average in RA compared to OA, this difference is not significant. Similarly, the proportion of CD68+ is not significantly different between OA and RA, although on average the proportion of CD68+ in OA is higher than is RA with 14,37% (± 8,04; n=4) against 11,19% (± 2,18; n=3) **(Fig 4.2.2.1 C)**. However, this difference is due to an out-lying patient in the OA population which has 28,09% of CD68+ in its synovium. Moreover, the proportion of CD206+ TRMs shows no significant difference between OA and RA synovium. Interestingly, we found that the expression of MERTK, CD68 and CD206 was different across the regions of the synovium. For instance, CD68 mainly accumulates in the LL with high fluorescence intensity, while in the SL CD68+ cells are more dispersed **(Fig 4.2.2.1 D)**. Furthermore, CD206 co-localizes with CD68 in the SL, but is less present in the LL. Interestingly, MERTK is also found in the LL and co-localizes with CD68, however, MERTK+ cells in the LL are not CD68+ or CD206+ and are often brighter than the MERTK+ cells found in the LL **(Fig 4.2.2.1 D)**. We see similar observation between OA and RA, and this population will be further investigated later in this section. Thus, CD206+ cells seem to be more present in the SL which could explain the small increase in RA where on average 9,01% (± 2,01; n=5) of the cells are CD206+ while only 7,2% (± 3,5; n=6) of the cells

are CD206+ in OA **(Fig 4.2.2.1 C)**. Although this difference is not significant, it supports the idea that the RA synovium has a more active SL. Nevertheless, we decided to fully characterize the localisation of the TRMs within the LL and the SL based on the expression of those 3 markers. Thus, we investigated the proportion of single positive MERTK+, CD68+, CD206+, double positive MERTK+CD68+, CD68+CD206+, MERTK+CD206+, and triple positive MERTK+CD68+CD206+ in the LL and SL in both OA and RA. Consistent with the visual observations, the majority of the TRMs in the LL are CD68+ and MERTK+ **(Fig 4.2.2.1 E).** Indeed, CD68+ represent on average 27,72% (± 7,43; n=4) of the LL in OA and 27,79% (± 9,12; n=3) in RA when MERTK+ compose 18,85% (±11,24; n=7) of the LL in OA and 17,93% (± 12,50; n=10) in RA. On the other hand, only 5,13% (± 3,67; n=6) and 8,32% (± 5,59; n=5) of the LL cells are CD206+ in OA and RA respectively **(Fig 4.2.2.1 E)**. However, in the SL CD206+ TRMs are more abundant and represent on average 12,90% (± 5,29; n=6) of the SL cells in OA and 12,89% (± 5,61; n=5) in RA followed by CD68+ which compose 4,22% (± 1,82; n=4) of the SL in OA and 7,23% (± 3,76; n=3) in RA. Finally, MERTK+ cells are the least represented among the SL population in both OA and RA with on average 1,39% (± 0,92; n=7) and 3,13% (± 2,52; n=10) respectively **(Fig 4.2.2.1 E)**. Statistically, the proportion of MERTK+ and CD68+ is significantly higher in the LL compared to the SL in both disease **(Fig 4.2.2.1 F)**. Inversely, CD206+ proportion is higher in the SL compared to the LL, although this comparison is only statistically significant in OA **(Fig 4.2.2.1 F)**. Then, we investigated the double positive populations. In accordance with the previous findings, the proportion of MERTK+ CD68+ is higher in the LL compared to the SL. Even though the MERTK+ CD68+ are almost absent from the SL (0,13% ± 0,05; n=3) in OA, the difference is not significant between the two regions due to a high variability between patients **(Fig 4.2.2.1 G)**. Similarly to OA, the most represented double positives cells are MERTK+ CD68+ since MERTK+ and CD68+ are the most abundant cells in the LL. Once again, this population is not present in the SL but the difference between the two regions is not statistically relevant in this small patient sample (n=3) **(Fig 4.2.2.1 G)**. Interestingly, the MERTK+ CD206+ described by the transcriptomic data is very rare and only few cells are positive for both MERTK and CD206 especially in the SL. Beside the fact that MERTK+ cells in the SL do not co-localized with either CD68 or

CD206, we could expect that the CD206+ present in the LL would express MERTK+. However, it is not the case as the CD206+MERTK+ population only represent 0,32% (± 0,5; n=6) of the OA LL **(Fig 4.2.2.1 G)**. If we report this proportion to the number of cells this represent between 1 and 10 cells maximum per regions which can easily be attributed to an overlapping signal rather than physiological co-expression. Furthermore, in RA we detect 1,31% (± 1,24; n=5) potentially a result of an overlapping staining too **(Fig 4.2.2.1 G).** However, for the same reasons stated in OA, plus the variability between patients, we did not classify those cells as a separated population but as staining artefacts. On the other hand, CD68 and CD206 visually colocalize in the SL in both OA and RA synovium **(Fig 4.2.2.1 G)** whilst in the LL, as most of the TRMs are CD68+ we can expect some overlap with the CD206 staining. However, the proportion of CD206+CD68+ in the SL is on average 1,87% (± 1,24; n=4) in OA and 2,64% (±1,52; n=2) in RA **(Fig 4.2.2.1 E, G)**. Moreover, the proportion of CD206+CD68+ in the LL shows no difference to the proportion observed in the SL **(Fig 4.2.2.1 G)**. Since the co-localization in the SL was obvious **(Fig 4.2.2.1 D)**, I decide to investigate the proportion of CD206+ CD68+ among the total population of CD68+ within the SL and the LL. Therefore, within the CD68+ TRMs of the lining on average 51,90% (±21,11; n=4) expressed CD206 **(Fig 4.2.2.1 H)**. This is particularly relevant on 2 OA patients (out of the 4 tested) which have more than 70% of the CD68+ expressed CD206+. Moreover, because the proportion of CD68 in the lining layer is higher compared to the SL the percentage of CD206+ in the CD68+ dropped **(Fig 4.2.2.1 H)**. In a similar way, in OA SL as the percentage of CD206+ is higher than percentage of CD68+ we observed a smaller proportion of CD68+ within the CD206+ than in the opposite scenario **(Fig 4.2.2.1 H)**. This is not always the case, for instance in the LL the percentage of CD68+ in the CD206+ is very heterogeneous between patients, probably explained by the reflection of the low expression of CD206+ in this region **(Fig 4.2.2.1 E, F)**. Finally, the proportion of triple positives TRMs was not found at the exception of one OA patients with the high number of CD206+ cells in the LL (DATA not shown).

In parallel to this research, our lab and collaborator are investigating the role of PDPN in the crosstalk between macrophages and fibroblasts and its link to inflammation. Therefore, we investigated the

proportion of PDPN expressed in the TRMs population. As expected, due to the localisation of PDPN expression in the LL, it mainly colocalized with CD68+ and MERTK+ TRMs in both OA and RA but not with the CD206+ TRMs **(Fig 4.2.2.1 I)**. Furthermore, we found a significant increase in the proportion MERTK+ PDPN+ in OA synovium compared to RA **(Fig 4.2.2.1 J)**. This might be explained by the fact that TRMs population of the lining are more disrupted in RA. Nevertheless, those results suggest that PDPN is expressed in the LL TRMs.

Taken together, these data indicates that the proportion of TRMs (based on the expression of MERTK, CD68 and CD206) is higher in the LL compared to the SL in both diseases. Moreover, no major differences were observed between OA and RA beside a slight increase of the number of LL TRMs in OA compared to RA whilst RA patients present a small (but not statistically significant) increase in the SL TRMs. Furthermore, the expression of MERTK, CD68 and CD206 is distributed differently throughout the synovium. Indeed, the majority of the TRMs in the LL express CD68 and MERTK while the majority of the TRMs in the SL are CD206+. In consequence, MERTK+ CD68+ TRMs localize in majority in the LL while the CD206+ and CD206+CD68+ are the main population of the SL. Moreover, MERTK+ CD206+ population could not be characterized as almost no cells were detected in any of the patients tested. In a similar way, the triple positive was not detected in sufficient number to be classified as a population.

A

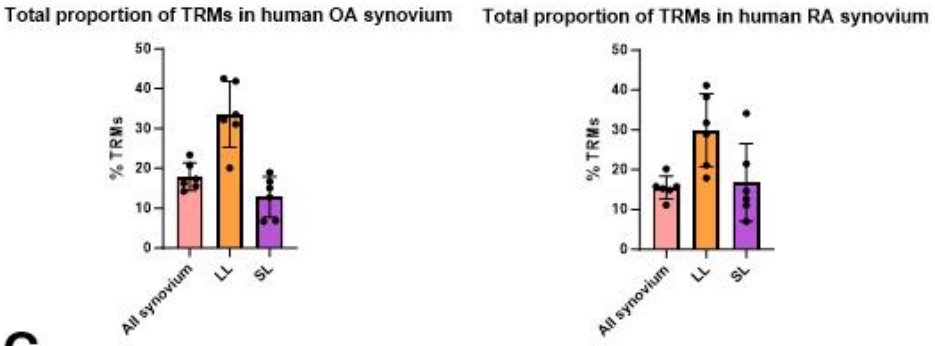
Total proportion of TRMs in human OA synovium
% TRMs
All synovium
LL
SL
Total proportion of TRMs in human RA synovium
% TRMs
All synovium
LL
SL

B

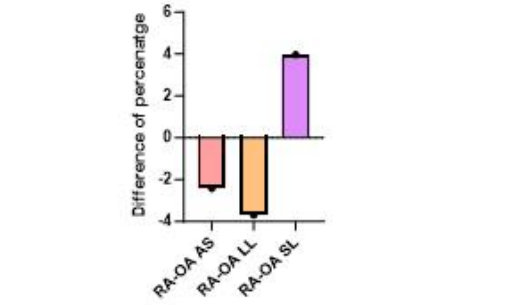
Difference of TRMs percentage between RA and OA
Difference of percentage
RA-OA AS
RA-OA LL
RA-OA SL

C

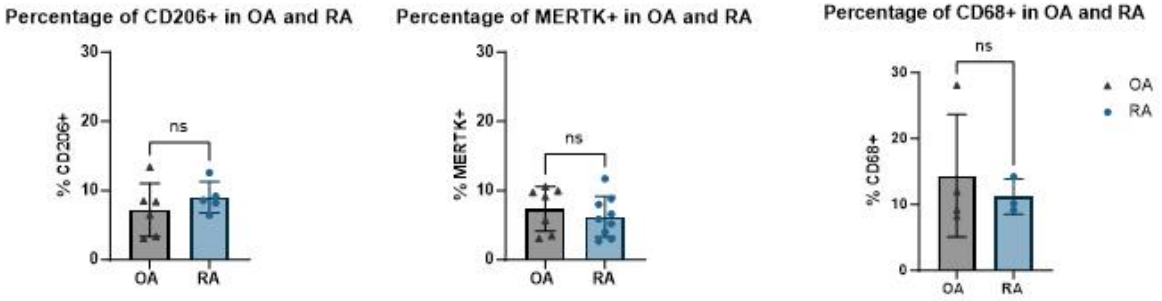
Percentage of CD206+ in OA and RA
% CD206+
ns
OA
RA
Percentage of MERTK+ in OA and RA
% MERTK+
ns
OA
RA
Percentage of CD68+ in OA and RA
% CD68+
ns
OA
RA
OA
RA

D

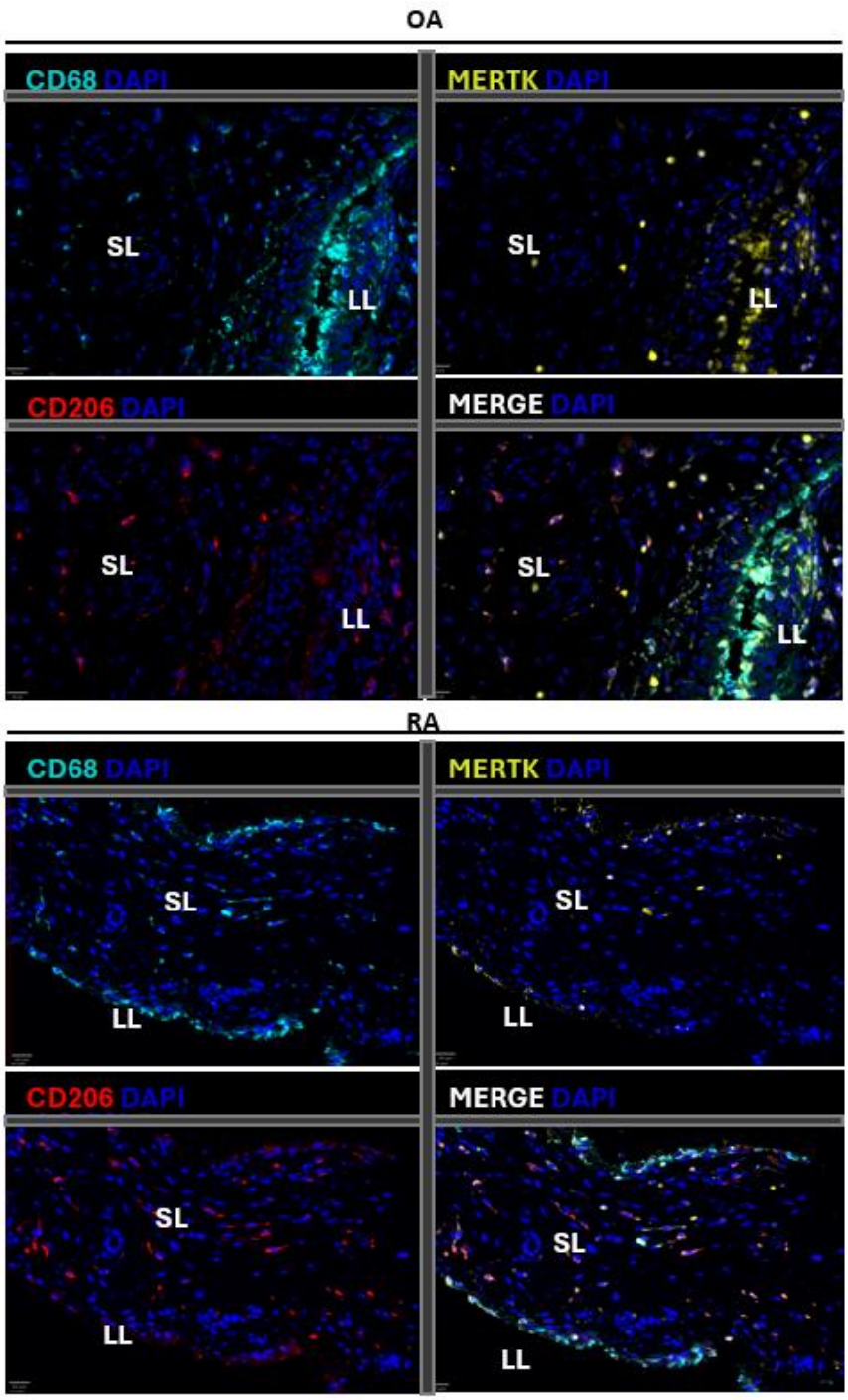
OA
CD68 DAPI
MERTK DAPI
CD206 DAPI
MERGE DAPI
SL
LL
RA
CD68 DAPI
MERTK DAPI
CD206 DAPI
MERGE DAPI
SL
LL

E

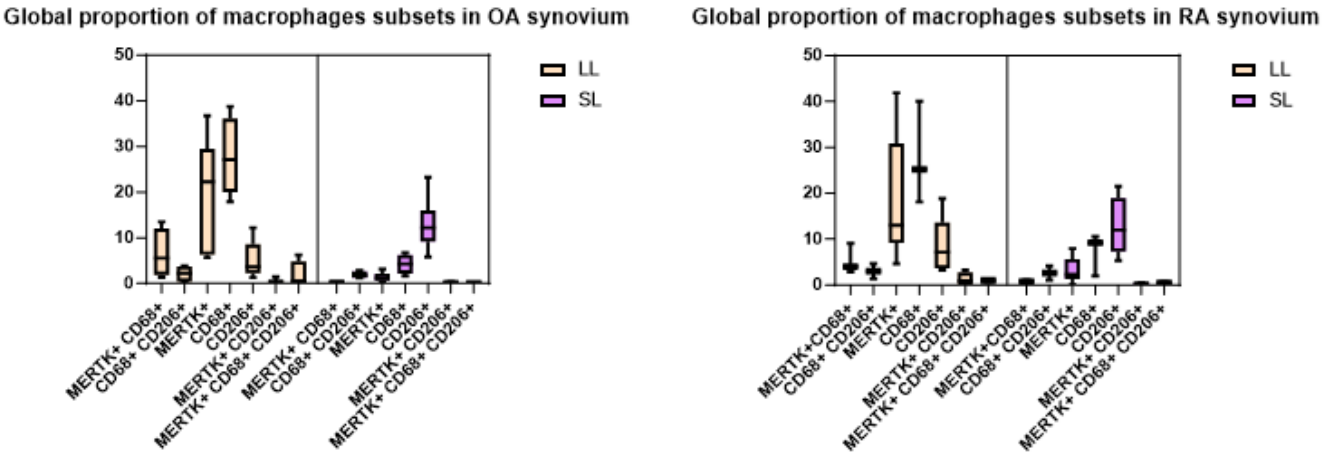
Global proportion of macrophages subsets in OA synovium
Global proportion of macrophages subsets in RA synovium
LL
SL
MERTK+ CD68+
CD68+ CD206+
MERTK+
CD68+
CD206+
MERTK+ CD68+ CD206+

F

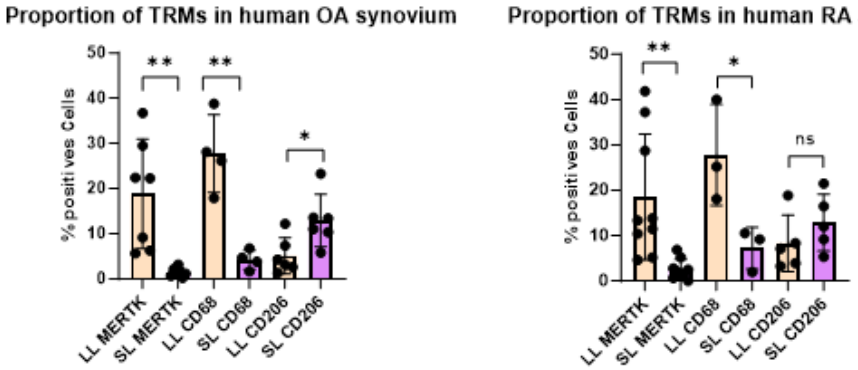
Proportion of TRMs in human OA synovium
Proportion of TRMs in human RA synovium
% positives Cells
LL MERTK
SL MERTK
LL CD68
SL CD68
LL CD206
SL CD206
ns

G

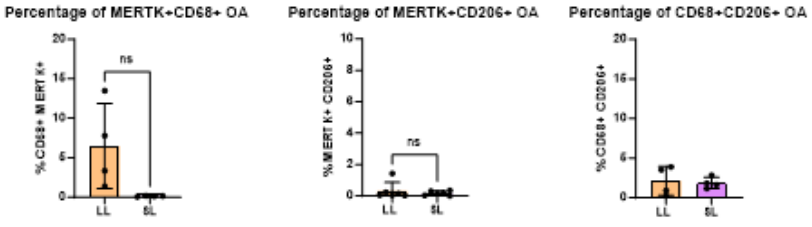
Percentage of MERTK+CD68+ OA
Percentage of MERTK+CD206+ OA
Percentage of CD68+CD206+ OA
ns
LL
SL

H

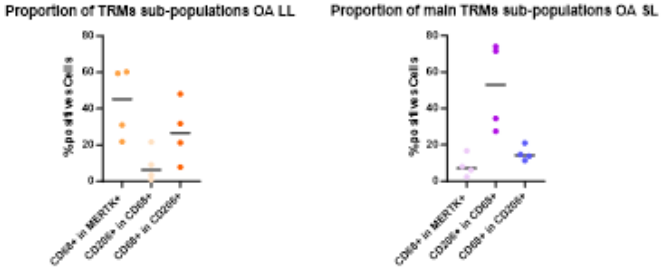
Proportion of TRMs sub-populations OA LL
Proportion of main TRMs sub-populations OA SL
% positives Cells

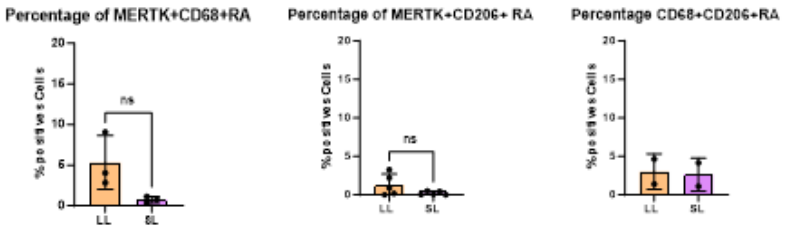
Percentage of MERTK+CD68+RA
Percentage of MERTK+CD206+ RA
Percentage CD68+CD206+RA
ns
LL
SL

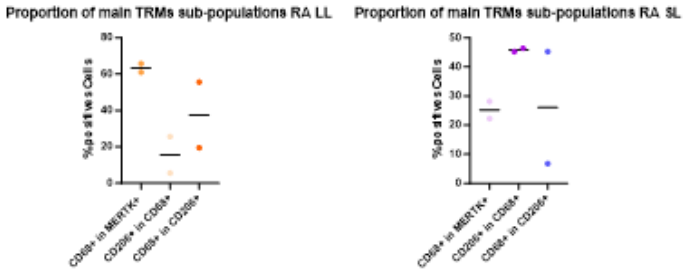
Proportion of main TRMs sub-populations RA LL
Proportion of main TRMs sub-populations RA SL
% positives Cells

I

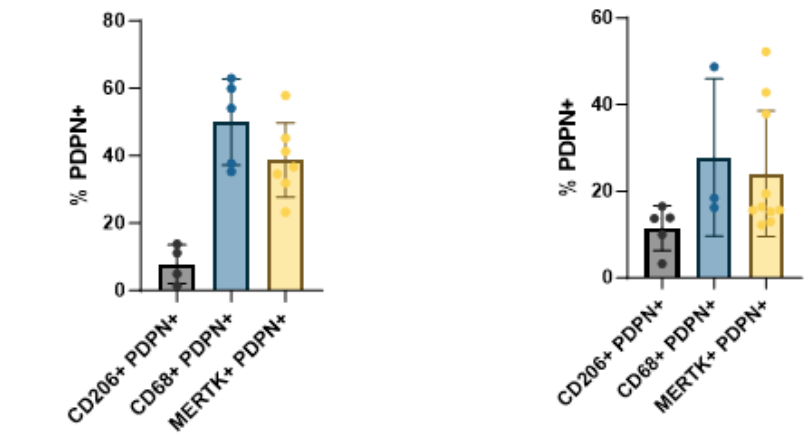
Percentage of PDPN+ in TRMs in OA
Percentage of PDPN+ in TRMs in RA
% PDPN+
CD206+ PDPN+
CD68+ PDPN+
MERTK+ PDPN+

J

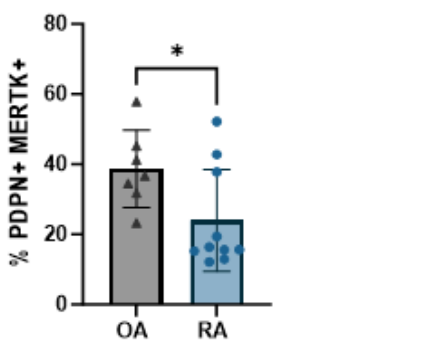
PDPN+ in MERTK+ in OA and RA
% PDPN+ MERTK+
*
OA
RA

**Figure 4.2.2.1: Characterization of the TRMs in OA and RA synovium by multiplex IF**

**A:** Total proportion of MERTK+ CD68+ CD206+ TRMs in all synovium (pink), LL (orange) and SL (purple) in OA (left) and RA (right). **B:** Difference of the TRMs proportion in RA minus the TRMs proportion in OA. AS: All synovium **C:** Comparison of the total proportion of MERTK+, CD68+ and CD206+ between OA (grey) and RA (blue). **D:** Multiplex IF staining showing the localization of CD68 (cyan), MERTK (yellow), CD206 (red) in OA (top panel) and RA (bottom panel). SL= sub-lining; LL=Lining layer. E: Relative proportions of the TRMs sub-population and their repartition into the LL (orange) and the SL (purple) in OA (left) and RA (right). F: Comparison of the proportion of MERTK+, CD68+ and CD206+ between the LL (orange) and SL (purple) in OA (left) and RA (right); paired student t-test. G: Comparison of the proportion of double positive MERTK+ CD68+, MERTK+CD206+, and CD206+CD68+ between the LL (orange) and SL (purple) in OA (left) and RA (right); paired student t-test. **H:** Percentage of CD68+ macrophages within the MERTK+ and percentage of CD206+ within the CD68+ in the LL (left panel) and SL (right panel) in OA (top) and RA (bottom). I: Percentage of PDPN+ in the CD206+ (grey), MERTK+ (blue), and CD68+ (yellow) TRMs in OA (left) and RA (right). J: Comparison of the total percentage of PDPN+ MERTK+ between OA (grey) and RA (blue). (*p < 0.05; **p < 0.01).

#### *4.2.2.2 Multiplex IF analysis of cellular senescence in TRMs*

Based on the expression of CD206, MERTK and CD68 observed above, we first investigated the proportion of p16+, p21+, yH2AX+ and p53+ in the MERTK+, CD68+ and CD206+ in the LL and SL of OA and RA synovium.

During the analysis, we noticed that the MERTK+ in the SL were brighter compared to the LL MERTK+ **(Fig 4.2.2.2 I)**. I first thought they might be the intermediate population repopulating the LL pool as they were mainly found at the interface between the LL and the SL **(Fig 4.2.2.2 I)**. However, in previous staining the exact same cells were staining for CD90 with a fluorescence intensity 20 times superior to the specific perivascular signal (data not shown). This interaction was lost when we changed the CD90 antibody. We concluded it was a non-specific interaction via the FC receptor. This is also observed for yH2AX staining that stain in a non-specific way to those cells **(Fig 4.2.2.2 J).** It is still interesting to speculate on the identity of those cells. Is it a regulatory macrophages population $MERTK^{HIGH}$ actively involved in efferocytosis? Alternatively, if we considered the non-specific interaction due to a high expression of FC receptor, they still could be macrophages, but they are negative for CD68+. Dendritic cells might be possible, but neutrophils are a better option as their shape is round. Nevertheless, we

excluded this population from the analysis as we cannot assumed the true phenotype of those cells. Thus, p16 appears to be more expressed in the CD68+ cells of the LL compared to the SL in both diseases. However, the differences were not significant though this may be due to the small sample size. Similarly, the percentage of CD206+ p16+ is not significantly different between the LL and SL, although on average, there is more p16+ CD206+ TRMs in the LL (12,74% ±10,98; n=5) than in the SL (5,81% ±5,1; n=5) in OA **(Fig 4.2.2.2 A)**. Moreover, a similar percentage of p16+ in the CD206+ TRMs is observed on average in RA synovium.

Next, the percentage of p21+ CD68+ is higher in the LL compared to the SL in all OA and RA patients but the limited patient number does not give statistical relevance to this difference **(Fig 4.2.2.2 B)**. Finally, within the CD206+ TRMs, the p21+ are on average more abundant in the LL (18,68% ±15,11; n=6) compared to the SL (8,27% ±6,17; n=6) in OA, this is also observed in the LL in RA (18,90% ±7,84; n=5) compared to the SL (8,09% ±6,39; n=5). Whilst the average proportion of p21+ CD206+ is higher in the LL compared to the SL, the differences are not statistically significant, perhaps due to the heterogeneity between patients.

Then, we assessed for the presence of DNA damage by looking at the proportion of yH2AX+ in the TRMs. First, we notice that on the 4 tested in OA 3 have more yH2AX+ CD68+ in the LL for an average of 6,1% (±3,17; n=4) compared to the SL where 2,79% (±2,80; n=6) of the CD68+ are yH2AX+ **(Fig 4.2.2.2 C)**. In RA, 2 out of 3 patients have more yH2AX+ CD68+ in the LL compared to the SL with an average of 7,69% (±4,16; n=3) and 4,36% (±1,64; n=3) respectively **(Fig 4.2.2.2 C)**. Furthermore, the percentage of yH2AX+ within the CD206+ is very heterogenous in OA, no pattern between patients can be identify as some have more yH2AX+ CD206+ in the LL, other more in the SL and other have similar percentage. Although the average suggests more positive cells in the LL (11,73% ±7,38; n=6) compared to the SL (8,0% ±5,8; n=6) in OA **(Fig 4.2.2.2 C)**. Additionally, the expression of p53 was measured to further investigate the stress response in the TRM populations. As described earlier, most of the p53 signal detected is in the LL. As expected, CD68+ p53+ TRMs are mainly found in the LL and are very rare in

the SL in both OA and RA. For instance, on average, 32,69% (±8,48; n=3) of the LL CD68+ are p53+ compared to only 4,83% (±3,36; n=3) in OA SL **(Fig 4.2.2.2 D)**. This also true in RA, we observed 43,46% (±26,27; n=3) of the CD68+ p53+ in the LL whereas only 2,18% (±0,57; n=3) in the SL **(Fig 4.2.2.2 D)**. At last, the percentage of CD206+ p53+ in the LL varies a lot between patients while it remains very low in the SL regardless of the disease **(Fig 4.2.2.2 D)**. For instance, within the SL, only 0,55% (±0,55; n=5) of the CD206+ are p53+ in OA and only 1,16% (±0,89; n=4) in RA although CD206+ are the most abundant TRMs in the SL. Examples of the staining are presented in E **(Fig 4.2.2.2 E)**.

As we could not compared the LL MERTK+ with the SL MERTK+ population, we compared the LL MERTK+ p16 expression between OA and RA. Interestingly, we noticed a significant increase of p16+ MERTK+ in the LL in RA compared to OA **(Fig 4.2.2.2 F)**. This difference is specific to p16 and is not seen with p21, p53 and yH2AX. Furthermore, other LL TRMs such as CD68+ have the same percentage of p16 in OA and RA suggesting that the difference is specific to the MERTK+ population **(Fig 4.2.2.2 F)**. This might underline a differential senescence into the TRMs MERTK+ between the diseases and may reflect a different proliferation. We can speculate that in OA the MERTK+ are more renewed compared to RA which could explain the reduction of this population often observed (26).

Next, we investigated the percentage of senescence in the MERTK+CD68+ (the main double positive population in the LL) and in the CD68+CD206+ (the main double positive population in the SL). As expected, the majority of MERTK+ CD68+ are p53+ in OA (54,60% ±4,19; n=4) and in RA (60,62% ±13,37; n=3) **(Fig 4.2.2.2 G)**. Interestingly, when we separate the MERTK+ that are CD68- in the LL and look at the expression of p53, we notice that the vast majority of the p53+ are in the MERTK+ CD68+ but not in the CD68- **(Fig 4.2.2.2 H)**. This result is also found in RA where the MERTK+CD68- are not positive for p53. Furthermore, this seems to be the same trend with the other senescence markers suggesting that p53 is mainly associated with CD68 expression but not MERTK. This could suggest that MERTK+ macrophages only expressed p53 when they are activated characterized by a high expression of CD68, or the expression of p53 increased the expression of CD68+ triggering more activation.

Furthermore, on average 20,14% (±6,66; n=4) and 24,34% (±14,9; n=3) of MERTK+CD68+ are p16+ in OA and RA respectively **(Fig 4.2.2.2 G)**. Interestingly, the proportion of p21+ is higher in the MERTK+CD68+ in RA (44,81% ±22,17; n=3) than in OA (17,55% ±4,64; n=3) **(Fig 4.2.2.2 G)**. But the variability between the RA patients is too high to conclude that there is a real difference between the two diseases. In addition, on average 10,48% (±4,39; n=4) of the MERTK+CD68+ have the DNA damage marker yH2AX+ in OA **(Fig 4.2.2.2 G)**. Similarly, in RA, the proportion of yH2AX+ cells are lower compared to the proportion of p21, p16, p53 found in the MERTK+CD68+ and represent 14,17% (±2,92; n=3) **(Fig 4.2.2.2 G)**. Finally, within the SL, CD68+CD206+ TRMs have a lower expression of the senescence markers compared to the LL population. This is especially true for p53, where only 3,04% (±2,42; n=3) in OA and 5,1% (n=2) in RA of the CD206+CD68+ expressed p53 **(Fig 4.2.2.2 G)**. Furthermore, yH2AX+ represent 8,87% (±3,44; n=3) of the CD206+CD68+ population which is close to the percentage observed in all the population studied earlier **(Fig 4.2.2.2 G)**. At last, p21+ are more common among the CD206+CD68+. Notably in OA, where 22,66% (±11,64; n=3) of the SL TRMs are p21+ **(Fig 4.2.2.2 G)**.

To conclude the analysis of senescence in the TRMs using multiplex histology, we found that there is a trend showing an increase of senescence in the LL compared to the SL. Indeed, in the populations mainly associated with the LL such as MERTK+ and/with CD68+, p16, p53 and p21 are increased compared to their counterpart in the SL. Moreover, the CD206+ population is mainly associated to the SL and only a small proportion of CD206+ cells are positive for p16, p21, yH2AX and p53 suggesting that TRMs are more subject to senescence and DNA damage when they are in the LL. In addition, the LL MERTK+ TRMs appeared more senescent in RA compared to OA suggesting different regulation between the disease that could lead to less efferocytosis in RA or more proliferation in OA LL.

**Figure 4.2.2.2: Multiplex IF analysis of cellular senescence in TRMs.**

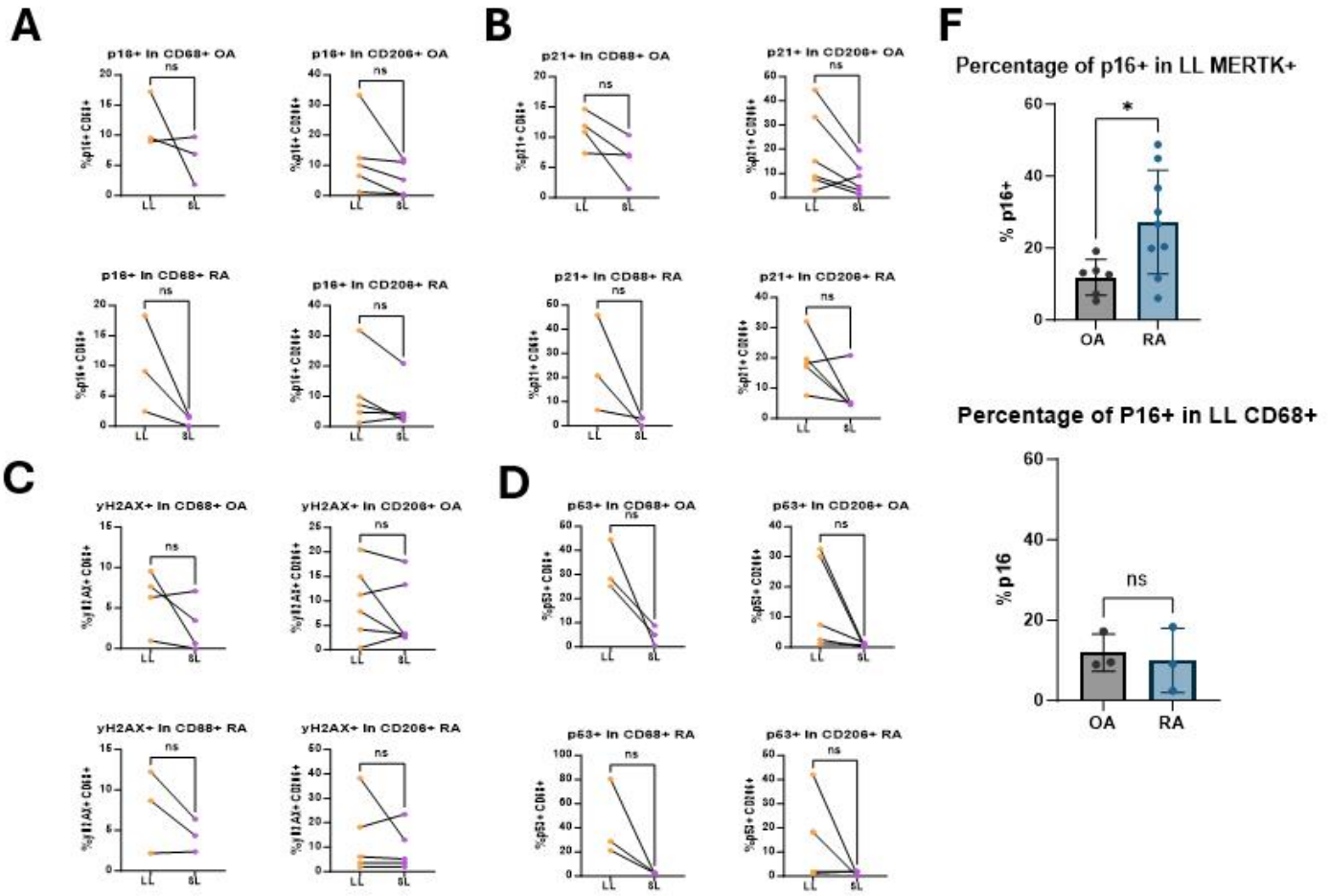


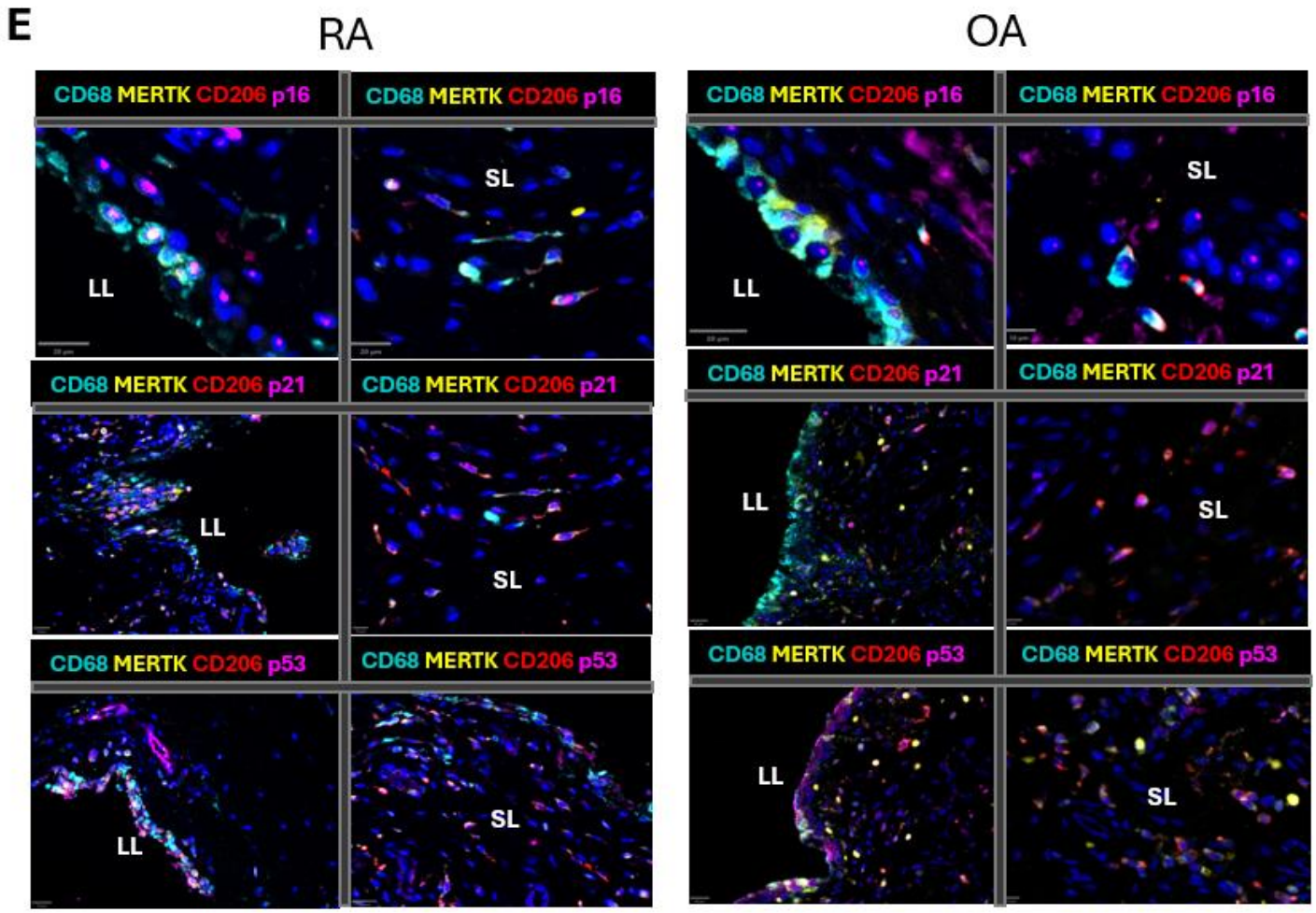

G

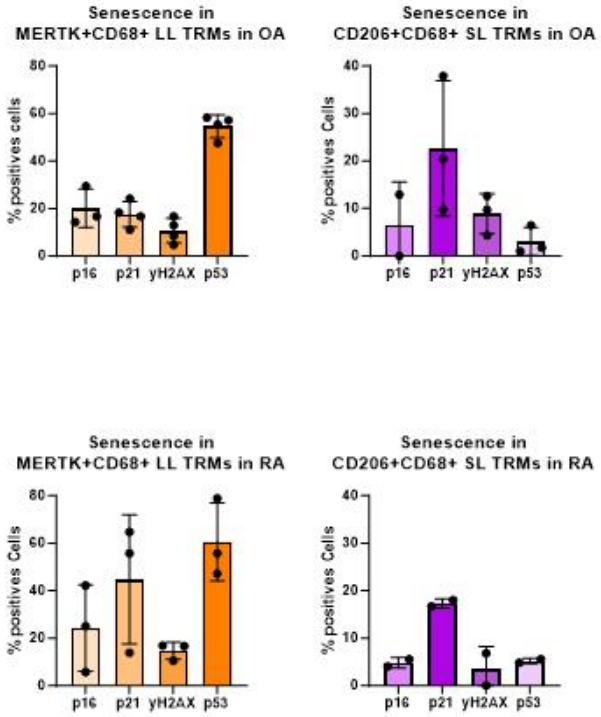
Senescence in MERTK+CD68+ LL TRMs in OA
% positives cells
p16 p21 yH2AX p53
Senescence in CD206+CD68+ SL TRMs in OA
% positives Cells
p16 p21 yH2AX p53
Senescence in MERTK+CD68+ LL TRMs in RA
% positives Cells
p16 p21 yH2AX p53
Senescence in CD206+CD68+ SL TRMs in RA
% positives Cells
p16 p21 yH2AX p53

H

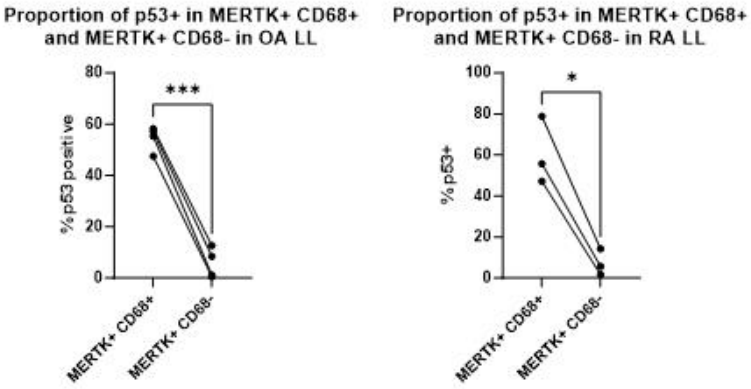
Proportion of p53+ in MERTK+ CD68+ and MERTK+ CD68- in OA LL
***
% p53 positive
MERTK+ CD68+
MERTK+ CD68-
Proportion of p53+ in MERTK+ CD68+ and MERTK+ CD68- in RA LL
*
% p53+
MERTK+ CD68+
MERTK+ CD68-

I

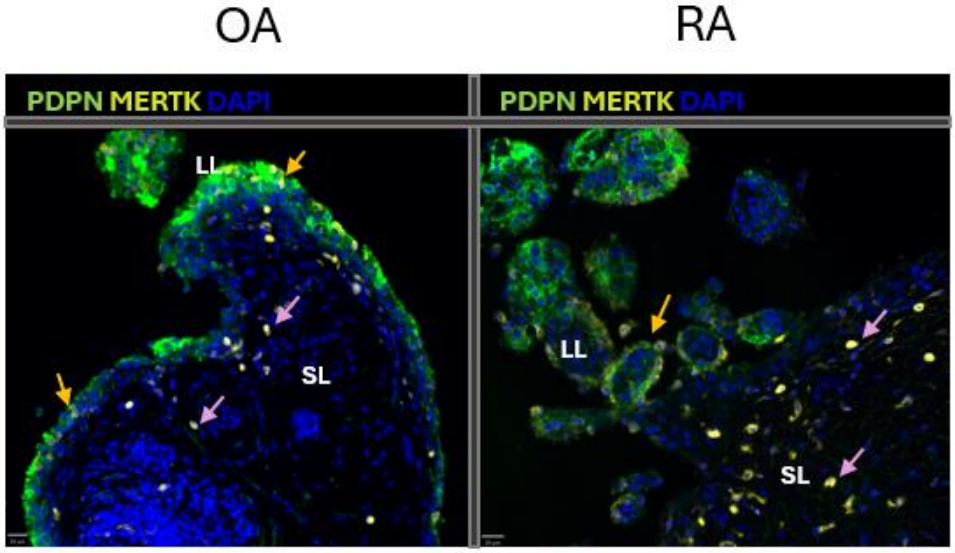
OA
RA
PDPN MERTK DAPI
LL
SL
PDPN MERTK DAPI
LL
SL

J

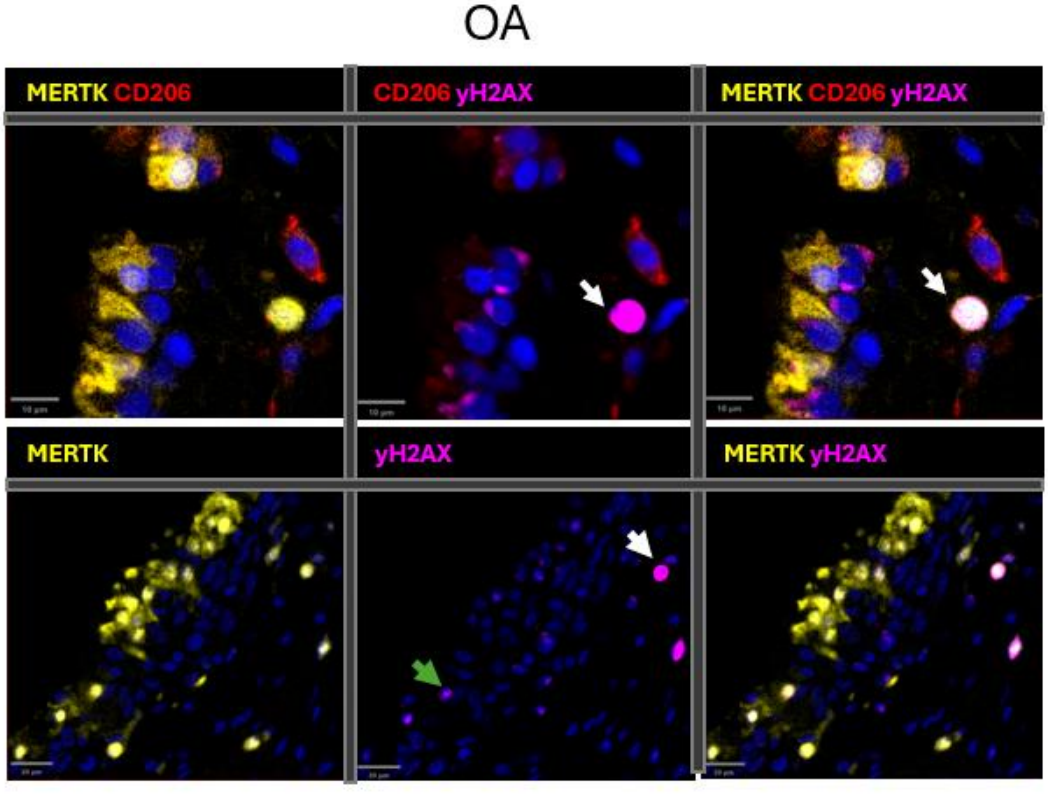
OA
MERTK CD206
CD206 yH2AX
MERTK CD206 yH2AX
MERTK
yH2AX
MERTK yH2AX

**Figure 4.2.2.2: Multiplex IF analysis of cellular senescence in TRMs.**

**A:** Percentage of p16 in CD68+ and CD206+ TRMs in the LL (orange) compared to the SL (purple) in OA (top) and RA (bottom), paired student t-test. **B:** Percentage of p21+ in CD68+ and CD206+ TRMs in the LL (orange) compared to the SL (purple) in OA (top) and RA (bottom), paired students t-test. **C:** Percentage of yH2AX in CD68+ and CD206+ TRMs in the LL (orange) compared to the SL (purple) in OA (top) and RA (bottom), paired students t-test. **D:** Percentage of p53 in CD68+ and CD206+ TRMs in the LL (orange) compared to the SL (purple) in OA (top) and RA (bottom), paired students t-test. **E:** multiplex IF staining showing p16+, p21+, yH2AX+, and p53+ (Magenta) in TRMs CD68 (cyan), MERTK (yellow), and CD206 (red) in LL and SL of OA (right panel) and RA (left panel), DAPI (blue). **F:** Top panel= Percentage of p16+ in LL MERTK+ in OA (grey) and RA (blue) and percentage of p16; Bottom panel= Percentage of p16+ in LL CD68+ in OA (grey) and RA (blue); unpaired student t-test. **G:** Percentage of p16+, p21+, yH2AX+, and p53+ in LL MERTK+CD68+ (orange) and CD206+ CD68+ (purple) in OA (top) and RA (bottom). **H:** Percentage of p53+ in MERTK+CD68+ compared to MERTK+ CD68- in the LL In OA (left) and RA (right), paired student t-test. **I:** multiplex IF staining showing the MERTK+ in the LL and the MERTK+ in the SL in OA (left) and RA (right); PDPN (green), MERTK (yellow), DAPI (blue); pink arrows= SL MERTK+, Orange arrows= LL MERTK+. **J:** multiplex IF showing non-specific staining of yH2AX (magenta) in SL MERTK+ cells compared to LL MERTK+; CD206 (red) MERTK (yellow), DAPI (blue). Green arrow = yH2AX+ nuclear signal White arrow = MERTK+ SL cells with non-specific signal. (*$p < 0.05$; ***$p < 0.001$).

#### *4.2.2.3 Analysis of the TRMs senescence using Spectral flow cytometry*

One advantage of histology is that when cells expressed the same markers, it is still possible to use their localization within the tissue to distinguish potential subsets. For instance, CD68 was expressed on most of the TRMs in the LL and the SL but it was possible to separate the CD68+ of the LL and the SL based on their respective localization. On the other hand, in flow cytometry it is more challenging to separate the subsets without specifics markers. Therefore, in the flow cytometry analysis I use CD68 and MERTK to investigate the TRMs population within the CD45+ CD11C-. The vast majority of CD45+ CD11C- macrophages in OA and RA patients were either MERTK+ or MERTK+CD68+ while only a small proportion were MERTK-CD68- and the CD68+ MERTK- were not detected in most patients **(Fig 4.2.2.3 A)**. This leads to the investigation of senescence in the MERTK+ and MERTK+ CD68+. As described, in histology, CD68+ MERTK+ and MERTK+ were associated mainly to the LL while a small proportion of MERTK+ was found in the SL. However, the SL MERTK+ appeared to have nonspecific staining for many markers questioning the true phenotype of this population **(Fig 4.2.2.2 F)**. Furthermore, transcriptomic

data classified all the TRMs as CD68+, MERTK+ regardless of their tissue location (25). When histology only reveals the highest expressing cells, FACS may be more representative of the transcriptomic data. In this case, MERTK+ and CD68+ are not sufficient to identify the LL from the SL TRMs. Nevertheless, we investigated the expression of p16, p21, p53, and the proportion of yH2AX in the MERTK+ and MERTK+ CD68+ macrophages. Overall, we observed, that MERTK+ and CD68+ shared the same senescence profile characterized by a high proportion of p16+, an heterogenous expression of p21+ among patients, a low proportion of yH2AX+ and no p53+ **(Fig 4.2.2.3 B)**. Then, when we compared the MERTK+ and the CD68+ MERTK+, we noticed that the proportion of p21+, p53+, and yH2AX+ but not p16+ are significantly increased in the MERTK+ compared to the CD68+ MERTK+ **(Fig 4.2.2.3 C)**. Similarly, in RA the same proportions are increased in the MERTK+ compared to the CD68+ MERTK+ but are not statistically significant **(Fig 4.2.2.3 C)**. Interestingly, we notice more heterogeneity between patients for all the markers in the MERTK+ in OA and RA.

In order to understand those variations, I tried to phenotype further the MERTK+ and CD68+ MERTK+ population using the expression of CX3CR1 and HLA-DR. Originally, we chose those markers to separate the LL and SL TRMs respectively. However, after further investigation we realized that those markers are good to classify the population in murine model but their expression in human remains unclear. Nevertheless, we identified 8 populations within the MERTK+ and CD68+ MERTK+ define in tables 1.2.4 A and B. Thus, the most frequent population in MERTK+ TRMs in OA and RA is CX3CR1+ HLA-DR+ and the most frequent population in the CD68+ MERTK+ is also CX3CR1+ HLA-DR**+ (Table 2 A, B)**. Interestingly, within the MERTK+ macrophages we observed 2 groups of patients with different proportion in the sub populations. Indeed, 4 patients have a high proportion of MERTK+ CX3CR1+ HLA-DR+ while the proportion of MERTK+ CX3CR1- HLA-DR- and MERTK+ CX3CR1+ HLADR- are low **(Fig 4.2.2.3 D)**. Oppositely, the second group have higher proportion of MERTK+ CX3CR1- HLA-DR- and MERTK+ CX3CR1+ HLADR- compared to the MERTK+ CX3CR1+ HLA-DR+ **(Fig 4.2.2.3 D)**. However, no differences between the two groups in the CD68+ MERTK+ are observed and the majority of MERTK+ CD68+ are CX3CR1+ HLA-DR+ **(Fig 4.2.2.3 E)**. Interestingly, the senescence is not the same in the

different sub population within the MERTK+ macrophages. Indeed, the proportion of p16+ and p21+ are higher in the HLA-DR+ macrophages compared to the HLA-DR- sub populations in both diseases **(Fig 4.2.2.3 F)**. Furthermore, there is a slight decrease in the proportion of p53+ and yH2AX in the HLA-DR+ sub population compared to the HLA-DR- suggesting that those cells have more DNA damage associated senescence than the HLA-DR+ sub population **(Fig 4.2.2.3 F)**. This senescence profile is not changing according to the group in which patients are belonging suggesting that the senescence observed is intrinsic to the population regardless of its proportion in tissue. However, the number of cells in some patients was low which may induce some error. Nevertheless, the patient in group 1 should have more p16+ and p21+ macrophages compared to the second group were most of the MERTK+ are HLA-DR negative have more DNA damage associated senescence. Furthermore, in the MERTK+ CD68+ population p16 and p21 is also higher in the HLA-DR+ sub population while the proportion of yH2AX+ is higher in the HLA-DR- **(Table 2 A, B)**.

In parallel, we were intrigued by the CD11c population. A recent study demonstrated that neutrophils expressed CD11c and its importance in the process of neutrophils maturation (119). As neutrophils plays an important role in RA and OA pathology, we investigated some of the senescence markers in the total CD11c+ cells. Notably, yH2AX as neutrophils are known to produce ROS during inflammation. Interestingly, we noticed that in RA, the proportion of yH2AX+ in the CD11c+ cells is increased on average compared the same population in OA **(Fig 4.2.2.3 G)**. Moreover, when compared to the percentage of yH2AX+ in CD11c- macrophages, the CD11c+ have a higher proportion of DNA damage in both OA and RA **(Fig 4.2.2.3 H)**.

In summary, in the FACS analysis, we were not able to separate the TRMs population of the LL and SL because of a lack of specific markers such as TREM2 (LL TRMs) or FOLR2 (SL TRMs) that should be include in the next FACS panel. However, based on the expression of MERTK, CD68, CX3CR1 and HLA-DR we manage to identify different macrophages sub populations present in different proportion according to the patient. For instance, 2 patients in OA and 1 in RA have a high proportion of CD68-

MERTK+ HLA-DR+ CX3CR1+ compared to others. This might suggest a higher level of infiltrated pro inflammatory monocytes HLA-DR+. Interestingly, those population exhibits a higher p16 and p21 expression compared to HLA-DR- while the later have an increase of yH2AX+ and p53+ in both diseases. While the possibility that those differences might be due to a non-specific binding to Fc receptor is not excluded, it is interesting to further characterized the implication of differential senescence in the infiltrated cells compared to the resident.

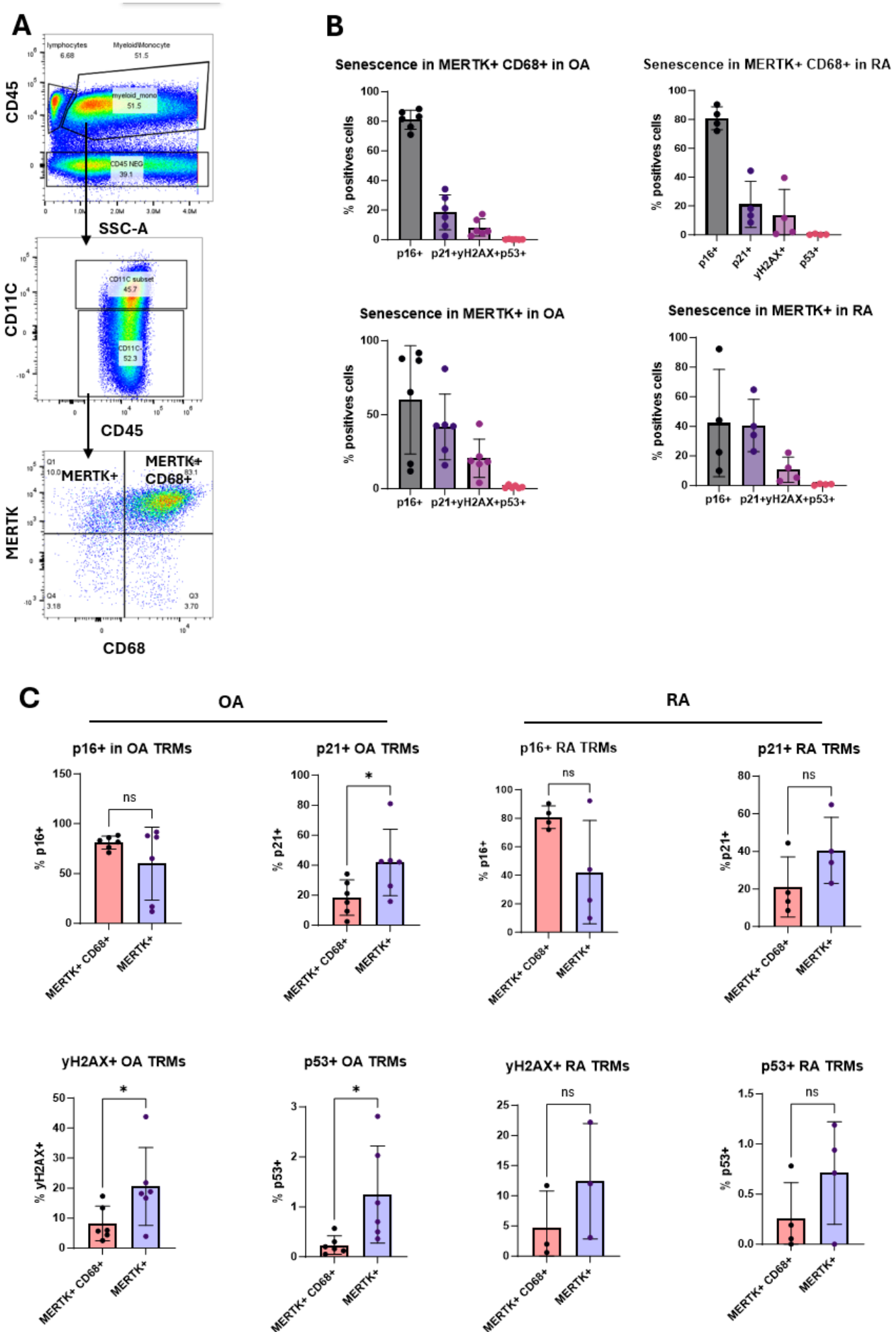
A
lymphocytes
6.68
Myeloid\Monocyte
51.5
CD45
myeloid_mono
51.5
CD45 NEG
39.1
SSC-A
CD11C
CD11C subset
45.7
CD11C-
52.3
CD45
MERTK
MERTK+
MERTK+
CD68+
83.1
Q1
10.0
Q4
3.18
Q3
3.70
CD68
B
Senescence in MERTK+ CD68+ in OA
% positives cells
p16+
p21+yH2AX+p53+
Senescence in MERTK+ CD68+ in RA
% positives cells
p16+
p21+
yH2AX+
p53+
Senescence in MERTK+ in OA
% positives cells
p16+
p21+yH2AX+p53+
Senescence in MERTK+ in RA
% positives cells
p16+
p21+yH2AX+p53+
C
OA
RA
p16+ in OA TRMs
% p16+
ns
MERTK+ CD68+
MERTK+
p21+ OA TRMs
% p21+
*
MERTK+ CD68+
MERTK+
p16+ RA TRMs
% p16+
ns
MERTK+ CD68+
MERTK+
p21+ RA TRMs
% p21+
ns
MERTK+ CD68+
MERTK+
yH2AX+ OA TRMs
% yH2AX+
*
MERTK+ CD68+
MERTK+
p53+ OA TRMs
% p53+
*
MERTK+ CD68+
MERTK+
yH2AX+ RA TRMs
ns
MERTK+ CD68+
MERTK+
p53+ RA TRMs
% p53+
ns
MERTK+ CD68+
MERTK+

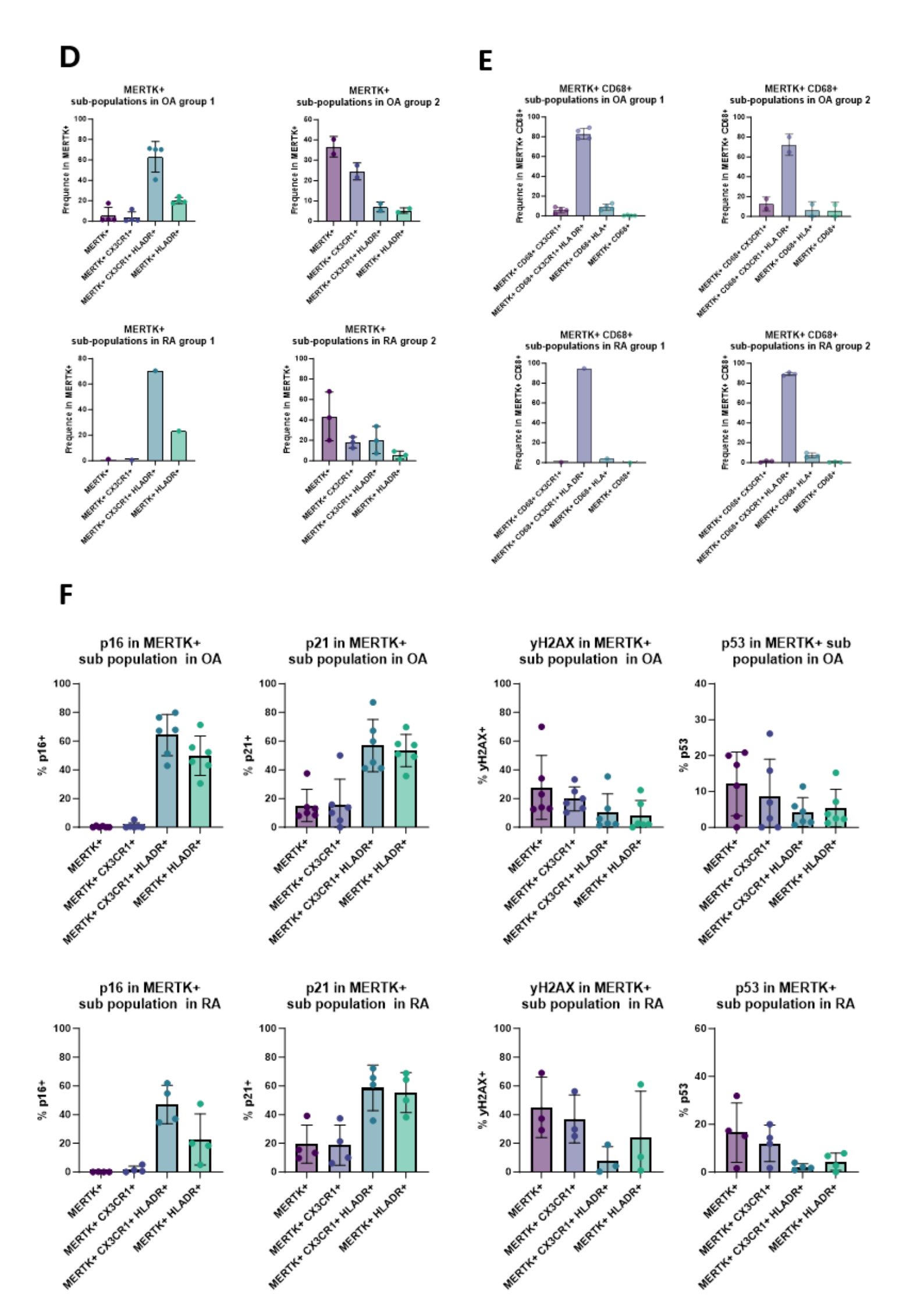
D
MERTK+
sub-populations in OA group 1
MERTK+
sub-populations in OA group 2
MERTK+
sub-populations in RA group 1
MERTK+
sub-populations in RA group 2
Frequence in MERTK+
MERTK+
MERTK+ CX3CR1+
MERTK+ CX3CR1+ HLADR+
MERTK+ HLADR+
E
MERTK+ CD68+
sub-populations in OA group 1
MERTK+ CD68+
sub-populations in OA group 2
MERTK+ CD68+
sub-populations in RA group 1
MERTK+ CD68+
sub-populations in RA group 2
Frequence in MERTK+ CD68+
MERTK+ CD68+ CX3CR1+
MERTK+ CD68+ CX3CR1+ HLA DR+
MERTK+ CD68+ HLA+
MERTK+ CD68+
F
p16 in MERTK+
sub population in OA
p21 in MERTK+
sub population in OA
yH2AX in MERTK+
sub population in OA
p53 in MERTK+ sub
population in OA
p16 in MERTK+
sub population in RA
p21 in MERTK+
sub population in RA
yH2AX in MERTK+
sub population in RA
p53 in MERTK+
sub population in RA
% p16+
% p21+
% yH2AX+
% p53
MERTK+
MERTK+ CX3CR1+
MERTK+ CX3CR1+ HLADR+
MERTK+ HLADR+

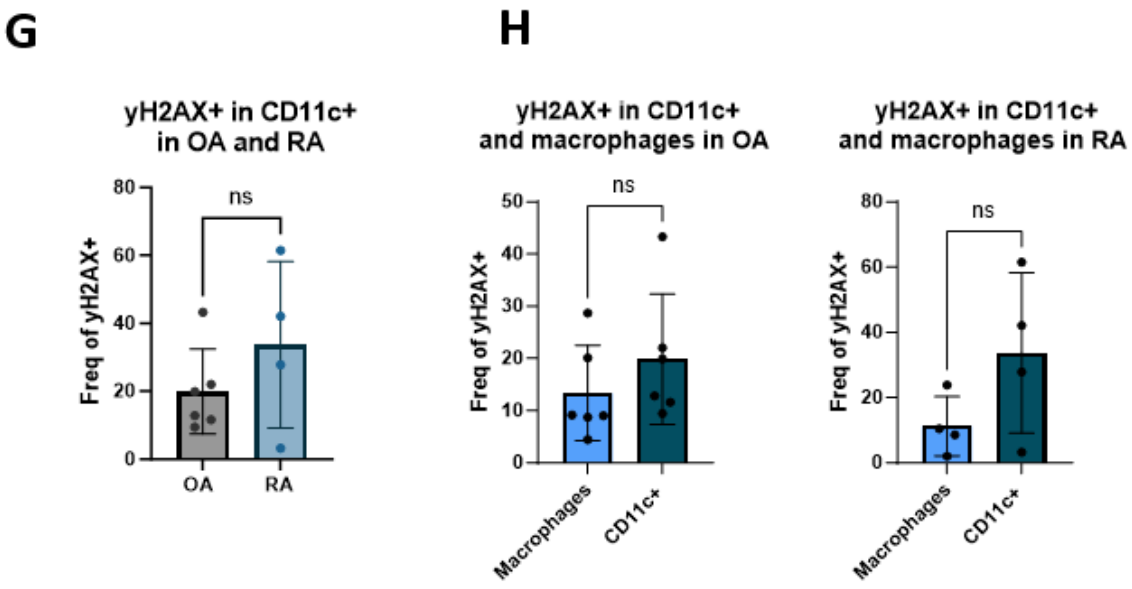


**Figure 4.2.2.3: Analysis of the TRMs senescence using Spectral flow cytometry**

**A:** Gating strategy to classify the TRMs population based on CD45+, CD11c-, MERTK+, and MERTK+ CD68+. **B:** Top panel = Percentage of p16+, p21+, yH2AX+, and p53+ in MERTK+CD68+ in OA (left) and RA (right). Bottom panel = Percentage of p16+, p21+, yH2AX+, and p53+ in MERTK+ in OA (left) and RA (right). **C:** Comparison of p16+, p21+, yH2AX+, and p53+ percentage between MERTK+CD68+ (light red) and MERTK+ (light blue) in OA (left) and RA (right). Paired Students t-test; OA (n=6), RA (n=4). **D:** Percentage of the subpopulations expressing CX3CR1or HLADR within the MERTK+ macrophages classified in 2 patients' groups: group 1 (left) in OA (top) RA (bottom) and group 2 (right) in OA (top) and RA (bottom). **E:** Percentage of the subpopulations expressing CX3CR1 or HLADR within the MERTK+ CD68+ macrophages classified in 2 patients' group: group 1 (left) in OA (top) RA (bottom) and group 2 (right) in OA (top) and RA (bottom). **F:** Percentage of p16+, p21+, yH2AX+, and p53+ in MERTK+ macrophages in OA (top) and in RA (bottom). **G:** Percentage of yH2AX+ in CD11c+ in OA (grey) and in RA (blue) **H**: Percentage of yH2AX+ in CD11c+ (dark green) compared to the percentage of yH2AX+ in macrophage (blue) in OA (left) and in RA (right); paired Students T-test OA (n=6), RA (n=4). (*p < 0.05).

## 4.2.3 lymphocytes

### *4.2.3.1 Analysis of the infiltrated lymphocyte populations*

" Synovitis" is seen in many forms of arthritis. Particularly in RA, as it has an autoimmune origin leading to chronic inflammation of the joint. However, synovitis is also common in OA patients as the regulation of the synovium is impaired leading to increased infiltration of immune cells in the SL. Among the main infiltrated cells, macrophages and myeloid are commonly found throughout the tissue. In addition, lymphocyte infiltration is also typical. Indeed, the presence of T cells and B cells clusters within the SL

indicate a fully established and chronic inflammatory state characterized by recruitment of immune cells, followed by the organization into aggregates, and failure to resolve. If the accumulation of lymphocytes persists, reorganization of the synovium may occur leading to the formation of tertiary lymphoid structures (TLS) supporting even further the survival of T and B cells. Those mechanisms are supported by fibroblasts which remodel the matrix and secret a range of chemokines and cytokines maintaining the survival and recruitment of leucocytes. Furthermore, immune senescence is characteristic of aging and is often associated with decrease in immune response and immune surveillance. It also participates to the overall low-grade inflammation (122). However, the impact of immune senescence on synovial pathology in RA and OA remains unclear.

First, we refined the analysis of the CD3, CD20 and CD45 staining to have a better resolution of the aggregates. Indeed, the cellular density in the aggregates is high leading to overlap of fluorescence, and a bad segmentation. To overcome this issue, we decreased the diameter value of cells expansion around the nuclei from 5µm to 3,5µm to capture more cells within the aggregates. Because of this, the number of detected lymphocytes is slightly increase compared to the population analysis in 1.2 but the proportion remains similar. Therefore, we first investigated the proportion of CD45+ cells in OA and RA patients. Although CD45 is a common marker of differentiated hematopoietic cells, it is not detected in CD68+ TRMs but strongly overlap with CD3+ and CD20+ cells **(Fig 4.2.3.1 A, B)**. As expected, we saw a higher proportion of CD45+ cells (12,20% ± 4,17; n=7) in RA patients compared to OA (7,65% ± 0,84; n=4) **(Fig 4.2.3.1 C)**. In line with this finding, the percentage of CD3+ T cells in RA (13,31% ± 4,72; n=10) is higher on average compared to OA synovium (4,12% ± 2,43; n=7) **(Fig 4.2.3.1 D)**. Furthermore, the number of B cells varies considerably between patients. Indeed, although most of RA patients have CD20+ cells in the synovium, their proportion is heterogenous and depends on the presence of aggregates. Nevertheless, on average, the synovium in RA is composed of 3,71% (± 2,73; n=7) B cells, while in OA, B cells were detected in only 2 patients and represent 1,07% (± 0,30; n=2) of the synovium **(Fig 4.2.3.1 D)**. Furthermore, when detected, CD20+ B cells are localized in clusters inside the aggregates while individual T cells can be found outside of the aggregates **(Fig 4.2.3.1 E)**.

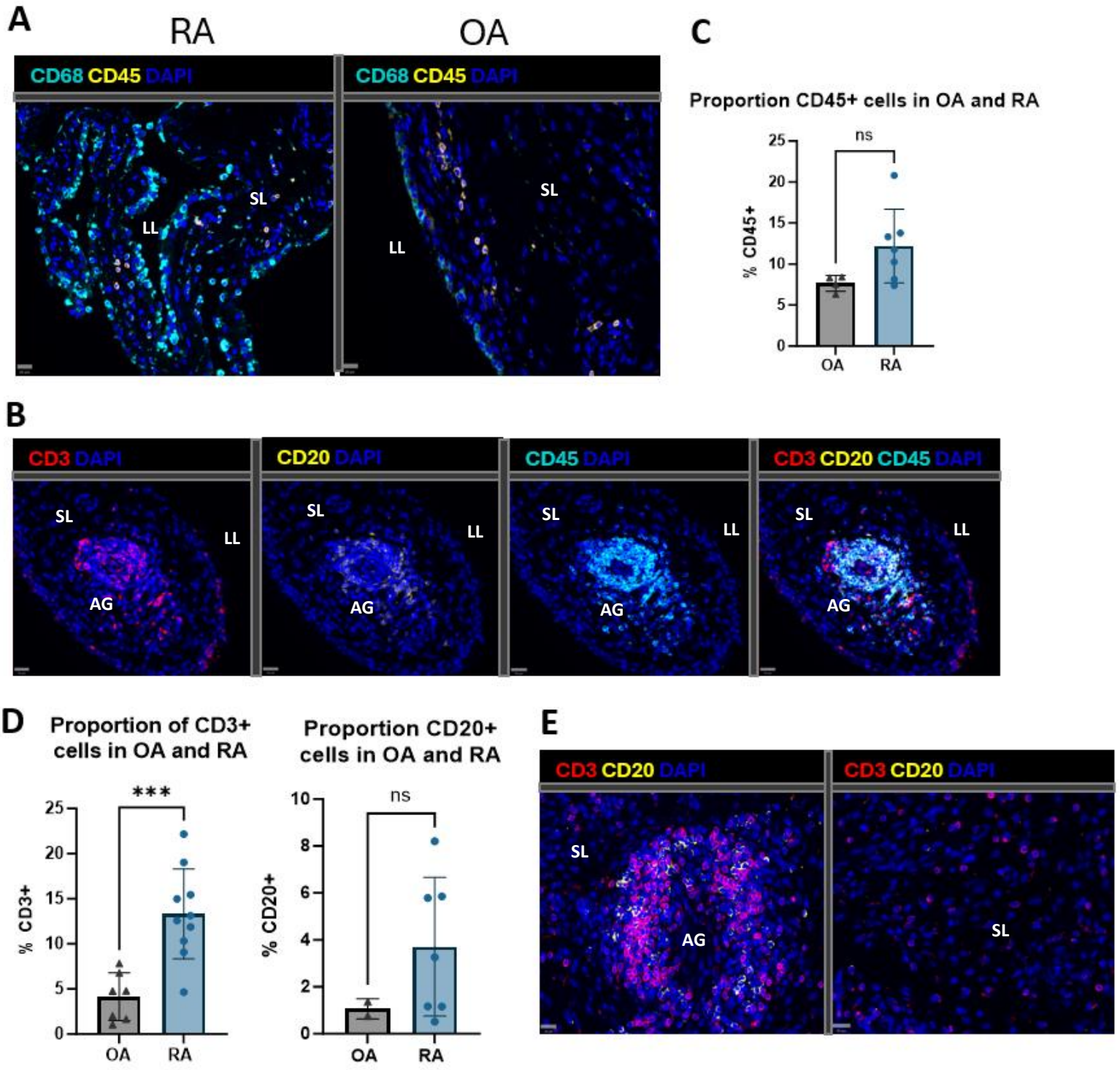


**Figure 4.2.3.1: Analysis of the infiltrated lymphocyte populations**

**A:** Multiplex IF staining showing the no colocalization between CD68 (cyan) and CD45 (yellow) in RA (left) and OA (right). **B:** Multiplex IF staining showing CD3 (red), CD20 (yellow) and CD45 (cyan) in a lymphocyte aggregate in RA synovium. **C:** Quantification of the percentage of CD45 in OA (grey) and RA (blue). Unpaired Students t-test OA (n=4), RA (n=7). **D:** Quantification of percentage of CD3 (left) and CD20 (right) in OA (grey) and RA (blue). Unpaired Students t-test for CD3 OA (n=7), RA (n=10); Unpaired Students t-test for CD20 OA (n=2), RA (n=7). **E:** Multiplex IF staining showing CD3 (red) and CD20 (yellow) in aggregates and in connective tissue in RA. LL=Lining layer; SL=Sub-lining; AG=Aggregate (***$p < 0.001$).

#### *4.2.3.2 Immune senescence by multiplex IF*

Once the population were classified, we investigated the proportion of p16+, p21+, yH2AX+ and p53+ in the CD45+ in OA and RA. On average, 10,09% (± 6,03; n=7) of CD45+ are p16+ in RA while in OA 11,26% (± 3,80; n=3) of CD45+ have intra-nuclear staining for p16 **(Fig 4.2.3.2 A)**. Moreover, no difference is observed between the proportion of CD45+ p21+ in both diseases and represent on average 10,66% (± 1,82; n=4) and 11,29% (± 5,17; n=7) in OA and RA respectively **(Fig 4.2.3.2 A)**. Furthermore, the percentage of yH2AX+ in CD45+ cells is equivalent in both diseases. Indeed, 14,1% (± 5,21; n=4) of CD45+ are yH2AX+ in OA while in RA this proportion is 15,39% (± 7,38; n=7) **(Fig 4.2.3.2 A)**. Finally, the proportion of p53+ CD45+ in OA (18,42% ± 9,70; n=4) is higher on average compared to RA (10,98% ± 6,34; n=7) **(Fig 4.2.3.2 A)**. However, the high variability of p53+ cells between the OA patients means that the difference observed is not significant. Altogether, no difference in senescence is observed between OA and RA synovium in the CD45+ populations. In addition, the percentage of yH2AX+ is higher than the percentage of p16 or p21 in both diseases suggesting that the senescence activation in immune cells might be induced by DNA damage.

Then, we investigated the percentage of senescence markers in CD3+ and CD20+ in both diseases. Firstly, in RA patients, 11,25% (± 6,35; n=11) of the CD3+ T cells are p16+ while only 2,32% (± 2,30; n=6) of CD20+ B cells are p16+ **(Fig 4.2.3.2 B, C)**. A similar observation is made in OA synovium, where on average 16,62% (± 9,15; n=4) of T cells and 2,63% (± 2,63; n=2) of B cells are p16+ **(Fig 4.2.3.2 B, D)**. Furthermore, the percentage of p21+ is also higher in the T cells compared to the B cells in RA synovium. Indeed, we observed that 13,52% (± 8,54; n=11) of T cells are p21+ when only 5,39% (± 3,62; n=6) of the B cells expressed p21 **(Fig 4.2.3.2 B, C)**. Contrariwise, the proportion of p21+ B cell in one OA patient seems abnormally high. After further investigation of the staining, the signal looks correct, however the number of CD20+ B cells in this patient is very low. Therefore, even a small number of positives cells increases the proportion which might not be representative of the total synovium.

Nevertheless, the percentage of p21+ in T cells in OA is similar on average to the percentage observed in RA **(Fig 4.2.3.2 B, D)**. In accordance with the findings in the CD45+ cells, the proportion of yH2AX+ in T cells and B cells is higher compared to the proportion of p16+ and p21+. Indeed, in RA synovium 18,65% (± 6,54; n=11) of T cells and 9,25% (± 9,73; n=6) of B cells are yH2AX+ **(Fig 4.2.3.2 B, C)**. Despite the fact that the percentage of yH2AX+ is lower compared to the percentage observed in T cells, we notice a high heterogeneity between patients. Furthermore, in OA the percentage of yHA2X+ T cells is 29,24% (± 24,65; n=5) **(Fig 4.2.3.2 B)**. Once again, we observed a high variability among the patients. For instance, in one patient up to 75,68% of T cells are yH2AX+, (the staining of this patient is used as example in figure 1.4.2 D) while another patient only has 3,06% of yH2AX+ CD3+. This might suggest differences in exposition to DNA damage Interestingly, the B cells in 2 OA patients tested have also a high proportion of yH2AX (28,95% ± 6,14; n=2) **(Fig 4.2.3.2 B, D)**. However, it is impossible to conclude that this percentage is biologically relevant or variability in the staining quality. Finally, the percentage of p53+ in the T cells population is averaging at 13, 31% (± 14,91; n=11) in RA **(Fig 4.2.3.2 B)**. Interestingly, we identified 2 groups of patients with high and low level of p53 in the RA cohort. The first group are tissues collected from JRP surgery and have significantly higher p53 in the T cells compared to the second group which are biopsies (**Fig 4.2.3.2 E)**. Furthermore, the percentage of p53+ in the B cells is also depending on the tissue type and is higher in the JRP cohort compared to the biopsies (**Fig 4.2.3.2 E)**. Nevertheless, on average the percentage of p53+ in B cells is lower compared to the T cells in both OA and RA. For instance, in OA no p53+ B cells were detected while on average 21,12% (± 15,79; n=5) of B cells are p53+ **(Fig 4.2.3.2 B)**.

Since the percentage of yH2AX+ is higher in the T cells compared to other senescence markers in both OA and RA, we investigated the DNA damage response in the CD3+ T cells. Surprisingly, we did not observe any specific pattern among patient in RA. Indeed, most RA patients have a slightly higher proportion of yH2AX+/p53+ compared to the yH2AX+/p53+/p21+ **(Fig 4.2.3.2 F)**. Furthermore, the activation of p53 and p21 independently of yH2AX varies according to the global level of senescence of the patients. It is important to notice that the DNA damage pathway in 2 of the biopsied patients

could not be analysed because no p53+ were detected. In contrast, in the OA cohort, the 2 patients with the higher level of senescence also have a high proportion of yH2AX+/p53+/p21+ suggesting that immune senescence in those patients might be increase in response to DNA damage **(Fig 4.2.3.2 F)**. However, in the 3 other patients, almost no yH2AX+/p53+ or yH2AX+/p53+/p21+ are detected, probably due to the low level of P21 and p53 in those patients.

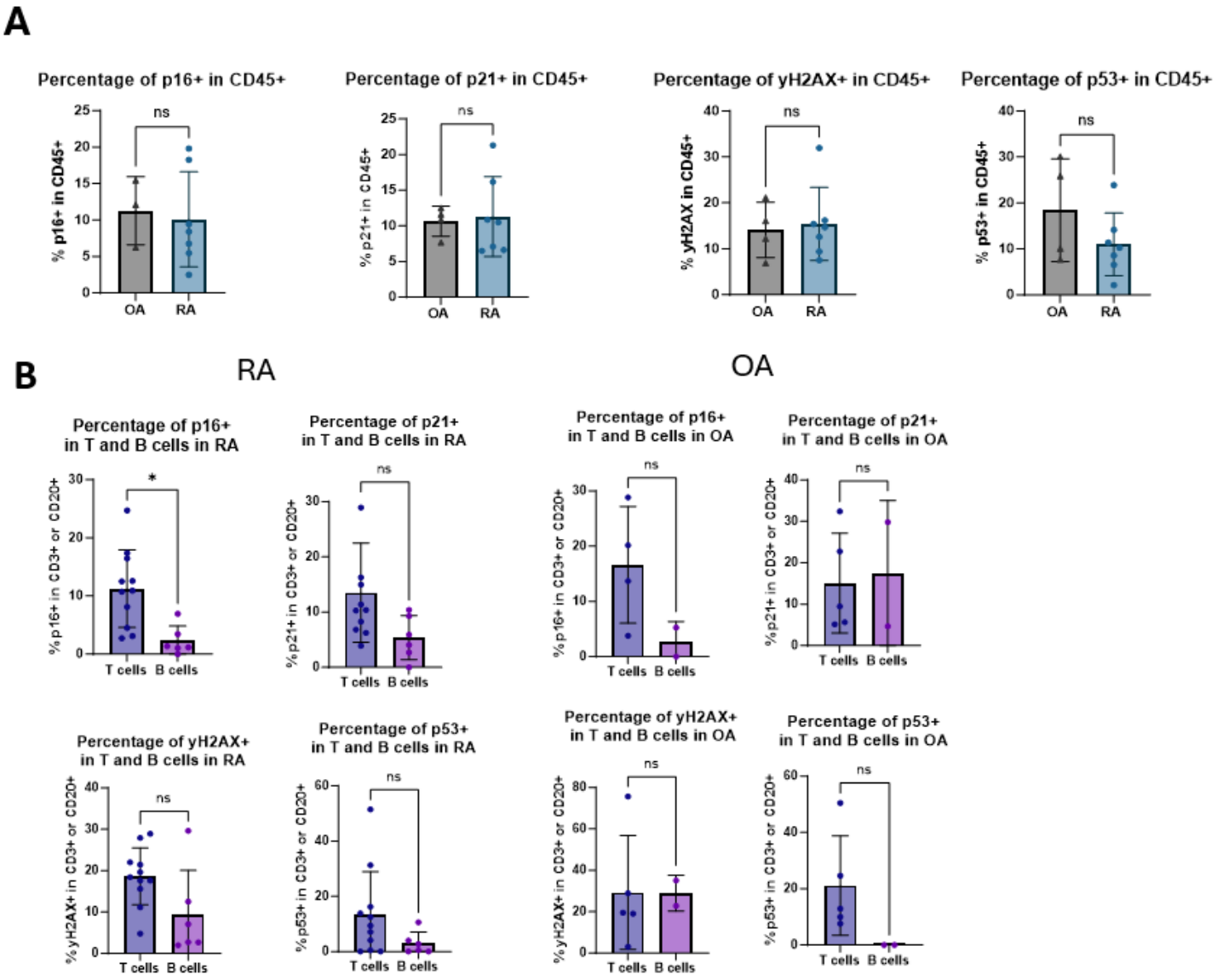


**Figure 4.2.3.2: Immune senescence by multiplex**

**A:** Percentage of p16+, p21+, yH2AX+, and p53+ in CD45+ in OA (grey) and in RA (blue), unpaired Student t-test OA (n=4), RA (n=7). **B:** Percentage of p16+, p21+, yH2AX+, and p53+ in CD3+ T cells (dark purple) compared to CD20+ B cells (magenta) in RA (left) and OA (right); unpaired Student t-test (*$p < 0.05$).

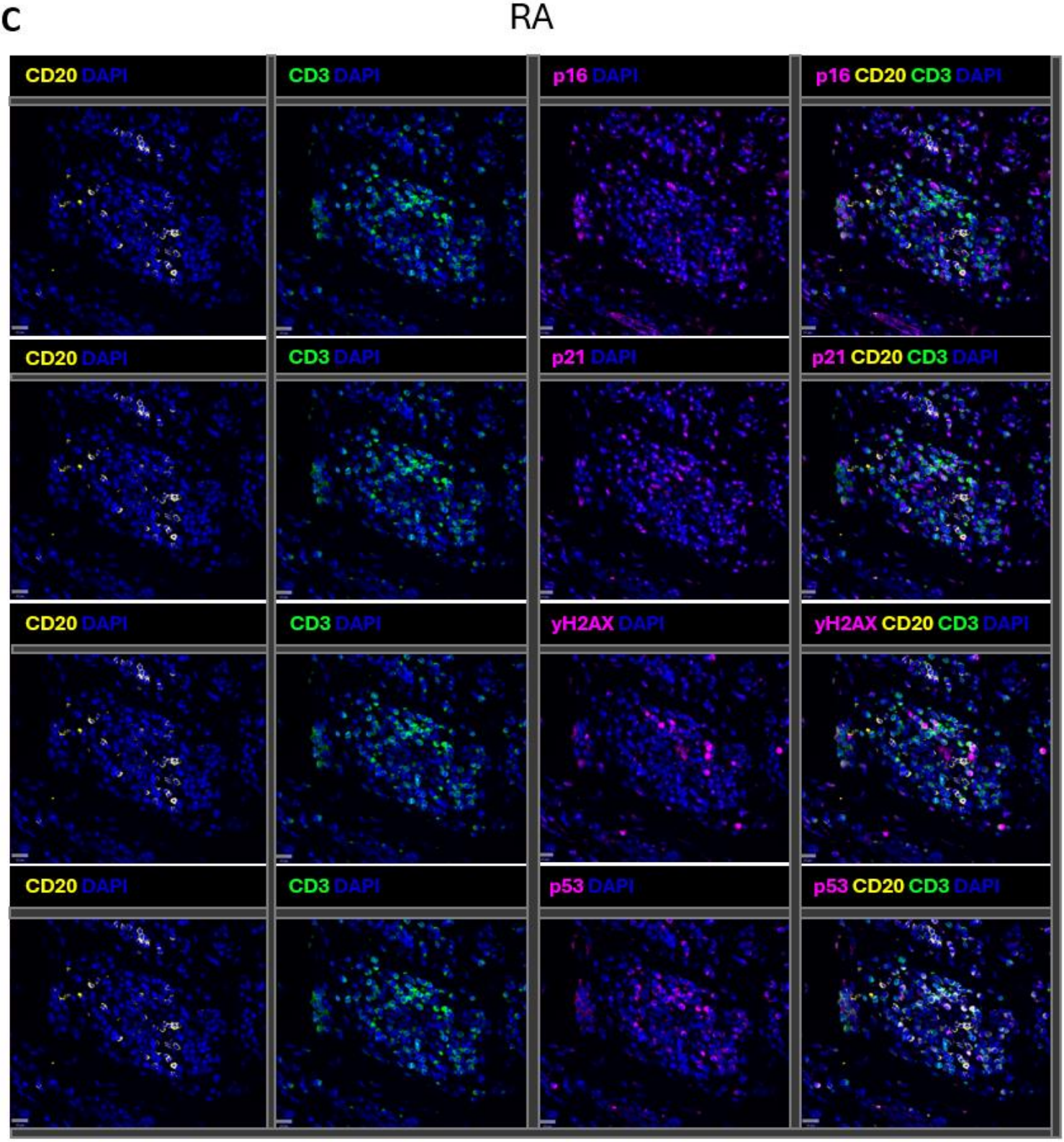


**Figure 4.2.3.2 (continued): Immune senescence by multiplex IF**

**C:** Multiplex IF staining showing p16, p21, yH2AX, and p53 (magenta) in lymphocyte aggregates in RA synovium; CD3 (green), CD20 (yellow).

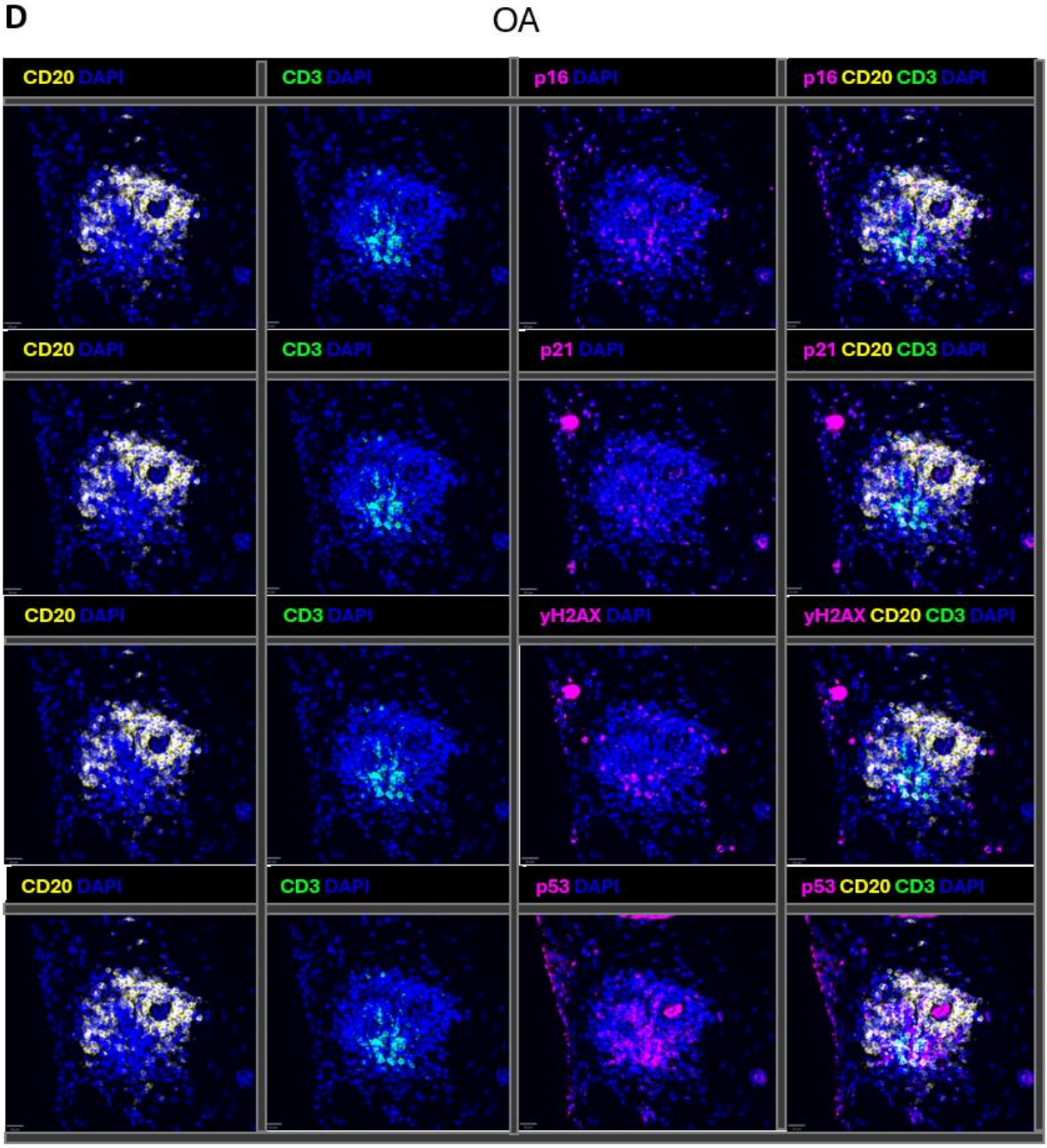


**Figure 4.2.3.2 (continued): Immune senescence by multiplex IF**

**D:** Multiplex IF staining showing p16, p21, yH2AX, and p53 (magenta) in lymphocyte aggregates in OA synovium; CD3 (green), CD20 (yellow).

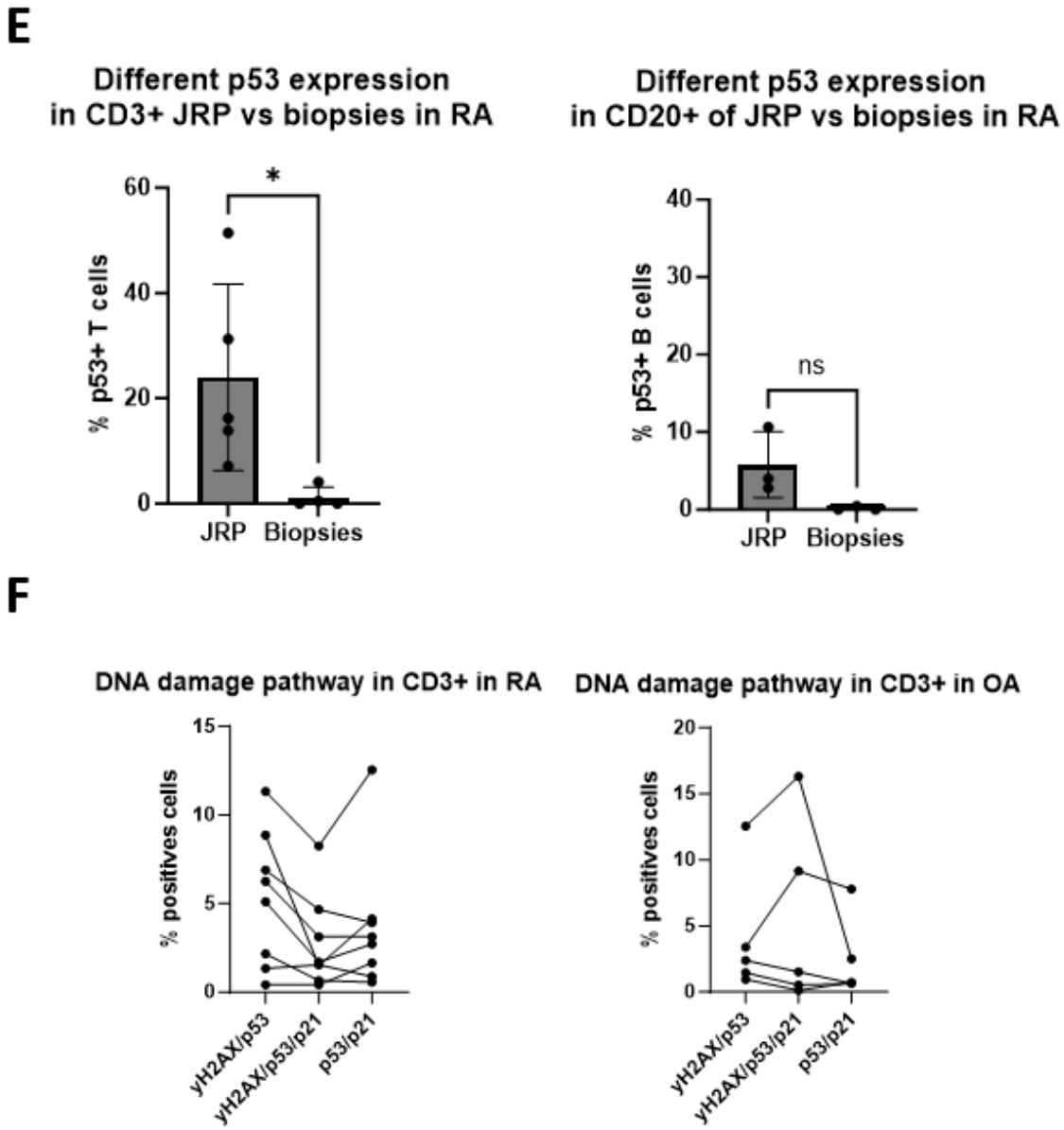


**Figure 4.2.3.2 (continued): Immune senescence by multiplex IF**

**E:** Percentage of p53+ in CD3 T cells (left panel) and CD20 B cells (right panel) in JRP patients compared to biopsies patients in RA; unpaired Students t-test. **F:** Percentage of yH2AX+p53+, yH2AX+p53+p21+, and p53+p21+ in CD3+ T cells in RA (left) and OA (right) (*$p < 0.05$).

#### *4.2.3.3 Immune senescence by flow cytometry*

Next, we investigated the senescence phenotype of the synovial infiltrated T and B cells using flow cytometry. After digesting the synovium, the main populations were analysed using the Spectral flow cytometer Cytek® Aurora. Lymphocytes were selected by the expression of CD45 and separated from the myeloid population on the basis of their size. Then, B cells were separated using the expression of CD19. From the CD19 negative cells, T cells were separated in the CD4+ and CD8+ subsets **(Fig 4.2.3.3 A)**. In the following results, the population denominated T cells are comprising the CD4+ and CD8+ excluding the double negative population.

Interestingly, the MFI of p16 in the T cells is significantly increase in OA compared the T cells in RA **(Fig 2.3.3 B)**. However, the MFI of yH2AX is higher in the T cells in RA compared to the T cell is OA **(Fig 4.2.3.3 B)**. Those differences were not observed in the multiplex analysis where no difference was observed between the 2 diseases in terms of immune senescence.

Like in the CellDIVE data, p16 is higher in the T cells compared to the B cells in both OA and RA. Indeed, on average, the MFI of p16 is 2,12 times higher in the T cells compared to the B cells in OA and 1,70 times higher in RA **(Fig 4.2.3.3 C top left)**. Similarly, the MFI of p21 is 1,91 times higher in the T cells compared to the B cells in OA and 1,70 times higher in RA T cells than B cells **(Fig 4.2.3.3 C bottom left)**. Interestingly, yH2AX MFI is on average higher in the B cells compared to the T cells. Indeed, there is 1,42 times increase of yH2AX MFI in the B cells in OA and 1,09 times increase in RA compared to the T cells **(Fig 4.2.3.3 C top right)**. In line with the histology, yH2AX is high in the B cells population in comparison to the other senescence markers. Furthermore, we observe a small increase in p53 MFI in the T cells population compared to the B cells in both diseases **(Fig 4.2.3.3 B bottom right)**.

Then, we asked if immune senescence affects differently the CD4+ helper and the CD8+ cytotoxic T cells in the synovium of OA and RA patients. Interestingly, the MFI of p16, p21, yH2AX, and p53 are not

different between the CD4+ and CD8+ suggesting that the class of T cells do not influence their senescence profile **(Fig 4.2.3.3 D)**.

Similarly to part 1.4.2, we explored whether the DNA damage response pathways were different between the diseases or cell populations. Therefore, I gated the p21+ and p21- in both T and B cells to investigate the percentage of yH2AX+ and p53+ in each subset **(Fig 4.2.3.3 E)**. First, we can notice that in accord with the MFI, the frequence of p21+ is 2,9 times higher in OA T cells compared to OA B cells and 2,42 times higher in RA T cells compared to RA B cells **(Fig 4.2.3.3 F)**. Furthermore, the proportion of p21+ observed in flow cytometry is higher to the proportion p21+ found in histology. Indeed, on average 69,3% and 67,23% of T cells are p21+ in OA and RA respectively when measured by the flow cytometry in opposition to the 15,09% and 13,52% observed in histology **(Fig 4.2.3.3 F; Fig 4.2.3.2 B)**. This might suggest different detection sensitivity between the techniques.

Next, we measured the percentage of yH2AX+ and p53+ within the p21+ and the p21- T and B cells in OA and RA. Thus, in OA patients we notice the same trend observed in T cells of the RA cohort analysed by histology, where most of patient have a small increase in the proportion of yH2AX+p53+ compared to the p21+yH2AX+p53+ **(Fig 4.2.3.3 G)**. Furthermore, the proportion of p53+p21+ T cells is higher in all OA patients compared to the p21+yH2AX+p53+. Moreover, the same trend is observed in the B cells in OA **(Fig 4.2.3.3 G)**. In addition, in the RA B cells we notice a opposite trend to the OA, where most patients have more p21+yH2AX+p53+ compared to yH2AX+p53+ **(Fig 4.2.3.3 G)**. However, in both OA and RA patients the percentage of those population is low which increases the risk of experimental false positive/negative. While the number of p21+yH2AX+p53+ and yH2AX+p53+ is low, most of the p21+ cells are yH2AX+p53- in T and B cells in both RA and OA **(Fig 4.2.3.3 H)**.

In conclusion, the immune senescence profile of the infiltrated B cells and T cells in similar between OA and RA patients despite different level of infiltration. Indeed, in both diseases, T cells are more positive for p16, p21 and p53 compared to the B cells population.

Furthermore, the percentage of yH2AX+ is higher in T cells and B cells compared to the other senescent markers. This observation is also observed by flow cytometry, where yH2AX MFI is increased in the B cells compared to the T cells. Moreover, no difference in senescence is observed between the CD4+ and CD8+ T cells subsets. These results might indicate a high percentage of DNA damage in the immune cells of the synovium leading to the activation of p53/p21 signalling. Surprisingly, the proportion of yH2AX+p53+ is low in most RA patients when the proportion of p21+yH2AX+p53+ is even lower. While, similar results are observed in the OA cohort analysed by flow cytometry, this is not the case for the RA patients in which T cells DNA damage activation are more heterogenous. Due to the limited number of patients and the variability between the analysis, it is difficult to characterize the DNA damage associated phenotype in the synovial T and B cells populations.

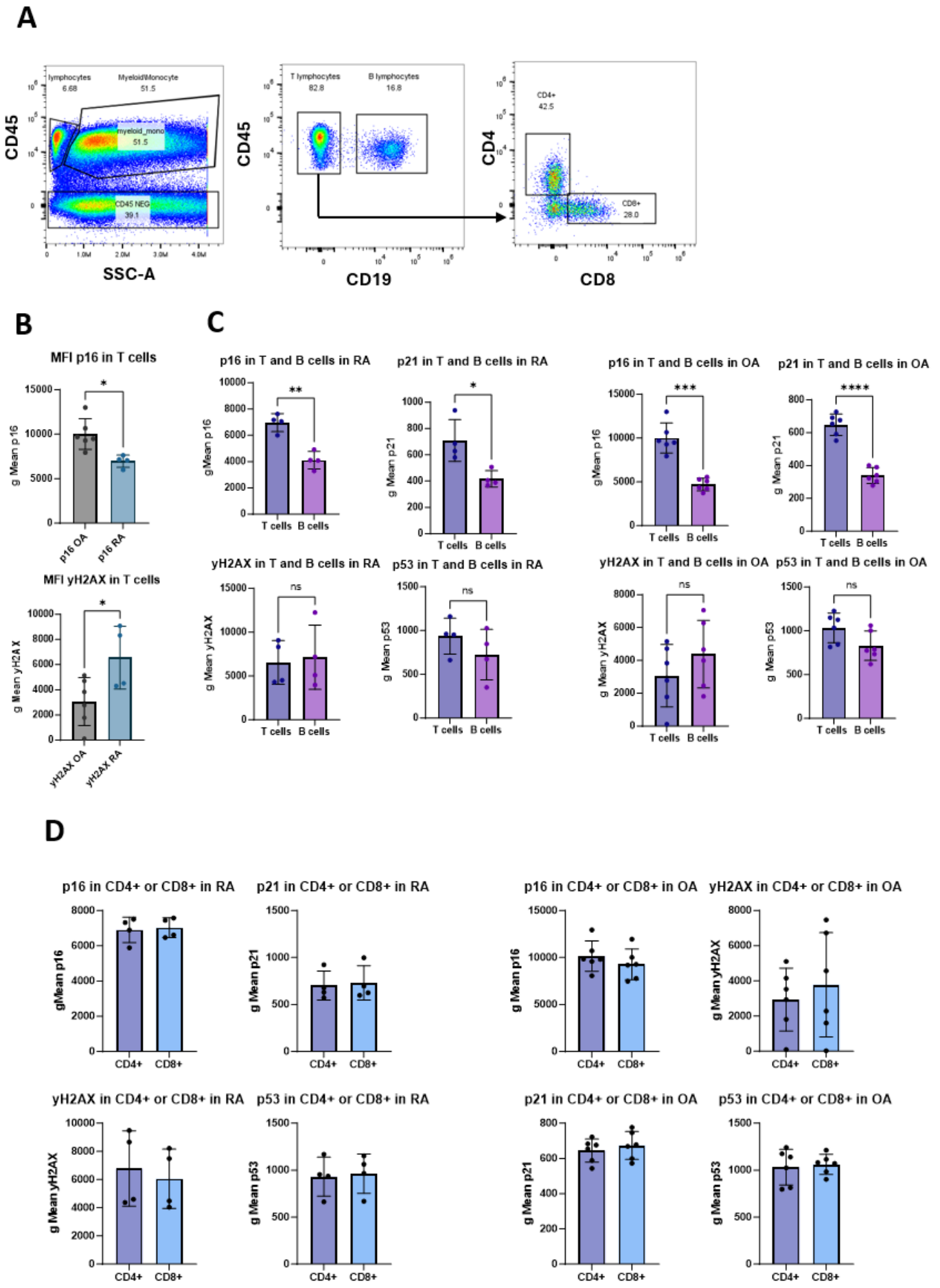
A
lymphocytes
6.68
MyeloidMonocyte
51.5
myeloid_mono
51.5
CD45 NEG
39.1
CD45
SSC-A
T lymphocytes
82.8
B lymphocytes
16.8
CD45
CD19
CD4+
42.5
CD8+
28.0
CD4
CD8
B
MFI p16 in T cells
g Mean p16
p16 OA
p16 RA
MFI yH2AX in T cells
g Mean yH2AX
yH2AX OA
yH2AX RA
C
p16 in T and B cells in RA
gMean p16
T cells
B cells
p21 in T and B cells in RA
g Mean p21
p16 in T and B cells in OA
gMean p16
p21 in T and B cells in OA
g Mean p21
yH2AX in T and B cells in RA
g Mean yH2AX
p53 in T and B cells in RA
g Mean p53
yH2AX in T and B cells in OA
g Mean yH2AX
p53 in T and B cells in OA
g Mean p53
ns
D
p16 in CD4+ or CD8+ in RA
gMean p16
CD4+
CD8+
p21 in CD4+ or CD8+ in RA
g Mean p21
p16 in CD4+ or CD8+ in OA
g Mean p16
yH2AX in CD4+ or CD8+ in OA
g Mean yH2AX
yH2AX in CD4+ or CD8+ in RA
g Mean yH2AX
p53 in CD4+ or CD8+ in RA
g Mean p53
p21 in CD4+ or CD8+ in OA
g Mean p21
p53 in CD4+ or CD8+ in OA
g Mean p53

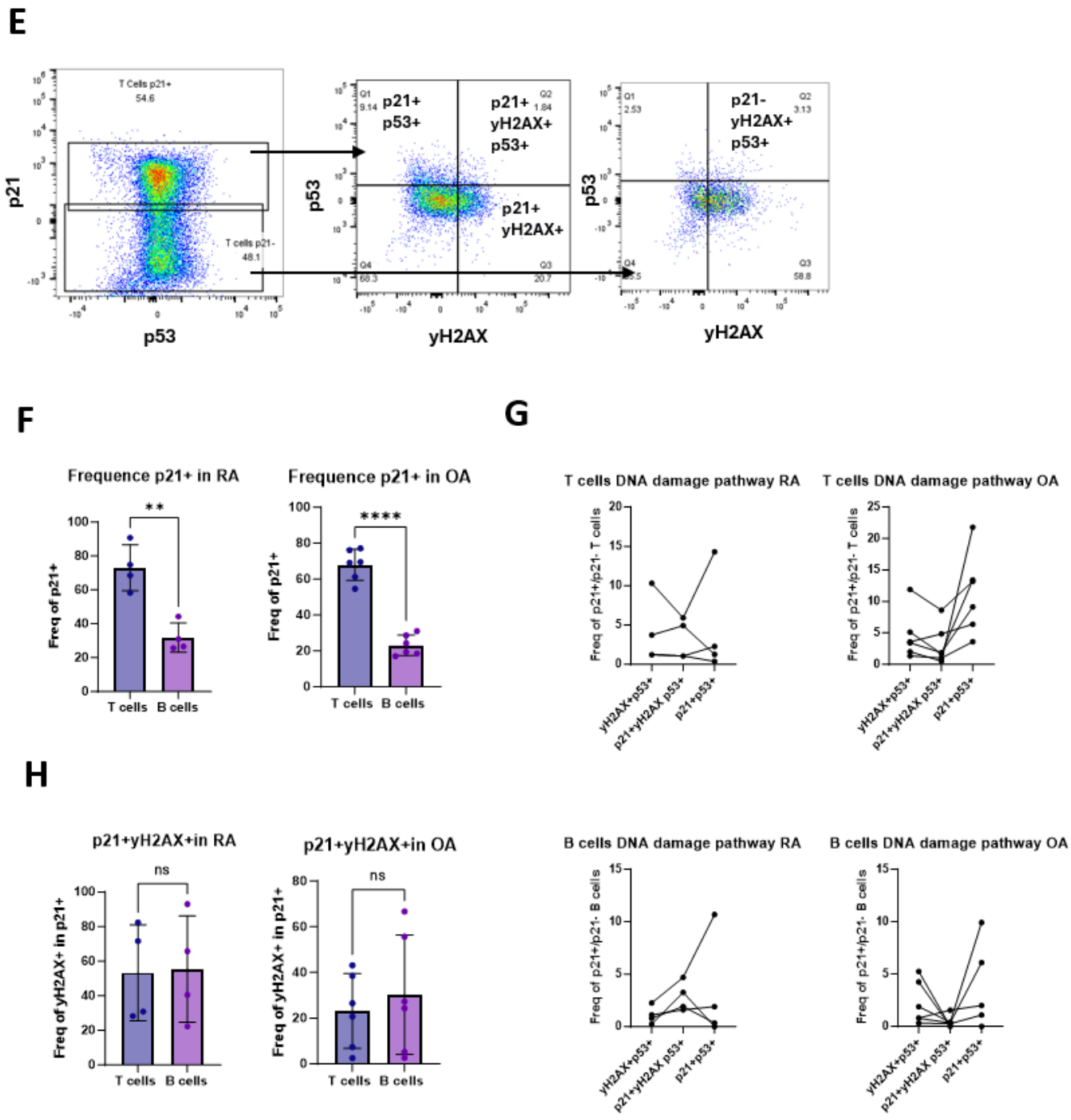


**Figure 4.2.3.2: Immune senescence by flow cytometry**

**A:** Gating strategy to classify B cells (CD45+ CD20+) and T cells (CD45+ CD20- CD4+ CD8+). CD4 and CD8 were classified based on CD4+ CD8- and CD4- CD8+ respectively. **B:** Quantification of the geometric mean fluorescence intensity of p16 (top) and yH2AX (bottom) in T cells in OA (grey) and RA (blue); unpaired Student t-test OA (n=6), RA (n=4). **C:** Quantification of the geometric mean fluorescence intensity of p16, p21, yH2AX, and p53 in T cells (purple) and B cells (magenta) in RA (left) and OA (right); Student t-test OA (n=6), RA (n=4). **D:** Quantification of the geometric mean fluorescence intensity of p16, p21, yH2AX, and p53 in CD4+ (dark blue) and CD8+ (light blue) in RA (left) and OA (right); Student t-test OA (n=6), RA (n=4). **E:** Gating strategy to classify the percentage of yH2AX+p53+, yH2AX+p53+p21+, and p53+p21+ in T cells. **F:** Percentage of p21+ in T cells (purple) and B cells (magenta) in RA (left) and OA (right); Student t-test OA (n=6), RA (n=4). G: Percentage of yH2AX+p53+, yH2AX+p53+p21+, and p53+p21+ in T cells (top) and in B cell (bottom) in RA (left) and OA (right). (*p < 0.05; **p < 0.01; ***p < 0.001; ****p < 0,0001).

### 4.2.4 Endothelial cells and Senescence

#### *4.2.4.1 Blood vessels type and endothelial cells classification by histology*

It is known that aging affects the homeostasis of the endothelium leading to a decrease of its regenerative capacity. Senescence in the endothelial progenitor cells is responsible for the decrease in endothelium repair (34). As in many senescent cells, ECs senescence is highly depending on the context, and can be characterized by the up regulation of p53/p21, increased of p16, presence of DNA damage, accumulation of ROS, decrease nitric oxide production, or up regulation of p38MAPK, eventually leading to loss of endothelium integrity (34, 37). Nevertheless, the impact of senescence in ECs of the microcirculation in the synovial homeostasis remains unknown. Here, we investigated ECs senescence using p16, p21, yH2AX and p53 during inflammation in OA and RA synovium.

To identified ECs, we used the expression of platelet endothelial cells adhesion molecule (PECAM-1) also called CD31. In preliminary staining, the expression of MCAM (CD146) was also investigated to detect mural cells in few OA and RA patients. As expected, CD31 is expressed in all the blood vessels (BVs) in OA and RA including capillaries, arterioles, and venules. Furthermore, MCAM expression allows the differentiation between the different type of vessels. Indeed, some vessels have a strong and uniform expression of MCAM adjacent to the CD31+ endothelial layer **(Fig 4.2.4.1 A, B, C)**. In those vessels, the morphology of the MCAM+ cells layer resembles SMCs suggesting that they are arterioles **(Fig 4.2.4.1 A, B, C yellow arrows)**. Moreover, capillaries are easily identified by their small size and are abundant compared to the number of arterioles **(Fig 4.2.4.1 A, B, C white arrows)**. Furthermore, by measuring the diameter of 25 randomly selected capillaries in the synovium of healthy, OA, and RA, we notice that the size of the capillaries in OA and RA are 2 times bigger compared to healthy synovium suggesting the role of inflammation in vessel dilatation **(Fig 4.2.4.1 D)**. The last vessels found also consist of a thin layer of ECs with partial MCAM staining on periphery but are distinguishable by their bigger size suggesting that they might be venules **(Fig 4.2.4.1 A, B, C blue arrows)**. However, we are

not excluding the possibility that they are capillaries dilated because of inflammation. Furthermore, CD90 is expressed around the capillaries and venules but not arterioles although NOTCH3 is detected in the perivascular population of the arterioles **(Fig 4.2.4.1 A)**. Finally, only one patient in OA had clearly identified lymphatic vessels characterized by the expression of PDPN **(Fig 4.2.4.1 E)**. Interestingly, ECs from lymphatic vessels are not CD31+ but expressed CD34+. Nevertheless, no difference in the proportion of CD31+ cells is observed between OA and RA **(Fig 4.2.4.1 F)**.

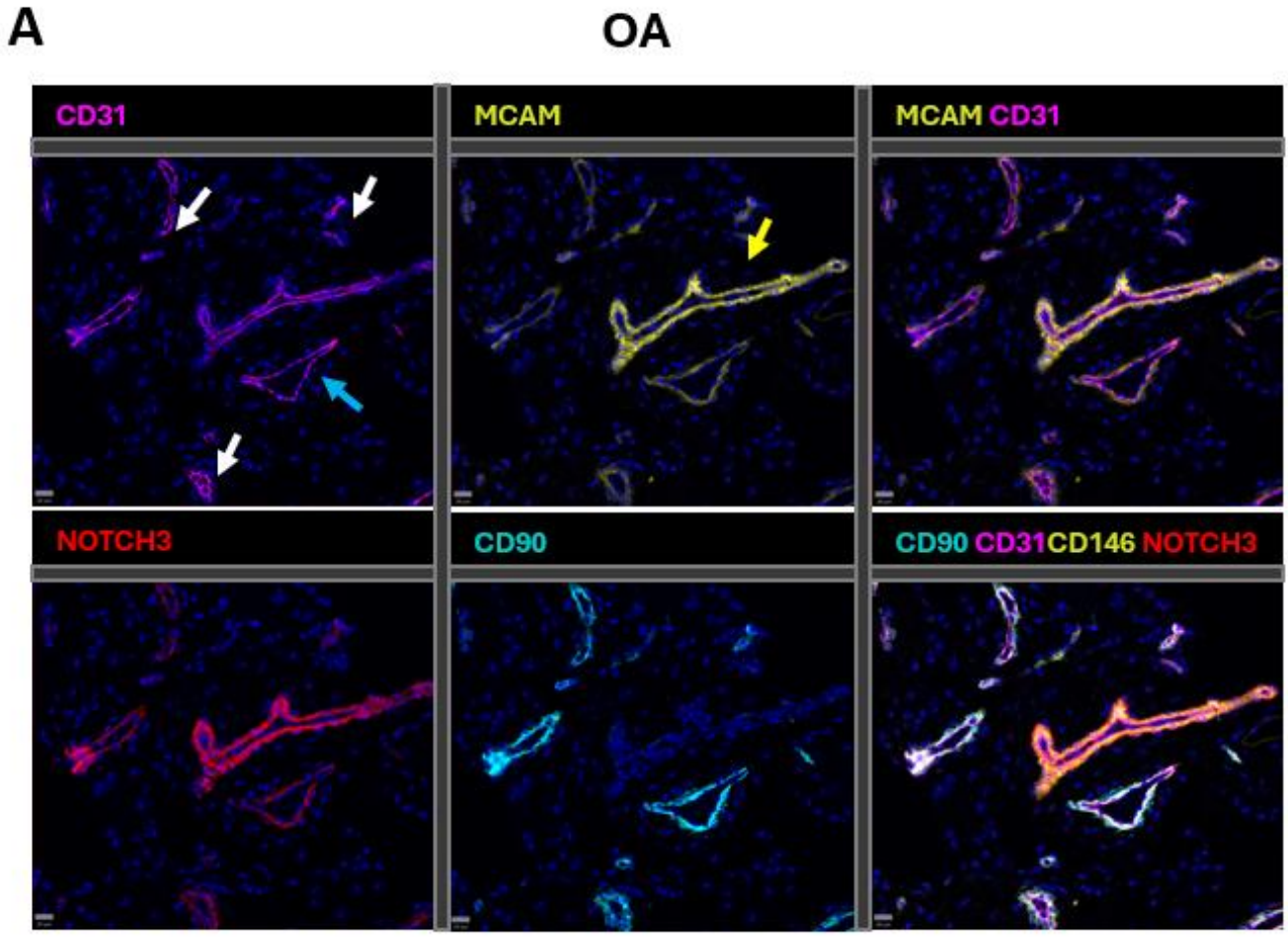


**Figure 4.2.4.1: Blood vessels type and Endothelial cells classification by histology**

**A:** Multiplex IF staining showing CD31 (magenta), MCAM (yellow), NOTCH3 (red), and CD90 (cyan) in OA synovium. White arrows show capillaries, blue arrows show venules, yellow arrows show arterioles.

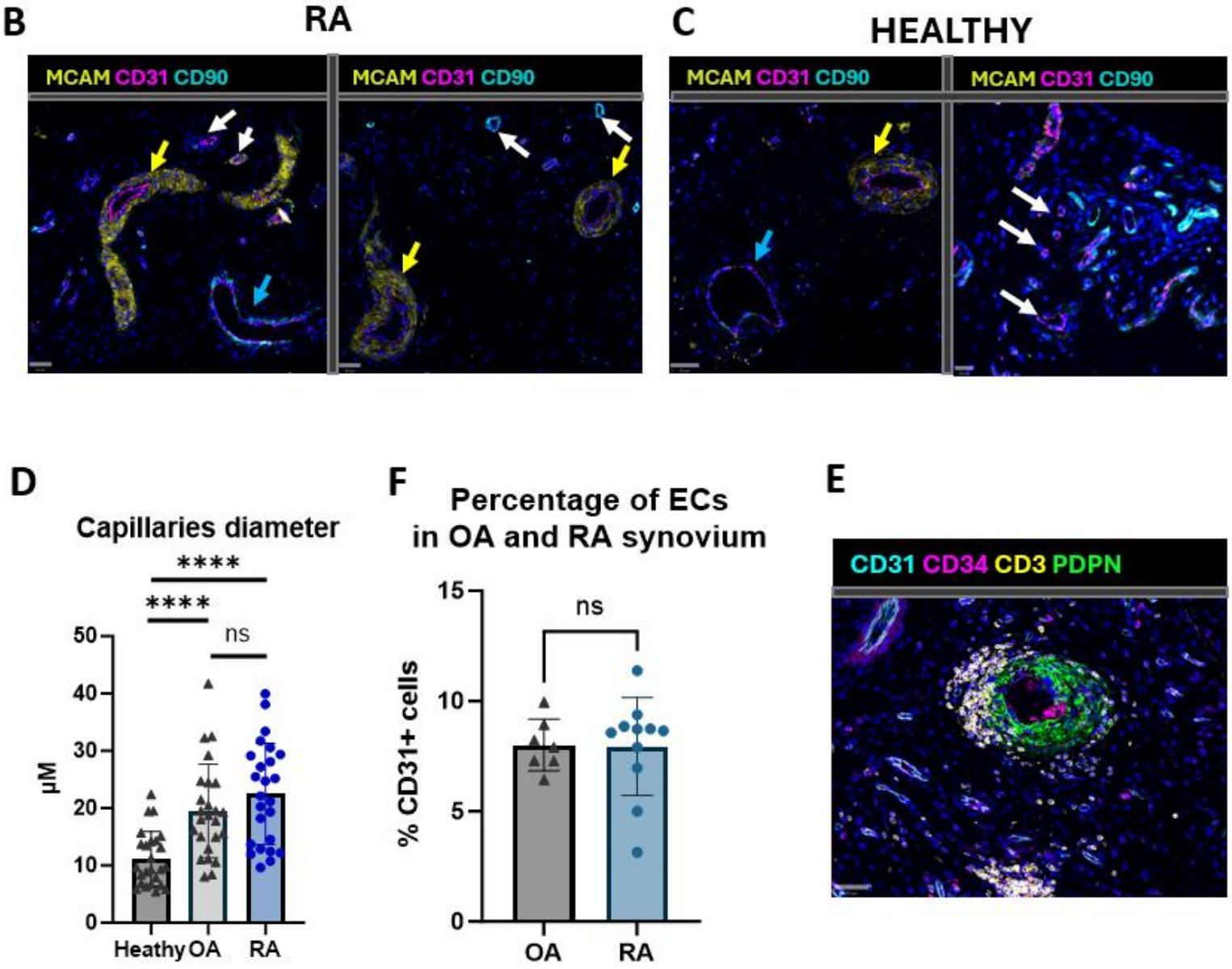


**Figure 4.2.4.1 (continued): Blood vessels type and Endothelial cells classification by histology**

**B:** Multiplex IF staining showing CD31 (magenta), MCAM (yellow), and CD90 (cyan) in RA synovium. White arrows show capillaries, blue arrows show venules, yellow arrows show arterioles. **C:** Multiplex IF staining showing CD31 (magenta), MCAM (yellow), and CD90 (cyan) in normal (healthy) synovium. White arrows show capillaries, blue arrows show venules, yellow arrows show arterioles. **D:** Measures the diameter of 25 randomly selected capillaries in OA, RA and healthy synovium using Qupath software. Unpaired Students t-test Capillaries (n=25), OA (n=1), RA (n=1), Healthy (n=1).**E:** Multiplex IF staining showing a lymphatic vessel in OA synovium. CD31(cyan) CD34 (magenta), CD3 (yellow), PDPN (green). F: Percentage of CD31+ in OA (grey) and RA (blue), Unpaired Student t-test, OA (n=7), RA (n=11) (****$p < 0{,}0001$).

#### *4.2.4.2 Histological analysis of the senescence in the ECs*

Next, we investigated the proportion of the senescence markers in the CD31+ ECs in both OA and RA synovium. Firstly, I wondered if ECs senescence from small capillaries or venules was different. Due to a lack of methods to quantify this difference, we looked the positivity of p16, p21, yH2AX and p53 in endothelium of capillaries and venules in both OA and RA and we did not see any difference. Indeed, positives cells were detected regardless of the size of the vessel. Unfortunately, without the MCAM staining it was difficult to identify the arterioles in the cohort analysed here. However, thanks to serial sections from the patients presented in figure 2.4.2 A, and B, we were able to identify arterioles based on the vessels structure. While some ECs from arterioles were positives for p16 and p21, the staining of p53 was localized in the SMCs but not present in the CD31+ cells. This seems to be true for most of the arterioles identified this way. Nevertheless, further staining including MCAM, αSMA and p53 are required to confirm this finding. For the rest of the analysis, the senescence makers were investigated in all the CD31+ ECs regardless of the vessels type.

Thus, on average 28,57% (± 14,30; n=6) of ECs are p16+ in OA synovium (**Fig 4.2.4.2 A, C)**. Similarly, in RA 24,74% (± 10,28; n=11) of ECs are also positive for p16 suggesting that ECs senescence through p16 activation is high in both diseases (**Fig 4.2.4.2 B, C)**. Furthermore, p21 is also high in the ECs. Indeed, 19,39% (± 8,86; n=6) and 23,09% (± 8,17; n=12) of ECs are p21+ in OA and RA, respectively **(Fig 4.2.4.2 A, B, C)**. Interestingly, the proportion of yH2AX+ in OA and RA ECs is significantly lower compared to the proportion of both p16+ and p21+. Indeed, on average, the proportion of yH2AX+ ECs in OA is 9,70% (±6,74; n=6) while in RA this proportion is 12,54% (±5,92; n=11) suggesting that perhaps ECs have a lower exposure to DNA damage in the context of arthritis **(Fig 4.2.4.2 A, B, C)**. Finally, the expression of p53 is widely heterogenous between patients in both diseases. Indeed, in some patients the majority of ECs are strongly positives for p53. This was observed in my preliminary IHC and IF staining where the expression of p53 was strongly overlapping with the BVs **(Fig 4.2.1.1 E)**. In echo to the pervious observation made on the lymphocyte populations, the RA tissues collected from biopsies

have a lower p53 expression within the SL compared to the JRP tissues. However, while 4 of the biopsies had low in p53 expression in T and B cells, here 2 of the biopsies have a high proportion of p53+ ECs cells. In addition, the disparity in p53 expression is also observed in OA patients where all tissue were collected after JRP surgery suggesting that this might be due to heterogeneity intrinsic to the patients. Nevertheless, 27,86% (±21,12; n=6) of ECs in OA are p53+, while in RA this percentage is 27,01% (±17,69; n=11) and is also significantly higher compared to the proportion of yH2AX+ **(Fig 4.2.4.2 A, B, C)**.

Then, we investigated the DNA damage senescence pathway by quantifying the proportion of yH2AX+/p53+, p21+yH2AX+p53+, and p53+/p21+ in the ECs of OA and RA patients. Similarly, to the previous analysis on the immune cells 2 patients with almost no p53+ ECs detected were excluded to prevent statistical anomalies. Thus, we noticed that in most patients the percentage of ECs yH2AX+/p53+ and p21+yH2AX+p53+ are lower compared to the proportion of p21+/p53+ **(Fig 4.2.4.2 D)**. Indeed, on average we observed 2 to 3 times more p21+/p53+ ECs compared to yH2AX+/p53+ and p21+yH2AX+p53+ **(Fig 4.2.4.2 D)**. As the proportion of yH2AX is low in the ECs those results are expected suggesting that the cellular senescence in the ECs might be driven by a persistent p53 activation leading to an increase of p21. However, the role of DNA damage in the activation of p53 remains unclear.

In summary, OA and RA patients affected by synovitis do not exhibit differences in the number and type of vessels present in the synovium. Diseased synovium has larger capillaries compared to healthy synovium as a result of inflammation. Furthermore, the perivascular niche of inflammatory CD90+ fibroblasts is not found around arterioles despite the expression of NOTCH3 suggesting that the activation of this subtype might be dependant of the cross talk between pericytes and endothelial but not SMCs. However, this hypothesis needs to be further explored and test *in vitro*.

Then, we show that cellular senescence is high in the ECs by the expression of p16, p21 and p53. The presence of DNA damage through phosphorylated H2AX is significantly underrepresented in the ECs of

RA synovium compared to the proportion of the other 3 hallmarks. Similar observations are made in OA synovium suggesting that the mechanism of ECs senescence is not dependent of the disease. Finally, among the p53+ ECs only a small proportion is positive for DNA damage, whilst the proportion of p21+/p53+ is 2 times higher on average. This could suggest that either ECs are less exposed to DNA stress or that they have a high repair activity through p53/p21 cell cycles arrest. Nevertheless, the high proportion of p16+ suggests that despite not having a strong DNA damage signature, ECs are undergoing senescence which can be related to vascular aging.

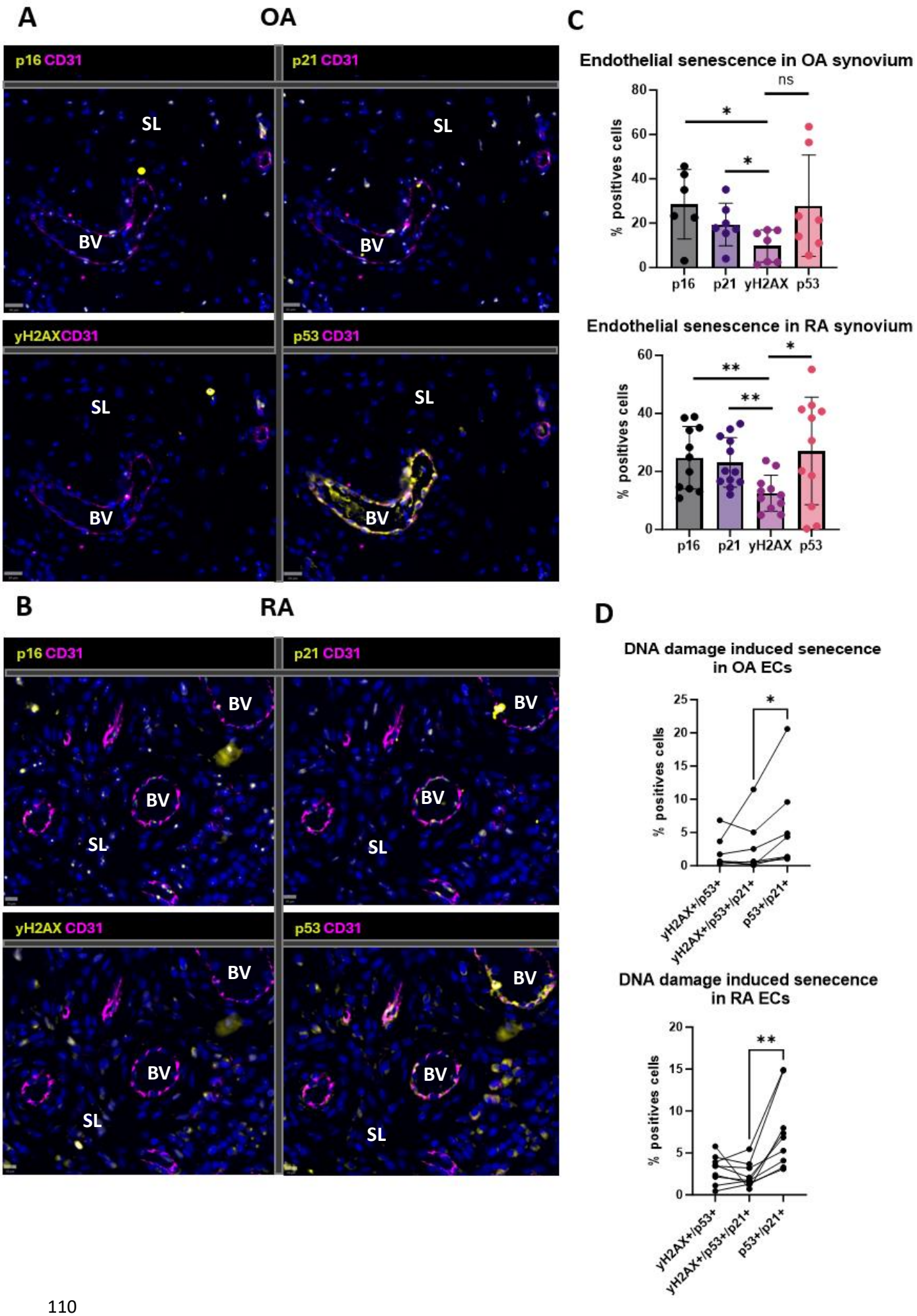
A
OA
p16 CD31
p21 CD31
yH2AXCD31
p53 CD31
SL
BV
B
RA
C
Endothelial senescence in OA synovium
% positives cells
p16
p21
yH2AX
p53
ns
Endothelial senescence in RA synovium
D
DNA damage induced senecence in OA ECs
yH2AX+/p53+
yH2AX+/p53+/p21+
p53+/p21+
DNA damage induced senecence in RA ECs

**Figure 4.2.4.2: Histological analysis of the senescence in the ECs in OA and RA synovium**

**A:** Multiplex IF staining showing p16, p21, yH2AX, and p53 (yellow) in blood vessels endothelium CD31+ (magenta) in OA synovium. **B:** Multiplex IF staining showing p16, p21, yH2AX, and p53 (yellow) in blood vessels endothelium CD31+ (magenta) in RA synovium. **C:** Percentage of p16+, p21+, yH2AX+, and p53+ in CD31+ endothelial cells in OA (top) and RA (bottom). Unpaired Student t-test, OA (n=7), RA (n=11). **D:** Percentage of yH2AX+p53+, yH2AX+p53+p21+, and p53+p21+ in CD31+ in OA (top) and in RA (bottom). Unpaired Student t-test, OA (n=7), RA (n=11) SL=Sub-lining; BV=Blood vessels (*p < 0.05; **p < 0.01)

### *4.2.4.3 ECs senescence in OA and RA synovium by flow cytometry*

Similarly to the multiplex analysis, we used CD31 to identify the ECs. In a first time, we made sure that the CD45- did not contain CD11c+ or MERTK+ myeloid as the expression of CD45 is low in some TRMs population. Then, in the "cleaned" CD45-, we separated ECs from the other stromal population using PDPN and CD31 and gated the all the CD31+ **(Fig 4.2.4.3 A)**. The first thing we noticed was the presence or absence of a $CD31^{low}$ PDPN+ between patients. Indeed, 3 out of 6 patients in OA have a high number of $CD31^{low}$ PDPN+ when in RA only 1 out of 4 have this population. Knowing that ECs also expressed CD34, we try to better characterize those populations based on the expression of CD34. In patients without $CD31^{low}$ PDPN+, most of the CD31+ were also CD34+ **(Fig 4.2.4.3 A)**. However, in patients with $CD31^{low}$ PDPN+, we observed the 4 following populations: CD31+ CD34+, CD31+, $CD31^{low}$ PDPN+, $CD31^{low}$ PDPN+ CD34+. The CD31+ population shows a proportion expression between PDPN and CD31 and have a similar profile than the unstained sample characteristic an unmixing error. Therefore, this population is not considered as endothelial cells.

Evidence shows that CD31 is expressed in immune cells such as circulating monocytes while PDPN can also be expressed on monocytes (123, 124). In addition to the analysis of the TRM populations that shows PDPN expressed on the TRMs of the LL especially in OA synovium **(Fig 4.2.2.2 I, J)** with a lack of PDPN+ CD31 observed in histology, we considered that the $CD31^{low}$ PDPN+ and the $CD31^{low}$ PDPN+ CD34+ could either be an unidentified infiltrated monocytes population or a nonspecific staining. The lack of staining in other immune cell markers such as CX3CR1, HLA-DR or CD68 make the identification of this population as monocytes difficult. However, endothelial cells from lymphatic vessels should

expressed PDPN, CD31 and CD34. Therefore, this population might be associated with the lymphatic system. However, the lymphatic vessels detected in histology were CD31- **(Fig 4.2.4.3 E)**. In consequence, as we were not able to properly identify this population it is not consider as part of the ECs, but their lymphatic origin is not excluded.

Thus, the population considered in this experiment as ECs is CD31+ CD34+ which is consistent among patients in both OA and RA and represent on average 24,75% (±17,87; n=6) of the CD45- in OA and 45,4% (±20,71; n=4) of CD45- in RA **(Fig 4.2.4.3 B)**.

Then, we compared the MFI of p16, p21, yH2AX and p53 in the CD31+ CD34+ ECs between OA and RA. No significative difference is observed for p16, p21, yH2AX or p53 intensity between OA and RA **(Fig 4.2.4.3 C)**. Although we noticed more heterogeneity in yH2AX intensity among the OA patients. Since the fluorescence intensity of p21, p53 and yH2AX was in the similar range of value. We decided to normalize the MFI of those markers to compare their intensity. Similarly to the histology data, there is a decrease in yH2AX in the ECs compared to p53 or p21 **(Fig 4.2.4.3 D)**. This decrease is significant in RA but not in OA due to the heterogeneity of yH2AX intensity. To further compared the expression of p16, p21, yH2AX, and p53 to the results provided by histology, we measured the proportion of positive cells of each marker in the CD31+ CD34+ population. Similarly to the finding in histology the proportion of yH2AX is deceased in the ECs compared to p21, p16 and p53 **(Fig 4.2.4.3 E)**. While in RA, this decreased is significant for those 3 markers, in OA only the proportion of p21+ is significantly higher than the yH2AX+ **(Fig 4.2.4.3 E)**. Nevertheless, the senescence profile of ECs is conserved between the two techniques. Finally, we measured the frequence of yH2AX+/p53+, p21+yH2AX+p53+, and p53+/p21+ in the CD31+ CD34+ to investigate if the senescence is associated with DNA damage. In accord with histology's data, the proportion of p21+yH2AX+p53+ is significantly lower in both diseases compared to the population of p53+/p21+ while most of the yH2AX+ are p21-, p53- **(Fig 4.2.4.3 F)**.

By using flow cytometry, we showed that the ECs characterized by the expression of CD31 and CD34 have a similar senescence profile observed in histology in which p16, p21 and p53 are the most

represented hallmarks and yH2AX+ ECs are rare. This leads to the same conclusions that vascular aging is affecting the ECs of the synovium regardless of the disease. However, the impact on vascular aging on the disease progression remains unknown.

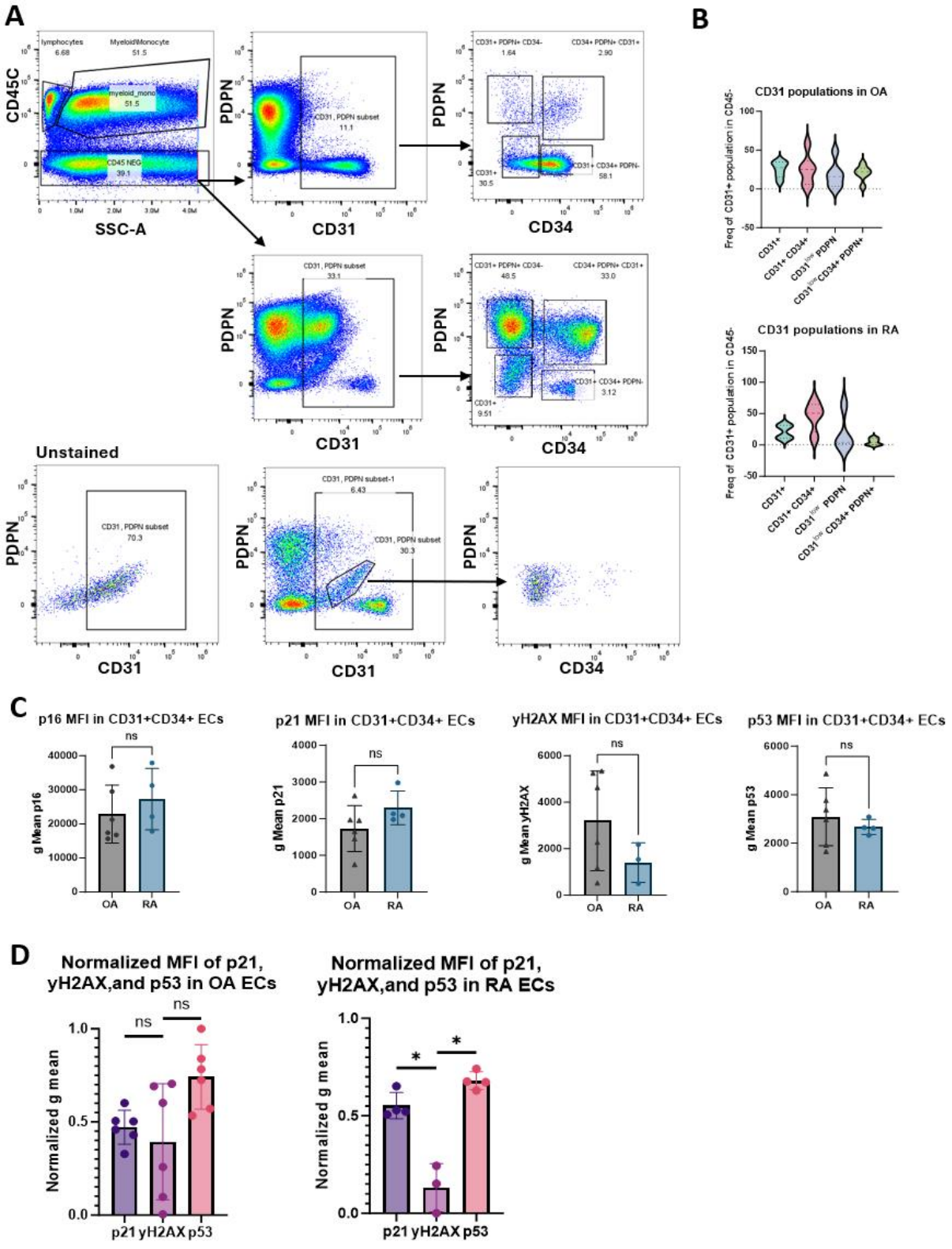

**Figure 4.2.4.3: ECs senescence in OA and RA synovium by flow cytometry**

**A:** Gating strategy to classify ECs. ECs are classified based on CD45- PDPN- CD31+ CD34+. 3 gates in top show one type of CD31+ PDPN+ profile in the cohort, 2 gates in the middle show the other type of CD31+ PDPN+ profile in the cohort. 3 gates in bottom show the similarities between the unstained control and the non-specific CD31+ population. **B:** Proportion of each CD31+ populations observed in OA (top) and RA (bottom). **C:** Quantification of the geometric mean fluorescence intensity of p16, p21, yH2AX, and p53 in CD31+ CD34+ ECs in OA (grey) and RA (blue), Unpaired Student t-test, OA (n=6), RA (n=4); yH2AX in RA (n=3). **D:** Normalized MFI of p21, yH2AX, and p53 in ECs in OA (left) and RA (right). Unpaired Student t-test, OA (n=6), RA (n=4); yH2AX in RA (n=3) (*p < 0.05).

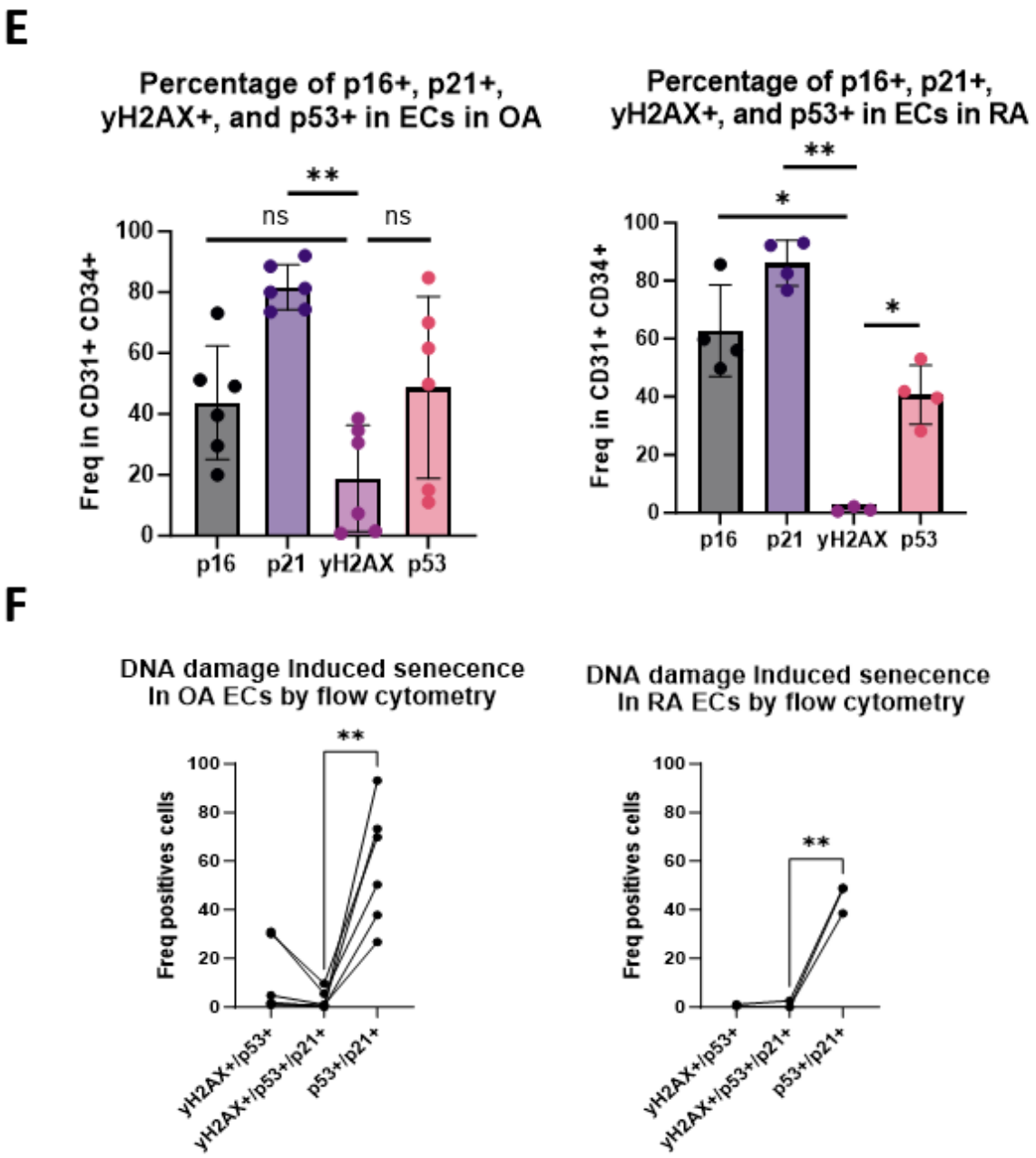

**Figure 4.2.4.3 (continued): ECs senescence in OA and RA synovium by flow cytometry**

**E:** Percentage of p16+, p21+, yH2AX+, and p53+ in CD31+ CD34+ endothelial cells in OA (left) and RA (right). Unpaired Student t-test, OA (n=6), RA (n=4); yH2AX in RA (n=3). **F:** Percentage of yH2AX+p53+, yH2AX+p53+p21+, and p53+p21+ in CD31+ CD34+ in OA (left) and RA (right). Unpaired Student t-test, OA (n=6), RA (n=4); yH2AX in RA (n=3) (*p < 0.05; **p < 0.01).

### 4.2.5 Cellular senescence in healthy synovium

Previous evidence points toward the idea that cellular senescence is occurring in most cell populations of the synovium in OA and in RA. However, cellular senescence is affecting both diseases similarly, and no difference is observed in term of proportion of senescent cells between OA and RA. Therefore, one question remains unclear, is the establishment of cellular senescence depends on shared mechanism between OA and RA or is simply intrinsic to the tissue during aging? To answer this question, we investigated the hallmarks of senescence in a normal synovium of a 43-year-old patient. Due to the rarity of healthy synovial tissue, only one patient could be analysed using multiplex histology. Firstly, we investigated the proportion of the synovial cell populations. Thus, 7,75% of normal synovium in composed by endothelial cells **(Fig 4.2.5 A)**. Moreover, 15,11% are PDPN+ MERTK-, although, as the CD68 staining did not worked this population should be composed of the LL fibroblasts and some CD68+ LL TRMs. Furthermore, 8,89% are CD90+ CD31- CD146- corresponding to the SL fibroblasts while 2,49% are mural cells. The MERTK staining was very low on this tissue and only 2,45% of the cells are MERTK+. Interestingly, normal synovium contains 3,75% of infiltrated CD3+ lymphocytes. Finally, the majority of the cells could not be classified with the markers available. Indeed, CD206, CD68, and CD45 did not work limiting the identification of many TRMs and infiltrated monocytes. Moreover, many Vimentin+ CD90- fibroblast-like cells are found dispersed into the SL, probably corresponding to normal fibroblast that composed the connective tissue.

Next, we investigated the proportion of p16+, p21+, yH2AX+ and p53+ in the population classified above. Firstly, we noticed that all the senescence markers are present in the normal synovium suggesting that senescence might occurs in normal joint independently of disease **(Fig 4.2.5 B)**.

Then, we compared the senescence in the PDPN+ LL fibroblasts to the CD90+ SL fibroblasts. Thus, we observed an increase of the percentage of p21+, yH2AX+ and p53+ but not p16+ in the LL compared to the SL **(Fig 4.2.5 C)**. Besides the expression of p16+, those findings are in line with the observation made in OA and RA synovium suggesting that the localisation of senescence the LL population might be driven by intrinsic factors link to the synovium architecture. Furthermore, the senescence profile of the ECs resembles the one found in OA and RA in the high expression of p16+ and p53+ **(Fig 4.2.5 D)**. However, the proportion of yH2AX+ is higher in this patient compared to the other patients in the OA and RA cohorts where yH2AX+ were low. Similarly, CD3+ T cells also exhibit a high percentage of p16+ and p53+ while a smaller proportion is p21+ **(Fig 4.2.5 D).** Interestingly, the percentage of yH2AX+ CD3+ is also higher in this patient compared to the lymphocytes in the OA and RA cohorts. Finally, the senescence in the MERTK+ macrophages in this patient is also characterized by a high p53 and p16 expression, a lower expression of p21 and a high yH2AX+ percentage **(Fig 4.2.5 D).**

Together, this indicates that cellular senescence in the synovium occurs independently of the disease state. Furthermore, the same populations are affected by cellular senescence including T cells, ECs, and TRMs. Besides a higher proportion of yH2AX+ in the ECs, T cells, and MERTK+ in this patient compared to the other RA and OA patients, the proportion of p16+, p53+ and p21+ are similar in OA and RA suggesting that the disease may not have an influence of the aging related senescence. Finally, the LL layers fibroblasts are also more senescent expected in p16 expression in this patient. This may suggest that the mechanisms that drives senescence in the LL are not link to the OA and RA but rather link to normal tissue aging in response to intrinsic stressors.

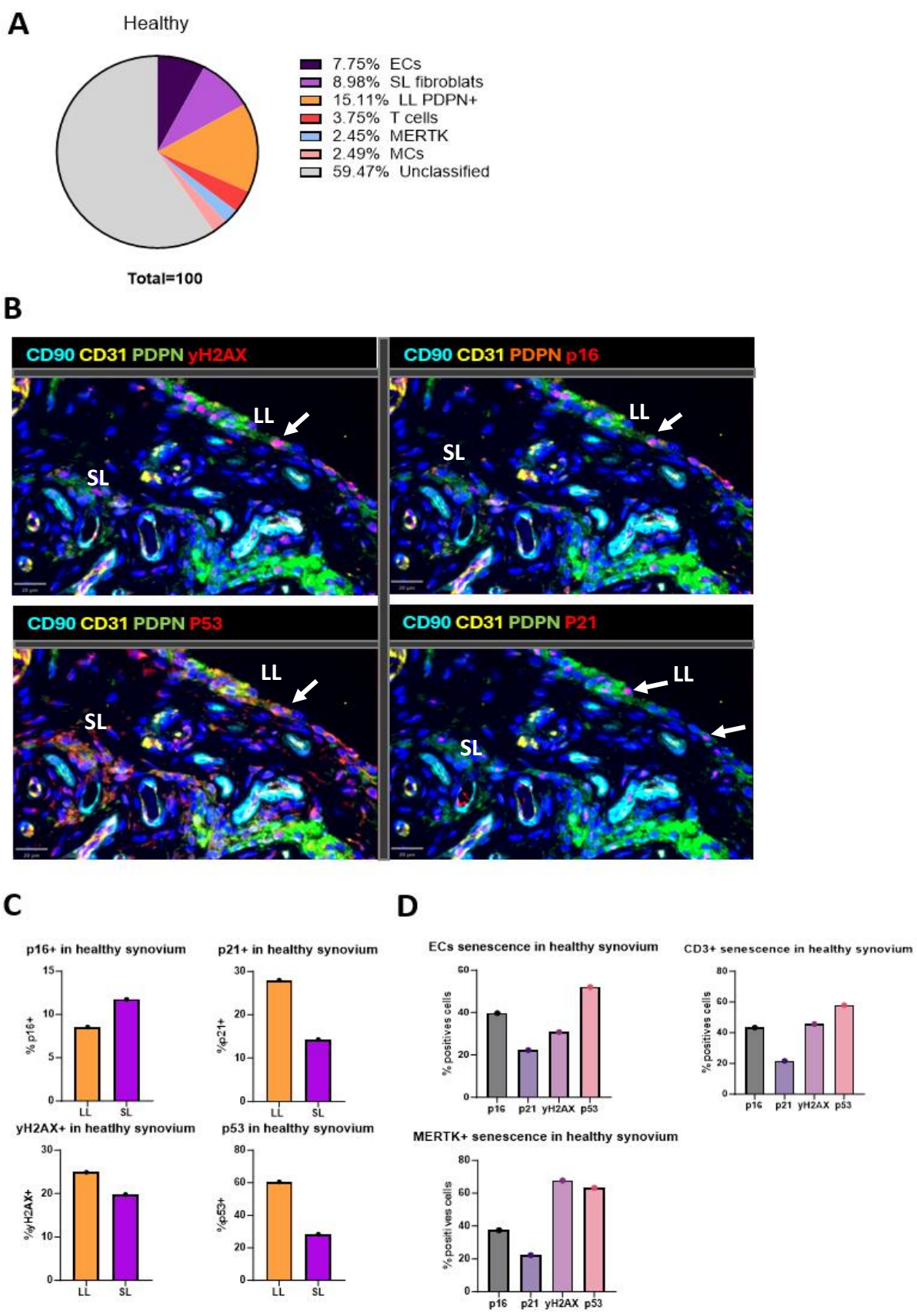


**Figure 4.2.5: Cellular senescence in healthy synovium**

**A:** Classification of the population observed in healthy synovium using multiplex IF panel. **B:** Multiplex IF staining showing yH2AX, p16, p53 and p21 (red), CD90 (cyan) CD31 (yellow), PDPN (green). **C:** Percentage of p16+, p21+, yH2AX+, and p53+ in LL fibroblasts (orange) and SL fibroblasts (purple) in healthy synovium (n=1). **D:** Percentage of p16+, p21+, yH2AX+, and p53+ in ECs (top left), T cells (top right) and MERTK+ (bottom left) in healthy synovium (n=1). White arrows= positive cells; LL=Lining layer; SL=Sub-lining.

## 4.3 Transcription of Hallmarks of Senescence in Human Synovium

### 4.3.1 Characterizing the transcription of CDKN2A and CDKN1A in OA and RA synovium

The implication of p16 in premature and replicative senescent cell is mainly dependant of its transcription. Many studies have identified the transcription factors Ets1 and 2 as positive regulator of the transcription of p16 by direct binding to its promoter resulting in cellular senescence in human fibroblasts (125). On the other hand, YB1 have been identified as a down regulator of p16 promoting cell growth (125, 126). This suggest that increasing p16 transcription is sufficient to induce premature and replicative cellular senescence. Furthermore, p21 transcription is activated directly by p53 (59). However, other interactors such as PCBP4, in a p53 independent manner, might regulate p21 by binding to its mRNA (127). However, it is unclear if it regulates p21 protein positively or negatively. Nevertheless, the transcription of *CDKN1A* (gene encoding for p21) and *CDKN2A* (gene encoding for p16) are critical in the establishment of cell cycle arrest and cellular senescence. Therefore, it is important to study the establishment of senescence with transcriptomic aspect. In a first time, we used the online available Sc-RNA seq data from the Accelerating Medicines Partnership (AMP) Rheumatoid Arthritis (RA) Phase I project (17) to address the expression of *CDKN2A* and *CDKN1A* in the synovial populations. This data set regroups 3 patient types including OA, leukocyte-poor RA, and leukocyte-rich RA. Therefore, the transcription of *CDKN2A* is spread throughout all the cell types without expression in a specific population **(Fig 4.3.1 A)**. Similarly, *CDKN1A* is expressed by all the synovial populations indifferently **(Fig 4.3.1 A)**. It is possible that the variation of expression of p16 and p21 are below the detection threshold and need to be investigated separately. Therefore, we investigated the transcription of *CDKN2A* and *CDKN1A* using fluorescence in situ hybridization (FISH). We used the RNAscope multiplex fluorescent kit allowing simultaneous staining of 3 mRNA probes in the same tissue.

In this context, we selected *PRG4* to classify the fibroblasts of the LL and *THY1* (CD90) for the SL fibroblasts. In combination with the previous fibroblast markers, we stained *CDKN2A* and *CDKN1A* in 10 RA patients and 6 OA patients and quantify the number of transcripts in synovial cells using the calculation methods described in methods. For unknow reason, *THY1* staining did not work in any of samples tested. Moreover, due to experimental variation some signals were either undetectable or oversaturated, especially with CDKN2A probes, leading to the removal of slides during the analysis. For the negative control, OA and RA slides were treated the same way but without probes to detected non-specific binding of the dyes.

The RNAscope signal consists of dots representing transcripts within the cells, when more dots than one dots are localized in the same sub-cellular region this form a cluster **(Fig 4.3.1 B, dots=white arrows; clusters=yellow arrows)**. In OA and RA synovium, we detected the presence of mRNA for p16 and p21 **(Fig 4.3.1 B)**. Then, we calculated the H-score of CDKN2A and CDKN1A in all the synovium to investigated different expression between OA and RA synovium. Therefore, the H-score for CDKN2A expression is 16,50 (±12,10; n=4) on average in OA, and 12,62 (±11,87; n=6) in RA patients **(Fig 4.3.1 D)**. Although, CDKN2A H-score is higher in OA, this difference is not significant due to high variability between the patients. Similarly, no significant difference in CDKN1A expression is observed between both diseases, with an average H-score of 21,81 (±7,72; n=6) and 17,29 (±9,79; n=10) in OA and RA respectively **(Fig 4.3.1 D)**. It is important to notice that the variability observed here might be both experimental and biological. Indeed, the cohort of patients we had access to was composed of old sections and fresh collected tissue, because of mRNA low stability we saw a difference is H-score between fresh and old slides. Yet, determining the localization of expression within the patients might help to better understand the context of senescence of the synovium. Thus, we calculated the H-score in the SL and LL in OA and RA patients. To determine accurately the LL, we used the expression of PRG4 while the SL was determined by the recognizable structures such as BVs or lymphocytes aggregates. Although, the majority of the patients in OA have more *CDKN2A* expression in the LL compared to the SL, this difference is not significant. Indeed, in OA, *CDKN2A* expression have a H-score of 20,63 (±10,92;

n=4) in the LL compared to the SL that have a H-score of 14,95 (±7,55; n=4) **(Fig 4.3.1 D)**. However, not enough slides were analysable to be statistically relevant. Furthermore, in RA, 5 out 6 patients have more CDKN2A mRNA in the LL compared to the SL, but one patient has a high expression of p16 in both sub regions. This could be explained by the fact that this patient has a high infiltrated synovium with lots of lymphocyte aggregates in which CDKN2A is highly expressed **(Fig 4.3.1 J)**. On the other hand, CDKN1A expression is significantly higher in the LL compared to the SL in both diseases. Indeed, the H-score of CDKN1A in OA LL is 33,13 (±8,13; n=6) while the H-score in the SL is 18,71 (±6,18; n=6) on average **(Fig 4.3.1 D)**. Similarly, in RA, 9 out of 10 patients tested have a higher H-score for CDKN1A in the LL compared to the H-score in the SL. Although the variability between patient in RA is greater than in the OA cohort the differential CDKN1A expression between the sub regions is significant with an average H-score of 28,51 (±24,14; n=10) in the LL compared to 19,16 (±19,47; n=10) in the SL **(Fig 4.3.1 D)**. The previous scores were measured using the combination of the dots scoring and the clusters scoring. Therefore, we investigated the H-score of the clusters alone to address any differences in the sub regions. As expected, in slides with clusters we see a small increase in the H-score of the LL for both CDKN2A and CDKN1A compared to the SL. However, this difference is not significant due to the very low number of clusters detected **(Fig 4.3.1 E)**. Then, we investigated the average number of dots per cells by diving the total number of dots detected by the number of positives cells. No significant difference in the number of dots per cells was observed between the LL and SL for CDKN2A and CDKN1A in both diseases **(Fig 4.3.1 F)**. However, between the expression of CDKN2A and CDKN1A, there is an increase of the average dots per cells in CDKN1A positive cells in both OA and RA, but this difference is only significant in the OA patients **(Fig 4.3.1 G)**.

As the primary aim of this experiment was to characterize the transcription of p16 and p21 in the LL and SL fibroblast populations, we try to colocalized the expression of CDKN2A and CDKN1A with PRG4 mainly expressed by LL fibroblasts and THY1 (CD90) expressed by the SL fibroblast populations. Since the THY1 probe did not work, we were only able to investigate the proportion of *CDKN2A* and *CDKN1A* positives in the *PRG4*+ cells. First, mRNA of p16 and p21 are both found in PRG4+ cells in OA and RA

**(Fig 4.3.1 F)**. Moreover, 21,81% (±7,56; n=4) of *PRG4*+ are *CDKN2A*+ in OA while in RA only 10,48% (±5,38; n=4) of the *PRG4*+ colocalized with *CDKN2A* **(Fig 4.3.1 I)**. Interestingly, we found that CDKN1A is also higher in OA PRG4+ cells with 42,81% (±10,14; n=5) compared to RA with 30,17% (±22,94; n=8) **(Fig 4.3.1 I)**. Although, those differences between the two diseases are not significant. Then, we asked if the difference between the proportion of *CDKN2A+ PRG4+* and *CDKN1A+ PRG4+* was significant. When we see a significative increase in *CDKN1A+ PRG4+* compared to CDKN2A+ PRG4+ in OA, this is not the case in RA despite the higher proportion of *CDKN1A+ PRG4+* observed **(Fig 4.3.1 J)**. Finally, we investigated the presence of CDKN2A and CDKN1A transcripts in other cell populations. Even though other makers could not be investigated in the same experiment some the structure of the synovium such as lymphocyte aggregates or blood vessels could still be identified with DAPI staining alone. Therefore, in OA and RA synovium we detected the presence of *CDKN2A*+ and *CDKN1A*+ in lymphoid aggregates, and blood vessels endothelium **(Fig 4.3.1 K, L)**. However, due to the lack of markers, it is not possible to attribute the expression to a specific cell type.

In summary, RNAscope analysis showed a variable expression of CDKN2A and CDKN1A but not significantly different between OA and RA synovium. Moreover, CDKN1A mRNA are significantly more expressed in the LL sub region compared to the SL in both diseases. The expression score of CDKN2A is also higher in the LL compared to the SL in OA and RA but not statistically significant. Furthermore, we found that CDKN1A+ cells have slightly more copies of p21 mRNA than the CDKN2A+ cells have p16 mRNA. Moreover, the H-score of *CDKN1A* is slightly higher in both LL and SL compared to the H-score of CDKN2A in the same sub region. While this might suggest more p21 activity than p16 this difference is not significant due to the variability between patients. in addition, the proportion of *CDKN1A+ PRG4+* is significantly increased compared to the *CDKN2A+ PRG4+* in OA suggesting more transcription of p21 in the LL fibroblasts. The same trend is observed in RA but is not significant. Finally, both CDKN1A and CDKN2A transcripts are found in ECs and Lymphocytes confirming the expression of p21 and p16 observed in those populations. Altogether, the transcription of p21 and p16 is found in most population

of the synovium, are more expressed in the LL compared to the SL confirming the senescence profile observed with multiplex histology.

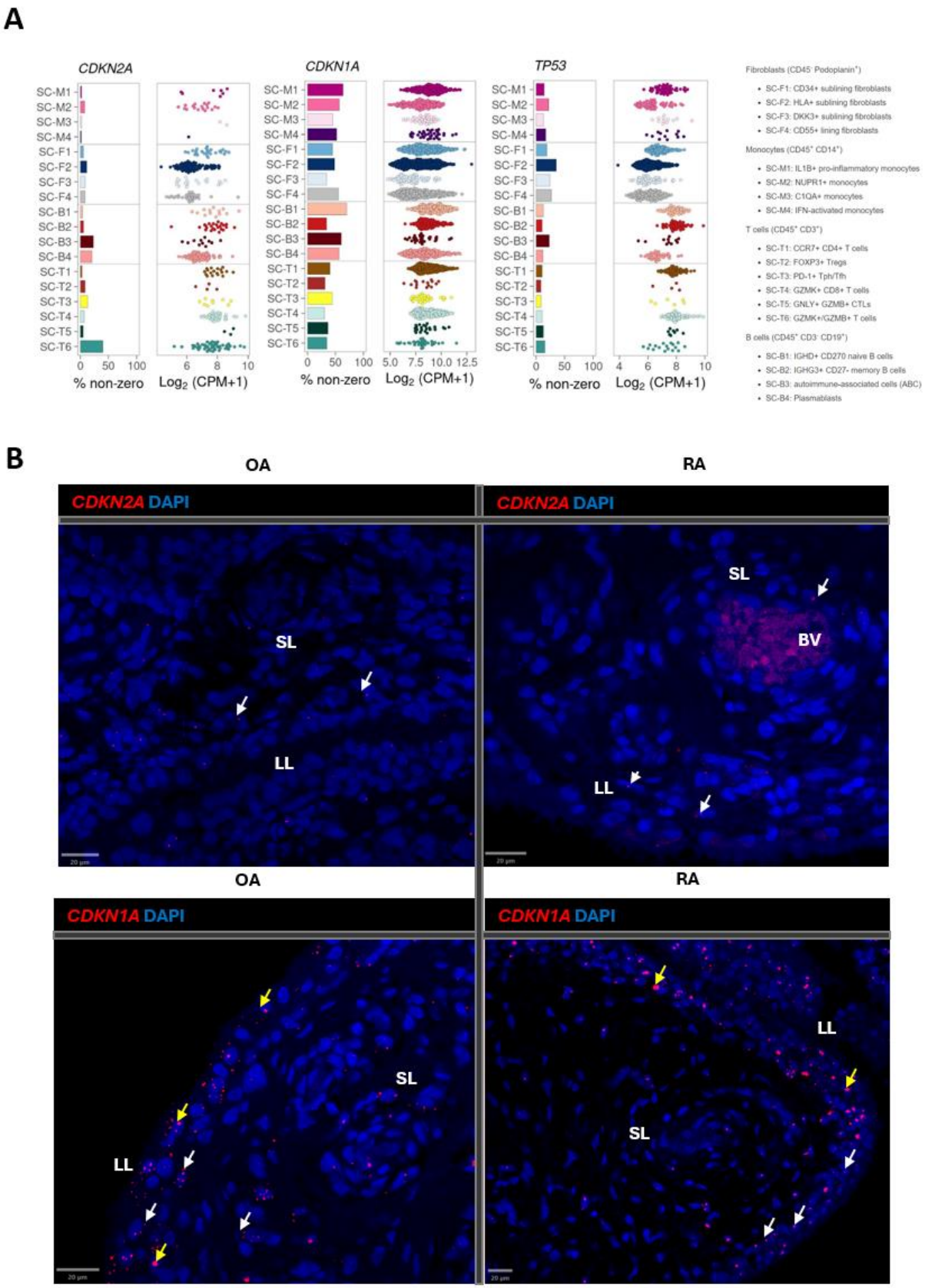


**Figure 4.3.1: Characterizing the transcription of CDKN2A and CDKN1A in OA and RA synovium**

**A:** Expression of *CDKN2A* (p16), *CDKN1A* (p21), and *TP53* (p53) in OA and RA synovium concatenated according to the Sc-RNA-seq Data set from the AMP phase I (17). **B:** RNAscope staining showing in red *CDKN2A* (p16) (top) and *CDKN1A* (p21) (bottom) in OA (left) and RA (right) synovium. White arrow = single dot, yellow arrow = cluster, BV =blood vessel, LL = Lining layer, SL = Sub-lining.

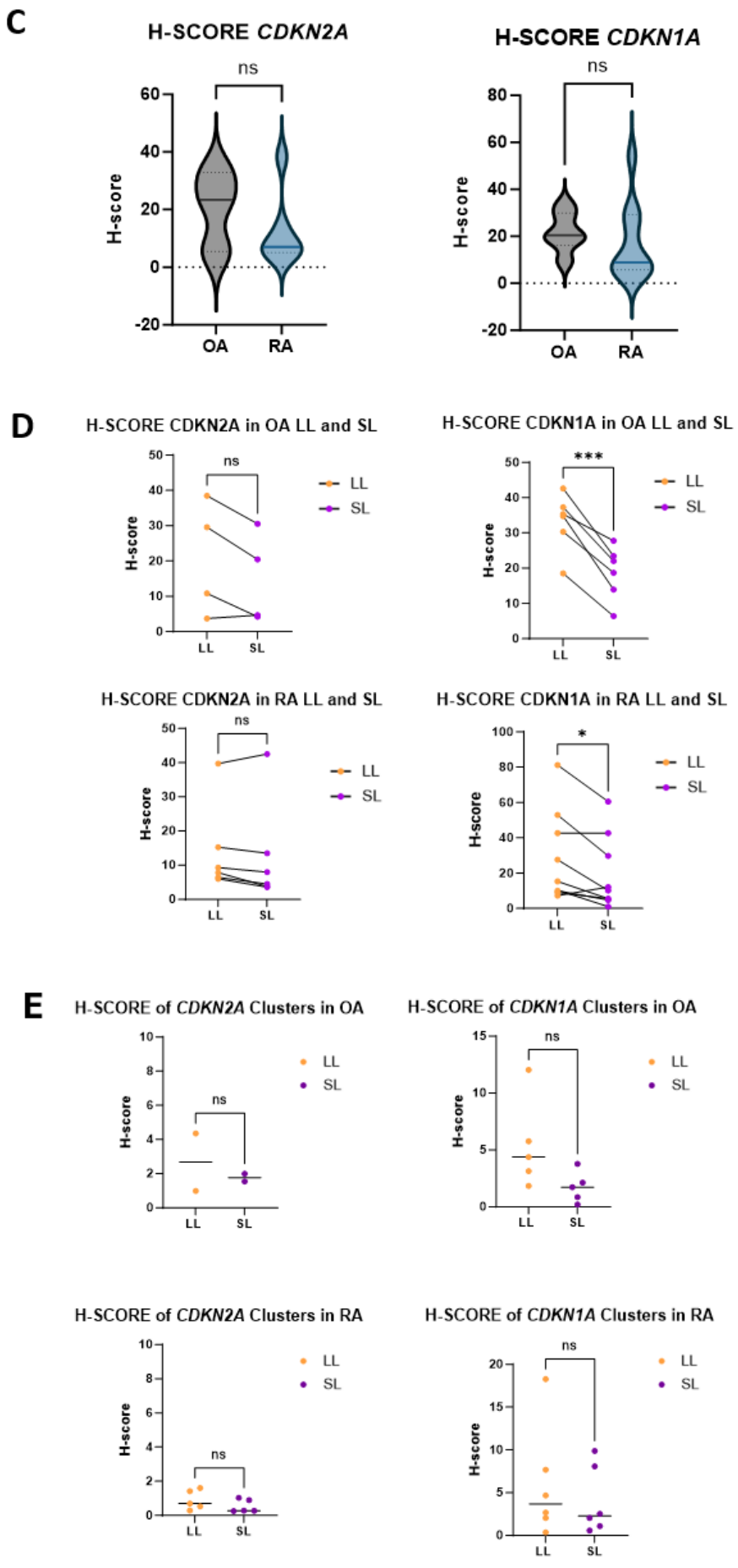


**Figure 4.3.1 (continued): Characterizing the transcription of CDKN2A and CDKN1A in OA and RA synovium**

**C:** H-score of *CDKN2A* (left), *CDKN1A* (right) in OA (grey) and RA (blue) synovium. Unpaired Students t-test for *CDKN2A*: OA (n=4), RA (n=6); Unpaired Students t-test for *CDKN1A*: OA (n=6), RA (n=10). **D:** H-score (dots + clusters) of *CDKN2A* (left) and *CDKN1A* (right) in the LL (orange) and SL (purple) in OA (top) and RA (bottom). Paired Students t-test for *CDKN2A*: OA (n=4), RA (n=6); Paired Students t-test for *CDKN1A*: OA (n=6), RA (n=10). E: H-score of *CDKN2A* clusters (left) and *CDKN1A* clusters (right) in the LL (orange) and SL (purple) in OA (top) and RA (bottom). Paired Students t-test for *CDKN2A*: OA (n=2), RA (n=5); Paired Students t-test for *CDKN1A*: OA (n=5), RA (n=6). (*p < 0.05; **p < 0.01; ***p < 0.001)

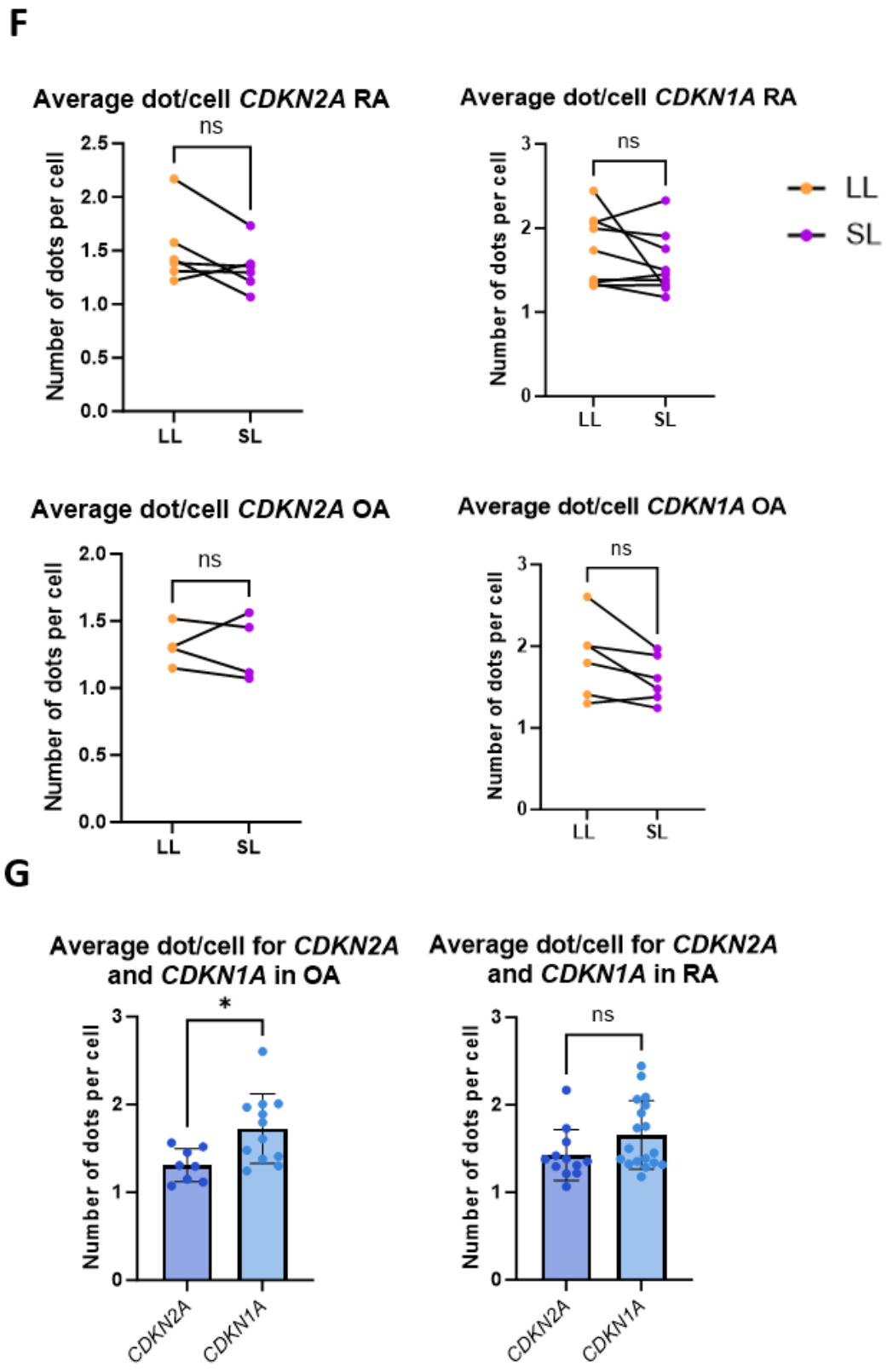


**Figure 4.3.1 (continued): Characterizing the transcription of CDKN2A and CDKN1A in OA and RA synovium**

**F:** Average dot per cell of *CDKN2A* (left) and *CDKN1A* (right) in the LL (orange) and SL (purple) in RA (top) and OA (bottom). G: Average dot per cell for *CDKN2A* (dark blue) compared to the average dot per cell of *CDKN1A* (light blue) in OA (left) and RA (right). The average dot/cell of the LL and SL were combined. Unpaired Students t-test for *CDKN2A*: OA (n=8), RA (n=12); Unpaired Students t-test for *CDKN1A*: OA (n=12), RA (n=20). (*p < 0.05).

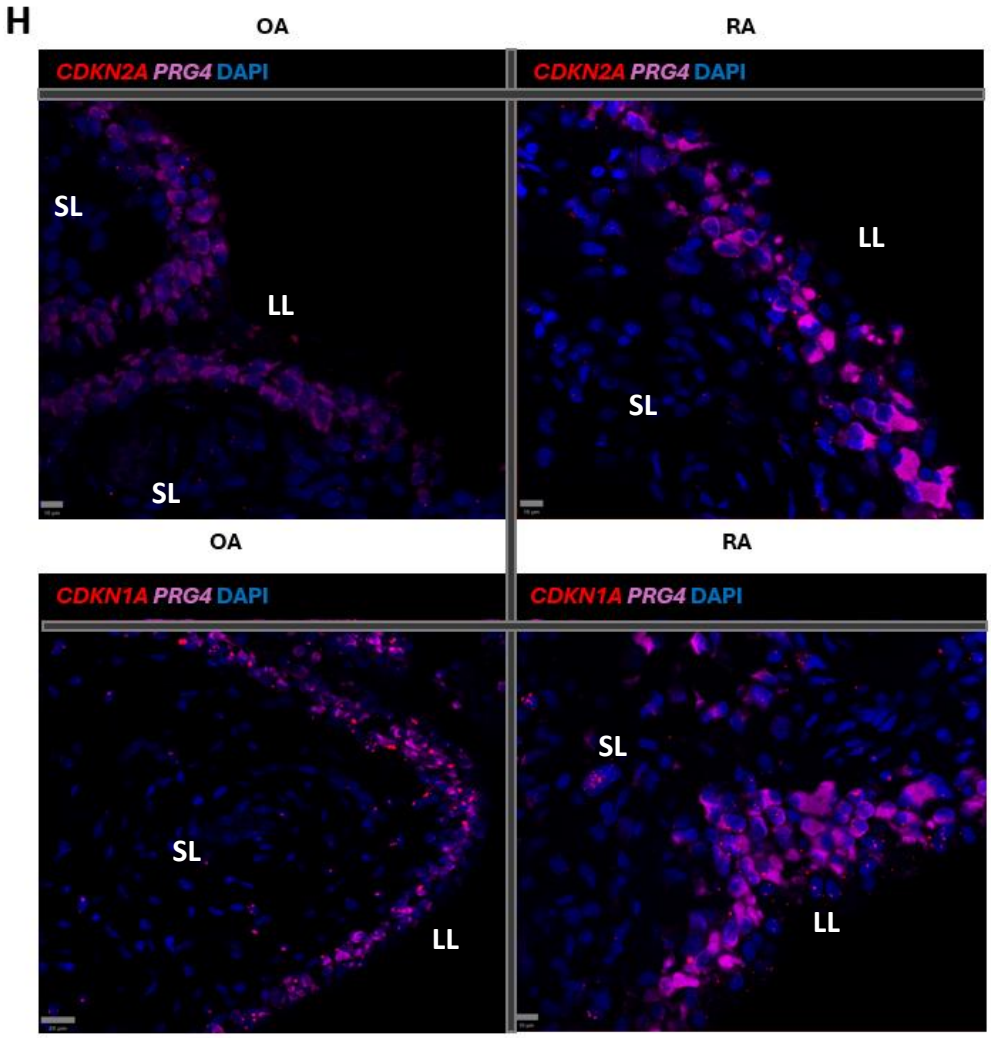


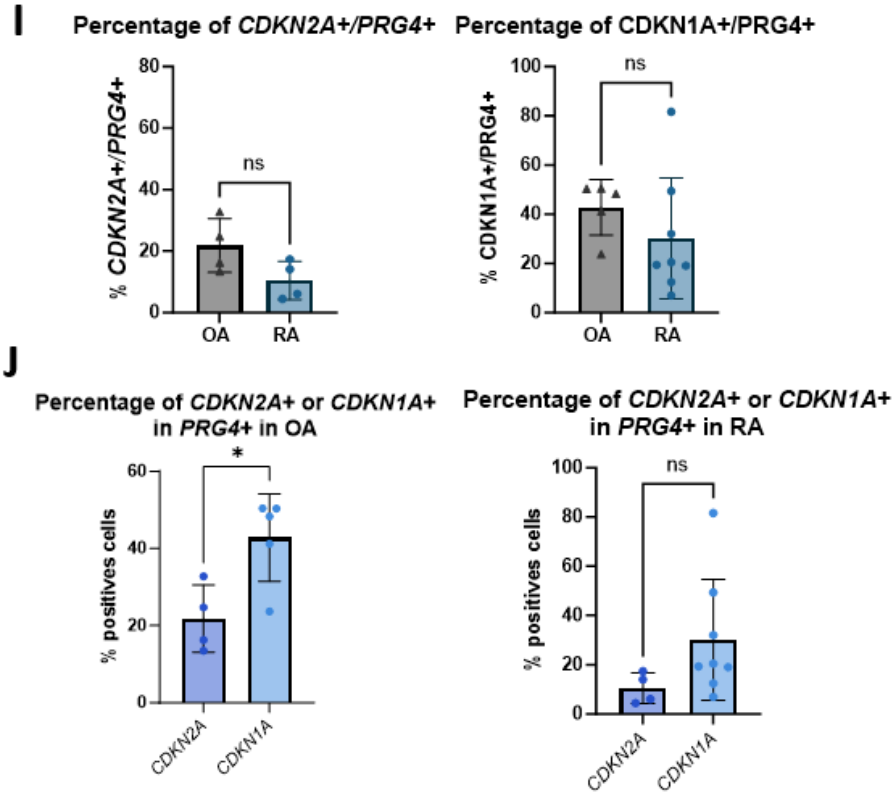


**Figure 4.3.1(continued): Characterizing the transcription of CDKN2A and CDKN1A in OA and RA synovium**

**H:** RNAscope staining showing in red *CDKN2A* (p16) (top) and *CDKN1A* (p21) (bottom) colocalization with *PRG4* (magenta) in OA (left) and RA (right) synovium. **I:** Percentage of *CDKN2A+* (left) and *CDKN1A+* (right) in *PRG4+* in OA (grey) and RA (blue). **J:** Comparison between the percentage of *CDKN2A+* in *PRG4+* (dark blue) with the percentage of *CDKN1A+* in *PRG4+* (light blue) in OA (left) and RA (right). LL=Lining layer; SL=Sub-lining; (*$p < 0.05$).

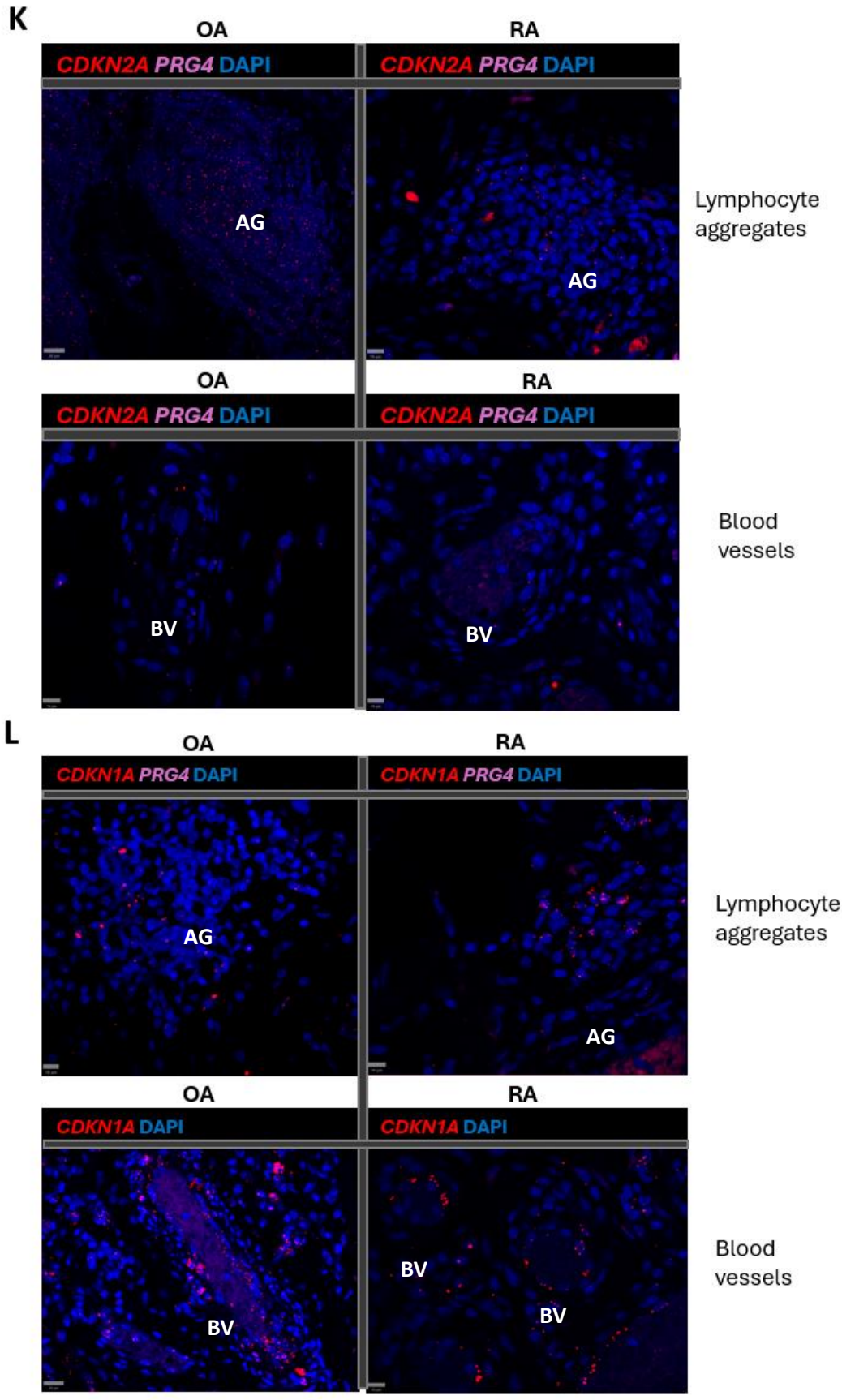


**Figure 4.3.1 (continued): Characterizing the transcription of CDKN2A and CDKN1A in OA and RA synovium**

**K:** RNAscope staining showing in red *CDKN2A* (p16) in lymphocyte aggregates (top) and blood vessels (bottom) in OA (left) and in RA (right). **L:** RNAscope staining showing in red *CDKN1A* (p16) in lymphocyte aggregates (top) and blood vessels (bottom) in OA (left) and in RA (right). BV=Blood vessels; AG=Aggregate.

# 5 Results chapter two: Does autophagy dysregulation increase cellular senescence?

## 5.1 TFEB expression in the human synovium

### 5.1.1 Global TFEB expression in OA and RA synovium

In this chapter, we aim to find some mechanism involved in the differential cellular senescence observed in chapter one to provide putative new regulations of aging in the synovium.

Autophagy has been recently in the centre of aging research and has now been accepted as an important hallmark of aging. Autophagy is the recycling machinery of the cell and regulates the degradation of defective mitochondria, aggregated or misfold proteins amongst other cellular components. As aged progress, autophagy decline leading to ER stress, mitochondrial dysfunction, and eventually cellular senescence. However, the relationship between autophagy and senescence remains unclear. One important transcription factor involves in the control of lysosome and autophagosome biogenesis is caller TFEB and is critical to establish autophagy. In this chapter we investigated the expression of TFEB in the synovial populations and correlate it with the previous findings on cellular senescence.

Similarly to the analysis of senescence, we investigated the expression of TFEB in the synovial cell populations using multiplex histology and spectral flow cytometry. We run thought issues in developing a working protocol for investigated TFEB with multiplex histology, for some unknown reasons the signal detected was either specific or in all tissue. Therefore, most of the patients tested were not analysable leaving 5 OA and 5 RA patients with a specific TFEB signal.

First, we investigated the differential expression of TFEB between OA and RA. Thus, TFEB expression is significantly reduced in OA compared to RA **(Fig 5.1.1 A)**. On average, 7,67% (± 3,35 n=5) of synovial cells are TFEB+ while 20,20% (± 5,64 n=5) of cells in RA synovium are TFEB+. Then, we measured the percentage of TFEB+ in the different region of the synovium and compared them between OA and RA.

Therefore, we observed that the proportion of TFEB+ in the LL is significantly decreased in OA compared to RA **(Fig 5.1.1 B)**. Despite the fact that the proportion of TFEB+ in the SL is higher in RA compared to OA, this difference is not significant, suggesting that the reduction of TFEB observed in OA in mainly associated with the LL **(Fig 5.1.1 B)**. Then, we investigated the differential expression of TFEB between the LL and the SL. Interestingly, in RA synovium, there is a significantly higher proportion of TFEB+ in the LL compared to the SL **(Fig 5.1.1 C)**. Moreover, this increase of TFEB+ cells in the LL is also found in OA but is not significant strengthen the idea that the decrease in autophagy in OA undergoes in the LL. However, this decrease is not observe by flow cytometry where the same overall TFEB fluorescence intensity is observed in both diseases **(Fig 5.1.1 D)**.

The activation of TFEB dependant of its sub-cellular localization, activated TFEB is nuclear while the inactive form is retained at the lysosomal membrane within the cytoplasm (94, 95). To investigated further the difference between OA and RA TFEB expression, we quantified the nuclear and cytoplasmic MFI of TFEB in the TFEB+ according to their location in the LL or SL. Therefore, on the first OA patients tested we observed a significant decrease of nuclear TFEB MFI in the LL compared to the nuclear MFI in the SL suggesting more activation in the SL compared to the LL **(Fig 5.1.1 E)**. In addition, there is a significant decrease of cytoplasmic TFEB in the SL compared to the cytoplasmic TFEB in the LL supporting the hypothesis of differential activation in this patient **(Fig 5.1.1 E)**. On the other hand, in one RA patient, the nuclear TFEB MFI is significantly increased in the LL compared to the SL **(Fig 5.1.1 F)**. Interestingly, in this patient the cytoplasmic MFI is increased in the SL compared to the LL **(Fig 5.1.1 F)**. To tested if this differential activation of TFEB was not only specific to those 2 isolated patients we analysed the sub-cellular localization of TFEB in the whole cohort. Thus, to perform the analysis across patients, we compared the ratio of the nuclear TFEB MFI of the LL divided by the nuclear MFI of the SL in both OA and RA. Interestingly, we observed a significative increase in the ration of nuclear LL/SL TFEB in RA compared to the same ratio in OA **(Fig 5.1.1 G)**. This demonstrated that RA have more intensity of TFEB in the nucleus in the LL compared to OA may be suggesting a differential activity of TFEB

between the two diseases. Next, we performed the same analysis on the cytoplasmic TFEB MFI but found no difference in the ratio of LL/SL cytoplasmic TFEB between OA and RA **(Fig 5.1.1 H)**.

Altogether, multiplex histology staining indicates that the global expression of TFEB is decreased in OA synovium compared to RA. Furthermore, this decreased in observed most specifically in the LL compared to the LL of OA patients. Moreover, the expression of TFEB in RA is higher in the LL suggesting that autophagy might be an important process of the LL homeostasis. In addition, this differential expression of TFEB between the LL and the SL is abrogated in OA due to the decrease of TFEB in the LL. Surprisingly, no difference in TFEB expression is observed by flow cytometry between OA and RA. Beside the different proportions of TFEB+ in OA and RA, the activity of TFEB in the LL compared to the SL is reduced in OA but enhanced in RA suggesting that in OA TFEB activity might be dysregulated in the LL but not in the SL.

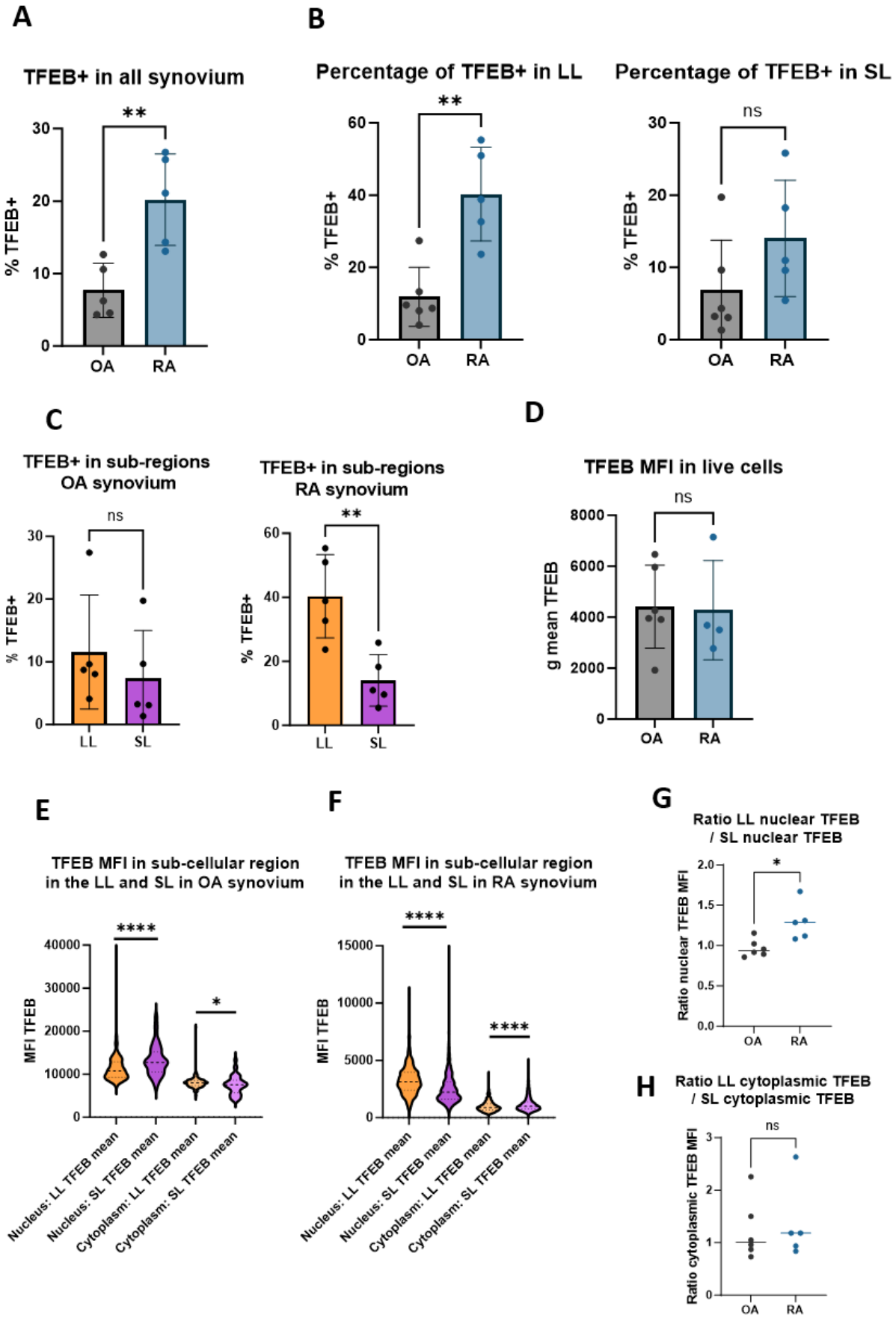
A
TFEB+ in all synovium
% TFEB+
OA
RA
**
B
Percentage of TFEB+ in LL
Percentage of TFEB+ in SL
ns
C
TFEB+ in sub-regions OA synovium
TFEB+ in sub-regions RA synovium
LL
SL
D
TFEB MFI in live cells
g mean TFEB
E
TFEB MFI in sub-cellular region in the LL and SL in OA synovium
F
TFEB MFI in sub-cellular region in the LL and SL in RA synovium
MFI TFEB
****
Nucleus: LL TFEB mean
Nucleus: SL TFEB mean
Cytoplasm: LL TFEB mean
Cytoplasm: SL TFEB mean
G
Ratio LL nuclear TFEB / SL nuclear TFEB
Ratio nuclear TFEB MFI
H
Ratio LL cytoplasmic TFEB / SL cytoplasmic TFEB
Ratio cytoplasmic TFEB MFI

**Figure 5.1.1 Global TFEB expression in OA and RA synovium**

**A:** Percentage of TFEB+ in total synovium in OA (grey) and RA (blue); unpaired t-test OA (n=5) RA (n=5). **B:** Percentage of TFEB+ in the LL (left) and in the SL (right) in OA (grey) and RA (blue); unpaired t-test OA (n=5) RA (n=5). C: Comparison between the percentage of TFEB+ in the LL (orange) with percentage of TFEB in the SL (purple) in OA (left) and RA (right); unpaired t-test OA (n=5) RA (n=5). D: TFEB MFI in OA (grey) and RA (blue) quantify in flow cytometry, unpaired t-test OA (n=6) RA (n=4). **E:** Nuclear and cytoplasmic MFI of TFEB in TFEB+ cells of the LL (orange) or in the SL (purple) quantified in multiplex IF in one OA patient. **F:** Nuclear and cytoplasmic MFI of TFEB in TFEB+ cells of the LL (orange) or in the SL (purple) quantified in multiplex IF in one OA patient. **G:** Ratio = mean of nuclear TFEB fluorescence intensity in the LL divided by the mean of nuclear TFEB fluorescence intensity in the SL in OA (grey) and RA (blue). Ratio <1 = more nuclear TFEB; unpaired t-test OA (n=5) RA (n=5). H: Ratio = mean of cytoplasmic TFEB fluorescence intensity in the LL divided by the means of cytoplasmic TFEB fluorescence intensity in the SL in OA (grey) and RA (blue). Ratio <1 correspond to more nuclear TFEB; unpaired t-test OA (n=5) RA (n=5). (*p < 0.05; **p < 0.01; ***p < 0.001; ****p < 0,0001).

### 5.1.2 TFEB expression in the fibroblast populations

Previous findings suggest that cellular senescence is increased in the PDPN+ LL fibroblasts compared to the CD90+ SL fibroblasts. This might indicate different TFEB expression which could lead to differential senescence. However, TFEB expression is mainly located in the LL in both OA and RA **(Fig 5.1.1; Fig 5.1.2 A)**. Therefore, when we investigated the proportion of TFEB+ in the PDPN+ MERTK- CD68- LL fibroblasts we see an increased compared to the CD90+ CD31- SL fibroblasts in both diseases **(Fig 5.1.2 B)**. However, this increase is not significant as some patients have more TFEB+ in the SL compared to the LL fibroblasts. Furthermore, in RA the percentage of TFEB+ LL fibroblasts is significantly higher than the percentage of TFEB+ SL fibroblasts **(Fig 5.1.2 C)**. This suggest that beside having a higher proportion of TFEB+ LL fibroblasts compared to TFEB+ SL, the reduction of TFEB observed between OA and RA is associated with a reduction of TFEB in the LL fibroblasts population. On the other hand, the proportion of TFEB+ in OA SL fibroblasts is also decreased compared to the RA SL fibroblasts but not significantly suggesting that those population might not be affected the same way by the decrease of TFEB **(Fig 5.1.2 C)**.

Next, we investigated the expression of TFEB in the $PDPN^{HIGH}$ and $PDPN^{LOW}$, classified previously as LL fibroblasts and SL fibroblasts respectively, using flow cytometry **(Fig 5.1.2 D)**. As described earlier, the expression of TFEB by flow cytometry did not show difference between OA and RA on the total live

cells but difference might still occur among the synovial populations. Therefore, we investigate the MFI of TFEB in the concatenated fibroblast populations between OA and RA, but no difference was detected **(Fig 5.1.2 E)**. Furthermore, the proportion TFEB+ in the $PDPN^{HIGH}$ is not increased in the RA patients compared to the OA patients **(Fig 5.1.2 E)**. Similarly, no difference is observed in the percentage of TFEB+ in the $PDPN^{LOW}$ population between the two diseases **(Fig 5.1.2 E)**. However, we can notice more heterogeneity in the percentage of TFEB+ among the OA patients compared to the RA cohort perhaps suggesting that TFEB is expression is more subject to dysregulation in OA. Furthermore, when we compared the $PDPN^{HIGH}$ and $PDPN^{LOW}$, there is a significant increase in the proportion of TFEB+ in the OA $PDPN^{HIGH}$ suggesting again the association of TFEB with the LL **(Fig 5.1.2 F)**. Similarly, in RA the $PDPN^{HIGH}$ have a higher TFEB+ proportion compared to the $PDPN^{LOW}$, but this difference is not significant. Interestingly, the MFI of TFEB in the PDPNHIGH is not increased compared to the MFI measured in PDPNLOW in both OA and RA **(Fig 5.1.2 G)**. This might suggest that even if the proportion of TFEB+ is increased there is not more TFEB expression within the cell.

Altogether, those data suggest that TFEB is potentially higher in the LL fibroblasts compared to the SL fibroblasts. However, histology data suggest that the reduction of TFEB observed in the total synovium in OA compared to RA is associated with a reduction of TFEB in the LL fibroblasts. Unfortunately, this difference is not observed in flow cytometry to confirm this statement.

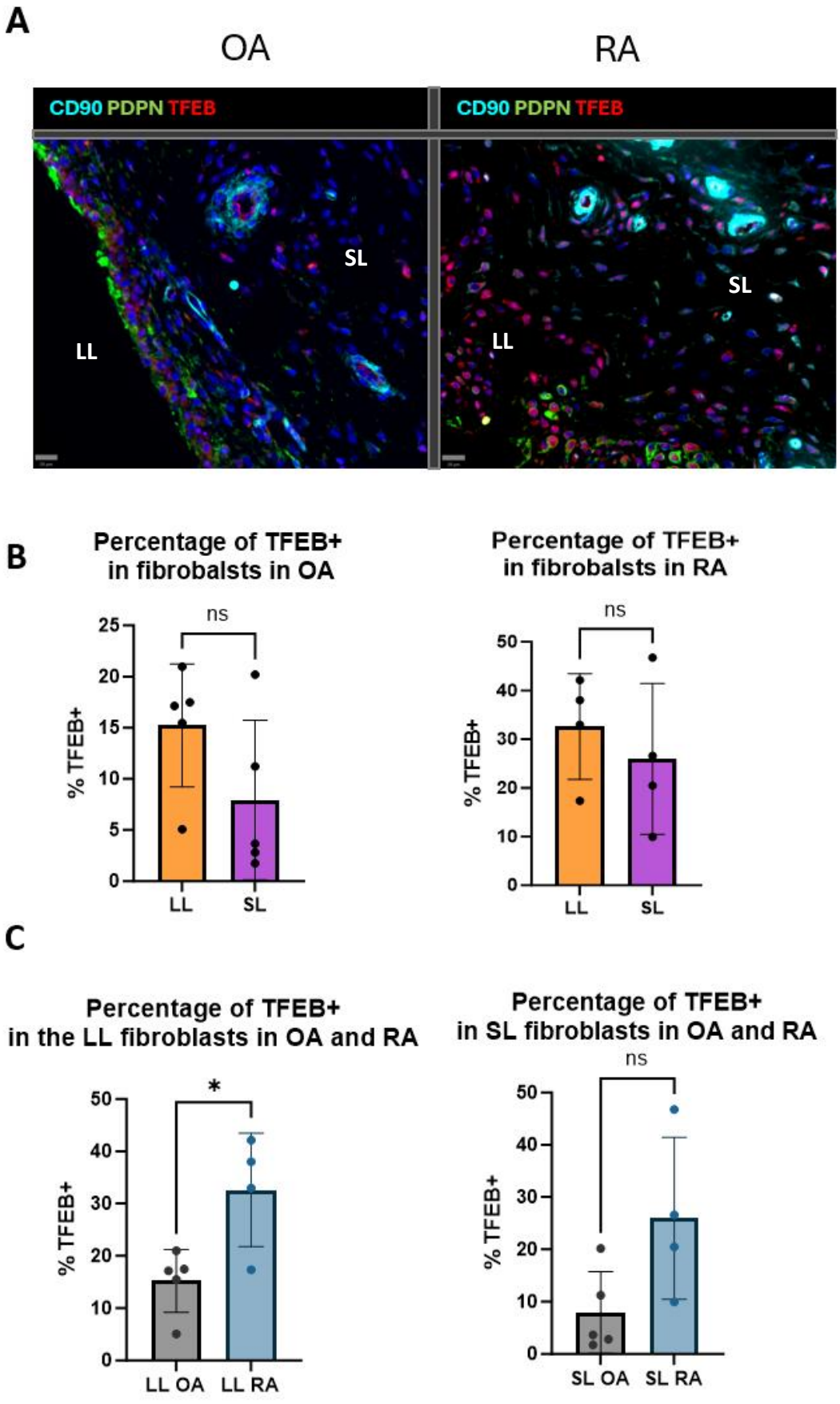


**Figure 5.1.2 TFEB expression in the fibroblast populations**

**A:** Multiplex IF staining showing TFEB (red), CD90 (cyan), and PDPN (green) in OA (left) and RA (right) synovium. B: Percentage of TFEB+ in LL fibroblasts (orange) and SL fibroblasts (purple) in OA (left) and in RA (right). C: Comparison of percentage of TFEB+ between OA (grey) and RA (blue) LL fibroblasts (left) and SL (right); LL=Lining layer; SL=Sub-lining; (*$p < 0.05$).

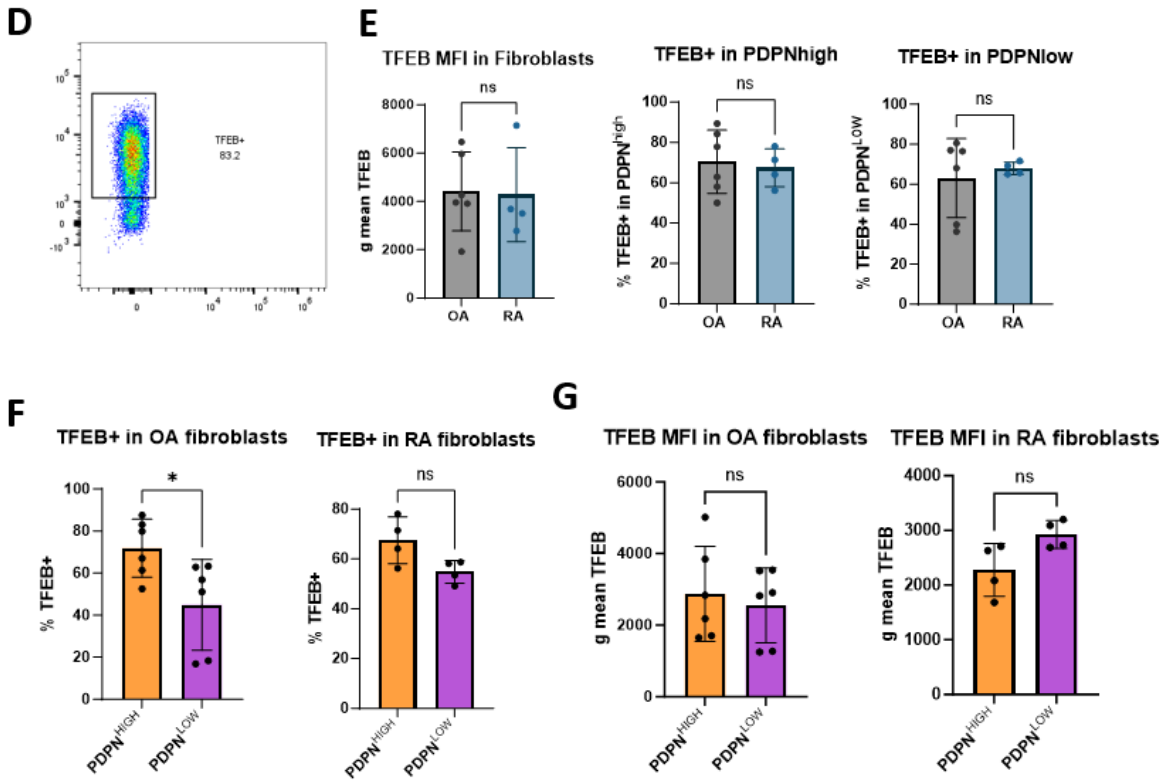


**Figure 5.1.2 TFEB expression in the fibroblast populations**

**D:** Gating strategy used to classify the TFEB+ in flow cytometry. **E:** Left: TFEB MFI in all fibroblasts in OA (grey) and RA (blue). Middle: TFEB+ percentage in PDPN$^{HIGH}$ in OA (grey) and RA (blue). Right: TFEB+ percentage in PDPN$^{LOW}$ in OA (grey) and RA (blue). Unpaired t-test OA (n=6) RA (n=4). **F:** TFEB+ percentage in PDPN$^{HIGH}$ (orange) compared to the percentage of TFEB+ in PDPN$^{LOW}$ (purple) in OA (left) and RA (right). **G:** TFEB MFI in PDPN$^{HIGH}$ (orange) compared to the MFI of TFEB in PDPN$^{LOW}$ (purple) in OA (left) and RA (right); Paired t-test OA (n=6) RA (n=4). (*$p < 0.05$).

### 5.1.3 TFEB expression in the macrophage populations

To further understand the autophagy regulation in the synovium it is critical to characterized TFEB expression in the macrophages as they are a major component of the synovium. Therefore, we looked at the expression of TFEB in the MERTK+, CD68+ and CD206+ macrophages of the synovium in the different sub-region of the synovium. First, we noticed that TFEB co-localized with MERTK+, CD68+ and CD206+ in OA and RA synovium **(Fig 5.1.3 A)**. However, the percentage of TFEB+ in macrophages is heterogenous among patients. For instance, some patients will have more that 40% of TFEB+ in LL

MERTK+ compared to other that have less than 10% of TFEB+ MERTK+ in the LL **(Fig 5.1.3 B)**. Nevertheless, the percentage of TFEB+ in LL MERTK+ is higher compared to the TFEB+ in SL MERTK+ **(Fig 5.1.3 B)**. This is significant in the RA patients but not in OA. Furthermore, the proportion of TFEB+ is also higher in the LL compared to the SL in 3out of 4 patients in OA while in RA 3 out of 3 patients have more CD68+ in the LL compared to the CD68+ in the SL **(Fig 5.1.3 B)**. Inversely, the proportion of CD206+ TFEB+ is higher in the SL in 3 out of 4 patients in OA and 2 out 3 patients in RA **(Fig 5.1.3 B)**. This is expected as the proportion of CD206+ is higher in the SL compared to the LL. Moreover, the proportion of TFEB+ in the LL MERTK does not change between OA and RA suggesting that the difference in senescence observed in this population might net be due to a differential autophagy **(Fig 5.1.3 C)**. Interestingly, there is no difference in the proportion of TFEB+ between OA and RA in the MERTK+CD68+ LL macrophages and SL CD206+ CD68+ suggesting that the difference seen between the two disease might not be related to a decrease of TFEB expression in the macrophage populations **(Fig 5.1.3 D)**.

Then, I investigated the expression of TFEB in the MERTK+ and CD68+ population by flow cytometry and no significant difference was observed in the MFI of TFEB in the MERTK+ and MERTK+ CD68+ in OA and RA **(Fig 5.1.3 E)**. Furthermore, the MFI of TFEB in the MERTK+ CD68+ is slightly increased compared to the MFI of TFEB in the MERTK+ macrophages in both OA and RA **(Fig 5.1.3 F)**. Interestingly, senescence was increased through p21, yH2AX and p53 in the MERTK+ compared to the MERTK+ CD68+ perhaps suggesting that the increase of TFEB might play a role in the decrease of senescence in those populations. However, this need to be further investigated with more direct mechanistic approaches.

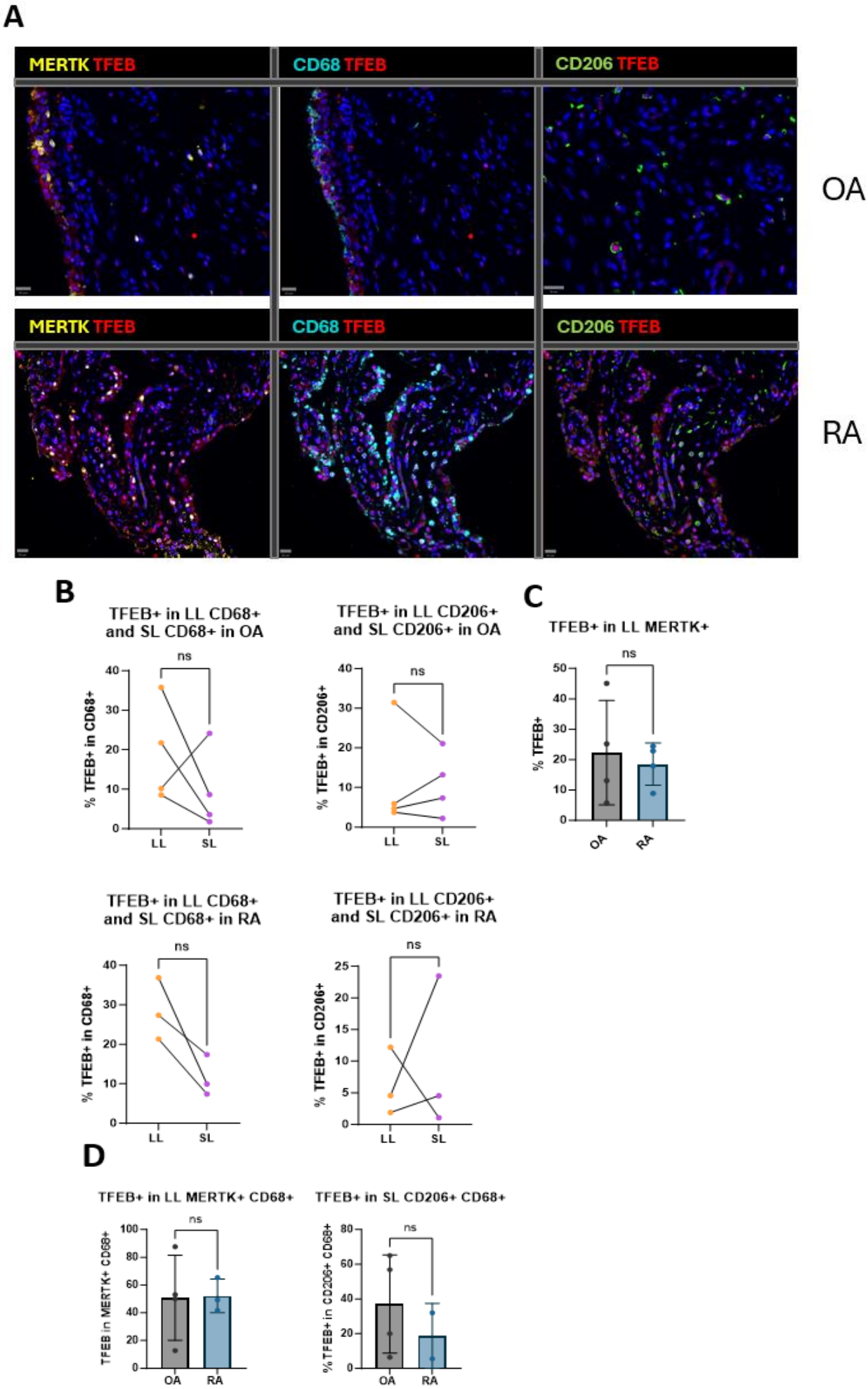
A
MERTK TFEB
CD68 TFEB
CD206 TFEB
OA
MERTK TFEB
CD68 TFEB
CD206 TFEB
RA
B
TFEB+ in LL CD68+ and SL CD68+ in OA
% TFEB+ in CD68+
ns
LL
SL
TFEB+ in LL CD206+ and SL CD206+ in OA
% TFEB+ in CD206+
ns
LL
SL
C
TFEB+ in LL MERTK+
% TFEB+
ns
OA
RA
TFEB+ in LL CD68+ and SL CD68+ in RA
% TFEB+ in CD68+
ns
LL
SL
TFEB+ in LL CD206+ and SL CD206+ in RA
% TFEB+ in CD206+
ns
LL
SL
D
TFEB+ in LL MERTK+ CD68+
TFEB in MERTK+ CD68+
ns
OA
RA
TFEB+ in SL CD206+ CD68+
% TFEB+ in CD206+ CD68+
ns
OA
RA

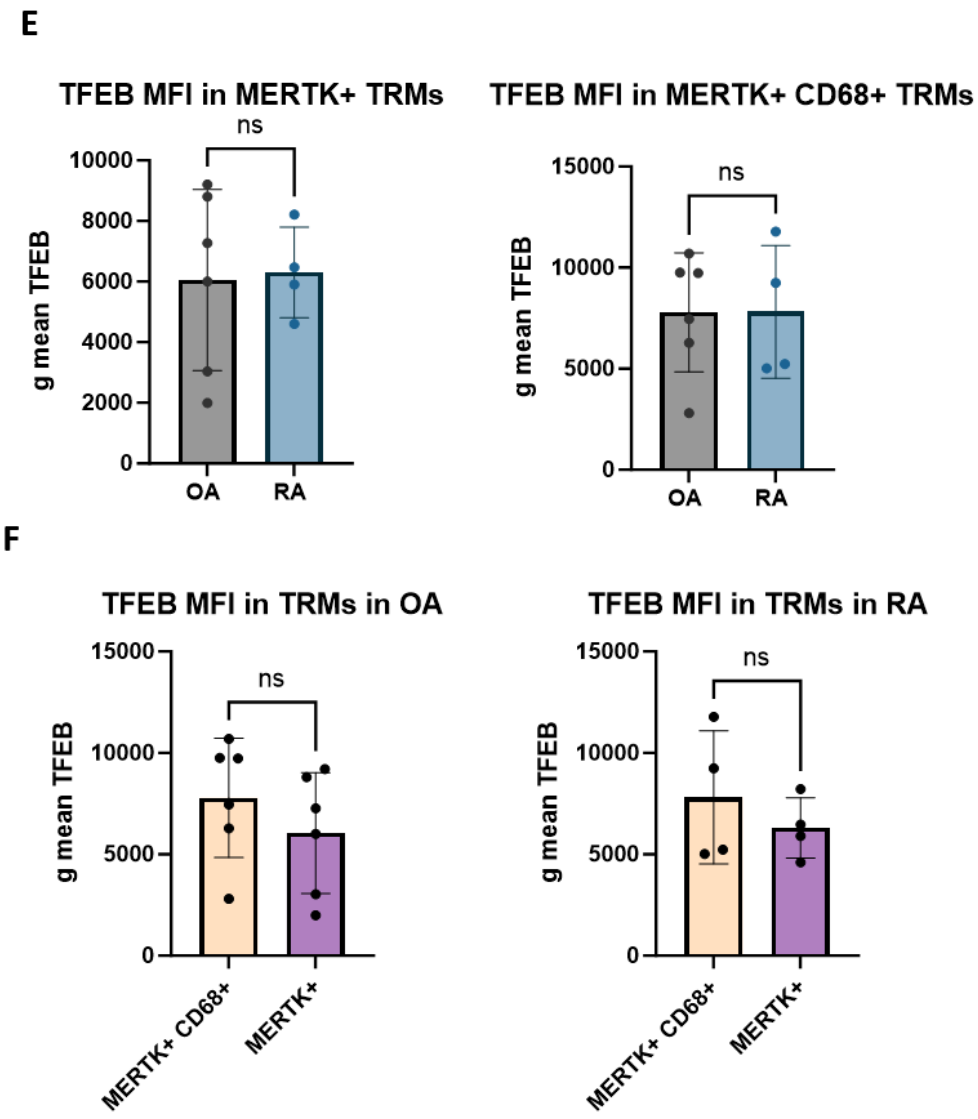


**Figure 5.1.3: TFEB expression in the macrophage populations**

**A:** Multiplex IF staining showing TFEB (red), CD68 (cyan), MERTK (yellow), and CD206 (green) in OA (top panel) and RA (bottom panel) synovium. **B:** Left: percentage of TFEB+ in LL CD68+ TRMs (orange) compared the percentage of TFEB+ in SL CD68+ TRMs (purple) in OA (top) and RA (bottom). Right: percentage of TFEB+ in LL CD206+ TRMs (orange) compared the percentage of TFEB+ in SL CD206+ TRMs (purple) in OA (top) and RA (bottom); paired t-test OA (n=4) RA (n=3). C: Percentage of TFEB+ in LL MERTK+ in OA (grey) and RA (blue); unpaired t-test OA (n=4) RA (n=4). D: Percentage of TFEB+ in LL MERTK+CD68+ (left) and in SL CD206+CD68+ (right) in OA (grey) and RA (blue); unpaired t-test MERTK+CD68+: OA (n=4) RA (n=3); unpaired t-test CD206+CD68+: OA (n=4) RA (n=2). **E:** TFEB MFI in MERTK+ (left) and MERTK+CD68+ (right) in OA (grey) and RA (blue); unpaired t-test OA (n=6) RA (n=4). **F:** TFEB MFI in MERTK+CD68+ (orange) compared to the TFEB MFI in MERTK+ (purple) in OA (left) and RA (right); unpaired t-test OA (n=6) RA (n=4).

### 5.1.4 TFEB expression in the infiltrated lymphocytes

While immune senescence is associated with loss of immune function, increasing autophagy improved B cell and T cell mediated immune response (128, 129, 130). In autoimmune diseases such as RA, impairing immune functions is key to prevent inflammation. For instance, the common use of Methotrexate (MTX) in RA therapies, aims to reduce the T cells and B cells activation. Therefore, we may ask if more autophagy is good in the context of chronic inflammation as it might increase B and T cells functions. On the other hand, immune senescence in the context of chronic inflammation may lead to worst outcomes. Nevertheless, little is known about autophagy and immune senescence during arthritis.

For this reason, we tried to quantify the expression of TFEB in the immune infiltered cell population including B cells and T cells in human OA and RA synovium using multiplex and flow cytometry. Due to inconsistency of both TFEB and CD20, we were not able to properly quantify TFEB expression in B cells by histology. However, during the optimization staining, we were able to successfully co-stain TFEB and CD19 in one OA patient **(Fig 5.1.4 A)**. Thus, in this patient, we observed a strong colocalization of TFEB and CD19 in lymphocytes aggregates while the proportion TFEB in T cells in reduced **(Fig 5.1.4 A)**. Then we investigated the proportion of TFEB+ in CD3+ and CD45+ cells in OA and RA and found no difference between diseases suggesting that autophagy is not decreased in OA patients **(Fig 5.1.4 B)**. Next, we compared the expression of TFEB in the CD3+ T cells against the CD45+ and CD45+ CD3- immune cells in the synovium. Moreover, in aggregates, we noticed that many cells are TFEB+ CD45+ but are not CD3+ **(Fig 5.1.4 C white arrows)**. Those cells might be B cells but in absence of specific markers this cannot be confirmed. Nevertheless, in OA we observed that the proportion of TFEB+ is higher in the CD45+ CD3- compared to the CD3+ while no difference is observed in RA **(Fig 5.1.4 D)**. To further characterized those findings in B cells, we investigated the MFI of TFEB in the CD19 in OA and RA. Thus, no differences are observed in the MFI of TFEB in the CD19+ B cells between the two diseases **(Fig 5.1.4 E)**. Similarly to the histology data, TFEB expression is also similar in T cells for both diseases **(Fig 5.1.4**

**E)**. However, the expression of TFEB is significantly increased in the B cells compared to the T cells in OA and RA. This is confirmed by both the increase of the proportion of TFEB+ and MFI of TFEB **(Fig 5.1.4 F)**. Furthermore, within the T cells, the proportion of TFEB+ in the CD4+ is significantly increased compared to the proportion of TFEB+ in the CD8+ in OA **(Fig 5.1.4 G)**. The MFI also indicates a decrease of TFEB in the CD8+ compared to the CD4+ in both OA and RA, but the difference is not significant.

In summary, TFEB expression in infiltrated cells do not change between OA and RA, confirming even more that the decrease of autophagy in OA is associated with a decrease of TFEB in the LL fibroblasts. Furthermore, we confirmed that TFEB is higher in the B cells populations compared to the T cells in both OA and RA. Other unpublished data are supporting the fact that B cells among other immune cells have the highest TFEB expression which is also the case in infiltrated cells in the synovium. Moreover, those data suggest that CD4 and CD8 T cells may have different regulation of TFEB that might play a role in their activity during inflammation.

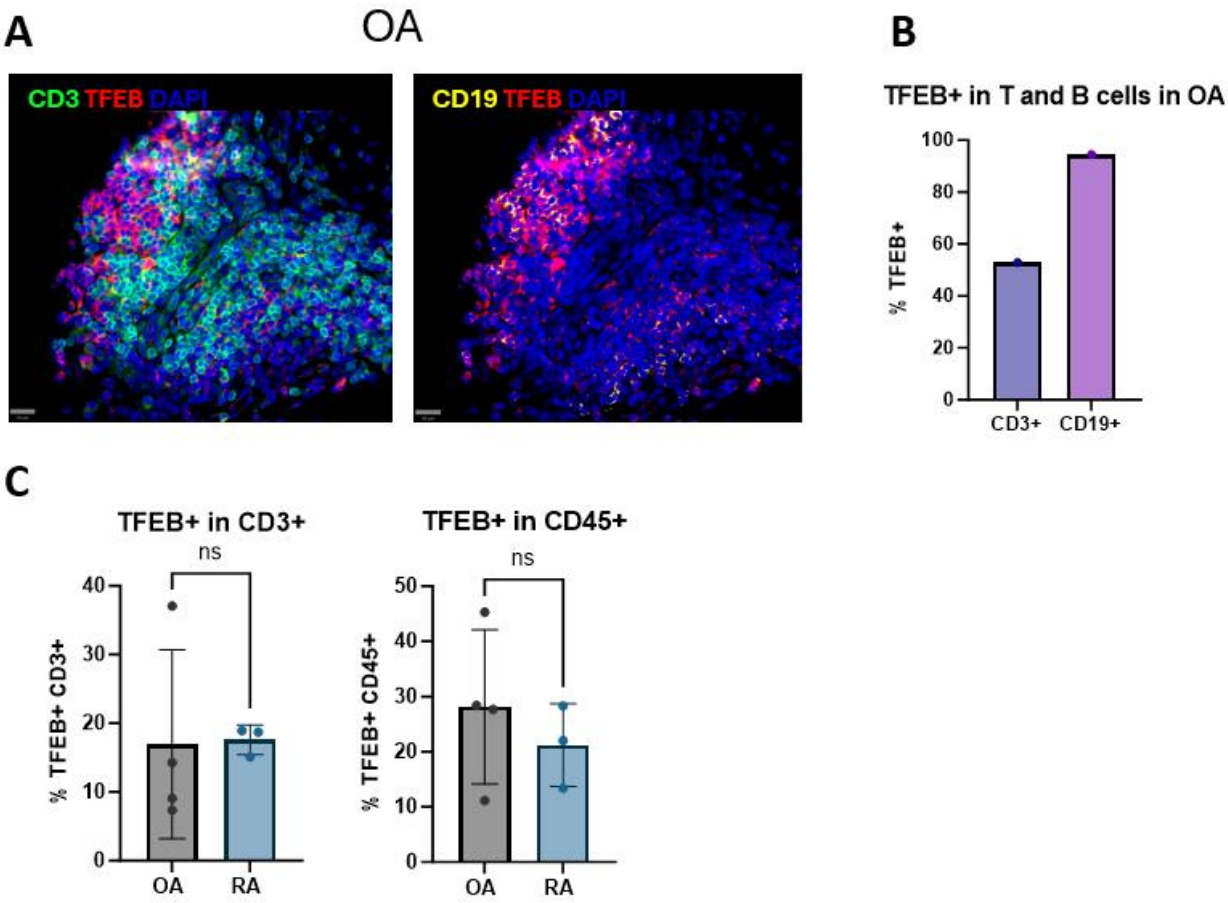


**Figure 5.1.4 TFEB expression in the infiltrated lymphocytes**

**A:** Multiplex IF staining showing TFEB (red), CD3 (green), and CD19 (yellow) in a lymphocyte aggregate in OA synovium. **B:** Percentage of TFEB+ in CD3+ T cells and CD19+ B cells in the OA patient in A. **C:** Percentage of TFEB+ in CD3+ T cell (left) and CD45+ immune cells (right) in OA (grey) and RA (blue); unpaired t-test OA (n=4) RA (n=4).

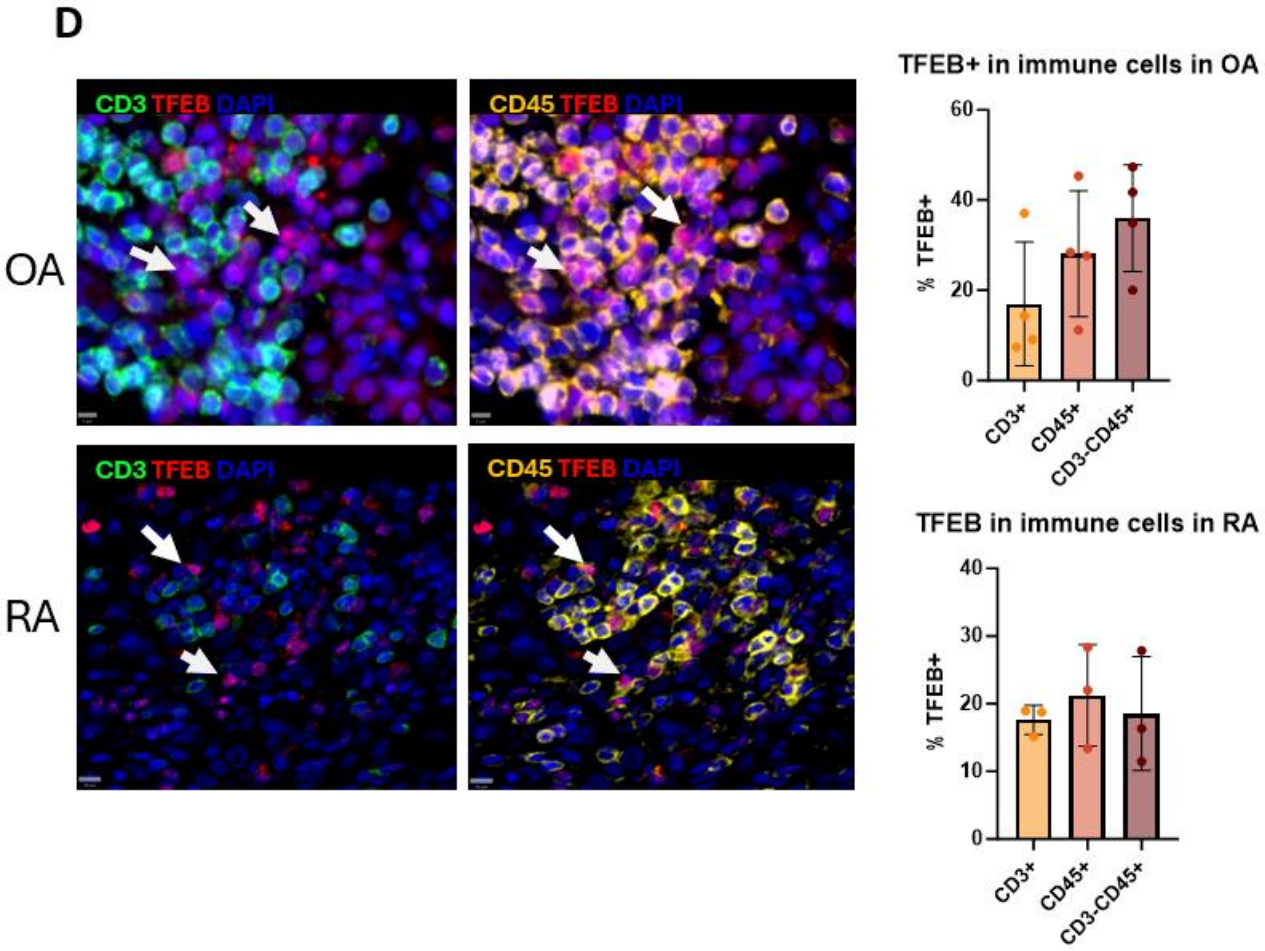
D
OA
RA
CD3 TFEB DAPI
CD45 TFEB DAPI
TFEB+ in immune cells in OA
% TFEB+
CD3+
CD45+
CD3-CD45+
TFEB in immune cells in RA
% TFEB+
CD3+
CD45+
CD3-CD45+

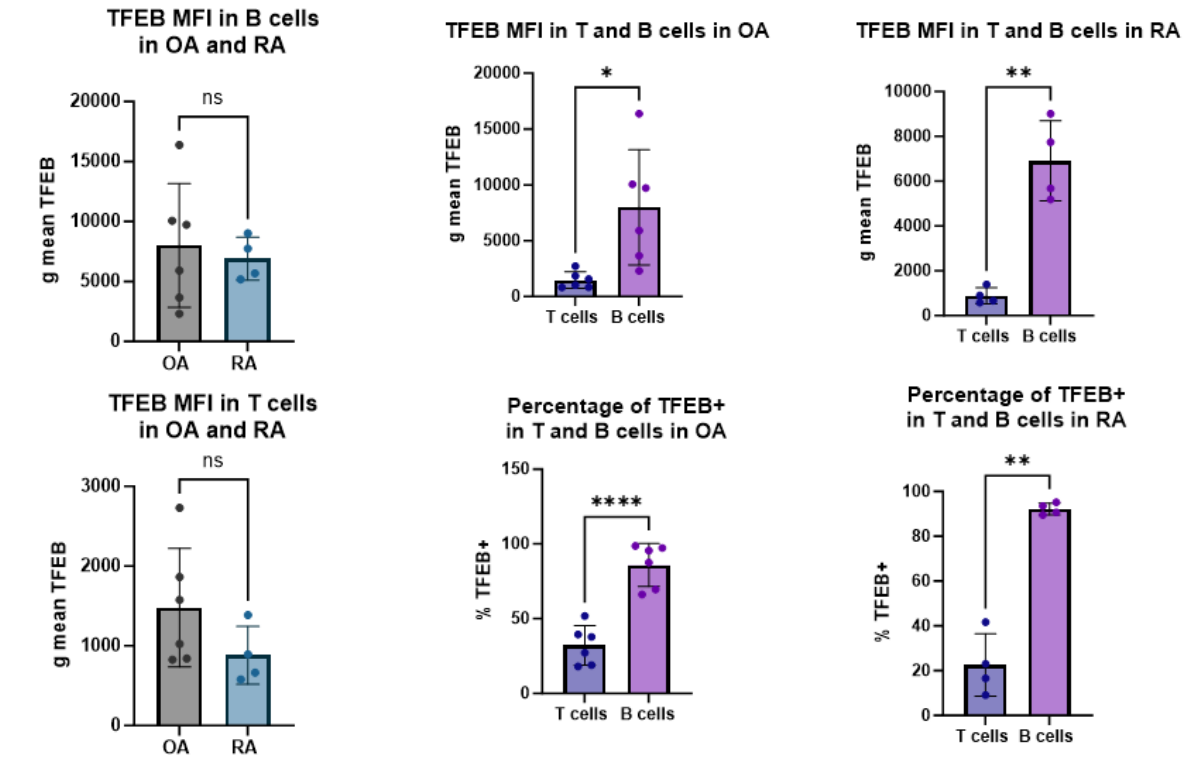
E
TFEB MFI in B cells in OA and RA
g mean TFEB
ns
OA
RA
TFEB MFI in T cells in OA and RA
g mean TFEB
ns
OA
RA
F
TFEB MFI in T and B cells in OA
g mean TFEB
*
T cells
B cells
TFEB MFI in T and B cells in RA
g mean TFEB
**
T cells
B cells
Percentage of TFEB+ in T and B cells in OA
% TFEB+
****
T cells
B cells
Percentage of TFEB+ in T and B cells in RA
% TFEB+
**
T cells
B cells

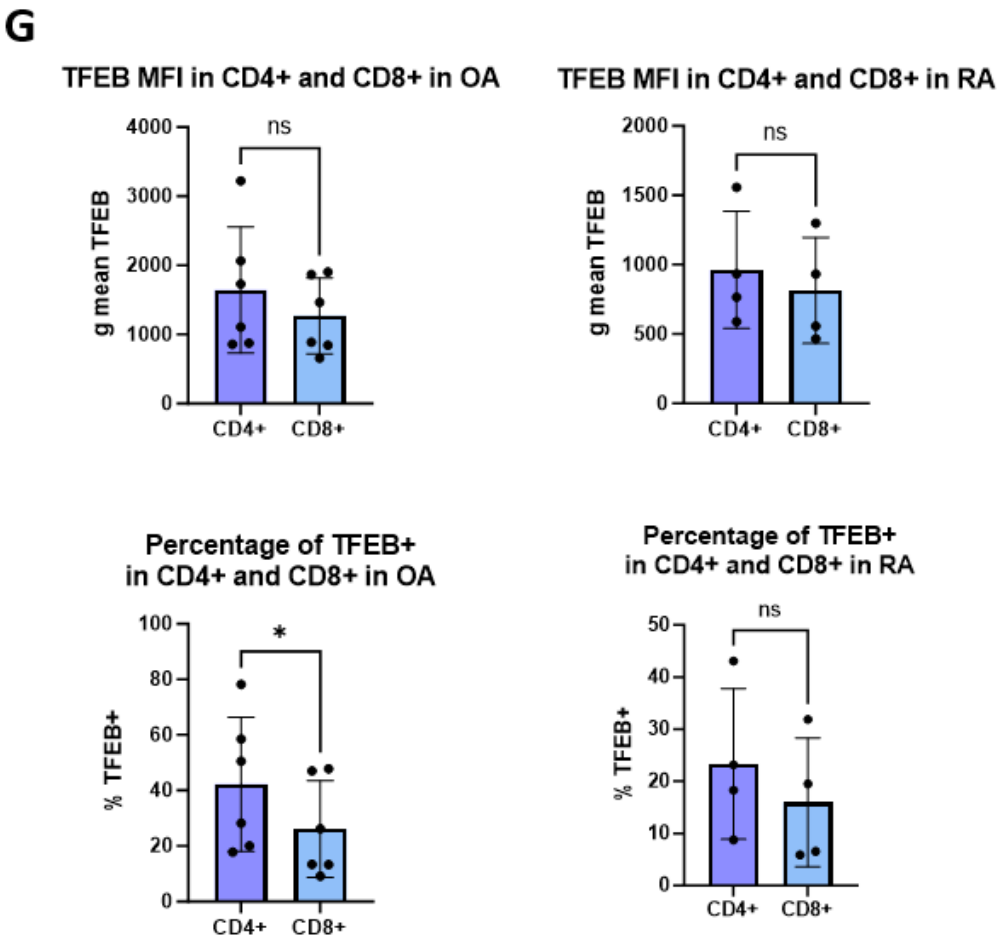


**Figure 5.1.4 TFEB expression in the infiltrated lymphocytes**

**D:** Multiplex IF staining showing TFEB (red), CD3 (green), and CD45 (yellow) (white arrows show TFEB+CD45+CD3- cells), and the quantification of the percentage of TFEB in CD3+, CD45+ and CD45+CD3- in OA (top) and RA (bottom). **E:** Flow cytometry measure of TFEB MFI in B cells (top) and T cells (bottom) in OA (grey) and RA (blue), unpaired t-test OA (n=6) RA (n=4). F: TFEB MFI (top) and TFEB+ percentage (bottom) in T cells (blue) and b cells (purple) in OA and RA synovium, paired t-test OA (n=6) RA (n=4). **G:** TFEB MFI (top) and TFEB+ percentage (bottom) in CD4+ (dark blue) and CD8+ (light blue) in OA and RA synovium, paired t-test OA (n=6) RA (n=4). (*p < 0.05; **p < 0.01; ****p < 0,0001).

### 5.1.5 TFEB expression in the endothelial cells

Recent evidence revealed the importance of autophagy in vasculature functions. Indeed, autophagy, particularly mitophagy, promotes ECs survival by protecting them from oxidative stress (131, 132). In reverse, decrease of autophagy induce ECs apoptosis and increase vascular permeability (131).

Moreover, autophagy appears to regulate angiogenesis processes either by promoting it under hypoxia or nutrient depravation or by limiting ECs migration and tube formation (131, 133, 134). Nonetheless, ECs autophagy is an active research area and the role of autophagy in the context of inflammation and aging in the joint is still under investigation.

Here, we investigated the expression of TFEB in the CD31+ ECs in OA and RA synovium using multiplex histology and flow cytometry. In a first time, TFEB is detected in both OA and RA blood vessels and colocalized with CD31 **(Fig 5.1.5 A)**. Furthermore, 28,29% (± 17,29; n=6) of ECs are TFEB+ on average in OA and 35,55% (± 14,02; n=5) are TFEB+ in RA **(Fig 5.1.5 B)**. Even though on average more ECs are TFEB+, the difference is not statistically different suggesting that TFEB is expressed in ECs similarly between the two diseases. Similarly, when we measure the TFEB MFI and TFEB+ frequence in the CD34+ CD31+ ECs using flow cytometry no difference is observed between OA and RA **(Fig 1.5 C)**. When investigating the TFEB expression by multiplex histology I noticed that in OA, TFEB staining appeared more localized in the cytoplasm than in the nucleus in the CD31+. Inversely, in RA TFEB staining appeared more nuclear. To quantify the nuclear and cytoplasmic staining of TFEB I investigated the MFI in the nuclei and cytoplasm of CD31+ TFEB+ cells of 1 OA and 1 RA patient. Thus, in both OA and RA, the MFI of TFEB is significantly higher in the nucleus compared to the MFI in the cytoplasm **(Fig 5.1.5 D)**. Interestingly, we observed a significant decrease of nuclear TFEB intensity in the OA ECs compared to the RA ECs suggesting more nuclear translocation of TFEB in RA endothelium. Furthermore, the intensity in the cytoplasm is significantly decreased in RA compared to OA suggesting that more TFEB is sequestered at the lysosome membrane in OA endothelium **(Fig 5.1.5 D)**. Together, this may underline a differential TFEB activation in the endothelium where TFEB is more activated in the ECs in RA compared to OA.

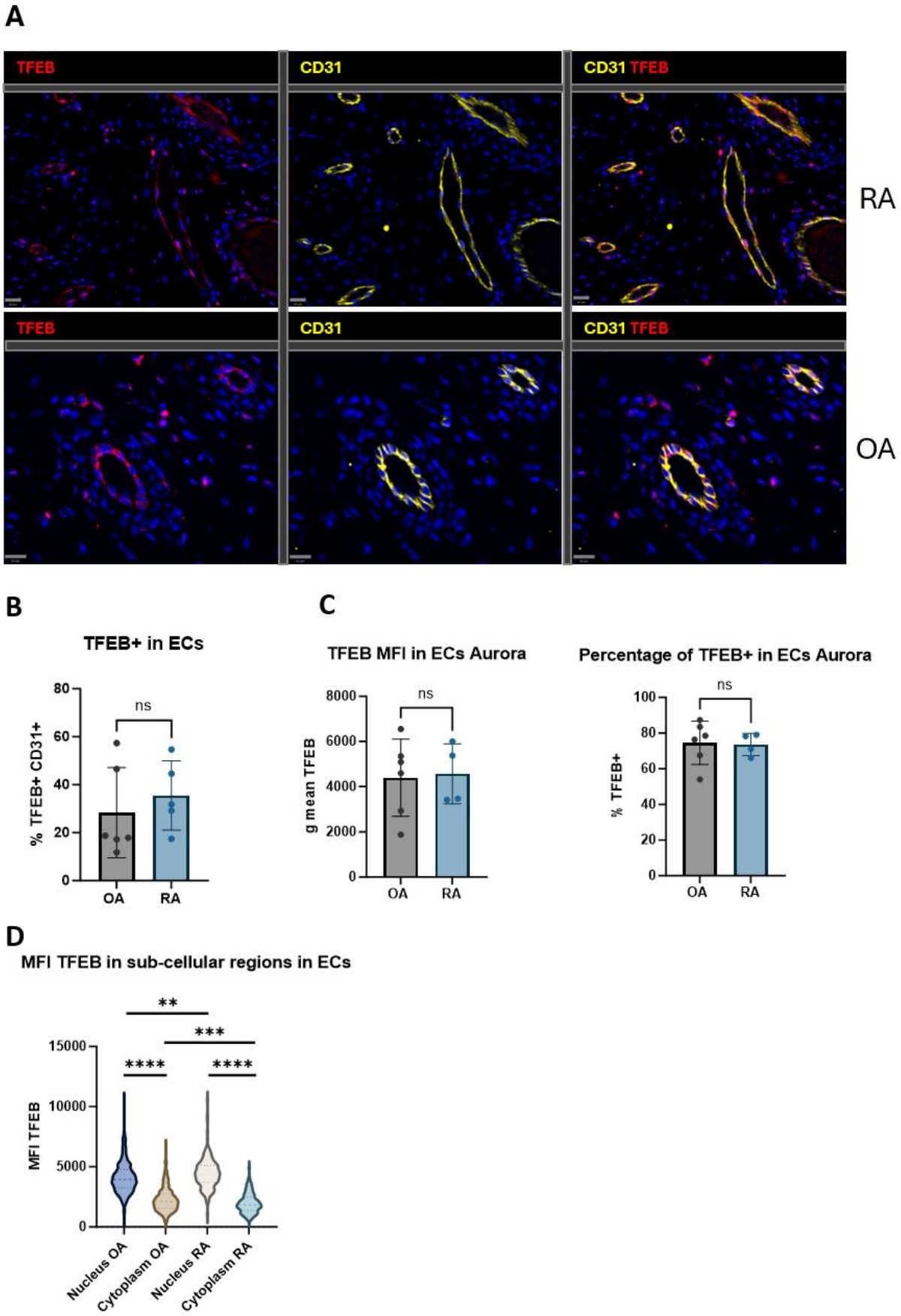


**Figure 5.1.5: TFEB expression in the endothelial cells**

**A:** Multiplex IF staining showing TFEB (red) and CD31 (yellow) in RA (top) and OA (bottom). **B:** Percentage of TFEB+ in CD31+ ECs in OA (grey) and RA (blue); unpaired t-test OA (n=6) RA (n=5). **C:** TFEB MFI (left) and percentage of TFEB+ (right) in CD31+ CD34+ ECs in OA (grey) and RA (blue) measure with flow cytometry; unpaired t-test OA (n=6) RA (n=4). **D:** Nuclear and cytoplasmic MFI of TFEB in TFEB+ ECs in one RA patient and one OA patient. (*p < 0.05; **p < 0.01; ***p < 0.001; ****p < 0,0001).

## 5.2 Transcription of TFEB in synovium

Our preliminary data to compared TFEB expression in cartilage of young and old in mice suggest that the dysregulation of autophagy with age is not entirely dependent of the expression of TFEB but its activation. Indeed, we do not see major changes in the expression of TFEB between old and young individual. However, post transcriptional regulation and the increase of TFEB inhibitors with aged may represent the main downregulation mechanism that decrease the autophagy via TFEB. Nevertheless, in the human joint the expression of TFEB is not fully characterized. Thus, I investigated the localization of TFEB mRNA in OA, RA and normal synovium using FISH multiplex RNAscope. Similarly, the previous results on *CDKN2A* and *CDKN1A*, and because of RNA poor stability, the detection of *TFEB* is dependent on the freshness of the tissue inducing variability in OA and RA cohort. We did not find a good way to normalize those data, therefore any comparison between patients is not robust. Nonetheless, the expression of *TFEB* is detected in both diseases **(Fig 5.2 A)**. However, no significative difference is observed in TFEB expression between the two diseases **(Fig 5.2 B)**. Moreover, the expression of TFEB is not increased in the LL in OA and RA compared to the SL suggesting that the increased in protein TFEB in the LL may not be a consequence of a higher expression **(Fig 5.2 C)**. Then, we investigated the average dot/cell in both LL and SL in OA and RA, but no difference is observed on average cells have 1.5 copies of TFEB mRNA **(Fig 5.2 D)**. As *PRG4* expression was detectable in some tissue, we investigated the proportion of *TFEB+ PRG4+* in OA, RA and normal synovium to determine if the proportion of TFEB expressing cell is higher in the LL fibroblasts. Thus, no difference is observed between OA, RA and healthy synovium regarding the proportion of *TFEB+ PRG4+* **(Fig 5.2 E, F)**. As we previously reported, TFEB was present in ECs and in immune cells especially B cells, this is also the case for the mRNA as it is highly detected in lymphocytes aggregates and bloods vessels **(Fig 5.2 E)**. Finally, in normal synovium, the expression of TFEB is mainly localized in the LL compared to the SL. However, the quality of the slide was not good and the signal detected was very weak making any interpretation only speculative. Furthermore, more investigation needs to be carried on normal synovium to truly understand how the context of the disease is influencing autophagy.

In conclusion, TFEB is expressed similarly in the LL and SL of OA and RA synovium suggesting that the difference observed in the protein level may be a consequence of post transcriptional regulations but not from transcription regulation. However, we cannot exclude that different transcriptional difference of TFEB might be observed between other cell types and between patients according to environmental factors.

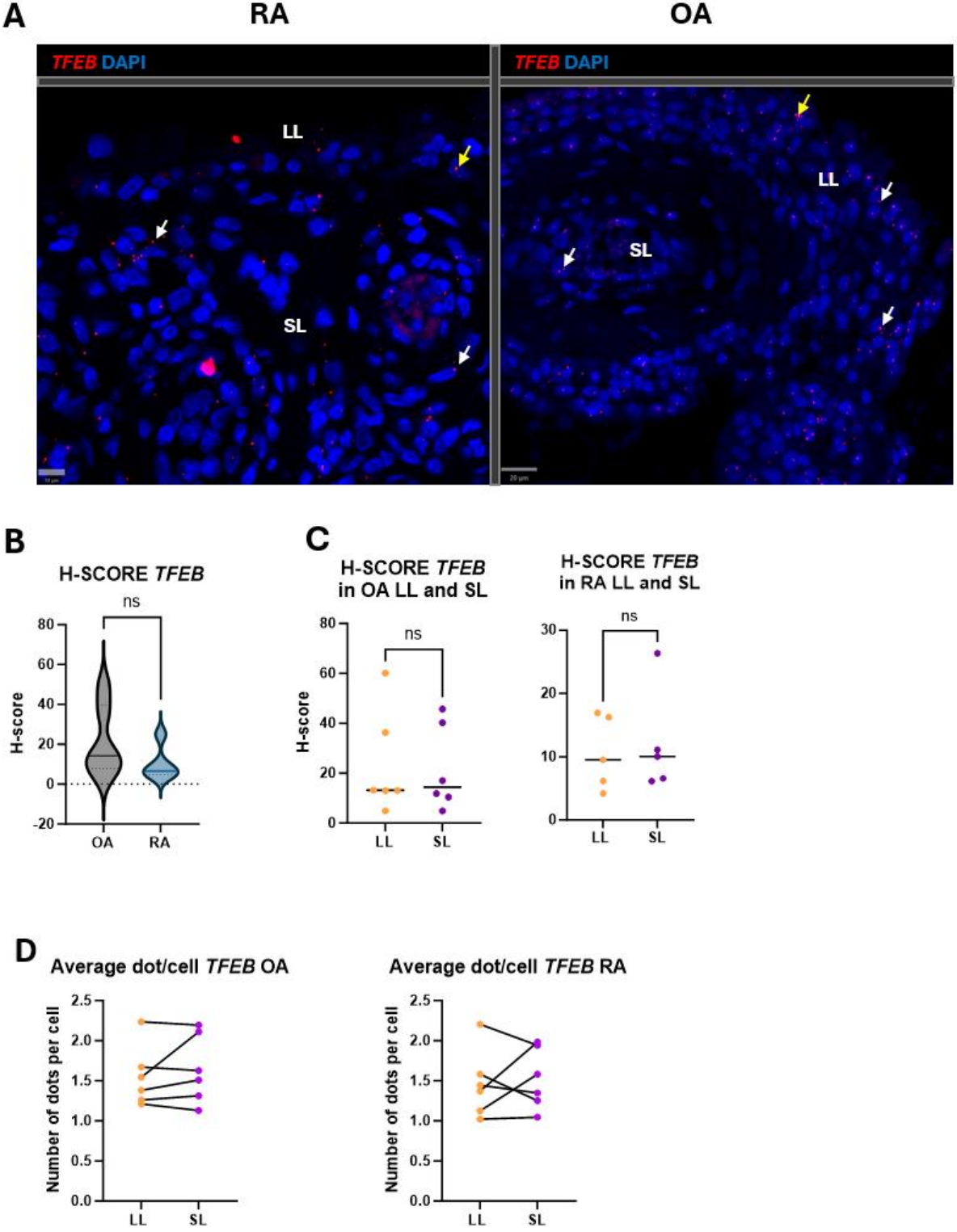


**Figure 5.2: Transcription of TFEB in synovium**

**A:** RNAscope staining showing *TFEB* (red) in RA (left) and OA (right) synovium. **B:** H-score of *TFEB* in the total synovium of OA (grey) and RA (blue); unpaired t-test OA (n=6) RA (n=6). **C:** H-score of *TFEB* in the LL (orange) and SL (purple) in OA (left) and RA (right); unpaired t-test OA (n=6) RA (n=6). **D:** Average dots per cell of *TFEB* in OA (left) and RA (right). **E:** RNAscope staining showing *TFEB* (red) and *PRG4* (magenta) in LL (top), lymphocytes aggregate (middle), and blood vessels (bottom) in RA (left) and OA (right) synovium. **F:** Percentage of *TFEB+* in *PRG4+* in OA, RA and healthy synovium; unpaired t-test OA (n=4) RA (n=5), healthy (n=1). **G:** RNAscope staining showing *TFEB* (red) and *PRG4* (magenta) in healthy synovium and the H -score in the LL (orange) and SL (purple).

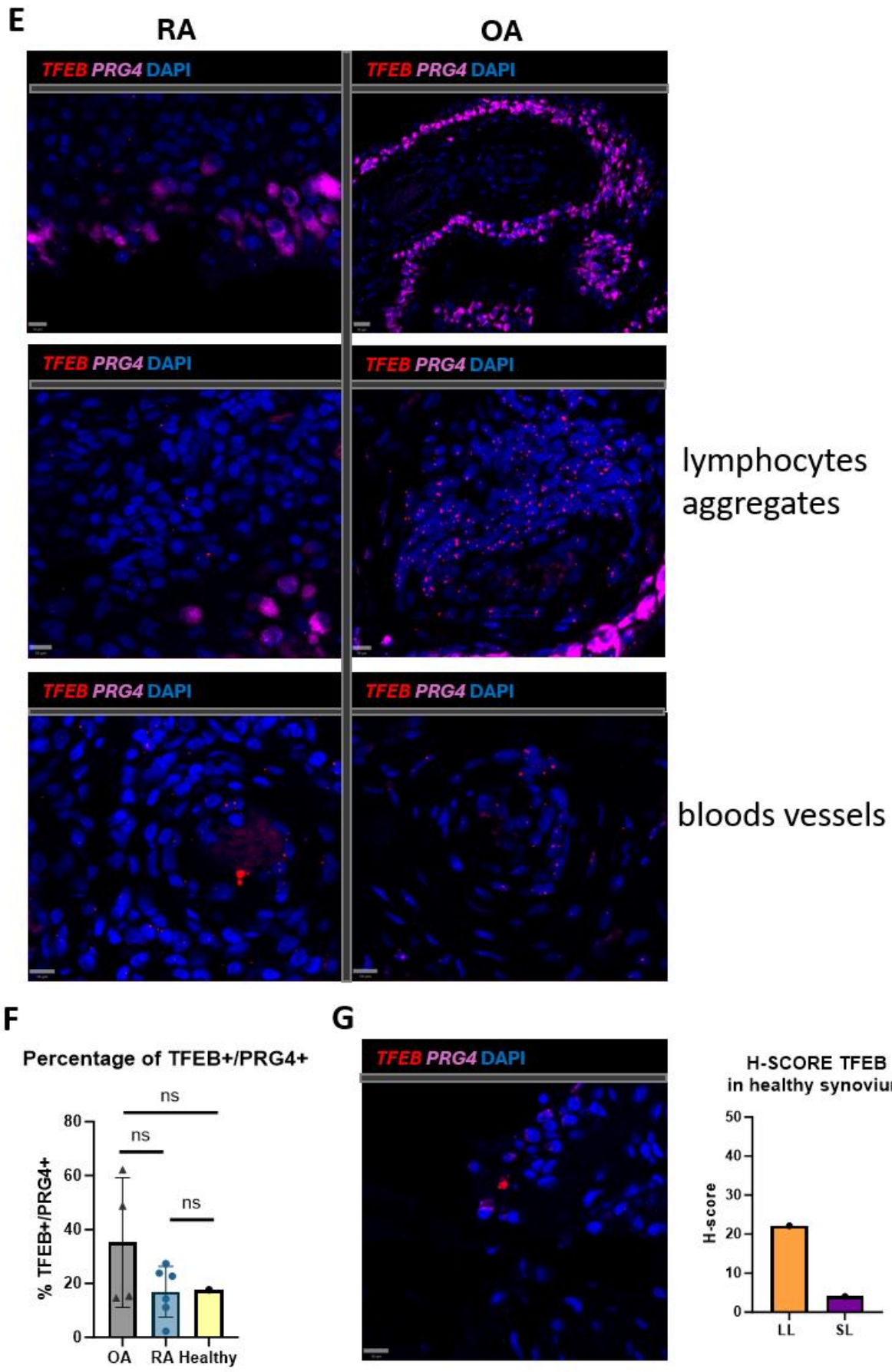


**Figure 5.2: Transcription of TFEB in synovium**

**E:** RNAscope staining showing *TFEB* (red) and *PRG4* (magenta) in LL (top), lymphocytes aggregate (middle), and blood vessels (bottom) in RA (left) and OA (right) synovium. **F:** Percentage of *TFEB+* in *PRG4+* in OA, RA and healthy synovium; unpaired t-test OA (n=4) RA (n=5), healthy (n=1). **G:** RNAscope staining showing *TFEB* (red) and *PRG4* (magenta) in healthy synovium and the H -score in

## 5.3 Corelation analysis between senescence, TFEB expression and patient metadata

### 5.3.1 TFEB and senescence

Many studies have reported the role of TEFB and its anti-aging and anti-senescence properties (128, 130, 135, 136). Yet, TFEB and senescence maintain a close mechanistic relationship. Indeed, evidence report that TFEB is involve in the DNA damage pathway and promote the stabilization of p53 protein level (137, 138). However, in the context of sustain damaged, the role of TFEB in the balance between apoptosis and senescence remains unknown. In the same vein, TFEB activation promotes lysosomal biogenesis in senescent cells increasing their survival suggesting the importance of autophagy even when cells are dysregulated (139). In consequence, understanding the relationship between senescence and TFEB in the context or arthritis may reveal new shared pathway and deepened our knowledge in age related diseases.

For this reason, we first investigated the expression of the hallmarks of senescence in all TFEB+ synovial cells in OA and RA synovium using the histology data. In both OA and RA, the proportion p21+ TFEB+ cell is significantly higher compared to the proportion of p16+ TFEB+ **(Fig 5.3.1 A)**. Furthermore, we observed an increase in the proportion of p53+ TFEB+ compared to the p16+ TFEB+ in both diseases **(Fig 5.3.1 A)**. However, this difference is not significant. Yet, the increase of proportion of p21 and p53 is TFEB+ cells may suggest that TFEB regulated p53 and subsequently p21 in a DNA damage repair context even though the proportion of yH2AX+ TFEB+ is significantly lower compared to the p21+ **(Fig 5.3.1 A)**. As previously described, the total proportion of TFEB is decrease in OA compared to RA **(Chap. 2. Fig 1.1 A)**. However, the proportions of p21+, p16+, yH2AX+ and p53+ in TFEB+ cells show no difference between OA and RA perhaps suggesting similar a common autophagy and senescence regulation in the synovium **(Fig 5.3.1 B)**.

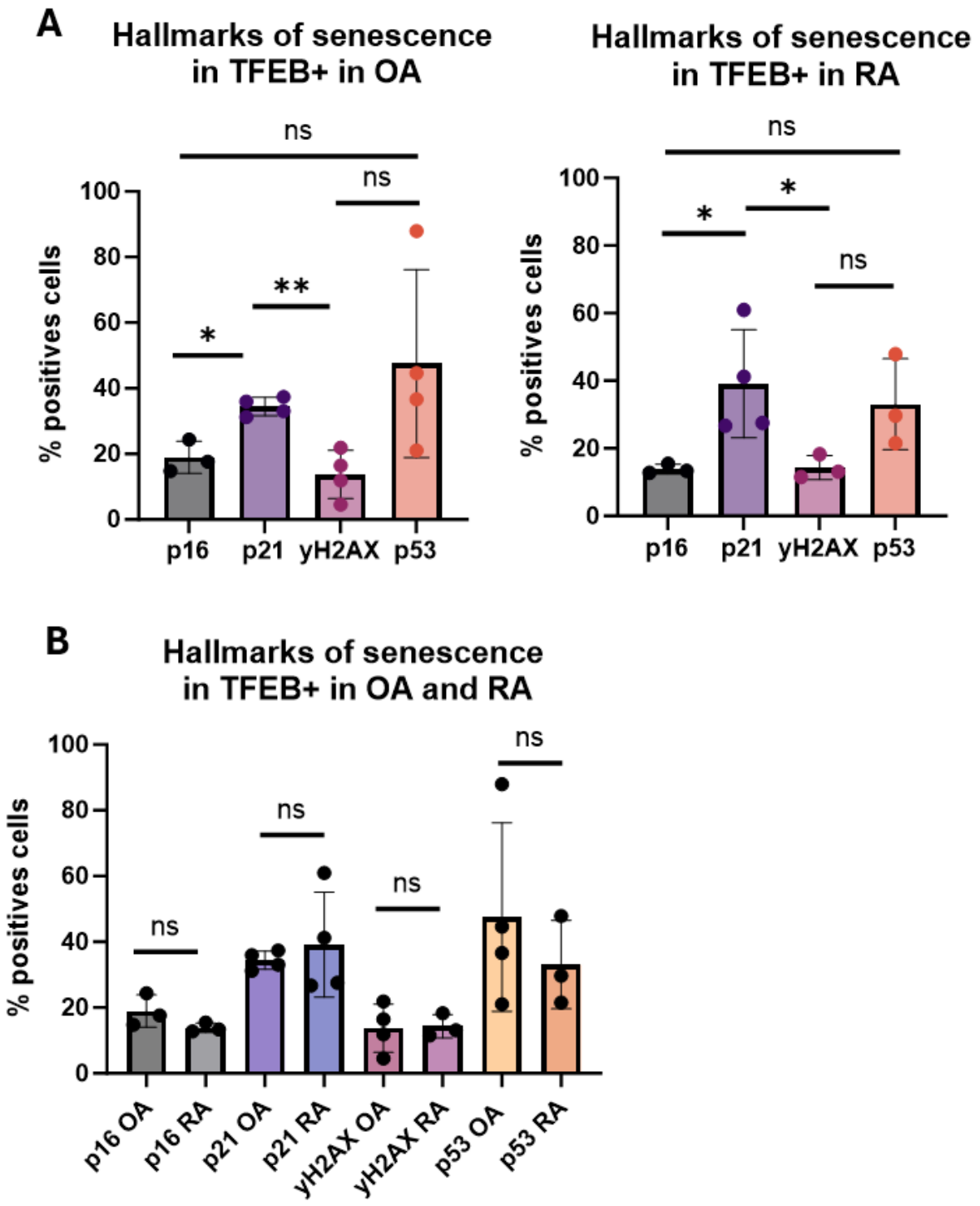


**Figure 5.3.1: Senescence hallmarks in TFEB+**

**A:** Percentage of p16+, p21+, yH2AX+, p53+ in TFEB+ in OA (left) and in RA (right) synovium measure by multiplex IF. Paired t-test OA (n=4); RA (n=3); OA p16 (n=3); RA p21 (n=4). **B:** Comparison of the percentage of p16+, p21+, yH2AX+, p53+ in TFEB+ between OA and in RA synovium. (*p < 0.05).

Next, we decided to corelated the expression of TFEB with the proportion of the marker of senescence to better understand its role in regulating senescence in OA and RA. Interestingly, we observed a positive correlation between TFEB expression with the proportion of yH2AX+ and p21+ in OA while in RA, TFEB expression negatively corelate with the proportion of p21+ and yH2AX+ **(Fig 5.3.1 C)**. Among those corelations, only the negative correlation between TFEB expression and yH2AX+ proportion is significant **(Fig 5.3.1 C, red box)**. However, this could suggest that in OA TFEB is dysregulated leading to an increase of DNA damage as suggested in a recent study showing that down regulation of TFEB leads to yH2AX accumulation (140). Conversely, in RA TFEB up regulation may lead to more DNA repair decreasing the proportion of yH2AX. Moreover, on all the RA cohort, we observed significant positive correlations between the proportion of p21+ with both p53+ and yH2AX+ proportion suggesting the DNA damage pathway through yH2AX and p53 induced cell cycle arrest via p21 **(Fig 5.3.1 D)**. This is also seen in OA but is not significant may be indicating more heterogeneity in the senescence activation in OA patients or simply that the number of patients is perhaps not sufficient to show significance.

The previous data are based on the global expression of TFEB and senescence in all the synovial cells. As previously described, the senescence is mainly found in the LL, especially in the LL fibroblasts. Thus, we correlated the expression of TFEB in with the proportion of the hallmarks of senescence in the LL and SL fibroblasts in both OA and RA. Interestingly, TFEB expression in OA fibroblasts do not correlate with p16 or p21 expression but positively correlate with yH2AX while negatively correlates with p53 **(Fig 5.3.1 D)**. Oppositely, TFEB in the RA LL fibroblasts positively correlate with p53 and p21 while negatively correlate with yH2AX and p16 suggesting again that TFEB may be involved in the DNA repair pathway leading to a reduction of damage as well as a decrease in p16 induced senescence **(Fig 5.3.1 D)**. Unfortunately, none of those correlations are significant but the smallest p values are found between TFEB and yH2AX in both diseases.

Next, we investigated the correlation between TFEB and senescence in the ECs as the data suggested that this population had high levels of TFEB and senescence. Indeed, there is a significant positive

correlation between p53 and TFEB in the ECs in both OA and RA underlining the crosstalk between TFEB and p53 **(Fig 5.3.1 G)**. In addition, TFEB have been shown to reduced ECs inflammation and alleviate leukocytes infiltrations in mice (141). Therefore, we tried to correlate the expression of TFEB in the ECs with the percentage of CD45+ in OA and RA synovium but no correlation is observed in this cohort probably because of the overlapping of pro-inflammatory factors involved in synovitis.

Altogether, TFEB appears to be involved in the DNA damage repair in both of and RA suggested by the higher proportion of p21+ TFEB+ and p53+ TFEB+. However, the decrease of DNA damage indicate by the proportion of yH2AX is associated with a high TFEB only in RA. This suggest that the protective role of TFEB and autophagy against DNA damage stress is impaired in OA but not in RA. This concept may be extended to the LL fibroblasts as we observed similar correlations. However, more data are required to confirm these findings. Moreover, TFEB expression significantly correlate with the increase of p53 in the ECs in both OA and RA suggesting a potential crosstalk in this specific context of endothelial senescence. Finally, the protective role of TFEB in ECs and its role to limit infiltration is not observed here, probably because of the global inflammation. Maybe downregulating TFEB in this context will increase vascular permeability and consequently infiltration. Nevertheless, the role of TFEB in the context of chronic inflammation need to be further investigated.

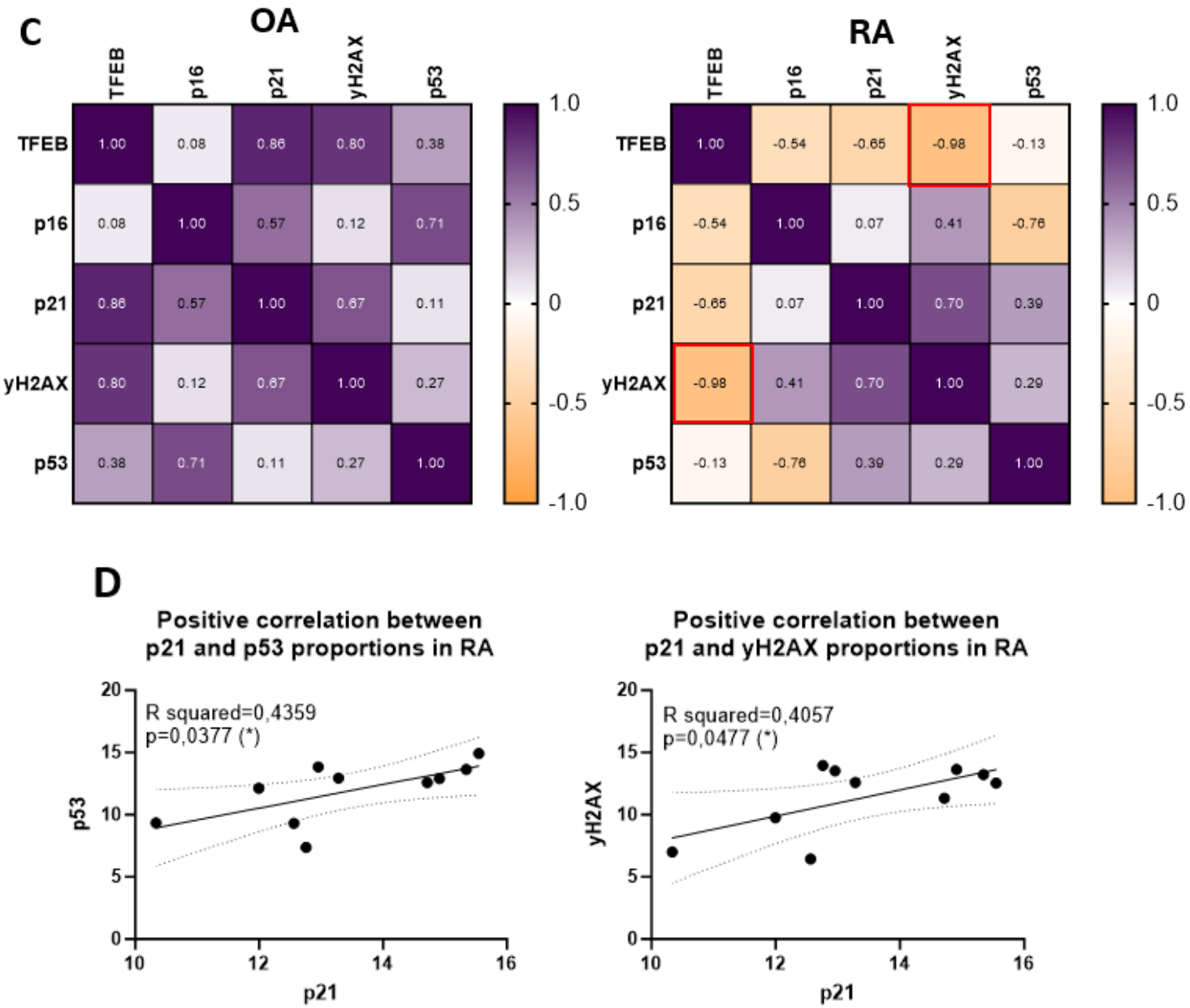


**Figure 5.3.1 (continued): Senescence hallmarks in TFEB+**

**C:** Pearson correlation of the percentage of TFEB+ with Percentage of p16+, p21+, yH2AX+, p53+ in OA (left) and RA (right); OA (n=4); RA (n=3); OA p16 (n=3); RA p21 (n=4); significant p value highlight in red: p value (%TFEB/%yH2AX) = 0.018; score= 1 (positive correlation), score = 0 (no correlation), score = - 1 (negative correlation). **D:** Linear regression between p21 and p53 proportion (left) with p21 and yH2AX proportion (right) in RA synovium (n=10). (*p < 0.05).

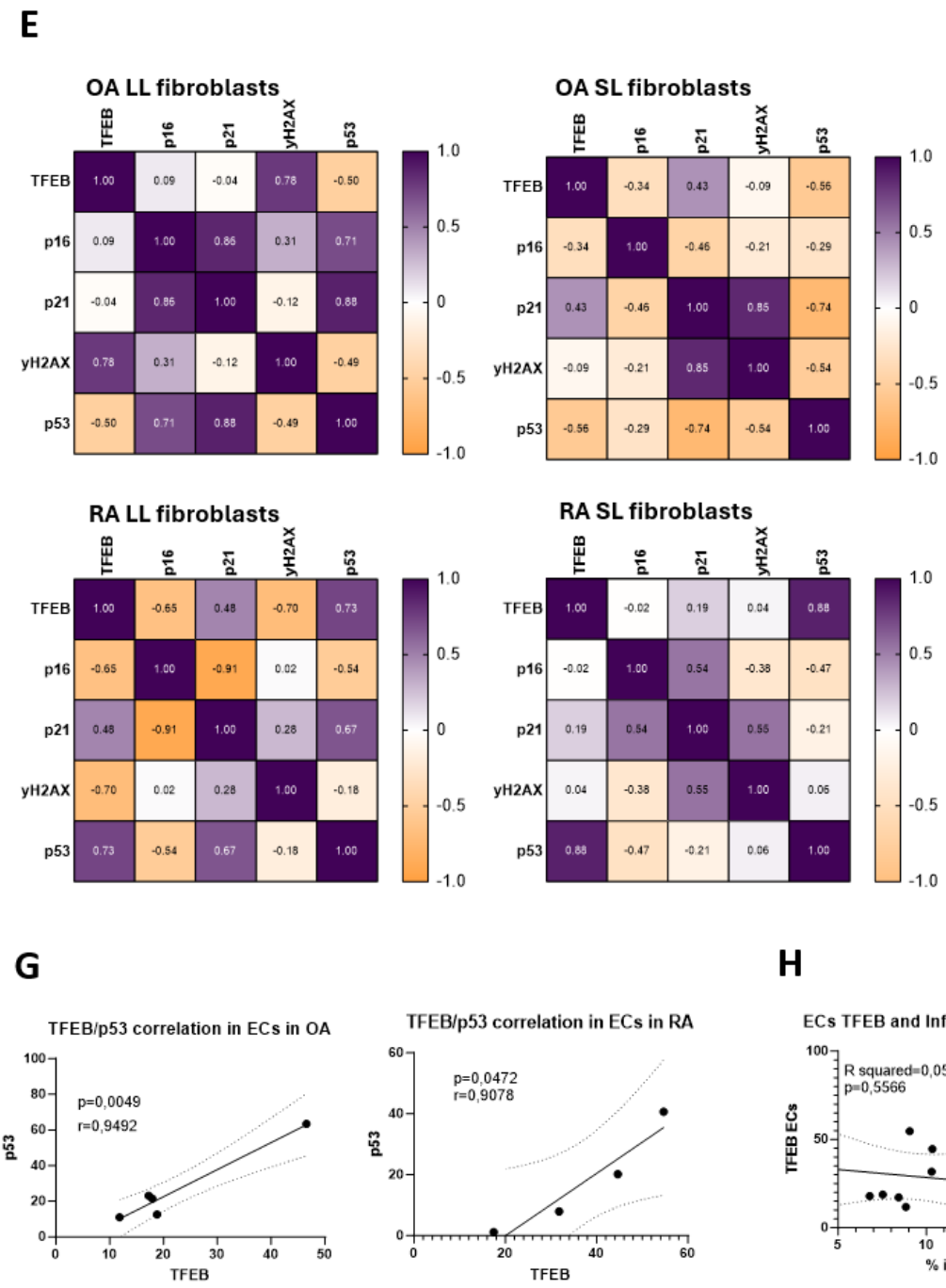


**Figure 5.3.1(continued): Senescence hallmarks in TFEB+**

**E:** Pearson correlation between the percentage of TFEB+ with p16+, p21+, yH2AX+, p53+ in OA (top) LL fibroblasts (left) and SL fibroblasts (right) and in RA (bottom) LL fibroblasts (left) and SL fibroblasts (right); OA (n=5), RA (n=4). **G:** Linear regression between the percentage of TFEB+ and p53+ in ECs in OA (left) and RA (right); OA (n=5), RA (n=4). H: Linear regression between the percentage of TFEB+ in ECs with the proportion of CD3+ T cells in RA and OA (n=8).

### 5.3.2 TFEB, senescence and patient background

Many factors are involved in arthritic diseases that can influence senescence, autophagy and inflammation. Both OA and RA are multi factorial diseases where age, sex, weight, and treatment influence the synovial state. Therefore, I investigated the link between TFEB and senescence with the accessible patient information including age, sex, BMI, treatment, diseases activity score (DAS28). Unfortunately, not all parameters where available for all the tissue. For instance, in the OA cohort, BMI was available in only half of the patients. Similarly, in RA, DAS28 or treatment with Nonsteroids Anti-Inflammatory Drugs (NSAID) was only available for the biopsies but not JRP. However, age and sex were available for all patients.

Thus, we correlated TFEB and senescence proportions with the age of patients in all patients concatenated. As expected, TFEB expression negatively correlate with age supporting the evidence a decline of autophagy with age **(Fig 5.3.2 A)**. Furthermore, the proportion of yH2AX significantly correlated with age supporting the idea that DNA damage accumulated with age via increase of cellular stress and telomere shortening **(Fig 5.3.2 B)**. A positive corelations between p21 and p53 with age is also observed but are not significant in the cohort. Surprisingly, the proportion of p16 do not corelated with age **(Fig 5.3.2 B)**. As already described in the RA patients, p21 positively corelated with p53 and yH2AX+ supporting the idea that the DDR through p53/p21 is involved upon DNA damage **(Fig 5.3.2 B)**. Then, we investigated the impact of age on senescence and TFEB within the RA and OA patients separately. In OA, we do not observe any significant correlation between age and senescence or TFEB mostly because the range in the age of the patients is only 19 years. However, in the RA cohort the range in the age of patient s is 47 years which allow a better analysis of the impact of age on TFEB and senescence. Thus, we observed the negative correlation between TFEB and age as well as the positive corelation between DNA damage accumulation and age in RA **(Fig 5.3.2 C)**. The proportion of p21 also correlate positively with age in RA but more young patients should be investigated to show significance.

Similarly, p53 positively correlate with age in both OA and RA but not significantly which may be explained by the low statistic range and the small sample size **(Fig 5.3.2 C, D)**.

Obesity is a common comorbidity factor in OA, and many studies report the impact of obesity on inflammation, and senescence (142). Interestingly, we observed a positive correlation between the proportion of p53 and p16 and the BMI of the patients **(Fig 5.3.2 E)**. However, these findings are not significant may be due to low range of the samples studied.

Regarding other patient information, we observed a positive correlation between the DAS28 and the age of the patients in the biopsy cohort in RA supporting the idea that age is an aggravating factor in RA **(Sup Fig 3 A)**. However, most of the patient metadata including positivity to Rheumatoid factor (RhF) or CCP do not show significant correlation with TFEB and senescence **(Sup Fig 3 A)**. Although, there is a significant positive correlation between p21 proportion and the treatment or not with NSAID, but only 4 patient is not enough, and this might just be a coincidence **(Sup Fig 3 A)**.

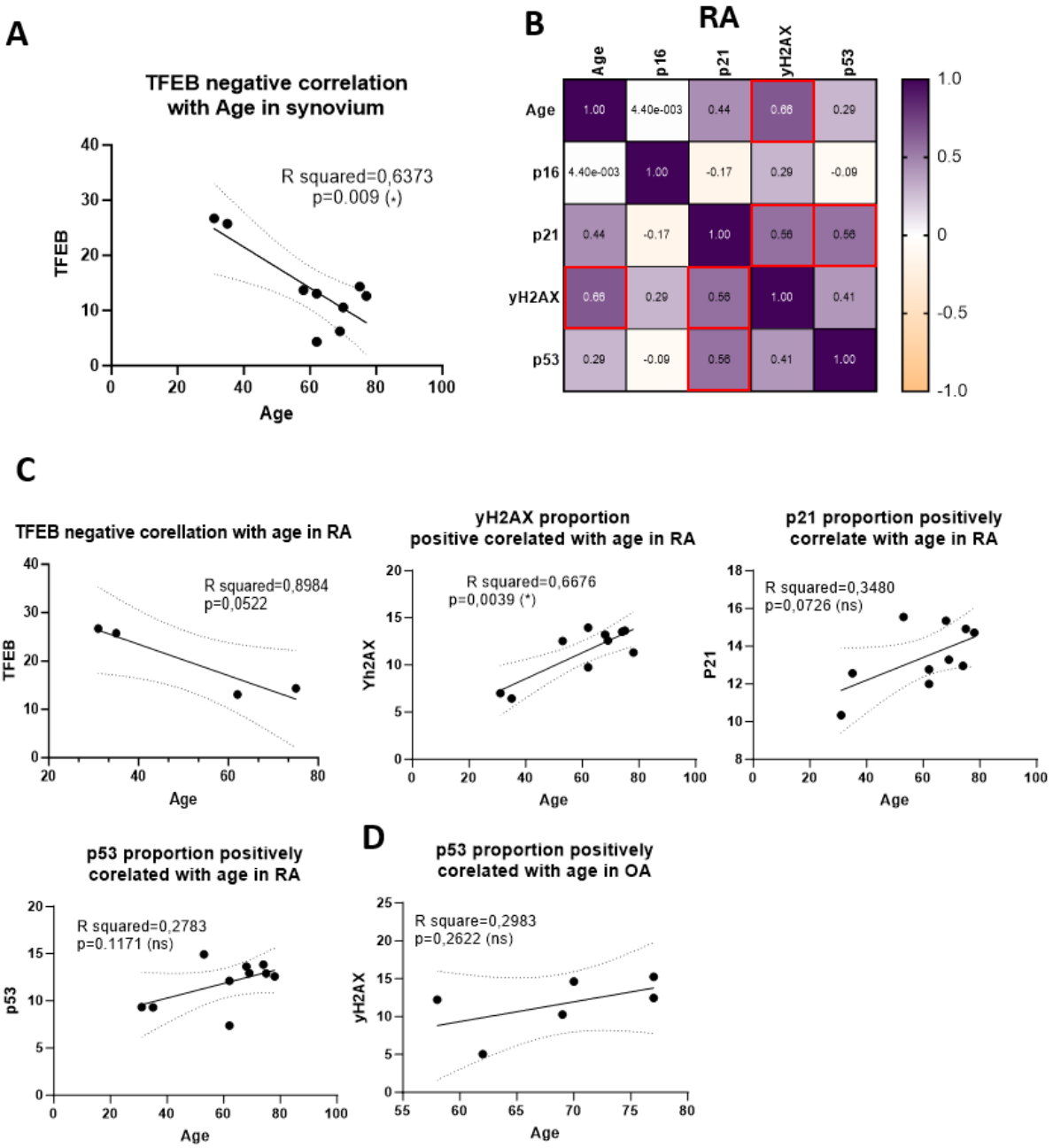
A
TFEB negative correlation with Age in synovium
R squared=0,6373
p=0.009 (*)
TFEB
Age
B
RA
Age
p16
p21
yH2AX
p53
1.00
4.40e-003
0.44
0.66
0.29
4.40e-003
1.00
-0.17
0.29
-0.09
0.44
-0.17
1.00
0.56
0.56
0.66
0.29
0.56
1.00
0.41
0.29
-0.09
0.56
0.41
1.00
1.0
0.5
0
-0.5
-1.0
C
TFEB negative corellation with age in RA
R squared=0,8984
p=0,0522
yH2AX proportion positive corelated with age in RA
R squared=0,6676
p=0,0039 (*)
Yh2AX
p21 proportion positively correlate with age in RA
R squared=0,3480
p=0,0726 (ns)
P21
p53 proportion positively corelated with age in RA
R squared=0,2783
p=0.1171 (ns)
p53
D
p53 proportion positively corelated with age in OA
R square=0,2983
p=0,2622 (ns)
yH2AX
E
Age and nuclear TFEB in the LL/SL ratio correlation in OA
R squared=0,6846
P value=0,1726 (ns)
Ratio nuclear TFEB LL/SL
Age and cytoplasmic TFEB in the LL/SL ratio correlation in RA
R squared=0,6802
P value=0,1752 (ns)
Ratio cytoplamsic TFEB LL/SL

**Figure 5.3.2: TFEB, senescence and patient background**

**A:** Linear regression between TFEB+ proportion in total synovium with the age of the patients in OA and RA (n=9). **B:** Pearson correlation between age and the percentage of p16+, p21+, yH2AX+, p53+ and TFEB+ in RA synovium; significant correlations are highlighted in red (*$p < 0.05$). **C:** Linear regression between age and TFEB+, p21+, yH2AX+, and p53+ percentage in total synovium in RA. **D:** Linear regression between age and p53+ percentage in total synovium in OA. **E:** Linear regression between age and nuclear TFEB MFI LL/SL ratio in OA (left) and in RA (right).

# 6 Conclusions: Key points

- Both techniques (multiplex IF and Flow cytometry) gave similar results, however the sensitivity between the techniques might be different.
- More markers are needed to fully characterize the sub-populations of fibroblasts and tissue resident macrophages (TRMs) in both histology and Flow cytometry.
- Several cell types remain unclassified in OA and RA with both techniques

Fibroblasts

- Multiplex histology analysis of senescence markers demonstrated that LL fibroblasts are significantly more positive for p16, p21, yH2AX and p53 compared to the SL fibroblasts in both OA and RA suggesting differential senescence in the synovium independent of the diseases.
- DNA damage pathway via the axis yH2AX/p53/p21 in the LL is different in both OA and RA suggesting different response to DNA damage in the two diseases.
- Flow cytometry shows increased p16, p21 and yH2AX in the LL $PDPN^{HIGH}$ expression compared to the SL $PDPN^{LOW}$ but p53 is expressed in both subsets in OA and RA.

Macrophages

- Multiplex analysis suggests that CD68+ MERTK+ TRMs are mainly associated with the LL while CD206+ CD68+ TRMs are localized in the SL.
- Expression of p16 and p53 is higher in the MERTK+ and CD68+ cells in the LL compared to the SL in OA and RA while the SL CD206 population are more p21+
- Flow cytometry analysis of macrophages indicate more p16+ and p21+ in the MERTK+ HLA-DR+ macrophages compared to the MERTK+ HLA-DR- that are more p53+ and yH2AX+ maybe suggesting a differential senescence between infiltrated monocytes and TRMs

lymphocytes

- Lymphocyte infiltration is observed in both OA and RA characterized by the presence of lymphocytes aggregates but the proportion of CD3+ T cells is significantly increased in RA compared to OA
- T cells have a significant increase of the senescence markers in both OA and RA compared to the B cells and this is shown in both techniques
- No difference of senescence is observed between CD4+ and CD8+ subsets

Endothelial Cells (EC)

- 4 types of vessels have been identified in the synovium: Venules, arterioles, capillaries and lymphatics
- Capillary size is increases with inflammation in both OA and RA compared to normal synovium, but the proportion of ECs is the same
- ECs have a higher percentage of p16, p21 and p53 compared to yH2AX

RNAscope (RNA analysis)

- CDKN1A (p21) transcription is significantly increased in the LL compared to the SL in OA and RA
- No significative difference in observed between LL and SL in the expression of p16
- Both p16 and p21 are expressed in PRG4+ but the percentage of p21 expressing PRG4+ fibroblasts is higher compared to the percentage of p16+ PRG4+ in OA
- P16 and p21 transcription is detected in lymphocytes aggregates and BV endothelium

Normal synovium

- Senescence as measured by yH2AX P21 P53 is increased in the LL compared to the SL but not p16 suggesting more DNA damage in the LL
- High senescence in ECs and T cells, MERTK+ macrophages suggests that cellular senescence might be an intrinsic property to the synovium
- More patients need to be tested

TFEB expression

- Multiplex histology demonstrates decrease of TFEB in OA synovium compared to RA
- TFEB is more associated with the LL, confirmed in Flow and Histology
- Histology suggests that the difference of TFEB between OA and RA is associated with a decrease of TFEB in the LL fibroblasts but not the other populations.
- No difference in TFEB expression between OA and RA is observed by FACS
- TFEB is higher in the LL TRMs, but no difference is observed between OA and RA
- TFEB is high in the B cells and low in the T cells supporting the protective role of autophagy against cellular senescence.
- TFEB is high in the ECs in OA and RA but no difference between the two diseases.
- Nuclear localisation of TFEB in ECs is higher in RA compared to OA suggesting more activation
- No difference of expression in the LL and SL measure by RNAscope suggesting post transcription mechanisms and activity to explain the differential TFEB observed
- TFEB is expressed in PRG4+, endothelium and aggregates

TFEB, senescence and patient information

- TFEB is associated with the expression of p21 and p53 underlining the role of TFEB in DNA damage response
- In RA TFEB negatively correlate with yH2AX proportion suggesting the protecting role of autophagy against DNA damage
- In OA TFEB correlate positively with yH2AX perhaps suggesting a dysregulation of TFEB
- Nuclear localization of TFEB is decrease in the LL in OA compared to RA supporting the hypothesis of a dysregulation of TFEB activity during OA.
- TFEB significantly correlated with p53 in the ECs suggesting a close relationship between TFEB and DNA damage response in the endothelium

- TFEB is decreased with age in the cohort supporting the importance of autophagy in age related diseases
- As expected, yH2AX positively correlate with age in RA, confirming the accumulation of damage is increased with age
- No significant correlation between clinical data and senescence

# 7 Discussion

Thanks to the emerging field of scRNA sequencing, it is now possible to deconstruct the tissue and revealed the heterogeneity of the sub-populations involved in healthy and dysregulated in disease. This had paved the way to understand the implication of fibroblasts and TRMs in arthritis. Yet, many mechanisms that regulates the behaviours of those cells are still unknown. It is accepted that inflammation is the main contributing factor of the heterogeneity of the fibroblast populations of the SL. From the moment between the expansion of the perivascular CD90+ fibroblasts to the establishment of an immune niche promoting infiltrated cells survival, fibroblast of the SL undergoes many activation states and phenotypes. During this time communication between ECs, immune cells and fibroblasts are critical underlining a new layer of complexity. Furthermore, the LL population although transcriptionally different from the SL populations may also display different activation states influenced the cell interactions with TRMs or neurones and disease state. Most of those regulations remains unknown today including the mechanisms involved in the expansion of the LL in OA. In this context findings new regulation pathways involving cellular senescence and autophagy may provide a new spectrum on the treatment of arthritis.

## 7.1 Phenotyping the right cells in the right tissue

One of the challenges in identifying sub-populations in diseases, is to find the right phenotype that allows a clear classification. Fibroblasts are heterogeneous cells with a high plasticity which make them able to respond to a wide range of stimuli. Because of this adaptability, fibroblasts in the wrong context could influence the diseases progression by promoting either inflammation or fibrosis (16, 18, 143). Synovial fibroblasts of the SL are a good example to understand this heterogeneity arising from pro-inflammatory context. Nonetheless, as the phenotypes diversify the classification of the sub population become more challenging.

Finding the appropriate approach to identify the sub-population within the tissue is critical. However, one technique is not enough to capture the complexity of the processes involved in the synovium

during arthritis. ScRNA-seq data provide a transcriptomic imprint of the tissue and allow the clustering of the population but do not give information on the protein expression or the localisation of the cell in each clusters. Similarly, flow cytometry will provide information on the expression, but the localization of the cells is lost during the digestion of the tissue. Histology, on the other hand, gives the information on the organization of the populations and lack of sensitivity to detected markers with low expression.

Here, difference between transcriptomic, flow cytometry and IF staining expression is confirmed when we investigated PDPN and CD90 using those techniques. Transcriptomic DATA from the Accelerating Medicines Partnership (AMP) Rheumatoid Arthritis (RA) Phase I indicates that PDPN is expressed by all synovial fibroblasts and CD90 in all the SL fibroblasts (17). Similarly, PDPN and CD90 were conventionally used in flow cytometry to distinguish LL (PDPN+ CD90-) and SL (PDPN+ CD90+) fibroblasts (16, 19). However, in histology, there is no overlapping staining between the two stromal markers, PDPN is almost exclusively found in the LL (beside lymphatic vessels), while CD90+ is restricted to the perivascular niche. Although it helps to classify the LL from the SL fibroblasts, it might exclude the populations with a lower expression of PDPN and CD90. For instance, CD90+ fibroblasts detected in the perivascular region may only represent one of the SL sub-population because of their NOTCH3 activation expressed a high proportion of CD90 compared to the other subtypes. Therefore, the DKK3+ regulatory, POSTN+, pro-inflammatory CXCL12+ and $HLA^{HIGH}$, as well as the intermediate population may not detectable based on CD90 expression only in histology.

To investigate the other population of SL fibroblasts in this DATA set, one solution could be to select the Vimentin+ CD206- CD68- cells observed in the connective tissue between the LL and the perivascular niche. Most of those cell have a fibroid shape and are negative for immune markers.

Similarly, the PDPN expression on the SL fibroblasts is not detectable indicating that the PDPN might be over expressed in the LL fibroblasts. The reason why PDPN might be over expressed in the LL fibroblasts is still under investigation and might depends on specific crosstalk between fibroblasts and

macrophages. It is not unreasonable to assume that TRMs and fibroblasts influences each other in the LL. This interaction may be via direct contact, secreted factors or even through the interaction with other cell types present in the LL that have not been investigate here.

Future works will focus on an adapted panel in both histology and flow cytometry including more selective markers to the sub-populations of the SL such as POSTN or DKK3, and for the LL fibroblasts including CLIC5 or CD55. The expression of CLIC5 and CD55 was tested in preliminary data but required more optimizations to be replicable.

Other mechanism involving the expression of CD34 may be further investigated. Beside the increase of CD34 in the pathological SL fibroblasts population, evidence suggest that CD3 deficient mice exhibits a worst case of arthritis due to an increase vascular permeability (144). Interestingly, the percentage of CD34 in the ECs and fibroblasts is heterogenous among patients in both diseases suggesting different outcomes of CD34 on inflammation.

One of the limit in the TRMs analysis was the lack of positional identity markers in both of my panels. Indeed, alone the expression of MERTK, CD68 and CD206 may not be sufficient to capture the sub-populations of the LL and SL, especially in flow cytometry. This will be tested with the use of the specific markers TREM2 for the LL and FOLR2 for the SL. Better characterization of the infiltrated populations in also needed to capture more of the synovial inflammatory context.

Another limitation in this study comes from the lack of different pathotypes between tissue and patient. Indeed, most of the synovium used in this study is coming from Joint replacement surgery (JRP). JRP can be considered as the last stage of the disease which limits or understanding of the mechanism in active disease. I believe the similarities observed between OA and RA synovium might be explain by a convergence of different form of arthritis into more homogenous pathotypes when subjects to similar injuries including inflammation, hypoxia and aging. Luckily, I had access to some tissue biopsies in the RA cohort, given more perspective on the regulation of senescence during active disease. Interestingly, the state of the diseases was not a major factor influencing cellular senescence.

Although p53 expression in T cell and ECs is reduced in the biopsy patients suggesting that in active diseases p53 may exhibits different regulations. Nevertheless, JRP tissue provides information on the late stages of the disease and are a good models to understand dysregulation leading to treatment failure. Not all the pathotypes are representing in this study, according to a semi-quantitative analysis, 3 RA patients out of 11 could be considered as diffuse myeloid due to the very low/absence B cells, while 8 patients were classified as lympho-myeloid (145, 146). The pauci-immune pathotype was not investigated.

Unclassified cells in this study represent a high percentage of the total synovium. Among them, one major actors that participate in RA inflammation are the neutrophiles. Among the infiltrated cells invading the joint during inflammation, neutrophils appears to be one of the first responder to arrive in the joint (147). They are present in the synovial tissues and are the predominant cell found in the synovial fluid in RA suggesting that neutrophils migrate throughout all tissues may lead to ECM modulation and many cell-cell communication. Furthermore, neutrophils are potent antigen presenting cells (APC) deeply involve in the presentation of citrullinated epitopes to CD4+ and B cells. This is particularly relevant in the context of patients with a high ACPA generation promoting the loop of inflammation and triggering more autoimmune target. One mechanism specific to neutrophils called the Neutrophils Extracellular Traps (NET) consists of the extrusion of DNA and granzymes in the extracellular environment. Local inflammation of the synovium triggers spontaneous NET activation of neutrophil (148). This process increases the antigen presentation of citrullinated peptides leading to more ACPA (148, 149, 150). Interestingly, synovial fibroblasts can internalize citrullinated epitopes originated from NET via RAGE-TLR9 pathway and present the peptides to CD4 T cells via MHC class II (149, 151). The pro-inflammatory fibroblasts sub-population up regulating CD74, and HLA might be actively involved in this process. In addition, we could suppose that MERTK+ macrophages participate in the clearance of the apoptotic neutrophils and NET to promote repairs (26). Fibroblasts expressing GAS6 (MERTK ligand) may enable those repair mechanisms explaining why this population is important in remission.

Similarly, neutrophils are also involved in synovitis in OA and their implication promotes cartilage degradation, inflammation and osteophytes development (152).

While the role, of neutrophils in inflammation in undeniable, there is another mechanism that may link metabolism and senescence and inflammation and therefore relevant to the arthritic pathologies. Indeed, neutrophils are heavy producer of ROS in the process of NET formation. It has been demonstrated that ROS production in neutrophils is increased both intra and extracellular (147). This might explain the increased of yH2AX+ proportion in the CD11c+ population observed with flow cytometry. Whereas the role of ROS production during inflammation is complex, its implication in promoting senescence in age related diseases is well established (153). We can reasonably think that the increase of extracellular $0_2$- converted in H2O2 spontaneously or via extracellular plasmatic NADPH oxidases (NOXs) may have a paracrine effect on the surrounding cells (154). Countless experiments use H2O2 as DNA damaging agents to induced cellular senescence. However, the physiological concentration of H2O2 release in the context of inflammation need to be investigate. In addition, it has been observed that intracellular ROS are increased in neutrophils found in the synovial fluid (SF) in RA. Moreover, ROS could be distributed via exosome secretion and directly impact the LL (155). It would be interesting to determine how the ROS produced by the SF neutrophils may affect the homeostasis of the LL. This process might be one of many involved in the increase of p53+, p21+ and yH2AX+ cells observed in the LL.

## 7.2 The challenges of detecting senescent cells

Finding senescent cells in the tissue has always been challenging due to their rarity in the tissue, their lack of specific biomarkers and the heterogenous context of cellular senescence induction. Today, many experts in the field have agreed that using one or two markers is not enough to properly detect senescent cells as many of those markers are involved in other processes (156). For instance, it has been reported that the polarization of macrophages toward M2 phenotypes induced the expression of p16 and increased SA-β-gal independently of p53 (157). Yet, those processes are reversible and not

related to senescence. In this context, the use of p16 alone to detect senescent macrophages is not sufficient. For instance, the increase of p16+ MERTK+ seen in RA compared to OA might be associated with an increase of polarization toward a repair phenotype. To test this hypothesis, investigating the expression of p16 in macrophages of RA patients undergoing remission would be helpful to better characterized their role in disease resolution (26). Similarly, most of the senescence markers used in this study are associated with cell cycle regulation. This is the case for p16, p21 and p53, which, besides being classically used by senescent cells to stop proliferation, are also expressed during normal cell cycle regulation (57). Alone, those markers are not sufficient to conclude on a definite senescent cells state and need to be associated with other hallmarks such as persistent DNA damage and DDR activation (156). In this study, the hallmark of DNA damage yH2AX was used to deepen the phenotyping of senescent cells. Despite the use of multiplex imagery and spectral flow cytometry, only 3 senescence markers were monitored in this study which limits the classification of senescent cells. To further distinguish true senescent cells from cells with a transitory cell cycle arret, other high-plex techniques should be further investigated. Many studies are using gene signature databases to classify senescent cells based on single cells RNA sequencing data. For instance, the SenMayo gene set is reported as a good method to identify senescent cells across tissues (158). Those approaches are currently being investigated in our lab to identify senescent cells and their role in OA. In addition, spatial mapping techniques such as Visium technology show promising results to identify cellular senescence signatures and clusters within the tissue (159). Furthermore, the emerging field of deep learning and AI allows the detection of new biomarkers of senescence such as the nuclear morphology (160). Therefore, a combination of techniques and the multiplicity of biomarkers is essential to characterize senescent cells, particularly in complex contexts such as arthritis.

## 7.3 Cellular senescence and normal aging of the synovium

Our data indicate that p16, p21, p53, and yH2AX positive cells are found in normal synovium. This suggests that normal aging processes increase the senescence phenotype in synovium independently of the disease. In a previous study, IHC staining of p16 shows that older OA and RA patients have similar number of p16+ cells compared to age matched healthy donor (110). However, the authors found that senescent cells accumulated prematurely in RA and OA synovium compared to heathy patients. In our study only one healthy tissue was investigated in the cohort. Surprisingly, this patient was younger than most of the patient in the cohort, yet presented a high number of p16, p21, p53 and yH2AX. Indeed, the normal synovium donor was 43 years old while the RA and OA cohorts had average ages of 62 and 71 years respectively. Nevertheless, similar percentage of senescent cells in the LL are observed when we compared age matched RA patients with the healthy donor (Data not shown). Here, we are limited by the number of healthy tissues available which prevent us addressing normal aging in the synovium. However, from the literature and our preliminary observations, we could hypothesize that normal aging increases senescence in the synovium LL independently of the disease. More normal synovial tissue from different aged patients is needed to verify that RA and OA promote the early accumulation of senescent cells. If the processes that promote cellular senescence in normal aging are driven by inflammation, metabolism dysregulation and autophagy dysfunction, it is not surprising that senescence accumulated faster in the context of arthritis.

## 7.4 Senescence and autophagy: implication of the metabolism

Our data suggest that p53, p21 and yH2AX are significantly higher in the LL fibroblasts compared to the SL fibroblasts and as a general statement, those markers accumulate in most of the cells in LL but not in the SL connective tissue and perivascular regions. Moreover, we also notice that the accumulation of p16+ cells (particularly fibroblasts) is also dominant in the LL compared to the rest of the synovium. This appears to be intrinsic to the synovium as both OA and RA exhibits an accumulation of senescence

in the LL. However, there is an increase in the proportion of p21+ within the LL fibroblasts in RA compared to OA. Contrariwise, yH2AX appears higher in OA LL fibroblasts in comparison to RA. To explain the accumulation of senescence in the LL, our postulate was that mechanism preventing senescence such as autophagy via TFEB expression was oppositely distributed within the synovium. Surprisingly, TFEB expression is higher in the LL fibroblasts compared to the SL fibroblasts in both diseases, although this difference is significantly more pronounced in RA. Therefore, both the hallmarks of senescence and TFEB are higher in the LL. Since both, cellular senescence and autophagy are mechanism to palliate cellular stress, those results are coherent and suggests that LL is differently affected by stressful events than the SL.

The microenvironment is highly dependent of the metabolism of the different cell types that compose it. The access to nutrient and oxygen drastically influences inflammation and changes the outcomes in pathological context. Therefore, it is critical to understand the metabolic profile in disease. Inflammation is known to induced hypoxia (161). Since the SL is the siege of inflammation, and the LL is deprived of vasculature, the hypoxic environment is exacerbated in the LL. This pro-inflammatory environment promotes glycolysis in the fibroblasts characterized by an up regulation of glucose transporter GLUT1 (162). According to transcriptomic DATA in RA, GLUT1 is even more up regulated in the LL fibroblasts (17). Unpublished scRNA-seq data set in OA also suggests that GLUT1 is enriched in the LL fibroblasts supporting the idea that the LL is more affected by hypoxia. A recent study indicates that a high expression of GLUT1 in gingival macrophages promotes inflammatory SASP release and increase of p16 and p21 via mTOR in presence of high glucose (163). If a similar mechanism is involved in the fibroblasts, we could suppose that the upregulation of GLUT1 in hyperglycaemic environment may promotes cellular senescence in the LL and exacerbates the risk factor between OA, diabetes and obesity (164).

Interestingly, mTOR is inhibited under hypoxia even in nutrient rich conditions (165, 166). The inhibition of mTOR could be one of the mechanism involved in the regulation of TFEB activation in the LL

fibroblasts under hypoxia. As inflammation is often increased in RA synovium compared to OA, we can suppose that hypoxia would be increased too in the LL in RA leading to further mTOR inhibition and finally more TFEB activation. This might be one of the explanation in the differential TFEB nuclear localization observed in the two diseases. Further evidence also suggests the role of hypoxia in the activation of autophagy (167). In addition, hypoxia increase mitochondrial ROS production adding more genotoxic burden to the environment (155). It is also possible that ER stress induced during hypoxia increased cellular senescence (168).

An interesting mechanism induced by the up regulation of glycolysis is the increase of lactate production. Indeed, lactate is increase upon inflammation and lead to the increase of fibroblasts mobility and IL-6 production (162). Interestingly, senescent RA fibroblasts in culture are more glycolytic after TNF-α stimulation than the non-senescent fibroblasts **(Sup. Fig 1 A, B)**. However, their mobility appears to be impaired even upon lactate stimulation **(Sup. Fig 1 C)**. This supports the increased inflammaging one of the principal consequence of senescent cells in tissue. Furthermore, macrophages are also impacted by the acidic environments of the synovium. Macrophages have an opposite reaction in presence of lactate leading to a reduction of migration and IL-6 production (162). This is adding more complexity in the metabolic relationship between fibroblasts and macrophages in the synovium.

Those mechanisms are probably not exclusive to RA and might be further explore in OA synovium. Recent studies focus on OA reveal that SFs from obese patients develop a pro inflammatory phenotype compared to normal weight patients highlighted by a higher IL-6 and CXCL8 expression (169). Furthermore, the metabolic profile in the synovial fluids from obese OA patients is different from the normal weight patient with a significantly higher concentration of lactate (170). The beneficial or detrimental role of lactate in the context of arthritis remains under investigation, while lactate may contribute to promote inflammation, some studies underline the role of lactate in the activation of autophagy (171, 172).

## 7.5 Autophagy, Cellular senescence, DNA damage and apoptosis: p53 as the common denominator

Mechanisms behind the hyperplasia of the LL observed in OA remains poorly understood. As previously described, LL in OA and RA are subjects to similar injuries including hypoxia, acidic and ROS rich environment, as well as a prolonged stimulation to pro-inflammatory signals. Yet, both structures are behaving differently during the disease progression. The first two hypothesis that come to mind explaining the hyperplasia in OA LL are either an increased proliferation of the TRMs and fibroblasts or an accumulation of the cells induced by impair apoptosis. Since proliferation markers such as ki67 do not seem to be expressed in the LL populations and that cellular senescence prevent apoptosis, we can suppose that the second hypothesis might be involved in OA. One problem with this hypothesis is that senescent cells accumulation in the LL in OA and RA are very similar whereas no difference of p16+ proportion is detected.

In this study the differences observed between OA and RA LL are the increase of p21 in RA, and the decrease in both TFEB level and nuclear localization in OA. However, in both diseases the LL display a high activation of p53. Interestingly, p53 is a central actor in the regulation of DNA damage, apoptosis, cellular senescence and autophagy.

First, I investigated if the differential autophagy activation could be attributed to p53. According to the literature, p53 have a dual role in inhibition/activation of autophagy according to its cellular localization (173, 174). Therefore, nuclear p53 may positively regulate autophagy via transcription mechanism while cytoplasmic p53 may be a repressor of autophagy and promoting cell death (173, 175). In this study, the LL staining of p53 is strictly cytoplasmic in OA and in active RA or JRP RA (Sup Fig 2 A). Following this proposal, it would suggest that if autophagy is regulated by p53, then this regulation would be the same in both diseases because of its localization into the cytoplasm. This goes in contradiction with the decreased TFEB activation seen in OA compared to RA. However, the increased or decreased of autophagy flux in this context has not been tested yet. Moreover, the

activation/expression of the key molecular components of autophagy such as Beclin-1, p62, LC3-II, ATG5 and ATG7 have not been addressed yet. Nevertheless, if the cytoplasmic accumulation of p53 leads to a decrease of autophagy this will be observed in both diseases which does not explain the differences in TFEB regulation as well as the differential hyperplasia in OA suggesting the involvement of other pathways.

Further evidence suggests that the activation p53 silenced GLUT1 expression by direct binding to *glut1* promoter while mTOR activate that transcription of GLUT1 (176). The activation of p53 is carried by its phosphorylation via AMPK (176). The absence of nuclear p53 staining in the LL could be an indication of an accumulation of inactive p53 repressing its transcriptomic targets. Counterintuitively, many synovial cells such as ECs and T cells that are in the state of cycle arret via p21 are also p53 meaning that p53 still maintain the activation of *cdkn1a*. However, other mechanism independent of p53 may be involve in later stage of the diseases. For instance, the high level of p21 mRNA and the accumulation of nuclear p21 in endothelial, LL fibroblasts, TRMs and T cells may be maintained by the activation the p38-MAPK. Indeed, p38-MAPK is known to promote the stabilization of p21 during G1 checkpoint (177).

Autophagy, DNA damage response and apoptosis sharded interconnected signalling pathways. Therefore, the activation of one response could lead to either promote or repress the other. While the relationship between autophagy and apoptosis remains controversial. For example, a target of p53 termed “damage regulated autophagy modulator” or DRAM1 is involved in the p53-mediated apoptosis by promoting autophagy (178). A more recent study suggests that DRAM1 acts as an inhibitor of mTOR and its target pS6 underlining its role in promoting autophagy and in regulating cell death/proliferation (179). This kind of relationship could be involved in the synovial LL too. As DRAM1 is a direct target of p53 and required its nuclear translocation, we could hypothesize that the cytoplasmic p53 is not able to activate the downstream target involved in induction of autophagy and p53-mediated cell death such as DRAM1. Therefore, in this specific context the activation of apoptotic

pathway involving autophagy may be impaired leading to accumulation of damaged cells. This will consequently promote cellular senescence inhibiting even further the apoptotic regulation. Interestingly, in the AMP II scRNA-seq data, DRAM1 appears downregulated in the LL fibroblasts but not in most the SL populations (sup Fig 2 B). It is unlikely that this mechanism alone could explained the increase senescence distribution of autophagy in the LL but in underline the complex relationship between autophagy, cellular senescence and cell death via p53.

Sirtuin 1 (SIRT1), a deacetylase involved in stress response and aging, could be a good candidate to better understand the role of p53-mediated apoptotic pathways in OA and RA synovium. Deacetylation of p53 by SIRT1 in presence of ROS prevents p53 nuclear translocation, impairing the transcription of targets of p53 involved in apoptosis (180). However, the accumulation of p53 in the cytoplasm promotes its interaction with the anti-apoptotic molecule BCL-2 within the mitochondria leading to releases of Cytochrome C and apoptosis (180). Dysregulation of SIRT1 may lead to the retention of p53 in the cytoplasm observed in the synovium while other pathways may impair the p53 transcription independent apoptosis.

As previously described, the environment in which the LL remains is highly genotoxic. Therefore, the activation of the DNA damage response is critical in this context. This is highlighted by the high proportion of yH2AX+, p53+ and p21+ found both macrophages and fibroblasts in the LL but not exclusively as ECs and T cells also have a high proportion of p21 and p53. Interestingly, LL fibroblasts positive for p53, p21 and yH2AX are also expressing p16 suggesting that cellular senescence is activated when damages accumulated, and the repair mechanism failed. However, many cells in the synovium could be in a state of premature senescence characterized by the expression of p53 and p21 but a low yH2AX signature.

Another piece of evidence supporting the activation of the DDR in the synovium is the significant positive correlation between p21 and γH2AX, as well as between p21 and p53. Interestingly, this

correlation is only observed in the RA patients but not in OA which could suggest an impaired DDR mechanism in OA.

TFEB is activate during DNA damage in a mTORC1 and p53 dependant manner (137). This regulation involves the repression of mTORC1 by p53 via the activation of the p53 target Sestrin 1 and 2 (Sesn1/2) which promote AMPK (137, 177, 181). Interestingly, TFEB knockout in mouse embryonic fibroblasts impaired the DDR upon DNA damage by repressing genes directly involved in DDR but also other target such a Sesn1 and Sesn2 or Dram1 (137). On the other hand, the activation of TFEB promote p53 transcription and stability which facilitate p53 mediated apoptosis after DNA damage injuries (137). Another study suggests an opposite mechanism of TFEB regulation by p53. The authors show that depletion of p53 promote the nuclear translocation of TFEB in lung cancer cells (182). This suggests a context dependent relationship between TFEB and p53.

Nevertheless, in the context of arthritis, we observed that TFEB is associated with p53 and p21, suggesting that TFEB participate in the DDR. For instance, the high level of TFEB, p21 and p53 while the proportion of yH2AX+ in the ECs could indicate that active repair mechanism is involved to protect the endothelium. This is further supported by the positive correlation between TFEB and p53 observed in the ECs in both RA and OA. Despite the strong activation of DDR, a high proportion of ECs also induced cell cycle arrets through p16 suggesting that the activation of cellular senescence is still present. It is possible that TFEB activation in ECs is involved in different pathways beside the DDR. Indeed, TFEB is involved in the regulation of angiogenesis (131). However, the role of autophagy as pro or anti-angiogenesis might be dependent of the context and is still debate. Interestingly, VEGF promote the phosphorylation of ULK1 (Unc-51-like autophagy-activating kinases 1) though AMPK (183). Therefore, we could hypothesize that VEGF dependant angiogenesis in the synovium may promote the activation of TFEB via the regulation of AMPK and ULK1 leading to the inactivation of mTORC1. This might be one of the mechanism behind the increase in nuclear TFEB in RA ECs compared to OA. In addition, promoting TFEB expression in ECs limits inflammation, immune infiltration and promotes antioxidant

factors independently of autophagy during atherosclerosis (141). Here, the nuclear activation of TFEB do not correlate with a lower percentage of CD3+ cell in the synovium. Nevertheless, the pro-inflammatory environment may overtake this regulation, and this process need to be further investigated as sheer stress and antioxidant response are critical parameter in the maintenance of the endothelium. Interestingly, a recent publication demonstrated that lactate activates CD31 which promotes autophagy in the ECs in RA, suggesting that the increase of TFEB in this population might also be regulated by metabolic pathway such as glycolysis (184). This encourages the perspective of treatment stimulating either TFEB expression or activation in the ECs in OA and RA.

Obesity is one of the most important co-morbidity factor in OA and might explain metabolic dysregulation. Furthermore, obesity increases cellular senescence SASP, ROS production, inflammation and M1 pro-inflammatory macrophages polarisation in adipose tissue and their surrounding environment (142). Once again, p53 appears to be a master regulator in many metabolic pathways in response to obesity and insulin resistance (185, 186).In this study, the p53 expression in the synovium positively correlate with the increase of BMI. However, the range of BMI in the OA patient's cohort was not sufficient to significantly prove this correlation.

The activation or inactivation of p53 appears central mechanism in the regulation of the diseases and this process may change toward the disease progression. Therefore, the inactivation of p53 may promote glycolysis, reduce autophagy via mTOR activation and influence apoptosis. In the process, AMPK seems a central regulator and should be investigated.

## 7.6 Promoting autophagy to prevent senescence

Indications of the protective effect of TFEB on senescence activation are clear in the B cell populations. Our preliminary data in accord with recent studies, suggest that B cell have a strong autophagic response due to a higher expression of TFEB (130). This is observed in the synovium, B lymphocytes are not affected by immune senescence whereas T cell are. Interestingly, TFEB is very high in the B cell compared to T cells suggesting that autophagy have a protective role by preventing damage and

reverse cellular senescence. In addition, despite the different infiltration of inflammation, no difference in the immune senescence and autophagy is observed between OA and RA suggesting that immune cells may undergo the same systemic regulation under aging. This need to be compared with non-infiltrated B cells and T cells in the afferent lymphoid structures. It has been demonstrated that B cell function is increased when autophagy is promoted via spermidine and TFEB (128, 130). While increasing B cell activity in an auto-immune context might be contradictory, the benefits of polyamine treatment such as spermidine may lead to positive outcomes on the overall joint homeostasis by reducing the damage burden of inflammaging and genotoxic stress. Many studies report that inducing autophagy promote the stem cell health a critical mechanism in cartilage homeostasis (187, 188).

Another promising effect to corroborate the implication of TFEB in promoting tissue homeostasis is observed in the significant negative correlation between TFEB expression and yH2AX in RA. Interestingly this effect is not found in OA patient supporting the hypothesis that TFEB is dysregulated in OA leading to impaired DDR mechanisms. This effect is exacerbated with age in the RA cohort where younger patients have the highest TFEB expression and the lowest yH2AX. As the age range between OA patients is low and most of the patients were old, I investigated the correlation between yH2AX proportion with age in the RA cohort when the younger patients are removed. This is leading to a loss of both negative, positive correlation and significance suggesting that aging may be the common factor of dysregulation of DDR in both diseases. Similarly, I verified that age difference between OA and RA patients was not responsible of the difference observed in nuclear localisation of TFEB. Interestingly, the age of patients does not influence the activation TFEB in OA and RA suggesting that the mechanism behind the differential TFEB nuclear localization may be disease dependant. Furthermore, in the LL fibroblasts, where we observed more dysregulation of TFEB in OA, TFEB negatively correlate with p53, positively correlate with yH2AX, and do not correlate with p16 or p21. The opposite correlation is observed in RA LL fibroblasts with positive correlation between TFEB and the DDR while DNA damage and senescence via p16 negatively correlate, further supporting the hypothesis of TFEB dysregulation in the DDR in OA LL fibroblasts. Unfortunately, more patients are needed to confirm that those

correlation are not due to random heterogeneity. Similarly, the lack of younger patients in the OA cohort limits our understanding on the regulation of TFEB in OA. Investigating TFEB and cellular senescence in post-traumatic OA will help to better understand the age-related mechanism observed in elderly patients.

## 7.7 Future perspectives

The direct or indirect mechanistic relationship between cellular senescence and TFEB induced autophagy in disease progression remains to be found. Despite the link established in this work, no evidence has demonstrated the molecular mechanism involved in TFEB and senescence regulation in the synovial populations. However, many approaches are being developed to answers those remaining questions.

One of the challenges in studying synovial fibroblasts *in vitro*, is the loss of tissue identity. Indeed, isolation of primary fibroblasts *in vitro* results in a "dedifferentiation" or an enrichment of the SL phenotype POSTN+, CD34+, CD90+ (116). This is applicable to the LL fibroblast too which adopts the same SL phenotype in addition to a loss of PDPN after many passages. Therefore, to maintain their identity in vitro, synovial fibroblasts need to be cultured in presence of the tissue's cues involved in the synovium. One option is to generate synovial organoids including endothelial cells to mimicking the perivascular NOTCH3+ niche and macrophages (preferably anti-inflammatory) to promote the formation of a substitute LL. Therefore, OA and RA primary fibroblasts were co-cultivated in presence of Human Umbilical cord Endothelial Cells (HUVECs) in a 3D environment composed of Matrigel **(Sup Fig 4 A)** according to the protocol described in Wei et al. studies (19). The expected induction of perivascular niche was seen in only one organoid generated with this process (**Sup Fig 4 B**). However, the majority of the 3D cultured lack of organization between HUVECs and fibroblasts resulting in spheroids with no tissue identity (**Sup Fig 4 C**). Similarly, the attempt to generate a LL using blood driven monocytes were unsuccessful so far. Because of the lack of reproducibility in the generation of the

organoids, investigate the mechanisms affecting LL and SL fibroblasts under TFEB overexpression and TFEB knockout remains in progress.

Finally, in vivo investigation of the role of TFEB in the progression of OA is currently investigated. The newly generated conditional TFEB KO under the *pdgfrα* promoter and *acan* (aggrecan) promoter, will deepen our understanding on the specific depletion of TFEB in fibroblasts and chondrocytes respectively. Those specific TFEB depletion will be investigated in a destabilisation of the medial meniscus (DMM) models of OA.

## 7.8 Final conclusions

This study highlights new potential regulations of the synovium in the context of synovitis through the spectre of DNA damage, cellular senescence and autophagy. While differential DNA damage response activation though p53 and p21 occurs in most of the synovium, the LL layer and the endothelium are the most affected. In those regions, the proportion of p16+ cell is higher compared to the rest of the synovium. This is also where most of the DNA damage (γH2AX) and the strongest DDR (p53, p21). In accord with our hypothesis, the LL fibroblasts appear to be particularly affected in this context. Interestingly, TFEB is more expressed in the regions with the higher DDR activity suggesting its role in the process. The exact role of TFEB in this context remain to determined, and raise new question on the relationship between autophagy, metabolism, apoptosis and cellular senescence. Does the activation of TFEB promote DNA damage repair? Does it promote apoptosis or cell survival? If TFEB promotes apoptosis, could the lower TFEB activation in OA explain the LL layer hyperplasia? If TFEB promote cell survival, does it increase or reduced cellular senescence in the context of genotoxic stress? Does the cytoplasmic localization of p53 influence the cell fate in the LL? Answering those questions will increase our understanding and reveal new facets of inflamed arthritis.

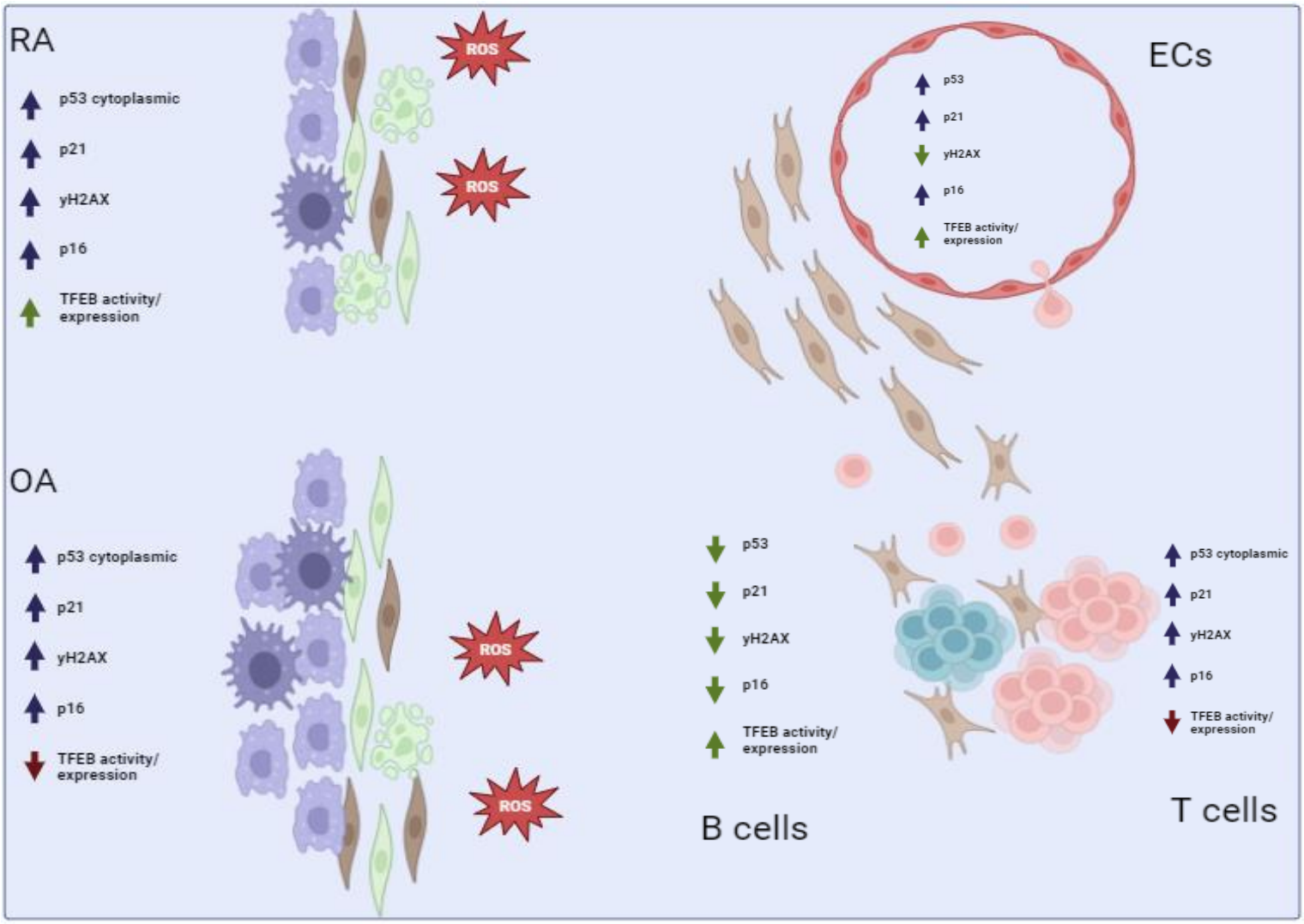


**Figure 7. 1: Schematic view of the regulation of the hallmarks of senescence and TFEB in the synovium**

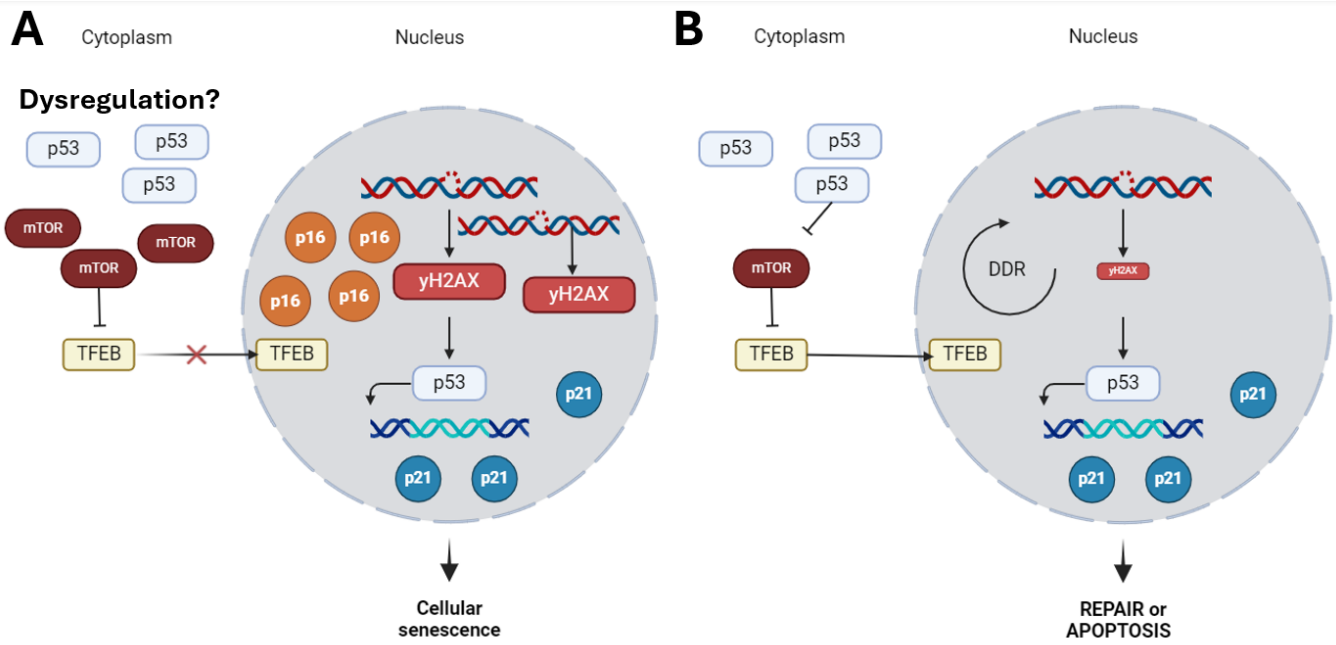


**7.2 Putative model of p53 and TFEB role in regulation of DNA damage and cellular senescence in the synovium**

**A:** Unknown dysregulation between cytoplasmic p53 and mTOR. In this context, mTOR accumulates and disables TFEB activation impairing the DNA damage response (DDR) and promoting cellular senescence. **B:** In this context, the interaction between p53 and mTOR is not dysregulated. Then, p53 inhibits mTOR preventing TFEB phosphorylation. TFEB activity increase DDR promoting repairs. This could enhance cell survival or apoptosis depending on the context.

Both of those mechanisms could happen simultaneously, depending on the context (hypoxia, hyperglycaemia, age) one or the other may be promoted.

## Table 2 A: senescence in macrophage populations in OA

| Population | Frequence (%) | p16 g Mean | Frequence p16+ (%) | Frequence p21+ (%) | Frequence yH2AX+ (%) | Frequence p53+ (%) |
|---|---|---|---|---|---|---|
| MERTK+ | 15,93 (±17,704; n=6) | 8873,5 | 0,34 (± 0,38; n=6) | 15,16 (± 10,64; n=6) | 27,73 (± 8,78; n=6) | 12,15 (± 8,93; n=6) |
| MERTK+ CX3CR1+ | 10,65 (±11,87; n=6) | 10666 | 1,06 (± 2,21; n=6) | 15,76 (± 16,93; n=6) | 19,80 (± 7,75; n=6) | 8,56 (± 10,53; n=6) |
| MERTK+ CX3CR1+ HLA-DR+ | 44,39 (±31,86; n=6) | 60752 | 64,32 (± 11,04; n=6) | 60,12 (± 18,14; n=6) | 10,11 (± 12,88; n=6) | 4,25 (± 2,08; n=6) |
| MERTK+ HLA-DR+ | 15,25 (±6,86; n=6) | 53844 | 49,80 (± 11,03; n=6) | 54,36 (± 11,18; n=6) | 8,15 (± 10,60; n=6) | 5,35 (± 2,23; n=6) |
| MERTK+ CD68+ CX3CR1+ | 8,08 (±4,41; n=6) | 19656 | 12,76 (± 9,39; n=6) | 3,91 (± 5,10; n=6) | 11,14 (± 2,76; n=6) | 0,73 (± 0,80; n=6) |
| MERTK+ CD68+ CX3CR1+ HLA-DR+ | 79,5 (±7,76; n=6) | 58859 | 55,47 (± 12,52; n=6) | 17,89 (± 11,98; n=6) | 4,56 (± 4,35; n=6) | 0,54 (± 0,13; n=6) |
| MERTK+ CD68+ HLA-DR+ | 7,99 (±4,51; n=6) | 55741 | 47,07 (± 9,38; n=6) | 32,37 (± 16,14; n=6) | 6,19 (± 8,65; n=6) | 0,50 (± 0,29; n=6) |
| MERTK+ CD68+ | 2,25 (±5,08; n=6) | 23284 | 15,80 (± 16,42; n=6) | 7,56 (± 10,96; n=6) | 7,23 (± 13,05; n=6) | 5,64 (± 8,23; n=6) |

## Table 2 B: Senescence in macrophage populations in RA

| Population | Frequence (%) | p16 g Mean | Frequence p16+ (%) | Frequence p21+ (%) | Frequence yH2AX+ (%) | Frequence p53+ (%) |
|---|---|---|---|---|---|---|
| MERTK+ | 32,86 (± 24,92; n=4) | 7274 | 0,06 (± 0,10; n=4) | 19,43 (± 13,07; n=4) | 45,13 (± 17,19; n=3) | 16,51 (± 10,73; n=4) |
| MERTK+ CX3CR1+ | 13,60 (± 8,47; n=4) | 8677 | 1,78 (± 2,04; n=4) | 18,72 (± 12,78; n=4) | 37,00 (± 13,72; n=3) | 11,99 (± 6,61; n=4) |
| MERTK+ CX3CR1+ HLA-DR+ | 32,82 (± 23,69; n=4) | 46431 | 47,05 (± 11,61; n=4) | 58,62 (± 13,08; n=4) | 7,82 (± 8,06; n=3) | 2,20 (± 1,13; n=4) |
| MERTK+ HLA-DR+ | 9,94 (± 8,17; n=4) | 31690 | 22,75 (± 15,42; n=4) | 55,35 (± 12,60; n=4) | 24,17 (± 26,33; n=3) | 4,36 (± 3,16; n=4) |
| MERTK+ CD68+ CX3CR1+ | 1,08 (± 0,73; n=4) | 8893 | 2,86 (± 3,40; n=4) | 4,39 (± 1,76; n=4) | 24,46 (± 25,13; n=3) | 2,08 (± 2,12; n=4) |
| MERTK+ CD68+ CX3CR1+ HLA-DR+ | 90,70 (± 2,66; n=4) | 46112 | 43,38 (± 13,97; n=4) | 17,40 (± 3,38; n=4) | 1,81 (± 7,94; n=3) | 0,55 (± 0,38; n=4) |
| MERTK+ CD68+ HLA-DR+ | 6,48 (± 2,20; n=4) | 35547 | 30,53 (± 11,25; n=4) | 40,30 (± 12,11; n=4) | 4,51 (± 5,01; n=3) | 0,42 (± 0,44; n=4) |
| MERTK+ CD68+ | 0,39 (± 0,32; n=4) | 10346 | 0,00 (± 0,00; n=4) | 63,05 (± 32,19; n=4) | 54,63 (± 35,30; n=3 | 21,22 (± 12,85; n=4) |

**Table 3: list of the markers used in multiplex IF staining and Spectral flow cytometry**

| AB multiplex IF panel | AB Flow cytometry panel |
|---|---|
| Stromal | |
| PDPN | PDPN |
| CD31 | CD31 |
| CD90 | CD90 |
| CD34 | CD34 |
| Immune | |
| CD20 | CD19 |
| CD45 | CD45 |
| CD3 | CD11C |
| | CD4 |
| | CD8 |
| TRMs | |
| MERTK | MERTK |
| CD68 | CD68 |
| CD206 | HLA DR |
| | CX3CR1 |
| Senescence | |
| P21 | P21 |
| P53 | P53 |
| P16 | P16 |
| yH2AX | yH2AX |
| Autophagy | |
| TFEB | TFEB |
| Pan cells | |
| Vimentin | HLA ABC |

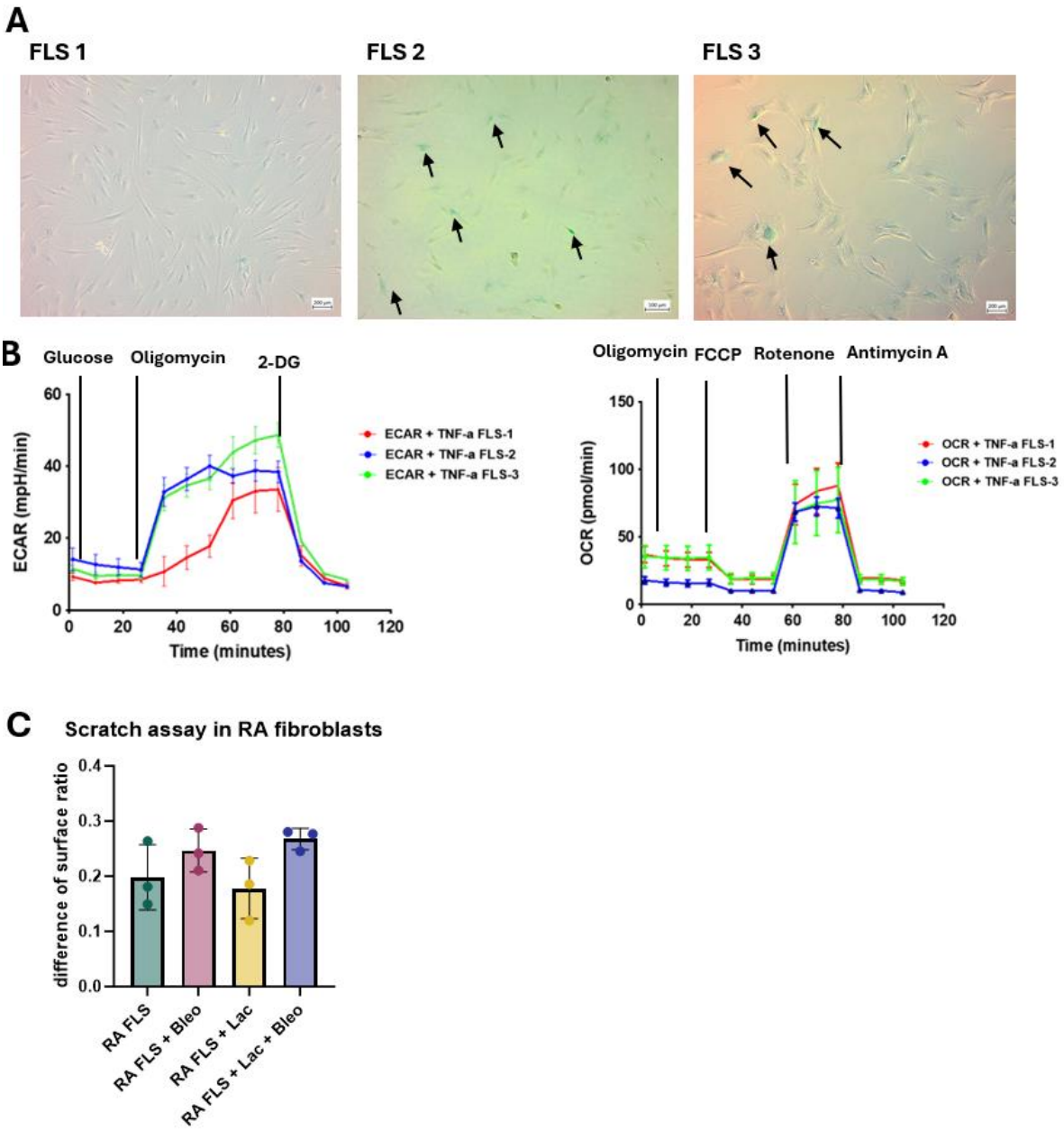


**Supplementary Figure 1: Metabolism and senescence preliminary exploration**

**A:** Senescence associated β-Gal staining of RA primary fibroblasts. FLS 1 (P4), FLS2 (P10), FLS3 (P7); black arrows show senescent cells. **B:** ECAR and OCR measured with Seahorses in RA fibroblasts. **C:** Scratch migration assay in RA fibroblasts and DNA damage induced senescence (BLEO) in presence or absence of lactate (n=3).

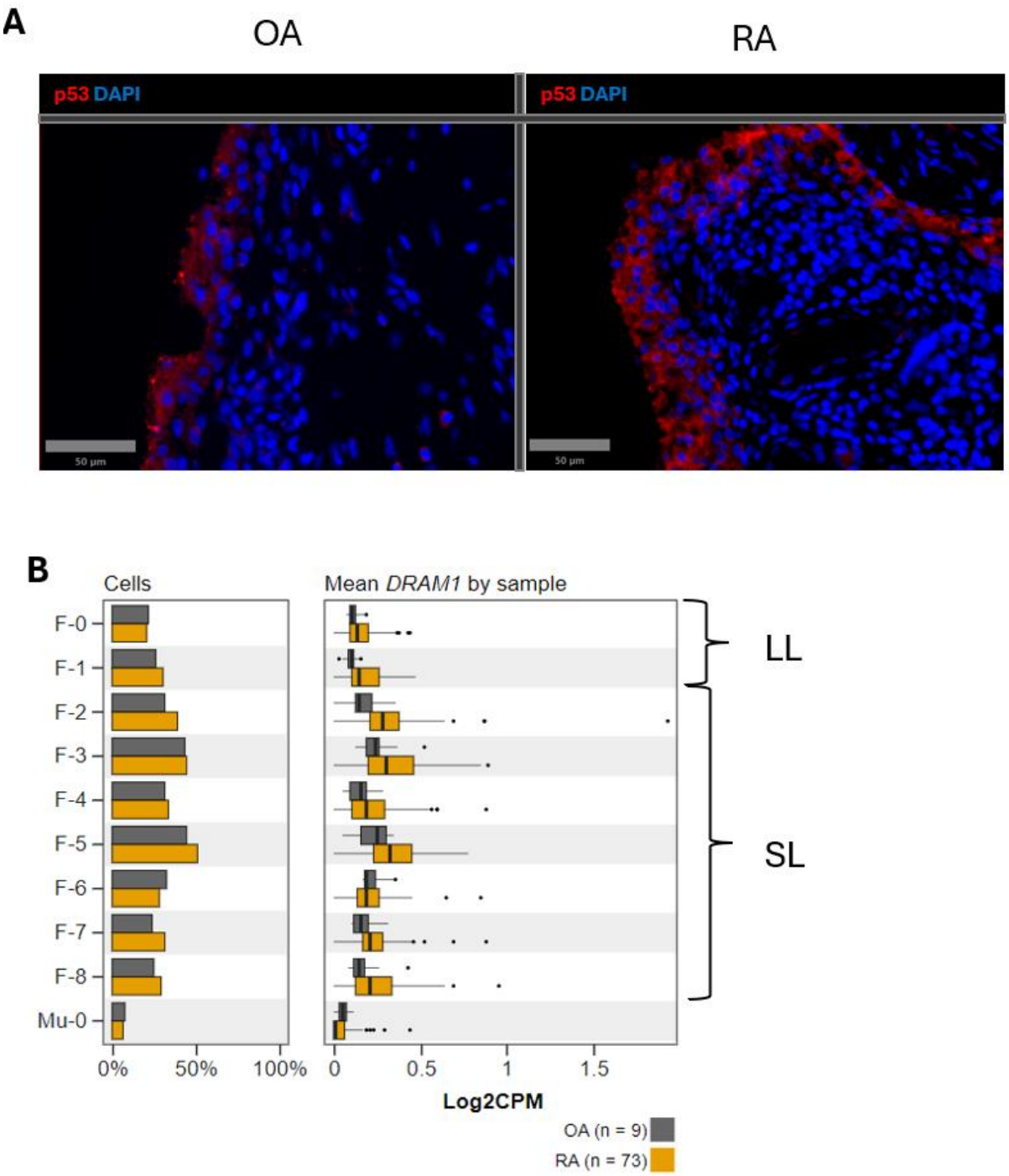


**Supplementary Figure 2: p53 cytoplasmic in regulation of DNA damage and autophagy**

**A:** Multiplex IF staining showing the cytoplasmic localization of p53 (red) in the LL in OA (left) and RA (right). B: Transcription of DRAM1 in OA and RA synovium based on the AMP phase II Sc-RNA-seq data set (189).

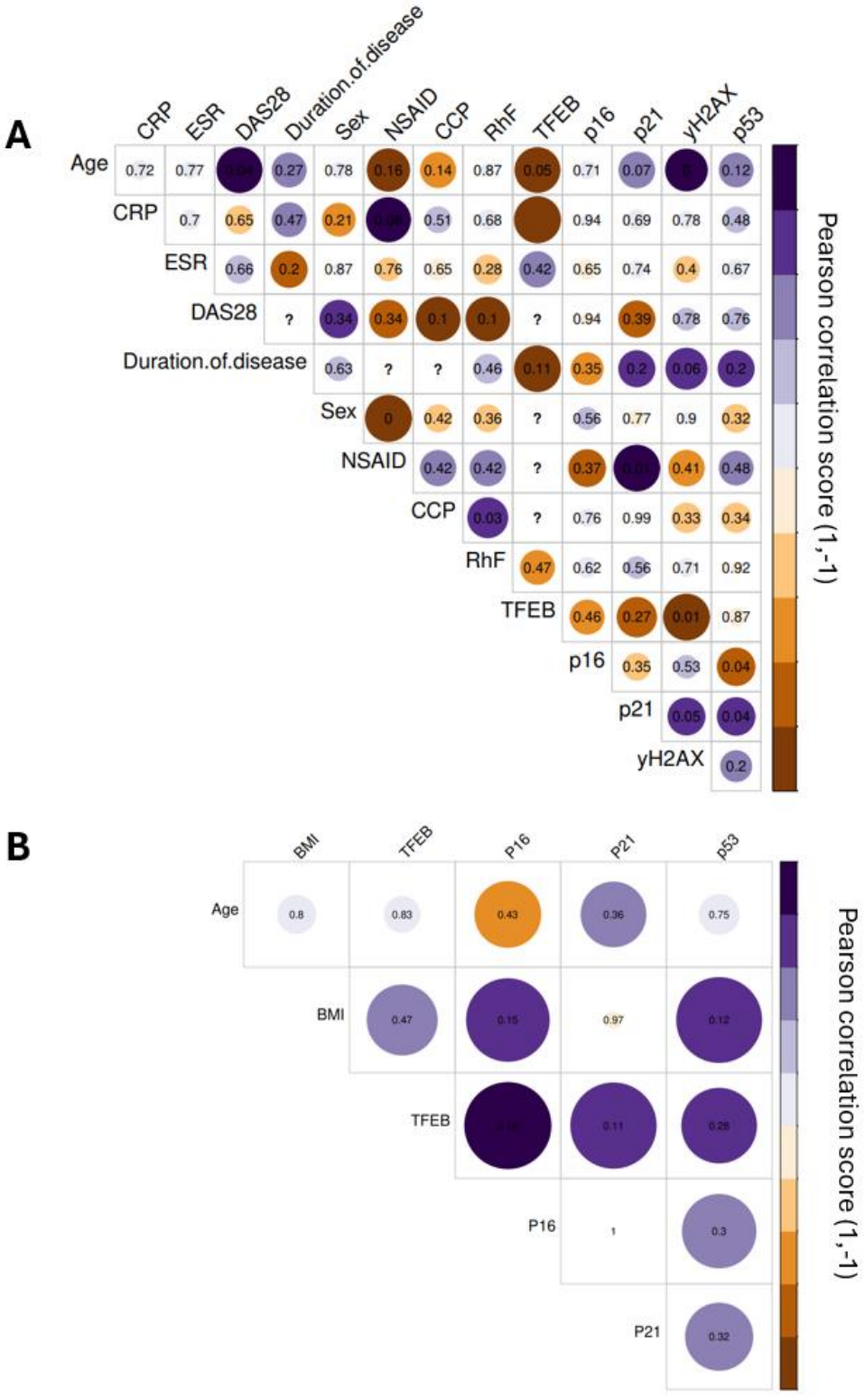


**Supplementary Figure 3: Patient Metadata correlation**

**A:** Pearson correlation of all the available metadata of the patient cohort in RA, p values are indicated in the centre of the circle, the color corresponds to the person correlation score. **B:** Pearson correlation of all the available metadata of the patient cohort in OA, p values are indicated in the centre of the circle, the color corresponds to the person correlation score.

# 8 Acknowledgement

I would like to thank the university of Birmingham and the Medical and Dental School of Birmingham to give me the opportunities to perform this research. Many thanks to the Medical Research Council Versus Arthritis (MRC VA) and Centre for Musculoskeletal Ageing Research (CMAR) to sponsor this research. During my PhD I had the chance to work in the best institution in rheumatology research in the UK, including the Rheumatology research group (RRG) in the Queen Elizabeth Hospital in Birmingham, the Kennedy institute of Rheumatology, and the BOTNAR research centre in Oxford granting me access to state-of-the-art technologies.

I am very grateful to Professor Andrew filer, Professor Simon Jones, Dr Jolet Mimpen and Professor Sarah Snelling in providing the human tissue in this study.

I could not have done this without the help of the Cell DIVE facilities teams in particular Dylan Windel, Ananya Bhalla and Sarah Hill. I would also like to thank the FACS facility manager Jon Webber for his teaching in flow cytometry.

Many thanks to Valentina Pucino for her great insights and her help in the project.

Next, I want to thank my supervisors, Professor Christopher Buckley who believed and me and gave this incredible opportunity, Professor Karim Raza for his warm support and help toward my PhD.

A special thanks to Dr Ghada Alsaleh for having me in her lab in Oxford, it was such a privilege to work with her. I would not have made it without her kindness and supports.

A warm thank you to Mathilde Pohin for her vital wisdom and friendship.

I also want to thank the Alsaleh group, especially the brilliant and amazing Loren Kell and Maria Kyriazi for bringing joy to the lab.

Many thanks to everyone that have helped me during this time that I could not name here.

Finally, I want to thank my parents, my family and my friends for their flawless supports.

# 9 Reference


1. de Brito Rocha S, Baldo DC, Andrade LEC. Clinical and pathophysiologic relevance of autoantibodies in rheumatoid arthritis. Adv Rheumatol. 2019;59(1):2.
2. Kurowska W, Kuca-Warnawin EH, Radzikowska A, Maslinski W. The role of anti-citrullinated protein antibodies (ACPA) in the pathogenesis of rheumatoid arthritis. Cent Eur J Immunol. 2017;42(4):390-8.
3. Catrina A, Krishnamurthy A, Rethi B. Current view on the pathogenic role of anti-citrullinated protein antibodies in rheumatoid arthritis. RMD Open. 2021;7(1).
4. Zhao J, Guo S, Schrodi SJ, He D. Molecular and Cellular Heterogeneity in Rheumatoid Arthritis: Mechanisms and Clinical Implications. Front Immunol. 2021;12:790122.
5. Martel-Pelletier J, Barr AJ, Cicuttini FM, Conaghan PG, Cooper C, Goldring MB, et al. Osteoarthritis. Nat Rev Dis Primers. 2016;2:16072.
6. van der Kraan PM, van den Berg WB. Osteophytes: relevance and biology. Osteoarthritis Cartilage. 2007;15(3):237-44.
7. Salman LA, Ahmed G, Dakin SG, Kendrick B, Price A. Osteoarthritis: a narrative review of molecular approaches to disease management. Arthritis Res Ther. 2023;25(1):27.
8. Bullock J, Rizvi SAA, Saleh AM, Ahmed SS, Do DP, Ansari RA, et al. Rheumatoid Arthritis: A Brief Overview of the Treatment. Med Princ Pract. 2018;27(6):501-7.
9. Cronstein BN, Aune TM. Methotrexate and its mechanisms of action in inflammatory arthritis. Nat Rev Rheumatol. 2020;16(3):145-54.
10. Wang Z, Huang J, Xie D, He D, Lu A, Liang C. Toward Overcoming Treatment Failure in Rheumatoid Arthritis. Front Immunol. 2021;12:755844.
11. Mok CC. Rituximab for the treatment of rheumatoid arthritis: an update. Drug Des Devel Ther. 2013;8:87-100.
12. Grassel S, Muschter D. Recent advances in the treatment of osteoarthritis. F1000Res. 2020;9.
13. Chu CQ. Highlights of Strategies Targeting Fibroblasts for Novel Therapies for Rheumatoid Arthritis. Front Med (Lausanne). 2022;9:846300.
14. Gauthier V, Kyriazi M, Nefla M, Pucino V, Raza K, Buckley CD, et al. Fibroblast heterogeneity: Keystone of tissue homeostasis and pathology in inflammation and ageing. Front Immunol. 2023;14:1137659.
15. Marsh LJ, Kemble S, Reis Nisa P, Singh R, Croft AP. Fibroblast pathology in inflammatory joint disease. Immunol Rev. 2021;302(1):163-83.
16. Croft AP, Campos J, Jansen K, Turner JD, Marshall J, Attar M, et al. Distinct fibroblast subsets drive inflammation and damage in arthritis. Nature. 2019;570(7760):246-51.
17. Zhang F, Wei K, Slowikowski K, Fonseka CY, Rao DA, Kelly S, et al. Defining inflammatory cell states in rheumatoid arthritis joint synovial tissues by integrating single-cell transcriptomics and mass cytometry. Nat Immunol. 2019;20(7):928-42.
18. Korsunsky I, Wei K, Pohin M, Kim EY, Barone F, Major T, et al. Cross-tissue, single-cell stromal atlas identifies shared pathological fibroblast phenotypes in four chronic inflammatory diseases. Med (N Y). 2022;3(7):481-518 e14.
19. Wei K, Korsunsky I, Marshall JL, Gao A, Watts GFM, Major T, et al. Notch signalling drives synovial fibroblast identity and arthritis pathology. Nature. 2020;582(7811):259-64.
20. Rauber S, Mohammadian H, Schmidkonz C, Atzinger A, Soare A, Treutlein C, et al. CD200(+) fibroblasts form a pro-resolving mesenchymal network in arthritis. Nat Immunol. 2024;25(4):682-92.
21. Ng MTH, Borst R, Gacaferi H, Davidson S, Ackerman JE, Johnson PA, et al. A single cell atlas of frozen shoulder capsule identifies features associated with inflammatory fibrosis resolution. Nat Commun. 2024;15(1):1394.
22. Lewis MJ. Predicting best treatment in rheumatoid arthritis. Semin Arthritis Rheum. 2024;64S:152329.

23. ETS1 is a key transcription factor that drives RANKL-expressing, tissue-destructive fibroblasts. Nat Immunol. 2022;23(9):1303-4.
24. Culemann S, Gruneboom A, Nicolas-Avila JA, Weidner D, Lammle KF, Rothe T, et al. Locally renewing resident synovial macrophages provide a protective barrier for the joint. Nature. 2019;572(7771):670-5.
25. Kurowska-Stolarska M, Alivernini S. Synovial tissue macrophages in joint homeostasis, rheumatoid arthritis and disease remission. Nat Rev Rheumatol. 2022;18(7):384-97.
26. Alivernini S, MacDonald L, Elmesmari A, Finlay S, Tolusso B, Gigante MR, et al. Distinct synovial tissue macrophage subsets regulate inflammation and remission in rheumatoid arthritis. Nat Med. 2020;26(8):1295-306.
27. Fullerton JN, Gilroy DW. Resolution of inflammation: a new therapeutic frontier. Nat Rev Drug Discov. 2016;15(8):551-67.
28. Salmon M, Scheel-Toellner D, Huissoon AP, Pilling D, Shamsadeen N, Hyde H, et al. Inhibition of T cell apoptosis in the rheumatoid synovium. J Clin Invest. 1997;99(3):439-46.
29. Lee A, Qiao Y, Grigoriev G, Chen J, Park-Min KH, Park SH, et al. Tumor necrosis factor alpha induces sustained signaling and a prolonged and unremitting inflammatory response in rheumatoid arthritis synovial fibroblasts. Arthritis Rheum. 2013;65(4):928-38.
30. Burman A, Haworth O, Hardie DL, Amft EN, Siewert C, Jackson DG, et al. A chemokine-dependent stromal induction mechanism for aberrant lymphocyte accumulation and compromised lymphatic return in rheumatoid arthritis. J Immunol. 2005;174(3):1693-700.
31. Barone F, Gardner DH, Nayar S, Steinthal N, Buckley CD, Luther SA. Stromal Fibroblasts in Tertiary Lymphoid Structures: A Novel Target in Chronic Inflammation. Front Immunol. 2016;7:477.
32. Yap H-Y, Tee S, Wong M, Chow S-K, Peh S-C, Teow S-Y. Pathogenic Role of Immune Cells in Rheumatoid Arthritis: Implications in Clinical Treatment and Biomarker Development. Cells. 2018;7(10):161.
33. Adams RH, Alitalo K. Molecular regulation of angiogenesis and lymphangiogenesis. Nature Reviews Molecular Cell Biology. 2007;8(6):464-78.
34. Wang P, Konja D, Singh S, Zhang B, Wang Y. Endothelial Senescence: From Macro- to Micro-Vasculature and Its Implications on Cardiovascular Health. Int J Mol Sci. 2024;25(4).
35. Guven G, Hilty MP, Ince C. Microcirculation: Physiology, Pathophysiology, and Clinical Application. Blood Purif. 2020;49(1-2):143-50.
36. Uhlen M, Fagerberg L, Hallstrom BM, Lindskog C, Oksvold P, Mardinoglu A, et al. Proteomics. Tissue-based map of the human proteome. Science. 2015;347(6220):1260419.
37. Scioli MG, Bielli A, Arcuri G, Ferlosio A, Orlandi A. Ageing and microvasculature. Vasc Cell. 2014;6:19.
38. Buckley CD, Amft N, Bradfield PF, Pilling D, Ross E, Arenzana-Seisdedos F, et al. Persistent induction of the chemokine receptor CXCR4 by TGF-beta 1 on synovial T cells contributes to their accumulation within the rheumatoid synovium. J Immunol. 2000;165(6):3423-9.
39. Ebert LM, Schaerli P, Moser B. Chemokine-mediated control of T cell traffic in lymphoid and peripheral tissues. Mol Immunol. 2005;42(7):799-809.
40. McGettrick HM, Ward LS, Rainger GE, Nash GB. Mesenchymal Stromal Cells as Active Regulators of Lymphocyte Recruitment to Blood Vascular Endothelial Cells. Methods Mol Biol. 2017;1591:121-42.
41. McGettrick HM, Buckley CD, Filer A, Rainger GE, Nash GB. Stromal cells differentially regulate neutrophil and lymphocyte recruitment through the endothelium. Immunology. 2010;131(3):357-70.
42. Filippi M-D. Mechanism of Diapedesis. Elsevier; 2016. p. 25-53.
43. Khaltourina D, Matveyev Y, Alekseev A, Cortese F, Iovita A. Aging Fits the Disease Criteria of the International Classification of Diseases. Mech Ageing Dev. 2020;189:111230.
44. Wagner KH, Cameron-Smith D, Wessner B, Franzke B. Biomarkers of Aging: From Function to Molecular Biology. Nutrients. 2016;8(6).
45. Lopez-Otin C, Blasco MA, Partridge L, Serrano M, Kroemer G. Hallmarks of aging: An expanding universe. Cell. 2023;186(2):243-78.

46. Volume Information. Evolution. 1957;11(4):i-viii.
47. Mitteldorf J. What Is Antagonistic Pleiotropy? Biochemistry (Mosc). 2019;84(12):1458-68.
48. Campisi J, d'Adda di Fagagna F. Cellular senescence: when bad things happen to good cells. Nat Rev Mol Cell Biol. 2007;8(9):729-40.
49. Hayflick L. The Limited in Vitro Lifetime of Human Diploid Cell Strains. Exp Cell Res. 1965;37:614-36.
50. de Lange T. Shelterin: the protein complex that shapes and safeguards human telomeres. Genes Dev. 2005;19(18):2100-10.
51. Shay JW, Wright WE. Telomeres and telomerase: three decades of progress. Nat Rev Genet. 2019;20(5):299-309.
52. Roake CM, Artandi SE. Regulation of human telomerase in homeostasis and disease. Nat Rev Mol Cell Biol. 2020;21(7):384-97.
53. Weterings E, van Gent DC. The mechanism of non-homologous end-joining: a synopsis of synapsis. DNA Repair (Amst). 2004;3(11):1425-35.
54. Mah LJ, El-Osta A, Karagiannis TC. gammaH2AX: a sensitive molecular marker of DNA damage and repair. Leukemia. 2010;24(4):679-86.
55. Rufini A, Tucci P, Celardo I, Melino G. Senescence and aging: the critical roles of p53. Oncogene. 2013;32(43):5129-43.
56. Mijit M, Caracciolo V, Melillo A, Amicarelli F, Giordano A. Role of p53 in the Regulation of Cellular Senescence. Biomolecules. 2020;10(3).
57. Vermeulen K, Van Bockstaele DR, Berneman ZN. The cell cycle: a review of regulation, deregulation and therapeutic targets in cancer. Cell Proliferation. 2003;36(3):131-49.
58. Massague J. G1 cell-cycle control and cancer. Nature. 2004;432(7015):298-306.
59. Engeland K. Cell cycle regulation: p53-p21-RB signaling. Cell Death Differ. 2022;29(5):946-60.
60. Michaloglou C, Vredeveld LC, Soengas MS, Denoyelle C, Kuilman T, van der Horst CM, et al. BRAFE600-associated senescence-like cell cycle arrest of human naevi. Nature. 2005;436(7051):720-4.
61. Liu B, Chen Y, St Clair DK. ROS and p53: a versatile partnership. Free Radic Biol Med. 2008;44(8):1529-35.
62. Passos JF, Nelson G, Wang C, Richter T, Simillion C, Proctor CJ, et al. Feedback between p21 and reactive oxygen production is necessary for cell senescence. Mol Syst Biol. 2010;6:347.
63. Crouch J, Shvedova M, Thanapaul RJRS, Botchkarev V, Roh D. Epigenetic Regulation of Cellular Senescence. Cells. 2022;11(4):672.
64. Munro J, Barr NI, Ireland H, Morrison V, Parkinson EK. Histone deacetylase inhibitors induce a senescence-like state in human cells by a p16-dependent mechanism that is independent of a mitotic clock. Exp Cell Res. 2004;295(2):525-38.
65. Davan-Wetton CSA, Pessolano E, Perretti M, Montero-Melendez T. Senescence under appraisal: hopes and challenges revisited. Cell Mol Life Sci. 2021;78(7):3333-54.
66. Hernandez-Segura A, Nehme J, Demaria M. Hallmarks of Cellular Senescence. Trends Cell Biol. 2018;28(6):436-53.
67. Zhou D, Borsa M, Simon AK. Hallmarks and detection techniques of cellular senescence and cellular ageing in immune cells. Aging Cell. 2021;20(2):e13316.
68. Wong ES, Le Guezennec X, Demidov ON, Marshall NT, Wang ST, Krishnamurthy J, et al. p38MAPK controls expression of multiple cell cycle inhibitors and islet proliferation with advancing age. Dev Cell. 2009;17(1):142-9.
69. Iwasa H, Han J, Ishikawa F. Mitogen-activated protein kinase p38 defines the common senescence-signalling pathway. Genes Cells. 2003;8(2):131-44.
70. Luo Y, Zou P, Zou J, Wang J, Zhou D, Liu L. Autophagy regulates ROS-induced cellular senescence via p21 in a p38 MAPKalpha dependent manner. Exp Gerontol. 2011;46(11):860-7.
71. Podhorecka M, Skladanowski A, Bozko P. H2AX Phosphorylation: Its Role in DNA Damage Response and Cancer Therapy. Journal of Nucleic Acids. 2010;2010(1):1-9.

72. Peters AHFM, Mermoud JE, O'Carroll D, Pagani M, Schweizer D, Brockdorff N, et al. Histone H3 lysine 9 methylation is an epigenetic imprint of facultative heterochromatin. Nature Genetics. 2002;30(1):77-80.
73. Mlynarczyk C, Fahraeus R. Endoplasmic reticulum stress sensitizes cells to DNA damage-induced apoptosis through p53-dependent suppression of p21(CDKN1A). Nat Commun. 2014;5:5067.
74. Liu Y, Sharpless NE. Tumor suppressor mechanisms in immune aging. Curr Opin Immunol. 2009;21(4):431-9.
75. Freund A, Laberge RM, Demaria M, Campisi J. Lamin B1 loss is a senescence-associated biomarker. Mol Biol Cell. 2012;23(11):2066-75.
76. Sikora E, Bielak-Zmijewska A, Mosieniak G. A common signature of cellular senescence; does it exist? Ageing Res Rev. 2021;71:101458.
77. Lopes-Paciencia S, Saint-Germain E, Rowell MC, Ruiz AF, Kalegari P, Ferbeyre G. The senescence-associated secretory phenotype and its regulation. Cytokine. 2019;117:15-22.
78. Jun JI, Lau LF. The matricellular protein CCN1 induces fibroblast senescence and restricts fibrosis in cutaneous wound healing. Nat Cell Biol. 2010;12(7):676-85.
79. Demaria M, Ohtani N, Youssef SA, Rodier F, Toussaint W, Mitchell JR, et al. An essential role for senescent cells in optimal wound healing through secretion of PDGF-AA. Dev Cell. 2014;31(6):722-33.
80. Munoz-Espin D, Canamero M, Maraver A, Gomez-Lopez G, Contreras J, Murillo-Cuesta S, et al. Programmed cell senescence during mammalian embryonic development. Cell. 2013;155(5):1104-18.
81. Gal H, Lysenko M, Stroganov S, Vadai E, Youssef SA, Tzadikevitch-Geffen K, et al. Molecular pathways of senescence regulate placental structure and function. The EMBO Journal. 2019;38(18).
82. Chuprin A, Gal H, Biron-Shental T, Biran A, Amiel A, Rozenblatt S, et al. Cell fusion induced by ERVWE1 or measles virus causes cellular senescence. Genes Dev. 2013;27(21):2356-66.
83. Montero-Melendez T, Nagano A, Chelala C, Filer A, Buckley CD, Perretti M. Therapeutic senescence via GPCR activation in synovial fibroblasts facilitates resolution of arthritis. Nat Commun. 2020;11(1):745.
84. Yao C, Guan X, Carraro G, Parimon T, Liu X, Huang G, et al. Senescence of Alveolar Type 2 Cells Drives Progressive Pulmonary Fibrosis. Am J Respir Crit Care Med. 2021;203(6):707-17.
85. Wiley CD, Brumwell AN, Davis SS, Jackson JR, Valdovinos A, Calhoun C, et al. Secretion of leukotrienes by senescent lung fibroblasts promotes pulmonary fibrosis. JCI Insight. 2019;4(24).
86. Waters DW, Blokland KEC, Pathinayake PS, Burgess JK, Mutsaers SE, Prele CM, et al. Fibroblast senescence in the pathology of idiopathic pulmonary fibrosis. Am J Physiol Lung Cell Mol Physiol. 2018;315(2):L162-L72.
87. Sousa-Victor P, Gutarra S, Garcia-Prat L, Rodriguez-Ubreva J, Ortet L, Ruiz-Bonilla V, et al. Geriatric muscle stem cells switch reversible quiescence into senescence. Nature. 2014;506(7488):316-21.
88. An S, Chen Y, Gao C, Qin B, Du X, Meng F, et al. Inactivation of INK4a and ARF induces myocardial proliferation and improves cardiac repair following ischemia-reperfusion. Mol Med Rep. 2015;12(4):5911-6.
89. Zhong Y, Wang G, Yang S, Zhang Y, Wang X. The role of DNA damage in neural stem cells ageing. J Cell Physiol. 2024;239(4):e31187.
90. Xu M, Bradley EW, Weivoda MM, Hwang SM, Pirtskhalava T, Decklever T, et al. Transplanted Senescent Cells Induce an Osteoarthritis-Like Condition in Mice. J Gerontol A Biol Sci Med Sci. 2017;72(6):780-5.
91. Jeon OH, Kim C, Laberge RM, Demaria M, Rathod S, Vasserot AP, et al. Local clearance of senescent cells attenuates the development of post-traumatic osteoarthritis and creates a pro-regenerative environment. Nat Med. 2017;23(6):775-81.
92. Gao SG, Zeng C, Li LJ, Luo W, Zhang FJ, Tian J, et al. Correlation between senescence-associated beta-galactosidase expression in articular cartilage and disease severity of patients with knee osteoarthritis. Int J Rheum Dis. 2016;19(3):226-32.

93. Glick D, Barth S, Macleod KF. Autophagy: cellular and molecular mechanisms. J Pathol. 2010;221(1):3-12.
94. Kim YC, Guan KL. mTOR: a pharmacologic target for autophagy regulation. J Clin Invest. 2015;125(1):25-32.
95. Cui Z, Napolitano G, de Araujo MEG, Esposito A, Monfregola J, Huber LA, et al. Structure of the lysosomal mTORC1-TFEB-Rag-Ragulator megacomplex. Nature. 2023;614(7948):572-9.
96. Bao J, Zheng L, Zhang Q, Li X, Zhang X, Li Z, et al. Deacetylation of TFEB promotes fibrillar Abeta degradation by upregulating lysosomal biogenesis in microglia. Protein Cell. 2016;7(6):417-33.
97. Settembre C, Di Malta C, Polito VA, Garcia Arencibia M, Vetrini F, Erdin S, et al. TFEB links autophagy to lysosomal biogenesis. Science. 2011;332(6036):1429-33.
98. Sardiello M, Palmieri M, di Ronza A, Medina DL, Valenza M, Gennarino VA, et al. A gene network regulating lysosomal biogenesis and function. Science. 2009;325(5939):473-7.
99. Palmieri M, Impey S, Kang H, di Ronza A, Pelz C, Sardiello M, et al. Characterization of the CLEAR network reveals an integrated control of cellular clearance pathways. Hum Mol Genet. 2011;20(19):3852-66.
100. Raza S. Autophagy and metabolic aging: Current understanding and future applications. Biochim Biophys Acta Mol Cell Res. 2024;1871(6):119753.
101. Kaushik S, Tasset I, Arias E, Pampliega O, Wong E, Martinez-Vicente M, et al. Autophagy and the hallmarks of aging. Ageing Res Rev. 2021;72:101468.
102. Klionsky DJ, Petroni G, Amaravadi RK, Baehrecke EH, Ballabio A, Boya P, et al. Autophagy in major human diseases. EMBO J. 2021;40(19):e108863.
103. Li YS, Zhang FJ, Zeng C, Luo W, Xiao WF, Gao SG, et al. Autophagy in osteoarthritis. Joint Bone Spine. 2016;83(2):143-8.
104. Carames B, Taniguchi N, Otsuki S, Blanco FJ, Lotz M. Autophagy is a protective mechanism in normal cartilage, and its aging-related loss is linked with cell death and osteoarthritis. Arthritis Rheum. 2010;62(3):791-801.
105. Zheng G, Zhan Y, Li X, Pan Z, Zheng F, Zhang Z, et al. TFEB, a potential therapeutic target for osteoarthritis via autophagy regulation. Cell Death Dis. 2018;9(9):858.
106. Price JS, Waters JG, Darrah C, Pennington C, Edwards DR, Donell ST, et al. The role of chondrocyte senescence in osteoarthritis. Aging Cell. 2002;1(1):57-65.
107. Jeon OH, David N, Campisi J, Elisseeff JH. Senescent cells and osteoarthritis: a painful connection. J Clin Invest. 2018;128(4):1229-37.
108. Liu Y, Zhang Z, Li T, Xu H, Zhang H. Senescence in osteoarthritis: from mechanism to potential treatment. Arthritis Res Ther. 2022;24(1):174.
109. Jeon OH, Wilson DR, Clement CC, Rathod S, Cherry C, Powell B, et al. Senescence cell-associated extracellular vesicles serve as osteoarthritis disease and therapeutic markers. JCI Insight. 2019;4(7).
110. Del Rey MJ, Valin A, Usategui A, Ergueta S, Martin E, Municio C, et al. Senescent synovial fibroblasts accumulate prematurely in rheumatoid arthritis tissues and display an enhanced inflammatory phenotype. Immun Ageing. 2019;16:29.
111. Aman Y, Schmauck-Medina T, Hansen M, Morimoto RI, Simon AK, Bjedov I, et al. Autophagy in healthy aging and disease. Nat Aging. 2021;1(8):634-50.
112. Carames B, Hasegawa A, Taniguchi N, Miyaki S, Blanco FJ, Lotz M. Autophagy activation by rapamycin reduces severity of experimental osteoarthritis. Ann Rheum Dis. 2012;71(4):575-81.
113. Chen X, Gong W, Shao X, Shi T, Zhang L, Dong J, et al. METTL3-mediated m(6)A modification of ATG7 regulates autophagy-GATA4 axis to promote cellular senescence and osteoarthritis progression. Ann Rheum Dis. 2022;81(1):87-99.
114. Zhang H, Li X, Li Y, Yang X, Liao R, Wang H, et al. CREB Ameliorates Osteoarthritis Progression Through Regulating Chondrocytes Autophagy via the miR-373/METTL3/TFEB Axis. Front Cell Dev Biol. 2021;9:778941.
115. Mimpen JY, Hedley R, Ridley A, Baldwin MJ, Windell D, Bhalla A, et al. Cellular characterisation of advanced osteoarthritis knee synovium. Arthritis Res Ther. 2023;25(1):154.

116. Elhai M, Micheroli R, Houtman M, Mirrahimi M, Moser L, Pauli C, et al. The long non-coding RNA HOTAIR contributes to joint-specific gene expression in rheumatoid arthritis. Nat Commun. 2023;14(1):8172.
117. Lo BC, Gold MJ, Scheer S, Hughes MR, Cait J, Debruin E, et al. Loss of Vascular CD34 Results in Increased Sensitivity to Lung Injury. Am J Respir Cell Mol Biol. 2017;57(6):651-61.
118. Rodrigues CR, Moga S, Singh B, Aulakh GK. CD34 Protein: Its expression and function in inflammation. Cell Tissue Res. 2023;393(3):443-54.
119. Hou L, Voit RA, Shibamura-Fujiogi M, Koutsogiannaki S, Li Y, Chen Y, et al. CD11c regulates neutrophil maturation. Blood Adv. 2023;7(7):1312-25.
120. Saul D, Jurk D, Doolittle ML, Kosinsky RL, Monroe DG, LeBrasseur NK, et al. Distinct secretomes in p16- and p21- positive senescent cells across tissues. bioRxiv. 2023.
121. Zinczuk J, Zareba K, Guzinska-Ustymowicz K, Kedra B, Kemona A, Pryczynicz A. p16, p21, and p53 proteins play an important role in development of pancreatic intraepithelial neoplastic. Ir J Med Sci. 2018;187(3):629-37.
122. Kell L, Simon AK, Alsaleh G, Cox LS. The central role of DNA damage in immunosenescence. Front Aging. 2023;4:1202152.
123. Kim SJ, Kim JS, Papadopoulos J, Wook Kim S, Maya M, Zhang F, et al. Circulating monocytes expressing CD31: implications for acute and chronic angiogenesis. Am J Pathol. 2009;174(5):1972-80.
124. Xie Z, Shao B, Hoover C, McDaniel M, Song J, Jiang M, et al. Monocyte upregulation of podoplanin during early sepsis induces complement inhibitor release to protect liver function. JCI Insight. 2020;5(13).
125. Kotake Y, Naemura M, Murasaki C, Inoue Y, Okamoto H. Transcriptional Regulation of the p16 Tumor Suppressor Gene. Anticancer Res. 2015;35(8):4397-401.
126. Kotake Y, Ozawa Y, Harada M, Kitagawa K, Niida H, Morita Y, et al. YB1 binds to and represses the p16 tumor suppressor gene. Genes Cells. 2013;18(11):999-1006.
127. Scoumanne A, Cho SJ, Zhang J, Chen X. The cyclin-dependent kinase inhibitor p21 is regulated by RNA-binding protein PCBP4 via mRNA stability. Nucleic Acids Res. 2011;39(1):213-24.
128. Alsaleh G, Panse I, Swadling L, Zhang H, Richter FC, Meyer A, et al. Autophagy in T cells from aged donors is maintained by spermidine and correlates with function and vaccine responses. Elife. 2020;9.
129. Zhou D, Borsa M, Puleston DJ, Zellner S, Capera J, Sanderson S, et al. Mapping autophagosome contents identifies interleukin-7 receptor-alpha as a key cargo modulating CD4+ T cell proliferation. Nat Commun. 2022;13(1):5174.
130. Zhang H, Alsaleh G, Feltham J, Sun Y, Napolitano G, Riffelmacher T, et al. Polyamines Control eIF5A Hypusination, TFEB Translation, and Autophagy to Reverse B Cell Senescence. Mol Cell. 2019;76(1):110-25 e9.
131. Hu M, Ladowski JM, Xu H. The Role of Autophagy in Vascular Endothelial Cell Health and Physiology. Cells. 2024;13(10).
132. Zhao L, Zhang CL, He L, Chen Q, Liu L, Kang L, et al. Restoration of Autophagic Flux Improves Endothelial Function in Diabetes Through Lowering Mitochondrial ROS-Mediated eNOS Monomerization. Diabetes. 2022;71(5):1099-114.
133. Schaaf MB, Houbaert D, Mece O, Agostinis P. Autophagy in endothelial cells and tumor angiogenesis. Cell Death Differ. 2019;26(4):665-79.
134. Fan Y, Lu H, Liang W, Garcia-Barrio MT, Guo Y, Zhang J, et al. Endothelial TFEB (Transcription Factor EB) Positively Regulates Postischemic Angiogenesis. Circ Res. 2018;122(7):945-57.
135. Hu G, Xia Y, Zhang J, Chen Y, Yuan J, Niu X, et al. ESC-sEVs Rejuvenate Senescent Hippocampal NSCs by Activating Lysosomes to Improve Cognitive Dysfunction in Vascular Dementia. Adv Sci (Weinh). 2020;7(10):1903330.
136. Abokyi S, Ghartey-Kwansah G, Tse DY. TFEB is a central regulator of the aging process and age-related diseases. Ageing Res Rev. 2023;89:101985.

137. Brady OA, Jeong E, Martina JA, Pirooznia M, Tunc I, Puertollano R. The transcription factors TFE3 and TFEB amplify p53 dependent transcriptional programs in response to DNA damage. Elife. 2018;7.
138. Juretschke T, Beli P. Causes and consequences of DNA damage-induced autophagy. Matrix Biol. 2021;100-101:39-53.
139. Curnock R, Yalci K, Palmfeldt J, Jaattela M, Liu B, Carroll B. TFEB-dependent lysosome biogenesis is required for senescence. EMBO J. 2023;42(9):e111241.
140. Slade L, Biswas D, Ihionu F, El Hiani Y, Kienesberger PC, Pulinilkunnil T. A lysosome independent role for TFEB in activating DNA repair and inhibiting apoptosis in breast cancer cells. Biochem J. 2020;477(1):137-60.
141. Lu H, Fan Y, Qiao C, Liang W, Hu W, Zhu T, et al. TFEB inhibits endothelial cell inflammation and reduces atherosclerosis. Sci Signal. 2017;10(464).
142. Narasimhan A, Flores RR, Camell CD, Bernlohr DA, Robbins PD, Niedernhofer LJ. Cellular Senescence in Obesity and Associated Complications: a New Therapeutic Target. Curr Diab Rep. 2022;22(11):537-48.
143. Lin Y, Xu Z. Fibroblast Senescence in Idiopathic Pulmonary Fibrosis. Front Cell Dev Biol. 2020;8:593283.
144. Blanchet MR, Gold M, Maltby S, Bennett J, Petri B, Kubes P, et al. Loss of CD34 leads to exacerbated autoimmune arthritis through increased vascular permeability. J Immunol. 2010;184(3):1292-9.
145. Meyerholz DK, Beck AP. Fundamental Concepts for Semiquantitative Tissue Scoring in Translational Research. ILAR J. 2018;59(1):13-7.
146. Lliso-Ribera G, Humby F, Lewis M, Nerviani A, Mauro D, Rivellese F, et al. Synovial tissue signatures enhance clinical classification and prognostic/treatment response algorithms in early inflammatory arthritis and predict requirement for subsequent biological therapy: results from the pathobiology of early arthritis cohort (PEAC). Ann Rheum Dis. 2019;78(12):1642-52.
147. Cascao R, Rosario HS, Souto-Carneiro MM, Fonseca JE. Neutrophils in rheumatoid arthritis: More than simple final effectors. Autoimmun Rev. 2010;9(8):531-5.
148. Khandpur R, Carmona-Rivera C, Vivekanandan-Giri A, Gizinski A, Yalavarthi S, Knight JS, et al. NETs are a source of citrullinated autoantigens and stimulate inflammatory responses in rheumatoid arthritis. Sci Transl Med. 2013;5(178):178ra40.
149. O'Neil LJ, Kaplan MJ. Neutrophils in Rheumatoid Arthritis: Breaking Immune Tolerance and Fueling Disease. Trends Mol Med. 2019;25(3):215-27.
150. Spengler J, Lugonja B, Ytterberg AJ, Zubarev RA, Creese AJ, Pearson MJ, et al. Release of Active Peptidyl Arginine Deiminases by Neutrophils Can Explain Production of Extracellular Citrullinated Autoantigens in Rheumatoid Arthritis Synovial Fluid. Arthritis Rheumatol. 2015;67(12):3135-45.
151. Carmona-Rivera C, Carlucci PM, Moore E, Lingampalli N, Uchtenhagen H, James E, et al. Erratum for Research Article "Synovial fibroblast-neutrophil interactions promote pathogenic adaptive immunity in rheumatoid arthritis" by C. Carmona-Rivera, P. M. Carlucci, E. Moore, N. Lingampalli, H. Uchtenhagen, E. James, Y. Liu, K. L. Bicker, H. Wahamma, V. Hoffman, A. I. Catrina, P. Thompson, J. H. Buckner, W. H. Robinson, D. A. Fox, M. J. Kaplan. Sci Immunol. 2020;5(43).
152. Chaney S, Vergara R, Qiryaqoz Z, Suggs K, Akkouch A. The Involvement of Neutrophils in the Pathophysiology and Treatment of Osteoarthritis. Biomedicines. 2022;10(7).
153. Davalli P, Mitic T, Caporali A, Lauriola A, D'Arca D. ROS, Cell Senescence, and Novel Molecular Mechanisms in Aging and Age-Related Diseases. Oxid Med Cell Longev. 2016;2016:3565127.
154. Sies H, Belousov VV, Chandel NS, Davies MJ, Jones DP, Mann GE, et al. Defining roles of specific reactive oxygen species (ROS) in cell biology and physiology. Nat Rev Mol Cell Biol. 2022;23(7):499-515.
155. Tafani M, Sansone L, Limana F, Arcangeli T, De Santis E, Polese M, et al. The Interplay of Reactive Oxygen Species, Hypoxia, Inflammation, and Sirtuins in Cancer Initiation and Progression. Oxid Med Cell Longev. 2016;2016:3907147.

156. Suryadevara V, Hudgins AD, Rajesh A, Pappalardo A, Karpova A, Dey AK, et al. SenNet recommendations for detecting senescent cells in different tissues. Nat Rev Mol Cell Biol. 2024.
157. Hall BM, Balan V, Gleiberman AS, Strom E, Krasnov P, Virtuoso LP, et al. p16(Ink4a) and senescence-associated beta-galactosidase can be induced in macrophages as part of a reversible response to physiological stimuli. Aging (Albany NY). 2017;9(8):1867-84.
158. Saul D, Kosinsky RL, Atkinson EJ, Doolittle ML, Zhang X, LeBrasseur NK, et al. A new gene set identifies senescent cells and predicts senescence-associated pathways across tissues. Nat Commun. 2022;13(1):4827.
159. Gurkar AU, Gerencser AA, Mora AL, Nelson AC, Zhang AR, Lagnado AB, et al. Spatial mapping of cellular senescence: emerging challenges and opportunities. Nat Aging. 2023;3(7):776-90.
160. Heckenbach I, Mkrtchyan GV, Ezra MB, Bakula D, Madsen JS, Nielsen MH, et al. Nuclear morphology is a deep learning biomarker of cellular senescence. Nat Aging. 2022;2(8):742-55.
161. Eltzschig HK, Carmeliet P. Hypoxia and inflammation. N Engl J Med. 2011;364(7):656-65.
162. Pucino V, Nefla M, Gauthier V, Alsaleh G, Clayton SA, Marshall J, et al. Differential effect of lactate on synovial fibroblast and macrophage effector functions. Front Immunol. 2023;14:1183825.
163. Wang Q, Nie L, Zhao P, Zhou X, Ding Y, Chen Q, et al. Diabetes fuels periodontal lesions via GLUT1-driven macrophage inflammaging. Int J Oral Sci. 2021;13(1):11.
164. Piva SR, Susko AM, Khoja SS, Josbeno DA, Fitzgerald GK, Toledo FG. Links between osteoarthritis and diabetes: implications for management from a physical activity perspective. Clin Geriatr Med. 2015;31(1):67-87, viii.
165. Brugarolas J, Lei K, Hurley RL, Manning BD, Reiling JH, Hafen E, et al. Regulation of mTOR function in response to hypoxia by REDD1 and the TSC1/TSC2 tumor suppressor complex. Genes Dev. 2004;18(23):2893-904.
166. Arsham AM, Howell JJ, Simon MC. A novel hypoxia-inducible factor-independent hypoxic response regulating mammalian target of rapamycin and its targets. J Biol Chem. 2003;278(32):29655-60.
167. Zaarour RF, Azakir B, Hajam EY, Nawafleh H, Zeinelabdin NA, Engelsen AST, et al. Role of Hypoxia-Mediated Autophagy in Tumor Cell Death and Survival. Cancers (Basel). 2021;13(3).
168. Chen PS, Chiu WT, Hsu PL, Lin SC, Peng IC, Wang CY, et al. Pathophysiological implications of hypoxia in human diseases. J Biomed Sci. 2020;27(1):63.
169. Nanus DE, Wijesinghe SN, Pearson MJ, Hadjicharalambous MR, Rosser A, Davis ET, et al. Regulation of the Inflammatory Synovial Fibroblast Phenotype by Metastasis-Associated Lung Adenocarcinoma Transcript 1 Long Noncoding RNA in Obese Patients With Osteoarthritis. Arthritis Rheumatol. 2020;72(4):609-19.
170. Farah H, Wijesinghe SN, Nicholson T, Alnajjar F, Certo M, Alghamdi A, et al. Differential Metabotypes in Synovial Fibroblasts and Synovial Fluid in Hip Osteoarthritis Patients Support Inflammatory Responses. Int J Mol Sci. 2022;23(6).
171. Sun W, Jia M, Feng Y, Cheng X. Lactate is a bridge linking glycolysis and autophagy through lactylation. Autophagy. 2023;19(12):3240-1.
172. Fedotova EI, Dolgacheva LP, Abramov AY, Berezhnov AV. Lactate and Pyruvate Activate Autophagy and Mitophagy that Protect Cells in Toxic Model of Parkinson's Disease. Mol Neurobiol. 2022;59(1):177-90.
173. Tasdemir E, Chiara Maiuri M, Morselli E, Criollo A, D'Amelio M, Djavaheri-Mergny M, et al. A dual role of p53 in the control of autophagy. Autophagy. 2008;4(6):810-4.
174. Tasdemir E, Maiuri MC, Galluzzi L, Vitale I, Djavaheri-Mergny M, D'Amelio M, et al. Regulation of autophagy by cytoplasmic p53. Nat Cell Biol. 2008;10(6):676-87.
175. Maiuri MC, Galluzzi L, Morselli E, Kepp O, Malik SA, Kroemer G. Autophagy regulation by p53. Curr Opin Cell Biol. 2010;22(2):181-5.
176. Zhou Y, Liu F. Coordination of the AMPK, Akt, mTOR, and p53 Pathways under Glucose Starvation. Int J Mol Sci. 2022;23(23).
177. Anand SK, Sharma A, Singh N, Kakkar P. Entrenching role of cell cycle checkpoints and autophagy for maintenance of genomic integrity. DNA Repair (Amst). 2020;86:102748.

178. Crighton D, Wilkinson S, O'Prey J, Syed N, Smith P, Harrison PR, et al. DRAM, a p53-induced modulator of autophagy, is critical for apoptosis. Cell. 2006;126(1):121-34.
179. Lu T, Zhu Z, Wu J, She H, Han R, Xu H, et al. DRAM1 regulates autophagy and cell proliferation via inhibition of the phosphoinositide 3-kinase-Akt-mTOR-ribosomal protein S6 pathway. Cell Commun Signal. 2019;17(1):28.
180. Yi J, Luo J. SIRT1 and p53, effect on cancer, senescence and beyond. Biochim Biophys Acta. 2010;1804(8):1684-9.
181. Budanov AV, Karin M. p53 target genes sestrin1 and sestrin2 connect genotoxic stress and mTOR signaling. Cell. 2008;134(3):451-60.
182. Zhang Z, Wang H, Ding Q, Xing Y, Xu D, Xu Z, et al. The tumor suppressor p53 regulates autophagosomal and lysosomal biogenesis in lung cancer cells by targeting transcription factor EB. Biomed Pharmacother. 2017;89:1055-60.
183. Spengler K, Kryeziu N, Grosse S, Mosig AS, Heller R. VEGF Triggers Transient Induction of Autophagy in Endothelial Cells via AMPKalpha1. Cells. 2020;9(3).
184. Cheung KC, Ma J, Wang L, Chen X, Fanti S, Li M, et al. CD31 orchestrates metabolic regulation in autophagy pathways of rheumatoid arthritis. Pharmacol Res. 2024;207:107346.
185. Krstic J, Reinisch I, Schupp M, Schulz TJ, Prokesch A. p53 Functions in Adipose Tissue Metabolism and Homeostasis. Int J Mol Sci. 2018;19(9).
186. Vergoni B, Cornejo PJ, Gilleron J, Djedaini M, Ceppo F, Jacquel A, et al. DNA Damage and the Activation of the p53 Pathway Mediate Alterations in Metabolic and Secretory Functions of Adipocytes. Diabetes. 2016;65(10):3062-74.
187. Chang NC. Autophagy and Stem Cells: Self-Eating for Self-Renewal. Front Cell Dev Biol. 2020;8:138.
188. Chen X, He Y, Lu F. Autophagy in Stem Cell Biology: A Perspective on Stem Cell Self-Renewal and Differentiation. Stem Cells Int. 2018;2018:9131397.
189. Zhang F, Jonsson AH, Nathan A, Wei K, Millard N, Xiao Q, et al. 2022.